



HAL
open science

Development of ionic electroactive actuators with improved interfacial adhesion: towards the fabrication of inkjet printable artificial muscles

Aiva Simaite

► **To cite this version:**

Aiva Simaite. Development of ionic electroactive actuators with improved interfacial adhesion: towards the fabrication of inkjet printable artificial muscles. Micro and nanotechnologies/Microelectronics. INSA de Toulouse, 2015. English. NNT: 2015ISAT0043 . tel-01591571

HAL Id: tel-01591571

<https://theses.hal.science/tel-01591571>

Submitted on 21 Sep 2017

HAL is a multi-disciplinary open access archive for the deposit and dissemination of scientific research documents, whether they are published or not. The documents may come from teaching and research institutions in France or abroad, or from public or private research centers.

L'archive ouverte pluridisciplinaire **HAL**, est destinée au dépôt et à la diffusion de documents scientifiques de niveau recherche, publiés ou non, émanant des établissements d'enseignement et de recherche français ou étrangers, des laboratoires publics ou privés.



Université
de Toulouse

THÈSE

En vue de l'obtention du

DOCTORAT DE L'UNIVERSITÉ DE TOULOUSE

Délivré par : *l'Institut National des Sciences Appliquées de Toulouse (INSA de Toulouse)*

Présentée et soutenue le 24/11/2015 par :

Aiva SIMAITE

Development of ionic electroactive actuators with improved interfacial adhesion: towards the fabrication of inkjet printable artificial muscles

JURY

FRÉDÉRIC MORANCHO
ROSE-MARIE SAUVAGE
PHILIPPE SOUERES
ERIC CATTAN
STÉPHANE REGNIER
CHRISTIAN BERGAUD
BERTRAND TONDU

Professeur d'Université
Ingénieur
Directeur de Recherche
Professeur d'Université
Professeur d'Université
Directeur de Recherche
Professeur d'Université

Président du Jury
Examinateur
Invité
Rapporteur
Rapporteur
Directeur de thèse
Co-directeur de thèse

École doctorale et spécialité :

GEET : Micro et Nanosystèmes

Unité de Recherche :

Laboratoire d'Analyse et d'Architecture des Systèmes (UPR 8001)

Directeur(s) de Thèse :

Christian BERGAUD et Bertrand TONDU

Rapporteurs :

Eric CATTAN et Stéphane REGNIER

PhD thesis

**Development of ionic electroactive actuators with
improved interfacial adhesion: towards the
fabrication of inkjet printable artificial muscles**

Aiva Simaite

Thesis prepared at:

LAAS-CNRS

NanoBioSystems and GEPETTO groups
7, avenue du Colonel Roche, BP 54200,
F-31031 Toulouse Cedex 4

Thesis was funded by:

French Ministry of Defence

The Armaments Procurement Agency (DGA)

November 24, 2015

Aiva Simaite

Development of ionic electroactive actuators with improved interfacial adhesion: towards the fabrication of inkjet printable artificial muscles

PhD thesis, November 24, 2015

Reviewers: Eric Cattan and Stéphane Regnier

Supervisors: Christian Bergaud and Bertrand Tondu

The Institut National des Sciences Appliquées de Toulouse (INSA de Toulouse)

Abstract

Ionic electroactive polymer based artificial muscles are promising alternative to traditional actuators, especially where compliant muscle-like response is desirable. Among them, conducting polymer actuators (*CPAs*) are most promising for biomedical applications, where biocompatibility, compactness and accurate positioning is essential. Nevertheless, development of applicable devices is hold down by their low efficiency and fast performance deterioration. The absence of a tactile, force or position feed-back is another feature limiting the development of functional devices. The goal of this thesis is to develop a fabrication technique for conducting polymer based actuators that could be up-scalable and enable facile integration of sensory feedback.

Inkjet printing is key technology in the field of defined polymer deposition as well as in fabrication of strain sensors. It is also one of the most promising alternatives to prevalent fabrication of conducting polymer actuators. Nevertheless, inkjet printed actuators were not yet realized due to rheological properties of conducting polymer solutions that challenge jetting and the complex solution - membrane interactions, that lead to poor adhesion or uncontrolled infiltration.

In order to enable this fabrication method, hybrid ion-storing membranes were developed. Argon plasma induced grafting-to of hydrophilic macromonomer with limited-in-depth deposition was used to obtain polyvinylidene fluoride (*PVDF*) membranes with hydrophilic upper surfaces and hydrophobic centre. Functionalized *PVDF* membranes were shown to withhold good adhesion to the conducting polymer films and preserve electrically insulating layer in between them. Hybrid membranes were demonstrated to be advantageous in fabrication of *CPAs* by drop casting and enable production of actuators with various morphologies. Furthermore, fabricated poly(3,4-ethylenedioxythiophene) polystyrene sulfonate (*PEDOT:PSS*) based actuators demonstrated long lifetime with no signs of delamination as well as large strain of more than 0.6%.

In addition, the complex nature of the physico-chemical mechanisms of the interactions between the polymer film and the porous membrane was better understood during this work. The conditions necessary in order to ensure strong adhesion as well as circumstances leading to uncontrolled infiltration were partially identified. These were used to set up limits to membrane preparation and polymer solution composition. Combining obtained knowledge with known requirements for inkjet printable solutions lead to the realization of the first inkjet printed *PEDOT:PSS* based ionic actuators.

Résumé

Les actionneurs à base de polymères électroactifs ioniques constituent une alternative prometteuse par rapport aux actionneurs conventionnels, en particulier lorsqu'une réponse comparable à celle d'un muscle naturel est recherché. Parmi eux, les actionneurs à base de polymères conducteurs constituent une voie prometteuse pour des applications biomédicale où la biocompatibilité, la compacité et un positionnement précis sont requis. Néanmoins, l'essor de dispositifs fonctionnels est fortement ralenti en raison de la faible efficacité d'actionnement et de la rapide dégradation des performances de ce type d'actionneurs. L'absence de rétroaction sur la force ou sur la position est également un autre aspect limitant le développement de cette approche. L'objectif de cette thèse est de proposer une technique de fabrication à grande échelle pour l'élaboration d'actionneurs à base de polymères électroactifs ioniques et permettant également l'intégration de capteurs pour un contrôle rétroactif.

L'impression par jet d'encre est une technologie clé pour le dépôt de polymères et une des plus alternatives les plus prometteuses pour la production d'actionneurs à base de polymères conducteurs. Cependant, la fabrication d'actionneurs par technique jet d'encre n'est pas encore totalement maîtrisée à cause des propriétés rhéologiques des solutions de polymères conducteurs qui rendent difficile le contrôle de l'éjection de gouttes mais également en raison de la nature complexe des interactions entre la solution et l'échantillon qui peut conduire à une faible adhésion et un mauvais contrôle de l'infiltration de l'encre.

Pour optimiser cette méthode de fabrication, des membranes hybrides contenant des ions ont été développées. Le greffage d'un monomère hydrophile par plasma argon avec un dépôt contrôlé en profondeur a été utilisé pour obtenir des membranes en polyfluorure de vinylidène (*PVDF*) avec des surfaces hydrophiles tout en conservant une zone centrale hydrophobe. Ces membranes hybrides ont permis d'obtenir, par dépôt de gouttes, des actionneurs de morphologies très variées à base de polymères conducteurs. En outre, la durée de vie d'actionneurs obtenus avec une solution conductrice de poly(3,4-ethylenedioxythiophene) polystyrene sulfonate (*PEDOT:PSS*) a été sensiblement augmentée avec des déformations de plus de 0.6% sans qu'aucun signe de délamination ne soit perceptible.

Enfin, la nature complexe des mécanismes physico-chimiques à l'origine des interactions entre le film polymère et la membrane poreuse a été mieux appréhendée durant ce travail. Les conditions nécessaires pour assurer une forte adhésion et les effets conduisant à un mauvais contrôle de l'infiltration ont été partiellement identifiés. Ces résultats ont permis de définir les paramètres clés concernant la préparation de la membrane et la composition de la solution polymère. En associant l'ensemble de ces résultats avec les exigences liées à l'utilisation de l'impression de solutions par jet d'encre, nous avons réalisé, en utilisant cette technique de dépôt, les premiers actionneurs ioniques à base de *PEDOT:PSS*.

Publications

The following publications are based on the work presented in this thesis:

1. Aiva Simaite, Bertrand Tondu, Fabrice Mathieu, Philippe Souères and Christian Bergaud; 'Simple casting based fabrication of PEDOT:PSS-PVDF-ionic liquid soft actuators', *Proc. SPIE 9430, Electroactive Polymer Actuators and Devices (EAPAD)*, 2015; 94301E; doi:10.1117/12.2083936.
2. Aiva Simaite, Bertrand Tondu, Philippe Souères and Christian Bergaud; 'Hybrid PVDF/PVDF-graft-PEGMA Membranes for Improved Interface Strength and Lifetime of PEDOT:PSS/PVDF/ Ionic Liquid Actuators', *ACS Applied Materials and Interfaces*, 2015; 7(36): 19966-77; doi:10.1021/acsami.5b04578.
3. Aiva Simaite, Fabien Mesnilgrete, Bertrand Tondu, Philippe Souères and Christian Bergaud; 'Towards inkjet printable conducting polymer artificial muscles. *Sensors and Actuators B: Chemical*, 2016; 229: 425-33; doi:10.1016/j.snb.2016.01.142.
4. Aiva Simaite, Aude Delegarde, Emmanuel Flahaut and Christian Bergaud; 'Spray-coated carbon nanotube carpets for creep reduction of conducting polymer based artificial muscles. *submitted*.

Acknowledgement

This thesis work was achieved thanks to collaboration and support of various people who I would like to gratefully acknowledge.

First of all, I would like to thank my supervisor Christian Bergaud. His never ending optimism was inspiring me to attempt to achieve things that at that moment looked rather impossible. Thanks to him I, stubbornly, have never gave up trying. I would also like to thank my supervisors in robotics group, Bertrand Tondu and Philippe Souères, who would always remind me the long term goals and potential of this project.

The work would not have been possible without continuous support of Fabian Mesnil-grente. During my thesis he was helping to find solutions to many technical problems i faced; conversations with him also served as a valuable inspiration that lead to many scientific contributions presented in this work. I would also like to acknowledge his work on inkjet printing presented in the Chapter 5.

The work presented at the end of the Chapter 4 on spray coating of carbon nanotubes was a collaboration with Aude Delgarde and Emmanuel Flahaut. I am sincerely grateful to them both for their contribution to this work.

I am also grateful for the enormous amount of help and teaching by Alexandre Rumeau and Nicolas Mauran. I want to thank Pascal Dubreuil and Aurélie Lecestre for their help with plasma grafting, Benjamin Reig for his EDX measurements and Fabrice Mathieu for helping to realise electrical characterization set-up for actuators. Other members of LAAS TEAM and I2C groups also contributed to this work for which I am very grateful.

I would never have been able to finish my dissertation without presence and help of my friends. There are no words that could express their importance to my work. Alexandre Ravet was there with me nearly every day of my thesis; coffee breaks with him helped a lot to cope with stress and not to give up. He and Pierrick Koch also deserve acknowledgement for the idea and realization of the dragon-fly. Furthermore, I want to thank Pierrick Koch for his essential help with video processing and all other lines of code. I also want to thank Ellon Paiva Mendes for his encouragement to learn MatLab and LaTeX and his patience teaching me. Finally, thank you to my all other friends who were there with me. I love you guys.

Abbreviations

Materials

CNTs carbon nanotubes

DMSO dimethyl sulfoxide

emimTFSI 1-ethyl-3-methylimidazolium bis(trifluoromethanesulfonyl)imide

MWCNTs multiwall carbon nanotubes

PDMS polydimethylsiloxane

PEDOT poly(3,4-ethylenedioxythiophene)

PEDOT:PSS poly(3,4-ethylenedioxythiophene) polystyrene sulfonate

PEG polyethylene glycol

PEGMA poly(ethylene glycol) methyl ether methacrylate

PEG400 poly(ethylene glycol) of $M_r = 400$

PEO polyethylene oxide

PPy polypyrrole

PVP polyvinylpyrrolidone

PSS polystyrene sulfonate

PVDF polyvinylidene fluoride

SDS sodium dodecyl sulfate

Created abbreviations for used materials

EG-PEDOT PEDOT:PSS with ethylene glycol as secondary dopant

G-PEDOT PEDOT:PSS with glycerol as secondary dopant

PEG-PEDOT PEDOT:PSS with PEG as secondary dopant

mPVDF PVDF-graft-PEGMA membrane

pPVDF pristine PVDF membrane

Characterization techniques

<i>AFM</i>	atomic force microscopy
<i>ATRP</i>	atom transfer radical polymerisation
<i>CV</i>	cyclic voltammetry
<i>EDX</i>	Energy-dispersive X-ray spectroscopy
<i>FT-IR</i>	Fourier transform infrared spectroscopy
<i>IR</i>	infrared
<i>RF</i>	radio frequency
<i>SEM</i>	scanning electron microscopy
<i>UV</i>	ultraviolet
<i>WCA</i>	water contact angle
<i>XPS</i>	X-ray photoelectron spectroscopy

Other

<i>CPAs</i>	conducting polymer actuators
<i>CPs</i>	conducting polymers
<i>DEAs</i>	dielectric elastomers
<i>EAPs</i>	electroactive polymers
<i>ILs</i>	ionic liquids
<i>IPMCs</i>	ionic polymer-metal composites
<i>IPNs</i>	interpenetrated polymer networks
<i>GD</i>	grafting density
<i>MD</i>	mixing depth
<i>SD</i>	spraying density
<i>SE</i>	spraying efficiency
<i>SMA</i>	shape-memory alloy

Contents

1	Introduction	1
1.1	Artificial muscles	1
1.1.1	Pneumatic actuation	2
1.1.2	Thermal actuation	2
1.1.3	Electric field actuation	4
1.1.4	Ion-based actuation	5
1.1.5	Other or combined actuation mechanisms	7
1.2	Applications of EAP based actuators	8
1.3	Motivation and Problem Statement	10
1.4	Thesis Structure	11
2	Hybrid PVDF/PVDF-graft-PEGMA membranes	13
2.1	Introduction	14
2.1.1	Functionalization of <i>PVDF</i> membranes	14
2.1.2	Polymer functionalization by gas plasma	17
2.2	Surface modification during irradiation: PVDF-graft-PEGMA by Ar plasma	20
2.2.1	Influence of plasma parameters	21
2.2.2	Limiting grafting depth	23
2.2.3	Controlling grafting depth	27
2.3	Conclusion	31
2.3.1	Future work	33
3	PEDOT:PSS and PVDF membrane: adhesion versus infiltration	35
3.1	Introduction	36
3.1.1	Adhesion between polymers	37
3.1.2	Polymer adsorption on the surface out of solution	39
3.2	Adhesion between <i>PEDOT:PSS</i> and <i>PVDF</i>	40
3.2.1	Adhesion evaluation method	40
3.2.2	Adhesion between pristine <i>PVDF</i> and <i>PEDOT:PSS</i>	41
3.2.3	Effect of the infiltration on the <i>PEDOT:PSS</i> -membrane adhesion .	45
3.2.4	Effect of the <i>PVDF</i> surface damage on adhesion	47
3.3	Adhesion between <i>PEDOT:PSS</i> and <i>PVDF-graft-PEGMA</i>	48
3.3.1	Influence of surface roughness	50
3.3.2	Influence of coating by physisorption	50
3.4	Comments on infiltration of <i>PEDOT:PSS</i>	53
3.5	Conclusion	56
3.5.1	Future work	56

4	PEDOT:PSS/mPVDF/ionic liquid actuators	59
4.1	Introduction	60
4.1.1	Volume change in the conducting polymer based actuators	61
4.1.2	PEDOT:PSS in ionic liquid	64
4.2	Fabrication	64
4.2.1	State-of-the-art	64
4.2.2	PEDOT:PSS/mPVDF/PEDOT:PSS actuators by drop casting	66
4.3	Characterization of PEDOT:PSS based actuators	68
4.3.1	Long time performance	73
4.4	The importance of a good adhesion	76
4.4.1	Lifetime	76
4.4.2	Performance	78
4.5	Influence of the mixing depth on actuators performance	79
4.6	Towards actuator performance improvement by altering <i>PEDOT:PSS</i>	83
4.6.1	Post-treatment of PEDOT:PSS	84
4.7	Conclusions	87
4.7.1	Future work	88
5	Towards inkjet printed artificial muscles	91
5.1	Introduction	91
5.1.1	Generation of droplets	91
5.1.2	Drop-substrate interaction and solidification	94
5.1.3	Inkjet of conductive polymers	94
5.2	Printing PEDOT:PSS on PVDF membrane	95
5.2.1	Ink-substrate interaction	95
5.2.2	Ink composition	99
5.3	Printing and characterisation of actuators	103
5.4	Conclusion	105
5.4.1	Future work	106
6	Summary of scientific contributions and closing remarks	107
6.1	Future Work	108
	Bibliography	111
A	Appendix 1: materials and experimental methods	143
A.1	Materials	143
A.1.1	Solutions	144
A.2	Chapter 2: Hybrid PVDF/PVDF-graft-PEGMA membranes	144
A.2.1	PEGMA deposition	144
A.2.2	Plasma irradiation	145
A.2.3	Characterization of PVDF membrane	146
A.3	Chapter 3: Adhesion	146
A.3.1	Fabrication of PVDF/PEDOT:PSS bilayers	146
A.3.2	Penetrating drop method	147
A.4	Chapter 4: PEDOT:PSS/mPVDF/ionic liquid actuators	148

A.4.1	Fabrication of actuators	148
A.4.2	Characterization of actuators	148
A.4.3	Post-treatment of actuators	150
A.5	Chapter 5: Towards inkjet printed artificial muscles	151
A.5.1	Ink preparation, printing and characterization	151
A.5.2	Printing and characterization of actuators	152
B	Appendix 2: additional figures	155
C	Résumé	163
C.1	Introduction	163
C.1.1	Muscles artificiels: état de l'art	163
C.1.2	Materials	167
C.1.3	Contexte et positionnement du problème	169
C.2	Membranes hybrides PVDF/PVDF-PEGMA	171
C.2.1	Contrôle de la profondeur de pénétration	173
C.3	PEDOT :PSS et membrane en PVDF : adhésion versus infiltration	175
C.3.1	Conclusion	179
C.4	Actionneurs ioniques PEDOT :PSS /mPVDF	179
C.4.1	Durée de vie	182
C.4.2	Vers des muscles artificiels fabriqués par technologie jet d'encre	183

Introduction

Contents

1.1	Artificial muscles	1
1.1.1	Pneumatic actuation	2
1.1.2	Thermal actuation	2
1.1.3	Electric field actuation	4
1.1.4	Ion-based actuation	5
1.1.5	Other or combined actuation mechanisms	7
1.2	Applications of EAP based actuators	8
1.3	Motivation and Problem Statement	10
1.4	Thesis Structure	11

There is a growing interest in robots working with or in close vicinity of humans. Making them compliant is one of the biggest challenges. For the next generation robots, adapted control strategies will need to be combined with lightweight materials, actuators, sensors and power sources. For example, traditional actuators have low power density, power-to-mass ratio and efficiency. These and other properties are limiting the creation of the dynamic micro-robots. Furthermore, their cost, bulkiness and the lack of integrated tactile or force feedback are limiting their applications in medicine.

Even though very limited at the moment, electroactive polymers (*EAPs*) have a potential of replacing prevalent actuators, where compliant muscle-like response is desirable. In addition, *EAPs* provide fabrication flexibility and could potentially be used for applications in medical devices (minimally invasive surgical and diagnostic tools) [131, 324, 381], prosthesis (hands and arms), robotics (as grippers and manipulators) [60, 149, 377], toys *etc.*

1.1 Artificial muscles

Artificial muscle is a generic term used for materials or devices that can generate reversible contraction, expansion, or rotation within one body due to an external stimulus (voltage, current, pressure, temperature, *etc.*) [270]. Based on the stimulus, they can be divided into (1) pneumatic, (2) thermal, (3) electric field and (4) ionic actuators. The comparison of the currently investigated artificial muscles is shown in *Fig. 1.1*. Their performance is often compared to the human skeletal muscle and some artificial muscles could produce larger strain (electric field driven actuators) or stress (ionic actuators). Nevertheless, the combination of the efficiency (40 %), strain

rate (50 %/s) and specific power (284 W/kg) of a human muscle are hard to match (Fig. 1.1b). The current state-of-the-art tendencies and challenges of prevalent artificial muscles are discussed in the following sections.

1.1.1 Pneumatic actuation

In pneumatic actuators the contractile and linear motion is generated by inflating and deflating an elastomer. They are extremely lightweight and compliant and are already widely used [74, 81, 149, 417]. Well-known McKibben-type actuators are being further developed in order to improve their lifetime and control [260, 378, 417]. In addition, new inflatable materials are being suggested such as the pneumatically-driven flexible microactuators (*FMA*s) [128, 129] or the embedded pneumatic networks of channels in elastomer (*PneuNets*) [149]. They generate more complex motions with the single source of pressure; gripping, bending, crawling motions can be created by simply changing their configuration and the size [256, 275, 278, 337]. Furthermore, stiffer and durable elastomers can be used in order to fabricate soft robots that are resistant to temperature, pressure and mechanical damage [256, 375].

Pneumatic artificial muscles rely on the air-producing equipment. Therefore, if damaged, they are likely to rupture and leak. Furthermore, their force is determined by both the pressure and the state of inflation, making them non-linear and difficult to control. This limits their applications where the delicate and precise movement is required. Therefore, as an alternative to the pneumatic actuation, other types of artificial muscles are being extensively studied.

1.1.2 Thermal actuation

Shape-memory alloy (*SMA*) materials such as Nitinol are the most well known lightweight solid-state alternative to conventional actuators. They undergo a phase and shape change with temperature or stress and for actuation purposes they are usually heated by running current through them (reviewed by [182]). Nevertheless, as most of the solid-state materials, *SMA*s fail after long cycling due to the microstructural crack propagation and fracture. Furthermore, cooling of the actuator is significantly slower than heating and causes a response asymmetry. Shape memory polymers (*SMP*s), actuated analogously, are promising alternatives to *SMA*s. They are low cost and are able to produce larger strains of up to 700% [200] (typical strain of *SMA*s is 0.1%). Furthermore, due to easier processing and synthesis flexibility, *SMP*s could be tailored to required applications (reviewed by [28, 360]).

Recently, a well known phenomenon of thermal expansion was used for the actuation of the twisted yarns of metals [270], carbon nanotubes (*CNT*s) [233], nylon or polyester [134]. The first actuators of this kind were produced by twist-spinning multiwall carbon nanotubes (*MWCNT*s) into a yarn and then overtwisting them until coiling [414]. When the length of the yarn is kept constant during heating, the yarn untwists and its diameter increases. Alternatively, when the change in the twist is restrained, during the actuation yarn contracts in length and its diameter increases. Twisting *MWCNT*s were shown

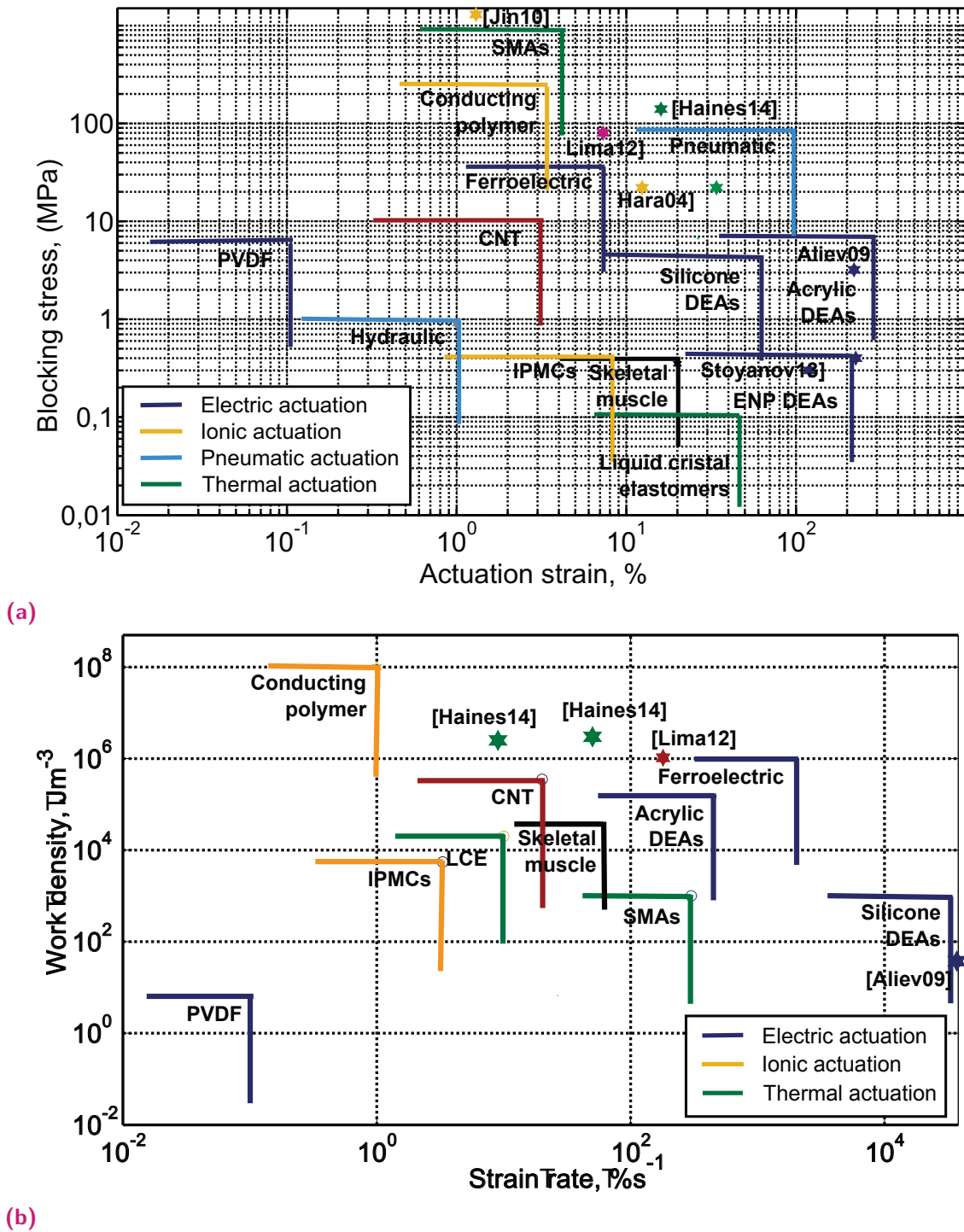


Fig. 1.1. (a) Stress versus strain and (b) work density versus strain rate of typical artificial muscles (defined by lines) and some state-of-the-art actuators (stars). Types of actuations: blue - electric, orange - ionic, green - thermal, red - CNTs, gray - others, black - mammal skeletal muscle. Adopted from [249, 269] and other sources mentioned in the text.

to increase their strength (up to 300 MPa), while coiling and wax-filling¹ amplifies the tensile stroke (from 0.7% to about 10%) and the work capacity. Even though MWCNTs yarns have remarkable electrical and mechanical properties, their fabrication is complicated and expensive. This encourages development of the artificial muscles, based on the twisted metal nanowires [270].

Recently, it was shown that much cheaper materials, such as nylon or polyester can be twisted, coiled and used as torsional muscles [134]. These actuators are able to contract by 49% and does not require the infiltration with the guest material. They can also be used for millions of cycles and produce mechanical work of 5.3 kW/kg. In comparison to CNTs, lower temperature is needed to drive these muscles. Therefore, they could be powered by changes in ambient temperatures or be woven into the smart textiles [134, 233]. Nevertheless, further work is needed to increase their electrothermal energy conversion efficiency that is currently only about 1 – 2%.

1.1.3 Electric field actuation

Piezoelectric ceramics are one of the materials that are able to produce mechanical stress because of the electric field and are used as actuators. Similarly, there are polymers that respond to electric field. For example, ferroelectric polymers, *i.e.* polyvinylidene fluoride (PVDF), can generate large strains (5%) due to the field-driven alignment of their polar groups. The main advantages of such polymers are low heat dissipation and fast response (*ms*). Therefore, actuators based on them can be used for applications such as varifocal microlenses [63]. Nevertheless, their actuation requires high voltages (150 MV/m), they are sensitive to defects and difficult to mass produce² [249, 269].

Dielectric elastomers

The most studied electroactive polymer actuators are based on dielectric elastomers (DEAs). They are typically made of a passive elastomer film that is sandwiched in between two compliant electrodes. When a voltage is applied, the electrostatic pressure between the electrodes (Maxwell Stress), arising due to the Coulomb forces, compresses the thickness and expands the area of the elastomer in between. Most of the actuator properties, *i.e.* the produced strain, force and specific energy density, depends on the generated electric field and, therefore, properties of the dielectric, *i.e.* relative permittivity and stiffness [37]. Most widely used dielectrics are silicone, polyurethane [307, 306] and polyacrylate [201, 157]. Typically, DEAs produce large strain³ (Fig. 1.1a) that presents one of their challenges, that is flexible and stretchable electrodes. For now, prevalent electrodes are based on the carbon powder, grease, rubber and metallic thin films (reviewed by [323]), but CNTs [355], metal ion implantation [93] and platinum salts [83] were suggested as an alternative.

¹The volume expansion of CNTs itself is very low, therefore infiltration with a guest material, *i.e.* wax, that has higher volume expansion was suggested [233].

²Electrostrictive graft elastomers based on PVDF copolymers, in which polar groups are attached as the side chains [395], require lower voltages (1.5 MV/m), but they also produce lower strains (4 %) and are relatively slower (< 133 Hz)

³Polyacrylate based DEAs produce highest strains (200 – 380 % in area in experiments, 20 % - commercially viable) and pressures (7.2 MPa). They are also known for the highest energy densities (> 0, 75 J/g) [37, 34] and efficiency (90%).

Overall, fabrication of *DEAs* requires low-cost, lightweight and conformable materials making them an excellent choice for actuators [37] and energy-harvesters [207]. Nevertheless, *DEAs* require high electric fields ($150 \text{ MV}/m$) and, consequently, voltages up to 5 kV , therefore their applications in medicine, biosciences and other fields that require contact with humans is very limited [249, 269].

Carbon nanotubes

Carbon materials can also be used as the electric field driven actuators. Thin, low density *CNTs* sheets can be produced from the *MWCNTs* forests and are capable of fast expansion in thickness (more than 200 % with a rate of $3.7 * 10^4 \text{ \%}/s$) making them faster than piezoelectrics. Nevertheless, as other electrically driven actuations, high voltages ($> 1 \text{ kV}$) are required limiting their applications [7].

1.1.4 Ion-based actuation

When actuation is required in vicinity of the human beings, in medicine or biosciences, it is essential to have low-voltage devices. The ion-based actuation relies on the mass transport of ions within the polymer and their uneven distribution that subsequently causes the volume or shape change. In this way, mechanical stress or strain of several percent can be produced with only $1 - 3 \text{ V}$. Several types of ionic *EAPs* are being investigated for applications as artificial muscles: ionic gels [252], ionic polymer-metal composites (*IPMCs*) [162, 374], conducting polymer actuators (*CPAs*) [24] and, more recently, carbon nanomaterial based composites [23, 204].

Ionic gels

Active hydrogels are three-dimensional polymer networks in which voids are filled with water. They can undergo a volume change as a response to an environmental stimulus and already have various applications [91] in biotechnology and medicine [25, 38]. As an emerging artificial muscles, ionic gels could potentially match the force and the energy density of a skeletal muscle at low voltages. In active ion gels, the reversible volume or shape change is a response to a chemical reaction, *e.g.* *pH* oscillations [125, 252], diffusion of a reactive substrate into the gel [212]. Because the flow of the solvent into the gel matrix is a diffusion controlled process, the response time of ionic gel is limited to several seconds. Nevertheless, fast gels could be made of thin films at a cost of a force⁴ [284]. In order to make the active gels more practical, the speed of their stimuli responsiveness and weak mechanical properties need to be improved [22, 151]. Furthermore, the robust electroding techniques need to be developed, that would not damage gel surface, *e.g.* the use of silver nanowires [2].

Ionic polymer-metal composites

Ionic polymer-metal composites (*IPMCs*) are made of a semipermeable polymer membrane sandwiched between metal electrodes. Semipermeable membranes are usually the ion-conducting polyelectrolytes, having a backbone chain of perfluorinated alkane terminated with ionic groups (*e.g.* SO_3^- for Nafion®, COO^- for Flemion®). These ion

⁴ The response time depends on the surface area to volume ratio while the force is proportional to the volume of the gel.

groups form hydrophilic cluster networks, where the solvent and the mobile counterions accumulate. Once an electric field is applied, cations along with the solvent move towards one of the electrodes, cause swelling and fast bending motion (more sophisticated actuation mechanisms are reported by [144, 240, 286, 287]). Factors influencing the electrochemomechanical response of the actuators, such as (1) the chemical composition and structure of the polymer [162, 189], (2) the morphology of the electrodes [374], (3) the nature of the mobile ions [29, 189, 288], (4) the solvent saturation [199] *etc.* are rather well understood and are extensively reviewed [80, 188, 336]. Due to the low actuation voltage and relatively large bending, *IPMCs* have potential applications in the underwater robotics (*e.g.* grippers [109], swimming devices [53, 185, 300]) and medicine (*e.g.* microgrippers [103], steerable catheters [324]).

One of their drawbacks is a back-relaxation - the actuation is followed by a slow relaxation due to the water diffusion out from the cation-rich area. In addition, *IPMCs* are sensitive to dehydration, hydrolysis above 1.23 V and tend to drift in the position or get permanently deformed when the direct current is applied. Furthermore, the lifetime of *IPMCs* is rather limited [313], primarily because of:

- Gradual water evaporation during cycling [196, 303]. The evaporation of water in air could be avoided if ionic liquids are used as electrolytes [29] but at a cost of the response speed and strain. Alternatively, devices could be encapsulated in *e.g.* parylene [192, 223], polydimethylsiloxane (*PDMS*) [382], other materials [4, 19]. Nevertheless, as a consequence of encapsulation, actuator stiffness increases and leads to a decrease of the deflection amplitude.
- Poor adhesion of metal electrodes to the membrane. In order to ensure sufficient adhesion between the membrane and the electroplated metals⁵, expensive and time consuming surface roughening techniques are required [43, 191]. Therefore, alternative adhesion improvement methods, *e.g.* polymer coating [41, 187], nano-powder casting [66] are being suggested.
- Damage of the electrode surface [303, 404]. In order to decrease the electrode cracking and degradation during bending cycles [41, 301] development of fabrication techniques, *e.g.* introducing novel electrodes [138, 186], is necessary.

Conducting polymers

Replacing metal electrodes with less rigid and brittle materials could solve several *IPMCs* limitations. Using conducting polymers (*CPs*) as electrodes is one of the alternatives. First of all, *CPs* provide electrical conductivity and ensure *IPMCs*-like behaviour. Secondly, the charge induced during the oxidation or reduction of the polymer is compensated by the ion ingress and egress. That subsequently causes a volume change of the polymer that is considered to be the primary factor leading to the actuation. The main advantages of *CPAs* are low voltage required for actuation and their biocompatibility making them the most promising candidates for applications in medicine and implantable devices. Furthermore, compared to their weight, they are able to induce a relatively large force and only small currents⁶ are needed to hold constant strain at DC

⁵ Metal salt reduction on the surface of the polymer.

⁶ Charge is dissipated because of the discharge through the electrolyte or electrochemical reactions.

voltage [154, 345]. On the other hand, fatigue, deterioration under cycling and slow response ($< 40 \text{ Hz}$) still needs to be improved. Conducting polymer actuators, their fabrication techniques and applications will be further discussed in *Chapter 4*.

Carbon nanotubes

The most recent ionic actuator type is based on carbon nanotubes (*CNTs*) and their composites suspended in the electrolytes [23] or ionic liquids (*ILs*) [18]. When the voltage is applied ($1 - 4 \text{ V}$), the *CNTs* surface is charged and electrolytes form an electric double layer around them. The electrostatic repulsion of the charges on the nanotubes causes the elongation of the carbon-carbon bonds, that consequently elongates the nanotube [23]. Due to their stiffness, networks of entangled nanotubes or yarns are needed to cause macroscopic deformations and even then, strain smaller than 1% are achievable [23]. On the other hand, due to the porosity and fast ion diffusion the strain rate of the *CNTs* actuators can reach $19 \text{ \%}/\text{s}$ ($< 10 \text{ ms}$ response time) [248]. Furthermore, their high elastic modulus (640 GPa) leads to huge work densities of $10^8 \text{ J}/\text{m}^3$.

Discovery of the 'bucky gel'⁷ [115] was followed by their applications as actuators [114]. 'Bucky gel' actuators have similar to the *IPMC* trilayer structure: the polymer impregnated with the ionic liquid in between two electrodes. Nevertheless, the motion is caused by the *CNTs* charging and subsequently the ion transport within and to the gel. The main advantages of the 'bucky-gel' actuators are their facile fabrication (layer-by-layer casting) and fast actuation times (respond to up to 100 Hz). Nevertheless, just as *CNTs* actuators, they are difficult and expensive to mass produce [217, 224, 383]. As a cheaper alternative, carbon black and carbon fiber mixtures with *ILs* are being investigated [371].

Composite materials

IPMCs suffer from the disadvantages caused by the rigidity of the electrodes, the conductive polymers are limited by their relatively low conductivity and the slow response and carbon nanotube actuators are expensive and energy inefficient. Therefore, there is growing interest in composite material electrodes that would combine advantages and reduce disadvantages of each type, e.g. carbon - conducting polymer composites [379, 362], *CNTs* mixtures with nanoparticles [370].

1.1.5 Other or combined actuation mechanisms

One of the limitations of *DEAs* is the low produced actuation pressure. In order to achieve stiffer actuated shapes, materials that combine properties of shape-memory polymers and dielectric elastomers can be used. Such materials are called bistable electroactive polymers (*BSEPs*), e.g. thermoplastic poly(*tert*-butyl acrylate) (*PTBA*) suggested by [409]. Bistable electroactive polymers are rigid at ambient temperature (below their glass transition temperature (T_g)) and can be actuated electrically as *DEAs* above T_g . Once cooled, actuated shape becomes and remains rigid with or without the electric field and until heated again. More rigid shape can support higher mechanical

⁷ Single walled carbon nanotube and ionic liquid gel-like composite.

loads at large strains. New *BSEPs* with better elasticity, transition temperature window and stability at high strains are being investigated [290, 321].

The multilayer structure of ionic polymer actuators that enables the bending deformation due to the expansion or contraction of one of the layers, can also be used for the electrothermal actuators. In this case, having significantly different thermal expansion coefficients and excellent adhesion are needed. One of the reported examples of such actuators are *PDMS* deposited on a large-area conducting *CNTs* paper [226]. Due to the two magnitude higher thermal expansion coefficient of *PDMS*, once the bilayer is electrically heated it bends towards the electrode. With the relatively low currents (hundreds of *mA*) and temperatures (40 – 120°C) high strains are achieved (bending angles of 200°).

Similarly, the hygroscopic nature of conducting polymers can be exploited [292, 294, 364]. In this case, the actuation could be controlled by (1) varying environments humidity, because of the absorption and desorption of the water vapour, or (2) electric field as water is being expelled from the polymer films due to Joule heating. Linear and rotor actuators using folded polypyrrole (*PPy*) films [294] and bending actuators of poly(3,4-ethylenedioxythiophene) polystyrene sulfonate (*PEDOT:PSS*) on *PDMS* [364] were so far reported.

Just as Faradic or non-Faradic charging causes conductive polymer expansion or contraction, nanoporous metallic materials were also shown to be able to produce a voltage induced reversible strain [398]. Nanoporous platinum [398], gold [33, 86], silver [87], their alloys [160] and nanohoneycomb nickel [56] produce strain larger than 0.1% with voltages lower than 1 *V*. During actuation, change of the surface properties⁸ of porous metal network causes volume expansion that is proportional to the surface-to-volume ratio. Nanoporous metals are stiffer and stronger compared to the polymer artificial muscles, and produce 10 times higher strain than conventional piezoelectrics with 1000 times lower voltage.

Recently, 'Onion artificial muscles' were reported [48], that could be considered a combination of the pneumatic *PneuNets* and the electric actuations. Micro-actuators that can both elongate and bend were produced by depositing gold electrodes on the acid-treated onion epidermal cell monolayer. The electrostatic forces deform cells ('inflate' or 'deflate') and due to stiff walls between them, cell actuator bends or elongates depending on applied voltage.

1.2 Applications of EAP based actuators

For now, the fastest approaching application of the electroactive polymer based actuators are electronic devices haptic feedback, Braille displays, headphones etc. Nevertheless, their lightweight and the low power consumption are also advantageous for actuation

⁸ In case of Pt and Au, the strain results from the double-layer charging, that consequently leads to the redistribution of the surface atoms and change of the interatomic distances (similar to *CNTs* actuators) [159]. On the other hand, the strain in the nanohoneycomb nickel is most likely induced by the difference of a lattice structure of the charged redox reaction products [56].

in space, robotics and medical devices. The choice of the type of the actuator needs to be made based on the specificity of the application.

Actuators in space

The need to reduce the mass and the power consumption of space travel vehicles is evident. Furthermore, space is a challenging environment, that requires materials that are stable at extreme temperatures, pressure, radiation, *etc.* Prevalent actuation technologies are based on piezoceramics or on hydraulic, pneumatic and electromagnetic devices and are failing to match these requirements. They could be possibly replaced by electroactive polymers. *EAPs* actuators are being investigated for performing or assisting tasks such as deployment of solar panels or antennae, haptics and telerobotics, walking or sliding robots *etc.*

Piezoelectric polymer based actuators are closest to the applications in spacecrafts for *e.g.* the control of orientation of surface mirror [77]. Nevertheless, mechanical amplification of displacement is still required and other artificial muscles are considered. One of the option is dielectric elastomer based artificial muscles, that were already investigated for control of large and lightweight mirrors [206] and as deployable microsatellite grippers [12]. Finally, ionic electroactive polymer based actuators have been tested for long term performance in space conditions. They were shown to be able to perform when irradiated or at low temperatures (if ionic liquids are used as electrolyte) [312] but their realisation as devices are still in an embryonic state.

Actuators in robotics

Due to their low power density, efficiency and power-to-mass ratio, traditional actuators are one of the key elements limiting the creation of dynamic micro-robots. Depending on the type of locomotion, strain, force and power requirement, artificial muscles of different types can be used: *DEAs* for walking [305], *IPMCs* and *CPAs* for swimming [55, 259] and crawling [280], piezoelectric ceramics for flying [245], *etc.* Large scale robots require large strain and force capabilities and good static and dynamic response. Each technology is being investigated and many actuators were presented to meet these needs (as discussed previously). Nevertheless only few of them can be implemented with a reasonable amount of control action [190, 269, 377]. One example is *DEAs*, that can be antagonistically configured for linear actuation and were implemented in inchworm microrobots as well as for multi-degrees of freedom motors [190, 65, 253].

The produced strain and force are the main limitations of *EAP* actuators for locomotion. On the other hand, their application as grippers are closer to realisation. Prototype conformable grippers based on *DEAs* were shown to be able to lift up weights 60 times heavier than their own weight [12, 338]. Unfortunately, the nonlinearity and time-variant dynamics of *DEAs* require advanced control algorithms, limiting their applications. Due to bending motion of ionic *EAPs*, micro-grippers are one of their main applications and prototype devices are being continuously reported [155, 179, 244]. In the case of ionic actuators, large time constants, unknown systems dynamics and positional drifts are main control challenges, but closed-loop [102] and feedforward [163] control strategies were suggested. The closed-loop control usually requires laser displacement or other sensors that are bulky and troublesome to implement. The

environment dependent behaviour [313] is challenging for feedforward controllers. Therefore possibilities of self-sensing actuators is one of the main current research axis [208].

Active smart textiles

Textiles could be considered smart if they consist of basic elements for sensing, activation and programming capability. The conducting polymers and carbon nanotubes can be easily integrated into the textile fabrics for creating electrically active areas. These areas would then allow change of textile structure depending on the stimuli [354]. Conventional polymer based actuators require electrolyte and produce the bending motion that complicates their integration in wearable textiles. As an alternative, thermoresponsive polymers and their yarns (discussed previously) were shown to be easily woven into the textile. The incorporated actuators could provide the exoskeleton functionality that would complement the biological muscles or could change the textile structure providing adaptive mass and heat transfer [134, 233].

Biomedical applications

Just as in the space, actuators used for biomedical devices have particular requirements, *i.e.* biocompatibility, compactness, accurate positioning, reasonable speed and strength [345]. Devices such as artificial sphincters, *i.e.* for treating the urinary incontinence, [20, 397], microsurgical instruments, especially for non-invasive surgery [271], implants for *e.g.* restoration of the facial movements [216] or blood vessel binders [150], catheters [218, 324] and endoscopes [405] are needed and have been suggested. Even though still in the early development state, conducting polymer based actuators are most promising for these applications. Their advantages include biocompatibility and biodegradability, relatively large strain and positioning at intermediate states, low required voltages, facile microfabrication, mechanical properties *etc.* Furthermore, their drawbacks limiting their applications in other areas, *i.e.* slow speed, dependence on electrolyte and creep are not critical for biomedical applications (less than 1 Hz actuation rate is satisfactory, large loads causing creep are not present and devices are usually required in liquid environment) [345].

In addition to mentioned applications, actuators could also be used in biosciences as cell manipulators [153] and mechanostimulators for controlling their growth, proliferation and differentiation [123, 363]. They can also be used to study the effect of mechanical stress on cells [3, 11]. Finally, the performance of conducting polymer based actuators was also investigated in cerebral physiological conditions for potential applications in guiding and positioning neural probes [76]. Despite the enormous potential, the efficiency needs to be significantly improved ($CPAs < 1\%$) in order to realise any of these devices.

1.3 Motivation and Problem Statement

The goal of this thesis is to develop ionic electroactive polymer based actuators, that could be used for applications in robotics. For this purpose fast, robust and up-scalable

fabrication technology is needed. Furthermore, for most of the applications, closed-loop control of the actuators is necessary that require sensory feed-back. Prevalent sensors, *i.e.* laser displacement, are bulky and hardly integrative, demanding alternative solutions. Inkjet printing is a key technology in the field of defined polymer deposition [120] and one of the most promising for production of soft electroactive polymer based actuators. Furthermore, it could also be used to fabricate and integrate strain sensors [8, 40, 69, 330, 325]. Nevertheless, there are several challenges limiting potential of inkjet printing: (1) solubility of conductive polymers and the availability of inks; (2) viscosity and surface tension of polymer solutions and jetting stabilization; (3) adhesion between ion-storing membrane and conductive polymer film; (4) diffusion of the ink through the pores of the membrane. These challenges are mostly related to the chemical nature of both, the conducting polymer solution and the ion storing membrane. Conducting polymer solution needs to fulfil requirements as printable ink, *e.g.* rheological properties, as well as an active layer of the actuators, *e.g.* good electrical and ionic conductivity, mechanical flexibility, ageing resistance. The membrane needs to provide volume for ion-storing as well as good ionic conductivity, excellent adhesion to conductive polymer and electrically insulating layer between two electrodes. In this work, we discuss these challenges in more details and suggest solutions, leading to the possibility to have first ever reported inkjet printed ionic conductive polymer based actuators.

1.4 Thesis Structure

Chapter 2

In a following chapter, we present hybrid ion-storing membranes, that have both upper surfaces hydrophilic and hydrophobic bulk. Hybrid membranes were developed in order to achieve good adhesion strength between the membrane and the electrodes while retaining electrically insulating layer in between. We start this chapter with an overview on the state-of-art of *PVDF* surface functionalization and plasma induced grafting of membranes. Then we introduce our fabrication method and finally, the characterisation of hybrid *PVDF/PVDF-graft-PEGMA* membranes.

Chapter 3

In *Chapter 3* we discuss in more details mechanisms of adhesion between two polymer materials and a special case when good adhesion needs to be ensured between the membrane and the solvent casted polymer. Theoretical background of adhesion between polymers will be followed by a discussion concerning joining *PEDOT:PSS* and *PVDF* in a context of producing conducting polymer based actuators. In this case, interface must not only be strong and stable once actuators are put into the ionic liquid, it also must be able to sustain large strain of several percent during the long lifetime.

Chapter 4

Further on, we will use previously discussed materials for fabrication of conducting polymer based actuators by drop-casting. This simple technique allows fast fabrication of devices with various geometries and compositions that can be used for better

understanding the working mechanisms of *PEDOT:PSS*, *PVDF* and ionic liquid based actuators. Even though these materials were used before, most of the publications were dealing with fabrication alternatives and fundamental understanding of working principles were rarely discussed. We will discuss performance of our devices in a context of known *PEDOT:PSS/PVDF* as well as state-of-the-art polypyrrole actuators. Finally, since efficiency of conducting polymer based actuators is rather low compared to other soft actuators [249, 269, 326], several ideas to improve the performance will also be discussed. We will introduce the preliminary results of post-treatment of *PEDOT:PSS* electrodes with surfactants, and carbon nanotube carpets.

Chapter 5

Finally, having hybrid *PVDF* membranes that ensure good adhesion between the membrane and the polymer, gives way to considering alternative fabrication techniques. One of them is ink-jet printing. After a short discussion on the challenges regarding printing conducting polymers on porous substrate, we demonstrate first ink-jet printed actuators, with strong interface. Potential of inkjet printing and possibilities of how to improve the process will also be discussed.

Chapter 6

Even if we were able to improve actuators performance to generate strain of up to 0.6%, performance of *PEDOT:PSS* actuators is still behind most of the state-of-the-art electropolymerized devices. Together with overview of the main achievements done during the time of this thesis, we will discuss the possibilities to further improve the process.

Hybrid PVDF/PVDF-graft-PEGMA membranes

Contents

2.1	Introduction	14
2.1.1	Functionalization of polyvinylidene fluoride (<i>PVDF</i>) membranes	14
2.1.2	Polymer functionalization by gas plasma	17
2.2	Surface modification during irradiation: PVDF-graft-PEGMA by Ar plasma	20
2.2.1	Influence of plasma parameters	21
2.2.2	Limiting grafting depth	23
2.2.3	Controlling grafting depth	27
2.3	Conclusion	31
2.3.1	Future work	33

A good insulating layer between two electrodes in conducting polymer actuators (*CPAs*) have to satisfy several requirements. First of all, it needs to provide sufficient softness and flexibility in order to obtain strains of several percent. This could be achieved by using very thin materials or membranes. Membranes are more advantageous especially because they can store electrolyte and therefore, actuators can be operated in air. In this case, a large available free volume is needed as well as a chemical stability and a good ionic conductivity. When the conducting polymer is synthesized electrochemically, the membrane should also provide the initial conducting layer. Finally, a good adhesion between the insulating layer and the conducting polymer is crucial for actuator lifetime.

The most widely used insulator for *CPAs* so far is probably *PVDF* ultrafiltration membranes. They are commercially available and have excellent mechanical properties and chemical resistance. In order to provide a conducting substrate, metal deposition or chemical synthesis are often used (*Section 4.2.1*), and a good adhesion is ensured by the interfacial layer created during the electropolymerization. Nevertheless, if the poly(3,4-ethylenedioxythiophene) polystyrene sulfonate (*PEDOT:PSS*) solution is used for the fabrication by solvent-casting, *PEDOT:PSS* and *PVDF* do not adhere. This leads to a partial separation of layers while handling and a complete delamination once actuator is immersed in a liquid (discussed in more details in *Chapter 3*). Therefore mainly hydrophilic membranes, *i.e.* polyurethane [295], cellulose [193] filled with ionic liquid were used. Hydrophilicity of the membranes ensures a good adhesion with *PEDOT:PSS* while ionic liquid blocks the pores preventing infiltration and occasional

connections between the electrodes. Nevertheless, the fabrication of such actuators is done one-by-one and is hardly up-scalable.

One of the possible properties causing the poor adhesion between *PEDOT:PSS* and *PVDF* is the chemical nature of materials: the hydrophobicity of *PVDF* and the hydrophilicity of the aqueous *PEDOT:PSS* solution. The contact angle between these materials is larger than 130° . Nevertheless, if hydrophilic *PVDF* is being used, *PEDOT:PSS* is immediately absorbed and in case where a trilayer configuration is needed - causes partial connections between the two electrodes. Therefore, the improvement of the adhesion is needed but the hydrophilic membranes cannot be used. Ikushima *et al* solved this issue by ultraviolet (*UV*) induced poly(ethylene glycol) methyl ether methacrylate (*PEGMA*) grafting on the surface of the *PVDF* membrane [148]. Inspired by their approach, we have developed technique for the partial functionalization of the membranes. Thus, hybrid membranes, that have hydrophilic pores to a certain depth are created.

In this chapter we shortly introduce the various available methods used to improve the *PVDF* membrane wettability, *i.e.* the plasma induced grafting. We also discuss in more details mechanisms of plasma diffusion, the interaction with the porous substrate and known factors that influence the morphology of the grafted polymers. Later we suggest a grafting-to method that allows functionalization of the membrane to a certain depth.

2.1 Introduction

PVDF membranes are not only used for the fabrication of *CPAs*, they are also often chosen for filtration, distillation, separation *etc.* They are preferred due to their mechanical strength, their good chemical resistance, thermal stability and ageing resistance. Nevertheless, their hydrophobicity causes wetting problems, that subsequently leads to a poor adhesion and fouling. Therefore, various surface functionalization methods are suggested in order to improve the hydrophilicity of membranes (recently reviewed by [175, 238, 319]).

2.1.1 Functionalization of *PVDF* membranes

Hydrophilic *PVDF* membranes can be obtained in three ways: (1) during the preparation of the membrane by blending; (2) by covalent and (3) non-covalent surface modification of existing membranes.

PVDF is not compatible with most of the hydrophilic polymers and direct blending is hard to achieve. Therefore, rather complicated synthesis methods are often needed [32, 39, 225, 318, 412]. Poly(vinylpyrrolidone) (*PVP*), polyethylene glycol (*PEG*) and poly(methyl methacrylate) (*PMMA*) are the most common hydrophilic polymers used for blending, but amphiphilic¹ block-copolymers, containing hydrophobic and hydrophilic parts are emerging as an alternative [358]. During the phase separation these kinds of additives arrange themselves so that the hydrophilic polymer chains

¹ having an affinity for two different types of environments

are exposed to the pore surface, while the hydrophobic part is entangled in the bulk. In a similar way, the incorporation of nanoparticles was also reported to improve the hydrophilicity of the membrane [272]. Unfortunately, successful blending methods do not only require rather complicated synthesis procedure, they also modify the bulk of the membrane, potentially altering their mechanical and thermal properties.

Alternatively, there exist several methods for the modification of already made *PVDF* membranes. One of them is a non-covalent coating, *i.e.* physisorption on the membrane surface with hydrophilic polymers or other molecules. Various oily liquids, amphiphiles and surfactants have a low water contact angle (*WCA*) with hydrophobic surfaces. They readily adsorb and flow through the pores of the membranes. This property is also used industrially for oil/water separation [424] or lubrication [222]. Nevertheless, the mechanisms of the process are still debatable [130, 353] and will be shortly discussed in *Chapter 3.4*. One of the drawbacks of the surface coating with amphiphilic molecules, is the instability of the layer (it can be easily washed away). In order to stabilize it, post-deposition treatments, *i.e.* cross-linking, polymerization, are needed (reviewed by Kang *et al*) [175]. In addition to the lack of long-term stability, the functionalization by adsorption also leads to the decrease of the membrane pore size, the water flux and even the pore clogging. Using them for soft actuators, could have a negative impact on the ionic conductivity and could decrease the free-volume available for ion-storing.

Finally, *PVDF* can also be functionalized by covalent modification. In this case only the surface of the membrane is modified, the bulk physical properties of the polymer are preserved and the pore size is rather unaltered. Furthermore, the functionalization is permanent and more stable than physisorption.

Covalent functionalisation of *PVDF* membranes

UV, O_3/O_2 , electron beam, plasma and other high energy irradiation is necessary in order to activate the *PVDF* surface. That usually leads to the defluorination, dehydrogenation or cleavage in the backbone of the *PVDF* and, subsequently, to the generation of radicals. Therefore, polymers with active moieties can be 'grafted-to' or 'grafted-from' *PVDF* backbone. The initiated radicals are relatively stable and the reaction precursor does not necessarily need to be in contact with the surface during the activation, *i.e.* the chemical reaction could be performed several minutes (or even hours) after the activation. The 'grafting-to' method, when the previously synthesized polymer is grafted on the surface, leads to the graft-polymer with a well known structure. Nevertheless, due to the low reactivity², the grafting density and homogeneity are hard to control. The 'grafting-from' method, where the monomer is grafted and the synthesis of the polymer follows, allows easier control of the grafting density and the length of the graft-polymer. Nevertheless, an insufficient control could lead to formation of long chains of the polymer that could reduce or even clog the pores.

PVDF is resistant to *UV* irradiation and a photo-initiator, *e.g.* benzophenon or its derivatives, is usually required. Radicals from the benzophenon are transferred to *PVDF* by dehydrogenation reaction as shown in *Fig. 2.1a* (more sophisticated mechanisms

² access of the functional groups might be hindered by polymer itself

reviewed by [84]). That is followed by a surface-initiated free radical graft copolymerisation of *e.g.* acrylate functional group [31, 317]. Photo-induced functionalization was shown to significantly increase the hydrophilicity of *PVDF* membrane surface (from 130° to 66°) and improve its antifouling properties [31, 148, 317].

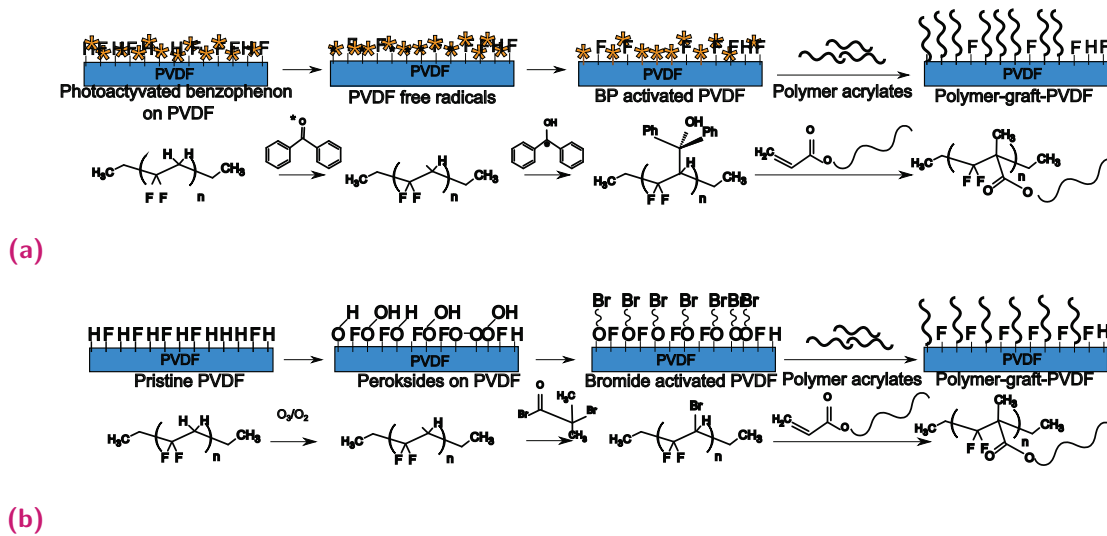


Fig. 2.1. Scheme and example of the grafting-to reaction of acrylate to *PVDF* membrane by (a) *UV* irradiation and (b) atom transfer radical polymerisation

Another way to activate *PVDF* membrane is irradiation with high energy electron beam [67]. During the γ -irradiation more stable main chain carbon-carbon or carbon-fluorine bonds are cleaved allowing post-activation grafting. Since monomers are not exposed to radiation, less branched graft polymers can be achieved. Furthermore, *UV* activation that may require several hours to achieve homogeneous grafting and γ -irradiation decreases surface contact angle to 0° in less than 30 seconds [78]. Nevertheless, that fast reaction might be difficult to control, and in case of 'grafting-from' method, leads to fast pore clogging. Furthermore, high energy irradiation does not only affects the bulk of the membrane. The polymer mobility at the crystalline-amorphous interphase regions is increased by chain-scissions that could degrade *PVDF* mechanical properties [238].

Plasma activation is an efficient way to activate *PVDF*. Due to its lower reactivity, the effect is also limited to only the surface of the polymer. Depending on the plasma power, active gas, distance, pressure and other parameters, surface dehydrogenation, defluorination and dehydrofluorination reactions may occur [304]. Oxidation reactions can also take place, when the oxygen plasma is used or when the activated surface is exposed to the ambient environment. Plasma on its own decreases water contact angle of the *PVDF* membranes, but it can also be used for the surface initiated grafting. A more detailed discussion on the plasma induced grafting is provided in Section 2.1.2.

Finally, the atom transfer radical polymerisation (*ATRP*), also called the 'living' polymerisation expands the choice of the monomers that are capable of the reaction. The reaction can be easily induced thermally after O_3/O_2 treatment [45, 46] or by using bromination [46]. More recently, methods involving activators generated by electron

transfer (*AGET*) were also shown to improve hydrophilicity [262]. A simplified reaction scheme for *ATRP* is shown in *Fig. 2.1b*. Even though grafting weight by *ATRP* is limited, *PEGMA* grafted on *PVDF* was shown to decrease water contact angle to 60° and leads to uniform and smooth surface coverage [46].

2.1.2 Polymer functionalization by gas plasma

'Cold' gas plasma³ is a partially ionised gas, consisting of reactive species such as electrons, ions, radicals, photons and passive gas molecules. It is a fast and possibly a solvent-free process, that allows functionalization of the surface without affecting the mechanical properties of the bulk. RF gas plasma⁴ can affect and modify polymer surface in different ways by: (1) plasma-enhanced chemical vapour deposition; (2) plasma etching and (3) surface activation and functionalization of polymers.

Plasma induced polymerization

Plasma-enhanced chemical vapour deposition refers to the excitation of an organic monomer gas (usually hydrocarbon CH_4 , S_2H_6 , C_2F_4 etc.), subsequent deposition and polymerization of it on the substrate (simplified scheme of the processes during plasma polymerisation is shown in *Fig. 2.2a* and are more explicitly reviewed by [211, 265, 266]). It usually creates amorphous, exceptionally branched and cross-linked polymer films with no obvious repeat unit. Due to the easy control over plasma parameters plasma polymerization can be used to synthesize very thin films (10 – 1000 Å) on various substrates of complex shapes. Nevertheless, plasma polymerization competes with polymer ablation and etching. Therefore, similar polymerization process can also occur after fragments and molecules are removed from the surface by heavy ion bombardment. Activated molecules could then be redeposited and reincorporated in the polymer surface. Plasma ablation is largely polymer dependent and is unlikely when *PVDF* is used.

Plasma etching of polymers

Plasma etching is often used in order to remove material from the surface. It is usually characterised by etching rate, anisotropy⁵ and selectivity⁶. The etching rate depends on: (1) plasma discharge parameters, e.g. type of gas, gas flow rate, plasma power, pressure, time (2) polymer chemical and physical properties. Depending on these parameters, surface could be etched by (1) chemical reactions, (2) ion bombardment and sputtering of the substrate and (3) *UV* irradiation and generation of free radicals, polymer backbone cleavage and subsequent reactions when exposed to oxygen.

Due to the reaction of atomic oxygen with the polymer surface, oxygen plasma is one of the most reactive etchants. Usually etching is initiated by the abstraction of hydrogens

³ Non equilibrium plasma, where ions and neutral molecules are at lower temperature (room temperature) than electrons. 'Hot' or equilibrium plasma - fully ionised and in thermal equilibrium as all reactive species are at the same temperature (usually 4000 K to 20000 K) is less practical.

⁴ Several plasma generation methods exists, i.e. direct current (*DC*), low-frequency (corona), microwave (*GHz* range) discharges, but for laboratory purposed and polymer treatment radio-frequency (*RF*) discharge plasma is most common.

⁵ $A = 1 - a_l/a_v$, where a_l and a_v are lateral and vertical etch rates respectively

⁶ $S = a_1/a_2$, where a_1 and a_2 are etch rates of two different materials

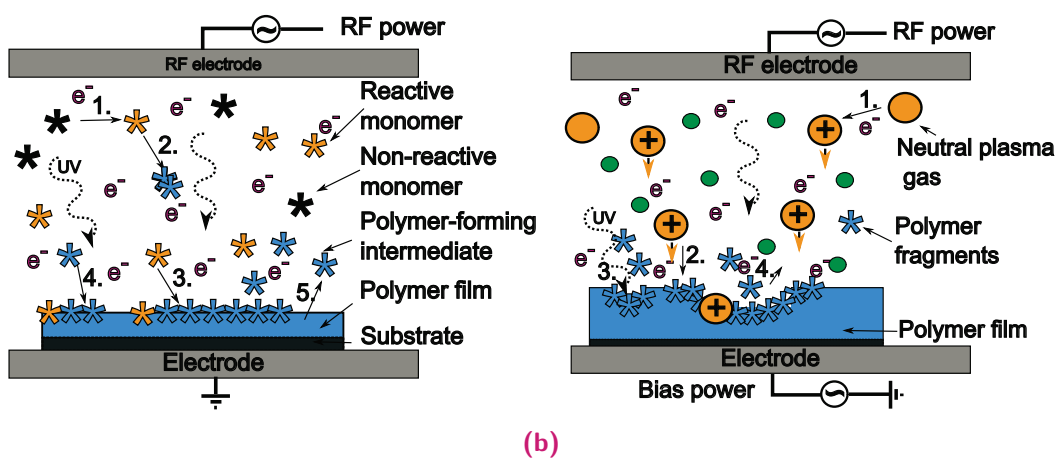


Fig. 2.2. (a) Scheme of the processes during plasma induced polymerization: (1) Monomer activation with reactive plasma species; (2) plasma state polymerization forming polymer-forming intermediates; (3) reactive monomer polymerization on the substrate; (4) polymerization of the polymer-forming intermediates on the surface; (5) ablation. (b) Scheme of the processes during plasma etching: (1) Activation of plasma gas creating cations; (2) damage of the polymer backbone by an impact with accelerated heavy ions; (3) generation of radicals on the polymer caused by *UV* irradiation; (3) ablation of the volatile impact products.

creating radicals or unsaturated moieties. These can subsequently be functionalized by molecular oxygen creating peroxides and weakening C–C bonds. Depending on the polymer, autoxidation can lead to chain scission and removal of the volatile etching products. Other gas plasma (especially Ar) has significantly smaller chemical etching rates, but can damage the polymer surface by sputtering. Usually ion bombardment is a slow process and its rate can be increased by the biasing of the electrode where the substrate is. A simplified scheme of the etching process is shown in *Fig. 2.2b*.

The change of the plasma parameters can significantly alter the etching rate. Type of used gas is one important factor and ions could be ranked as $\text{Ar} < \text{CF}_4 < \text{CO}_2 < \text{air} < \text{O}_2$, where Ar is the least reactive and O_2 the most. Increasing the density of the plasma reactive species or their speed (power, temperature and bias) also accelerates etching but usually, the properties of the polymer are playing the major role. For example, polymers containing no oxygen and no halogen (other than fluorine) are the most resistant to etching and aromatic side groups could further increase the resistance [367]. Semi-crystalline polymers are more resistant to etching than amorphous ones, as diffusion of reaction particles into a polymer is impeded. Thus, high power (200 W) and bias (20 W) as well as mixtures of reactive gas (40% CF_4 and 60% O_2) are required to successfully etch polymers such as *PVDF* [158, 267]

Surface activation and functionalization of polymers

Plasma is also an efficient way to introduce the reactive chemical groups to the otherwise non-reactive polymeric surfaces. The activated surfaces can then be used for increasing adhesion between polymers, their wettability and for further chemical reactions *e.g.* in order to improve the biocompatibility and immobilization of biomolecules. Amine, carboxy, hydroxy and aldehyde groups can be anchored by reactive gas plasma, *i.e.* oxygen, ammonia, carbon dioxide, hydrogen and nitrogen mixture, alkyl alcohol,

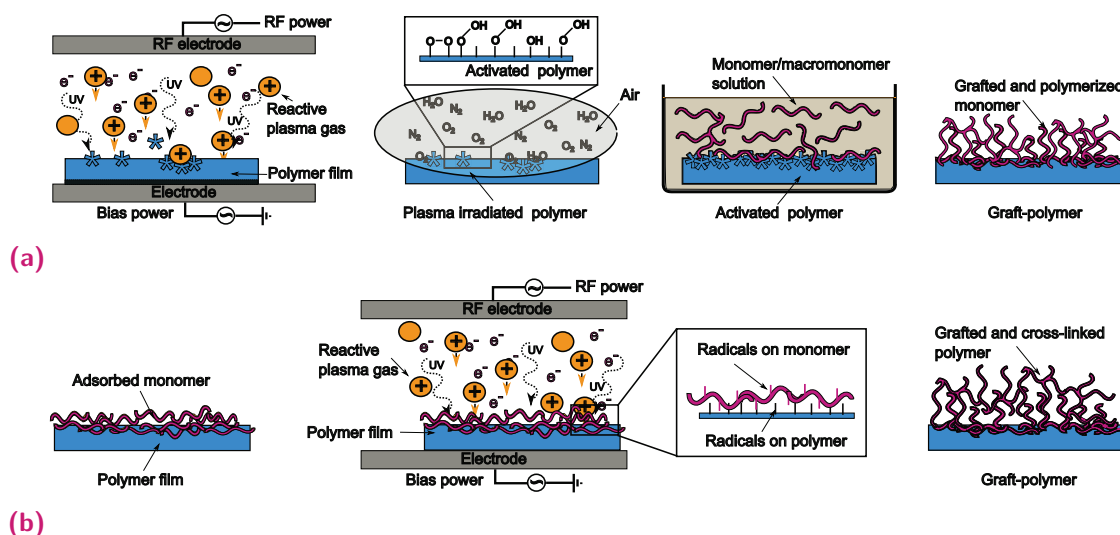


Fig. 2.3. (a) (1) Generation of radicals on the surface of the polymer film by plasma irradiation; (2) activation of the polymer surface with oxygen moieties during the exposure to the air; (3) incubation of the activated polymer in the solution containing polymer-to-be-grafted monomer or macromonomer. (b) (1) Immobilization of the monomer or macromonomer on the surface of the substrate; (2) activation of both: the polymer surface and monomer precursor by plasma creating radicals on both; (3) simultaneous reaction between active species: anchoring of the reaction precursor to the substrate and cross-polymerization.

acrylic acid *etc* (reviewed by [291, 341]). In a special case, when very hydrophobic surfaces are needed, fluorine plasma can be used to form fluorinated groups [70, 220]. Unfortunately, due to oxidation and recombination reactions, most of the activated surfaces have relatively short life-time, therefore their application or subsequent covalent reactions should follow immediately.

In addition to possible reactions with plasma reactive species, radicals generated on the surface could cause cleavage of polymer chains. This could influence their mechanical properties if chain mobility is increased or cross-linking of the polymer increases its molecular weight [132]. Nevertheless, surface radicals can also be used for subsequent chemical reactions, similarly to γ -irradiation [45, 64, 177, 420] or molecules-to-be-grafted can be deposited on the surface and anchored during irradiation [44, 46, 390]. In both cases, monomers can be used as reaction precursors for induced polymerization [64, 177, 420] or already synthesized polymers with functional groups can be grafted [44, 45]. Simplified reaction mechanisms for post-irradiation grafting and functionalization during irradiation are depicted in *Fig. 2.3a* and *2.3b* respectively.

During irradiation, radicals can be produced on both, the polymer-to-be-grafted and the substrate, leading to the competing reactions of: (1) the substrate and the polymer, (2) cross-linking of polymers and (3) cross-linking of the substrate [390]. Depending on the plasma conditions various structures, such as brush-like or network-like, can be obtained [44]. Furthermore, the grafting weight can be controlled by irradiation time, plasma power and amount of the precursor. Nevertheless, etching and degradation

compete with the polymerization after longer grafting times [30, 390]. Finally, plasma irradiation creates very thin functionalized layers (in order of 7.5 nm) that do not change the porosity of the membrane and do not affect their mechanical and thermal properties [46, 390]. Etching is less likely if post-irradiation grafting is used and both monomers [420] and macromonomers [45, 177] can be polymerized. In this way much thicker grafting layers are achieved, that could lead to the complete surface coverage and, if porous materials are used, significant decrease in the pore size [45, 177].

Surface grafting is a powerful technique in order to increase surface wettability (to 20° in less than 100 s) and biocompatibility, that is essential for microfiltration [44, 45, 64, 177, 420] and other applications in medicine and biotechnology [58, 108, 126, 408]. Furthermore, it was also shown to be promising in enhancing adhesion between polymers [148, 366] and can be used in order to improve the adhesion between *PEDOT:PSS* and *PVDF*.

2.2 Surface modification during irradiation: PVDF-graft-PEGMA by Ar plasma

Surface modifications of *PVDF* and other fluoropolymers have been studied by many researchers. Like for other polymers, defluorination and oxidation reactions are most common and treatment in N₂, O₂, H₂ and Ar plasmas increases its hydrophilicity. Nevertheless, fluoropolymers seem to be more resistant to oxygen plasma (dehydrogenation rather than defluorination is dominant) and are heavily damaged only by argon [94, 304, 384]. Therefore in order to realize grafting during or after irradiation, Ar plasma is usually used. Due to the experimental work-flow, post-irradiation grafting leads to an increased asymmetry of the membranes. The surface of the membrane that is being exposed to the plasma is usually more active and is subsequently more densely covered [64, 177, 420]. Furthermore, the control of the plasma activation in the pores of the materials is difficult and often the functionalization of all the membrane pores cannot be avoided. Finally, for our applications very thin grafting layers are needed, so that porosity of the membranes and their ion-storage volume remain maximum. Therefore, grafting during irradiation, was considered to be a more suitable method.

Due to its availability and versatility *PEG* is often used as a grafting polymer, especially when hydrophilicity and biocompatibility need to be improved. *PEG* functionalized with methacrylate at the end is more reactive and can be grafted on *PVDF* membrane by various means, e.g. *ATRP* [45, 46], *UV* activation [31, 317], plasma [44, 46]. The chemical structure of both, *PVDF* and *PEGMA*, as well as their reaction product is shown in Fig. 2.4a. The Fourier transform infrared spectroscopy (*FT-IR*) spectra (Fig. 2.4b-2.4c) show the change in their *IR* signatures during the covalent reaction. It can be used for characterization of the surface coverage after functionalization (detailed method is provided in Section A.2). Small shift from 1727 cm⁻¹ to 1715 cm⁻¹ for conjugated *OCO* stretching vibration of methacrylate group and *OCO* in esters respectively is the main signature of the covalent reaction. If compared to only *PVDF* membrane, *CH* stretch at 2900 cm⁻¹ appears, that shows presence of alkyl *CH* vibrations from *PEGMA* backbone.

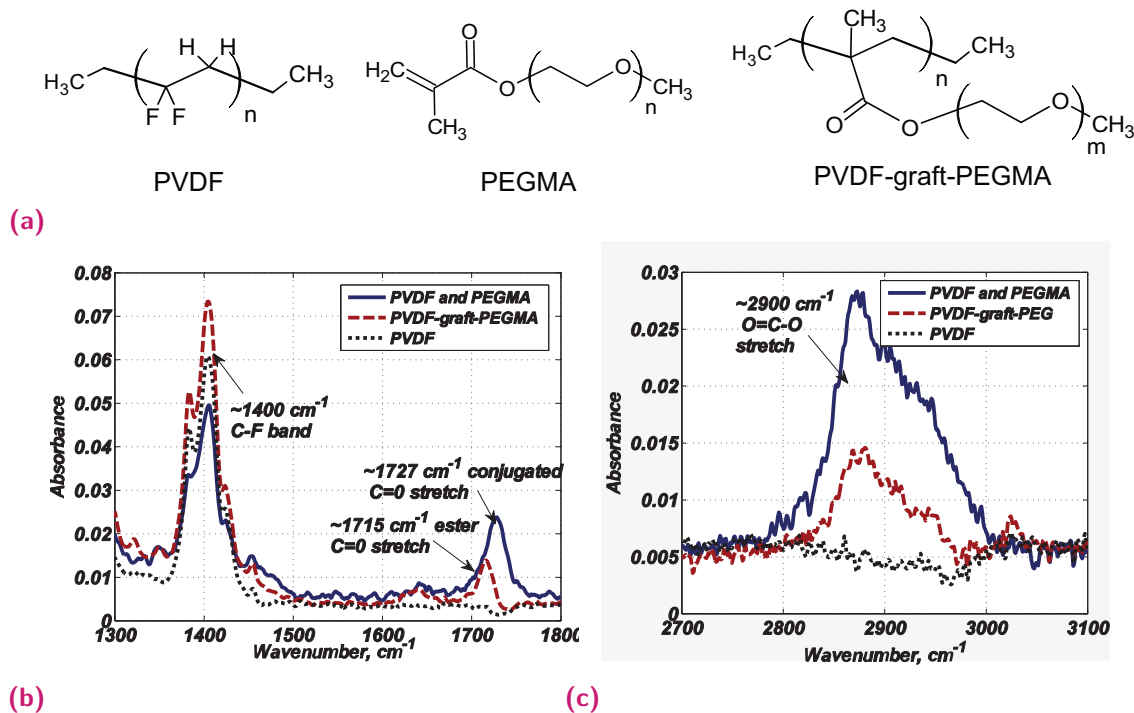


Fig. 2.4. (a) Chemical structure of PVDF, PEGMA and PVDF-graft-PEGMA and their IR signatures between (b) $1300 - 1800\text{ cm}^{-1}$ and (c) $2700 - 3100\text{ cm}^{-1}$

For the characterization of the grafting density and the surface coverage, the ratio of the integrated areas of the peak around 1400 cm^{-1} signifying CF bond and OCO ester stretch will be used (the range used for integration is shown in Fig. 2.5b).

2.2.1 Influence of plasma parameters

The grafting of a hydrophilic polymer by direct irradiation was first realized by Wang *et al* [390]. They immobilized PEG ($M_n - 1000$) by dipping PVDF membranes (porosity of $0.65\ \mu m$) in its solution for 5 minutes and irradiated dried membranes with low-pressure Ar plasma ($100\ Pa$ pressure, gas flow rate of $20\ sccm$). They showed that radio frequency (RF) power higher than $15\ W$ and for duration longer than $60\ s$ causes etching and degradation of the PVDF membrane. We observed the same tendency for larger grafting times, as mass-loss was observed for minutes long irradiations. Therefore, only the grafting performed at low power ($10\ W$) and short times up to $30\ s$ (experimental details provided in Section A.2.1) will be further discussed. Fig. 2.5a shows that the surface coverage is smoothest after only 20 seconds. The significant increase in the roughness (from $188\ nm$ to $435\ nm$) is observed for the longer grafting times. Nevertheless, the increase in roughness due to the etching is unlikely. FT-IR measurements show increase in OCO–CF ratio (Fig. 2.5c) and after $30\ s$ grafting CF signal is nearly gone. This means a very dense surface coverage with PEGMA, that is thick enough to prevent IR wavelength from reaching PVDF. Therefore, increasing roughness could be an indication of the faster polymerization of PEGMA on the uppermost areas of the membrane.

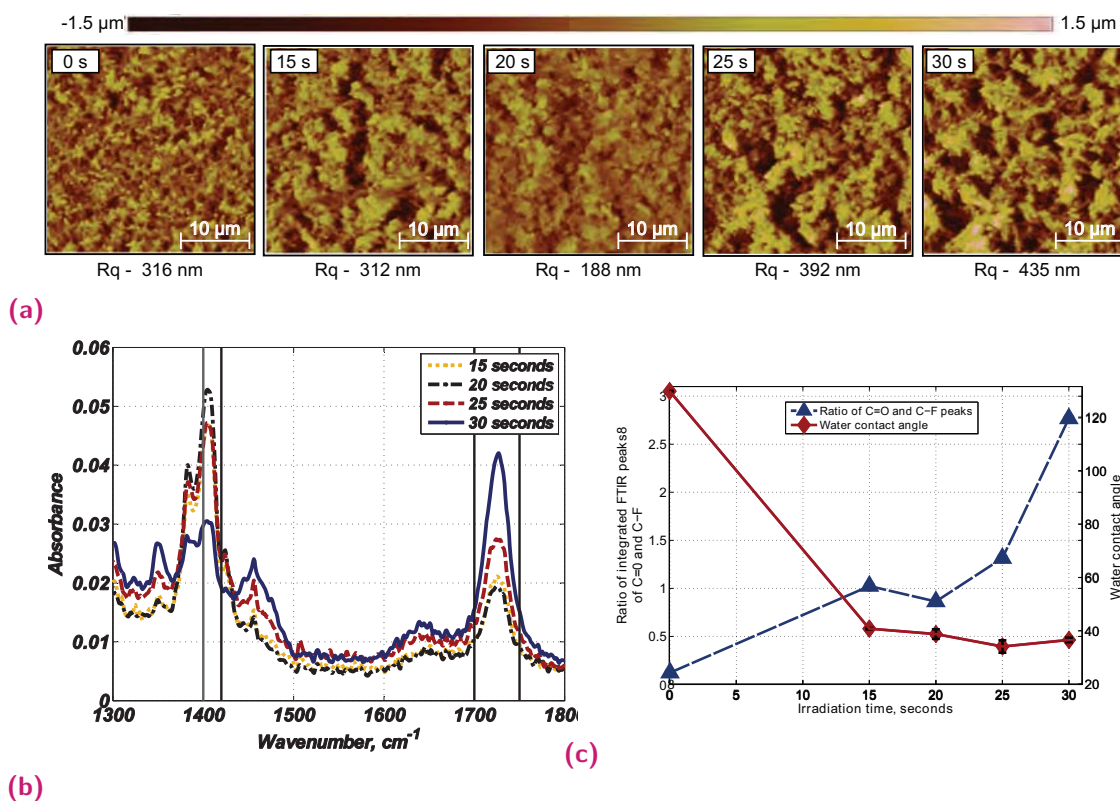


Fig. 2.5. (a) atomic force microscopy (AFM) surface scans of PVDF membranes after PEGMA grafting with different plasma irradiation times. Measured average roughness is indicated below. (b) FT-IR spectra of the same membranes and (c) Ratio of integrated OCO–CF FT-IR peaks (blue \triangle) and measured water contact angle (red \diamond)

Water contact angle dependence on the grafting time is also shown in Fig. 2.5c. In agreement with FT-IR results, even 15 seconds are sufficient to decrease WCA from 130 to 40°. The deviation of the measurement value is also very small throughout the membrane indicating homogeneous coverage. Moreover, WCA does not change when increasing irradiation time, suggesting that hydrophilic coverage does not degrade and remains homogeneous.

One of the differences of our experiment in comparison to the previously published, is a lower plasma pressure (40 mTorr). It has two competing effects on polymerization and etching. At higher pressures more reactive plasma species are available, but it also increases the density of molecules, leading to smaller free path (λ^7), more collisions between molecules and less with the surface of the membrane. Therefore an optimal pressure exists, as was demonstrated by [64]. For a given free path, the diameter of the pores of the membrane will determine the transport mechanism of the plasma and therefore the activation depth. For example, in pores larger than 10 μm viscous flow occurs, meaning that gas collide with each other rather than with the membrane. Nevertheless, in our case the ultrafiltration membranes are used at low pressures and

⁷ average distance travelled between collisions, $\lambda = kT/(\pi d^2 P \sqrt{2})$, d - diameter of the molecule and P is the pressure

the free path of the molecule is much larger than the diameter of the pores⁸. Therefore, once exposed to plasma gas, membranes are permeated with gas in a fraction of a millisecond⁹ and collisions occur with mostly the membrane pores. Therefore in most of the previously reported cases, even when atmospheric pressure plasma was used ($\lambda_{Ar} = 0.25 \mu m$ and pore size of $0.1 \mu m$ [44]), pores of the membrane were activated leading to grafting [44, 46, 64, 177, 390, 420].

Controversially, Choi *et al* reported that at 20 W Ar plasma power and at 5 Pa pressure, less than 30 μm of membrane thickness is being activated for membranes with $0.1 \mu m$ pore diameter. Our experiments show similar results. During plasma grafting at 40 mTorr, 5 W, for 15 – 30 s on $0.1 \mu m$ PVDF membranes with PEGMA immobilized by dipping, grafting was not detectable with FT-IR on the other side of the membrane (even though slight decrease in the water contact angle was observed from $130^\circ \pm 1.7$ to about $108.7^\circ \pm 7.4$). This indicates a partial penetration-through. Nevertheless, grafting at even lower powers (down to 1.6 W) or higher pressures (up to 60 mTorr) on both sides of the membrane leads to full functionalization showing that plasma penetrates to at least half of the membrane thickness¹⁰.

2.2.2 Limiting grafting depth

Once the aqueous solution of PEDOT:PSS is deposited on the hydrophilic membrane, it penetrates through it, creating connections between electrodes. Therefore, the hydrophilic membranes are not applicable for the fabrication of actuators. We concluded that controlling the activation depth of the membrane, by varying plasma parameters is not effective and two adjustments to the process were considered: (1) limiting the activation by plasma depth by blocking the pores of the membrane and (2) limiting the deposition of the precursor to a certain thickness (Fig. 2.6c).

Gas diffusion through liquids is at least 10000 times slower than in gases [72]. Therefore, if the pores of the membrane are filled with liquid, the permeability of the membrane will be determined mainly by the solubility of the gas in this liquid. At room temperature, PEGMA is a viscous liquid ($9 m^2 s^{-1}$). Just like PEG, it possesses some hydrophobic characters that lead to its fast adsorption on the surface and pores of hydrophobic membranes [152]. Therefore, once immersed in pure PEGMA, PVDF pores are completely filled with the liquid, and their interaction is sufficiently strong to form solid state composite¹¹. The filled membrane can be considered as a non-porous one. Therefore, during irradiation by plasma, reactive ion species will most likely be neutralised as soon as liquid phase is encountered leading to grafting on only the top surface of the membrane (Fig. 2.6b).

⁸ in our case, $\lambda_{Ar} = 1.2 mm$ and the pore size $0.1 \mu m$) leading to Knudsen flow, where mass flux per unit area depends only on the density gradient of the gas: $J = D_k \frac{\phi}{\tau} \frac{M_W}{RT} \frac{\Delta P}{\Delta L}$, where $D_k = 0.66r \sqrt{\frac{8RT}{\pi M_W}}$, $\frac{\phi}{\tau}$ are membrane obstruction factor where ϕ and τ are porosity and tortuosity and l its thickness, r - pore radius, M_W - molecular weight of the gases, Δp - pressure difference across the membrane

⁹ assuming initially empty cylindrical pores, gas flux is $0.21 kg m^{-2} s^{-1}$ and subsequently permeation time is $0.8 \mu s$

¹⁰ The penetration through the pores of the membrane was observed after PEDOT:PSS deposition. This can occur only if membrane is hydrophilic as will be discussed in Chapter 3.

¹¹ there is no significant liquid flow from the membrane in air

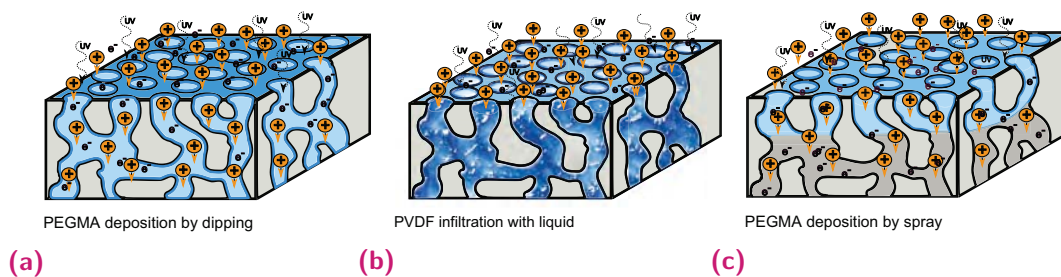


Fig. 2.6. Schemes showing three different precursor deposition strategies and subsequent plasma membrane interactions: (a) deposition by dipping in diluted solution leading to precursor adsorption on the surface of the membrane and subsequently activation and grafting by plasma throughout the thickness; (b) deposition by dipping in viscous liquid that prevents plasma gas diffusion and activation to the pores; (c) deposition by spraying that limits precursor deposition to a certain depth.

Alternatively, the functionalization will also be localized if the availability of the reaction precursor is limited (Fig. 2.6c). Due to its hydrophobic interaction with *PVDF*, *PEGMA* immediately adsorbs on its walls. Therefore, a method to deposit very small quantities of *PEGMA* is needed. One possibility is using compressed air spray coating [133]. The spray is produced when the compressed air stream is mixed with the solution. The ejected droplet size as well as their speed depends on many parameters (discussed later in Section 2.2.3), but optimised process leads to the deposition of small quantities of materials in nearly solvent-free state. Lateral surface diffusion rate for *PEG* on hydrophobic surface, depends on its molecular weight, adsorbed surface concentration, presence of solvent *etc.*, but in general, for concentrated thicker layers it is $< 0.5 \mu\text{m}^2\text{s}^{-1}$ and for monolayer $< 5.0 \mu\text{m}^2\text{s}^{-1}$ (for comparison, in solution $> 10 \mu\text{m}^2\text{s}^{-1}$) [418]. Theoretical studies of the nature of the polymer adsorption and surface kinetics is still a large challenge in the field [236], but we assume that once a small *PEGMA* droplet reaches the surface of the membrane, it is adsorbed, and only the presence of the residual solvent drives lateral diffusion [344].

As shown in Fig. 2.7 both methods, filling (dip) and spraying lead to the functionalization of the *PVDF* membranes. Dipping in diluted *PEGMA* solutions (as in Section 2.2.1 and shown in Fig. 2.6a) leads to grafting mass of about 3.4 ng/mm^2 after 15 s irradiation. In comparison, 'filled' and 'spray' functionalization lead to a significantly lower grafting, 0.12 ng/mm^2 and 0.08 ng/mm^2 respectively. Furthermore, during these experiments, samples were slightly biased (1 W) therefore grafting depth is not limited by plasma diffusion. The comparison of obtained results is shown in Fig. 2.7. In both cases the *WCA* successfully decreased to less than 40° and *OCO*–*CF* ratio increases to more than 0.6 showing successful functionalization and surface coverage. Interestingly, even though 'filled' membranes have a larger *OCO*–*CF* ratio, indicating better surface coverage, the water contact angle for sprayed membranes is significantly smaller: $32.1^\circ \pm 6.3$ and $< 10^\circ$ respectively. In fact, *WCA* of the membranes prepared by spraying, could not be precisely measured due to the fast spreading and adsorption of the droplet to the pores of the membrane. This already suggests possible differences in grafting depths.

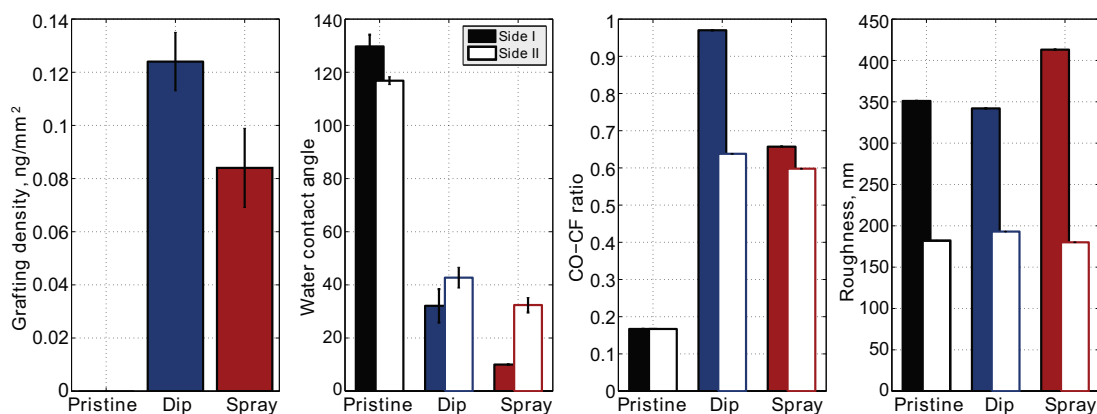


Fig. 2.7. Comparison of membranes prepared by filling the pores (dip) and spray coating (spray): (a) grafting density; (b) water contact angle; (c) integrated *FT-IR* OCO–CF ratio; (d) roughness of the membranes. Filled and empty bars indicate measurements on two sides of the membranes.

Another important aspect that is shown in *Fig. 2.7* is that there is a difference in the grafting for the two sides of the membrane. It could be caused by the initial asymmetry of the membranes that is a consequence of the fabrication by phase-inversion. The *AFM* images of both sides of the pristine *PVDF* membrane on two sides are shown in *Fig. 2.8*. The surface roughness is $333 \pm 24 \text{ nm}$ and $182 \pm 2 \text{ nm}$ respectively. First of all, the difference in the surface roughness can explain the variation in the *WCA*. For the pristine membranes, *WCA* is 130° and 110° for the rough and smooth side respectively. As described by Wenzel, rough and chemically hydrophobic surfaces are more hydrophobic and the rough hydrophilic surfaces are more hydrophilic [399]. Therefore, the *WCA* decreases more for the rough side of the membrane: from 130° to about 10° on the rough side and from 110° to about 30° for the smooth side (*Fig. 2.7*).

In comparison to the initial roughness difference, plasma does not significantly change it (*Fig. 2.8*). Especially the morphology of the smooth side of the membrane remains unchanged whatever the *PEGMA* deposition method is used. Nevertheless, the morphology changes due to *PEGMA* grafting are visible on the rough side. The large grafting mass (by dipping in diluted solution) leads to a visible surface coverage (*Fig. 2.5a*). Similarly, irradiation of the membrane with filled pores leads to a dense surface coverage (OCO–CF ratio 0.98) but also to a very homogeneous grafting ($R_q = 307 \text{ nm}$). While for the membranes with small amount of *PEGMA* sprayed, reaction tends to be localized on the higher parts of the membrane further increasing roughness of the surface to 372 nm .

Surface morphology, grafting mass and *FT-IR* results agree with the assumption that the active plasma species are being stopped by the liquid in the pores of *PVDF*. As it can penetrate only several angstroms, only the upper surface, to the depth of the order of its roughness (several micrometers) can be modified. Nevertheless, but due to the vast availability of the reaction precursor it leads to a very dense coverage (larger grafting mass and OCO–CF ratio). Furthermore, since the pores of the membrane are not modified, the *WCA* is higher than for membranes prepared by spraying *PEGMA* and does not lead to infiltration. During spray coating large amount of the precursor will be deposited on the uppermost part of the membrane. However, due to the velocity

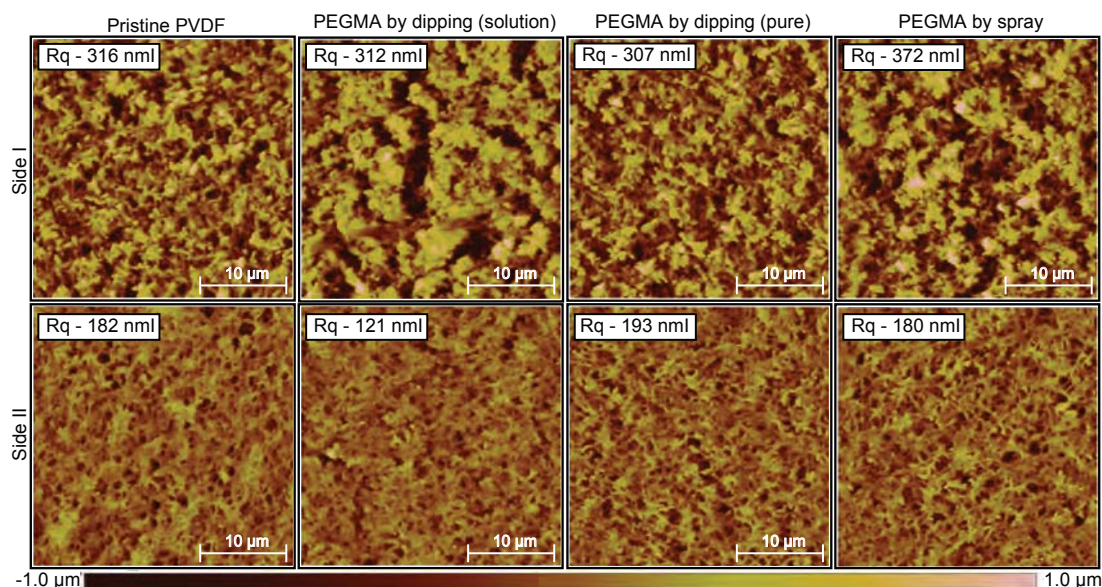


Fig. 2.8. AFM surface scans of the two sides of the pristine and functionalized membranes. *PEGMA* deposition method is indicated above.

of the droplets or the presence of the residual solvent, *PEGMA* might as well diffuse to a certain extent into the pores. Nevertheless, in comparison to 'filling', smaller amount will be available for grafting leading to less functionalization but, likely, in larger depth.

Grafting depth

In order to confirm these observations, *PEDOT:PSS* water solution was deposited by drop casting on both sides of the membrane (as in *Appendix A.4.1*). To estimate the reaction depth and the thickness of the hydrophilic *PVDF*, we used Energy-dispersive X-ray spectroscopy (*EDX*) sulphur scan of *PVDF/PEDOT:PSS* sandwich. We observed that hydrophilic *PVDF* membranes of the same porosity lead to diffusion of *PEDOT:PSS* (with 1 vol% poly(ethylene glycol) of $M_r=400$ (*PEG400*)) through the membrane but does not infiltrate into the hydrophobic *PVDF* membranes. Therefore we assume that *PEDOT:PSS* would penetrate into the *PVDF* membrane only down to the functionalization depth. *Fig. 2.9a-2.9b* show *EDX* line scans along the cross-section for sulphur (that is only present in *PEDOT:PSS*) and fluorine (only in *PVDF* membrane). The region where both signals are present (mixing depth (*MD*)), corresponds to the width of the grafting layer.

In both cases, the grafting depth was limited. Therefore the hybrid hydrophobic-hydrophilic *PVDF* membranes were made retaining the hydrophobic *PVDF* center of the membrane (along the cross-section at least 50 μm in the middle are hydrophobic (*Fig. 2.9a* and *2.9b*)). Nevertheless, the grafting profiles along the cross-section are very different. When the plasma diffusion is limited by filling the pores with a viscous liquid, fast and gradual decline of *PEDOT:PSS* in the *PVDF* membrane is observed. On the other hand, the spraying of the precursor leads to a step-like *PEDOT:PSS* penetration profile. In this case, we can assume that relatively dense functionalization of the pores up to 20 μm in depth is achieved and it leads to filling of pores with *PEDOT:PSS*. As can

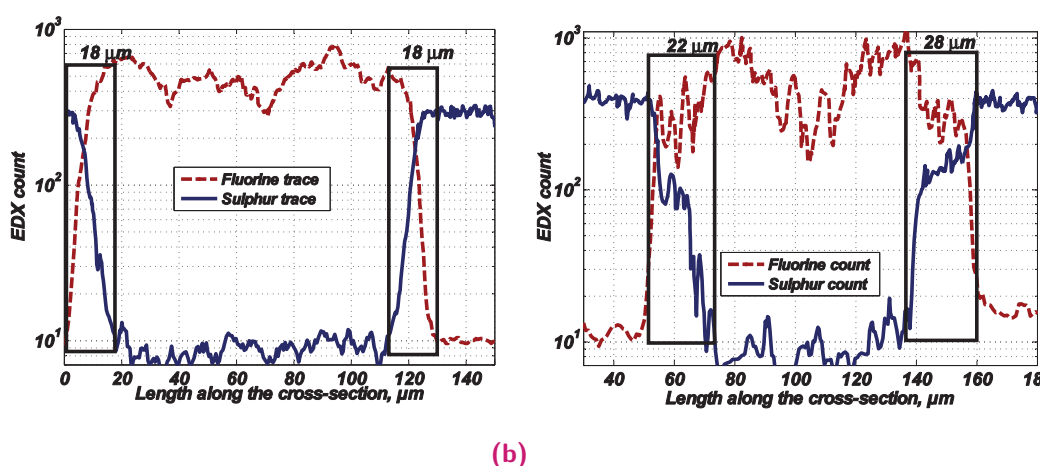


Fig. 2.9. EDX sulphur (blue) and fluorine (red) line scans across the cross-section of the PEDOT:PSS/PVDF-graft-PEGMA/PEDOT:PSS trilayers, where PEGMA was deposited on PVDF by (a) dipping and filling the pores, (b) spray coating.

be seen in Fig. 2.9b, for 20 μm on each side of the membrane, PEDOT:PSS EDX count is roughly 30% smaller than for PEDOT:PSS on the surface. It corresponds to 70% porosity of the membrane. Fast decline of sulphur amount follows to about 10, that is a noise level¹² of the measurement. On the other hand, it seems that only the surface was well activated and functionalized for the 'filled' membranes. Nevertheless, small amount of PEDOT:PSS can be detected for about 18 μm in depth and could be an indication of small plasma diffusion through the liquid or PEDOT:PSS infiltration through the pores of the hydrophobic membrane.

To sum up, both methods are suitable for limiting the depth of the plasma grafting by direct irradiation. Nevertheless, filling the pores with the grafting precursor leads to a very dense polymerization. That could consequently block the pores of the membrane on its surface and have a negative impact on the ionic conductivity of the electrolytes stored in the membrane. In addition, in this case, polymerization is sensitive to the preparation of the membrane. The excess of liquid on the surface (in our case, it was removed by placing membranes on filtration paper) could prevent irradiation of PVDF backbone, making the process hard to control. Finally, as a certain amount of precursor was infiltrating into the pores of the membrane, the control of the spray coating parameters could allow tuning of the mixing depth.

2.2.3 Controlling grafting depth

Spray coating

The spray coating process depends on many spray-gun parameters, e.g. the nozzle size, pressure, the chemical nature of the precursor and the solvent, the spraying environment and the substrate (experimental details are provided in Appendix A.2.1). Therefore spraying efficiency (SE)¹³ and homogeneity of the film are hardly predictable. If low boiling point solvent is used, such as ethanol, it evaporates on-flight before reaching the

¹² level of the fluorine trace outside the PVDF membrane

¹³ fraction of the mass of the precursor deposited to the mass of the precursor sprayed

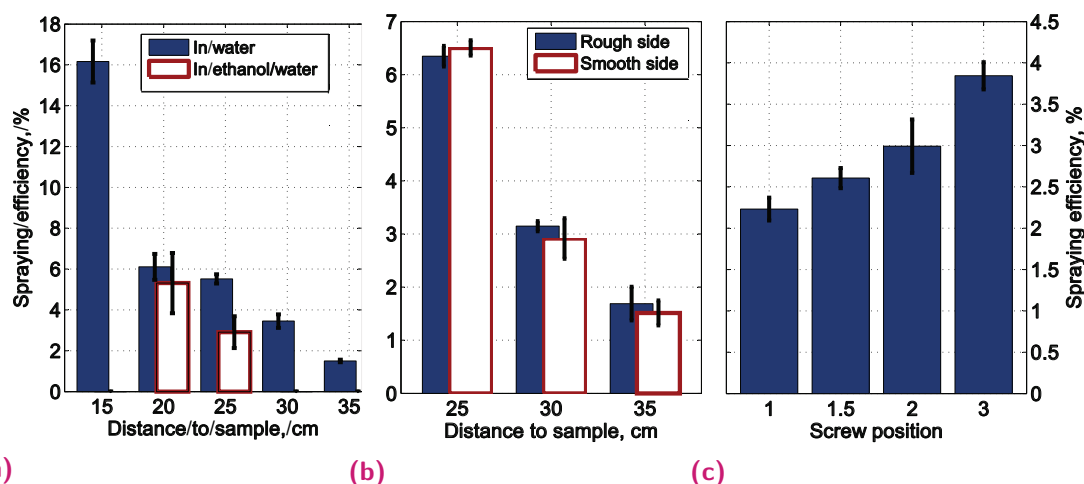


Fig. 2.10. Spray efficiency of *PEGMA* in ethanol/water solution on *PVDF* membranes with different spray parameters

substrate and completely dry precursor leads to the less homogeneous films[1]. It can be seen in *Fig. 2.10a*, that even in the 50% azeotropic ethanol and water mixture, the variation in *SE* is larger than when *PEGMA* aqueous solution is sprayed. Nevertheless, if water is used as a solvent, larger droplets are reaching the surface of membrane and large amounts of the residual solvent could cause *PEGMA* infiltration into the membrane.

The flight time determines the amount of residual solvent, therefore, the distance of the spray gun from the membrane is one of the key parameters determining the spraying efficiency (*Fig. 2.10a-2.10b*). Valve opening¹⁴ leads to the control of the size of the ejected droplet and the cone angle of the spray and is also affecting the amount of precursor deposited (*Fig. 2.10c*). Nevertheless, it also affects the spray time, therefore an optimum half turn position was maintained during further experiments. Air pressure determines the ejection speed of the droplet and is another key parameter. The velocity of the drop will subsequently determine its evaporation rate as well as an impact force (full optimization was not performed). Finally, the morphology of the surface on which *PEGMA* is sprayed might also affect the deposited mass as shown in *Fig. 2.10b*. It is likely that roughness influences the surface diffusion rate of *PEGMA* as smoother surfaces would lead to larger surface concentrations [62, 418, 419]. Nevertheless, observed differences are too small and within the measurement error and therefore will not be further considered.

In our case *PEGMA* solution in 10 vol% ethanol/water azeotropic mixture, $2\text{kgf}/\text{cm}^2$ pressure, half-turn valve opening, was used as it was shown to lead to the most homogeneous deposition. By changing the distance of the spray gun to the membrane from 35 cm to 20 cm (*i.e.* the size of the droplet that reaches the membrane is changed) large spectrum of spray and graft densities were obtained as shown in *Fig. 2.11*. Even small amounts of *PEGMA* sprayed (spraying density (*SD*) and grafting density (*GD*) indicated in the legend) lead to reaction on the surface and its full coverage as suggested

¹⁴ Defined as a screw position in number of quarter turns

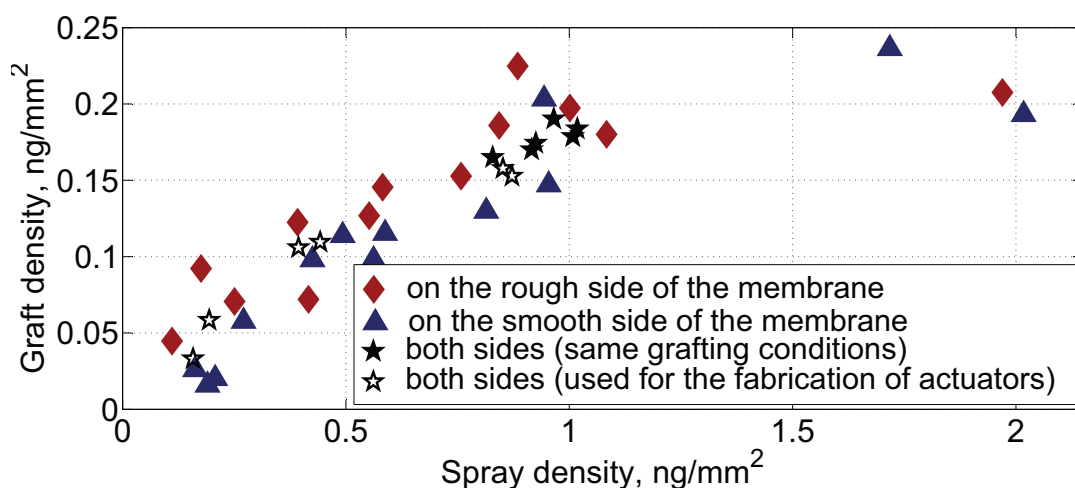


Fig. 2.11. Grafting density versus density of PEGMA sprayed on the rough (blue) and smooth side (red) at different conditions. Black stars - sprayed on both side and averaged.

by saturation of the OCO–CF ratio of the membranes grafted on the smooth side (Fig. 2.12a). As the roughness of the surface further increases for the grafting on the rough side (Fig. 2.12c and 2.13), larger OCO–CF ratio could be explained as a result of decreased accessibility of the membrane to infrared (IR) wavelength. Interestingly, large amounts of PEGMA deposited ($SD - 0.47 \text{ ng/mm}^2$) lead to relatively low grafting densities ($GD - 0.058 \text{ ng/mm}^2$). That is also an indication of the fast and dense surface coverage, that might prevent plasma from reaching the precursor in the pores.

Fig. 2.12b shows the WCA dependence on surface roughness and chemical composition. For pristine membranes, WCA is 130° and 110° for the smooth and rough side respectively. Surface roughness influences wetting in the sense that the WCA on the rough chemically hydrophobic surfaces is larger and WCA on the rough hydrophilic surfaces is even lower.[399] Therefore, the water contact angle decreases much faster to about 20° when the rough side is functionalized. Grafting on the smooth side leads to a decrease to about 40° . It is also worth noting that even though small grafting densities ($> 0.06 \text{ ng/mm}^2$ that correspond to SD of about 0.12 ng/mm^2 and OCO–CF ratio before saturation) lead to WCA lower than 100° , surface coverage is less homogeneous as suggested by high WCA measurement error. Therefore, for fabrication of membranes we suggest using a grafting density of at least 0.07 ng/mm^2 .

In summary, the surface roughness of the substrate seems to influence PEGMA grafting behaviour. When grafting on the rough side, slightly larger grafting efficiency can be expected as shown in Fig. 2.11. Our results suggest that reaction might be faster on the uppermost areas of the membrane, further increasing its roughness (Fig. 2.11 and B.1). Surface coverage seems to be more homogeneous (no significant roughness change) on the smooth side. Finally, surface area of the membrane (measured by Krypton adsorption and Brunauer–Emmett–Teller (BET) theory) does not change significantly with functionalization ($5.19 \pm 0.33 \text{ m}^2/\text{g}$ for pristine and functionalized membranes)

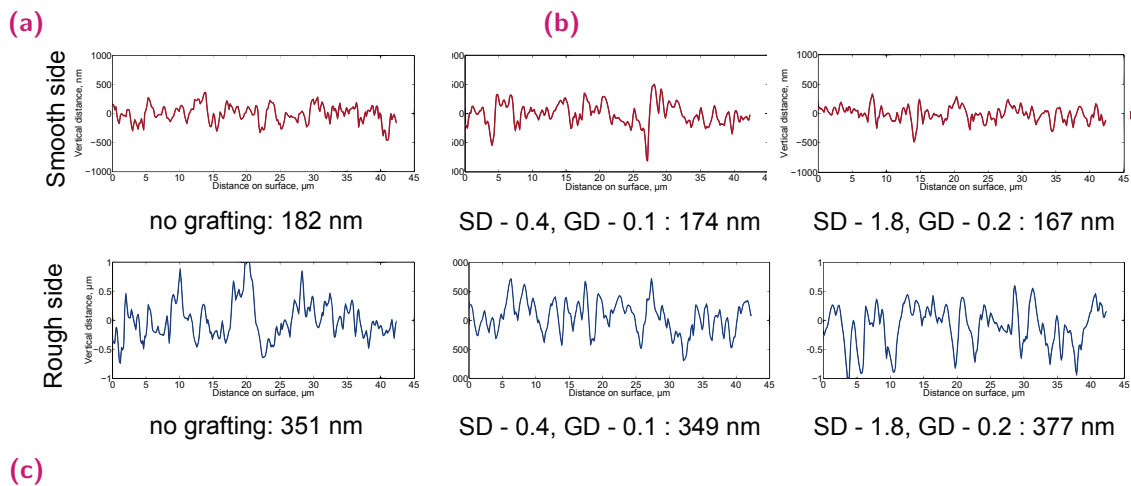
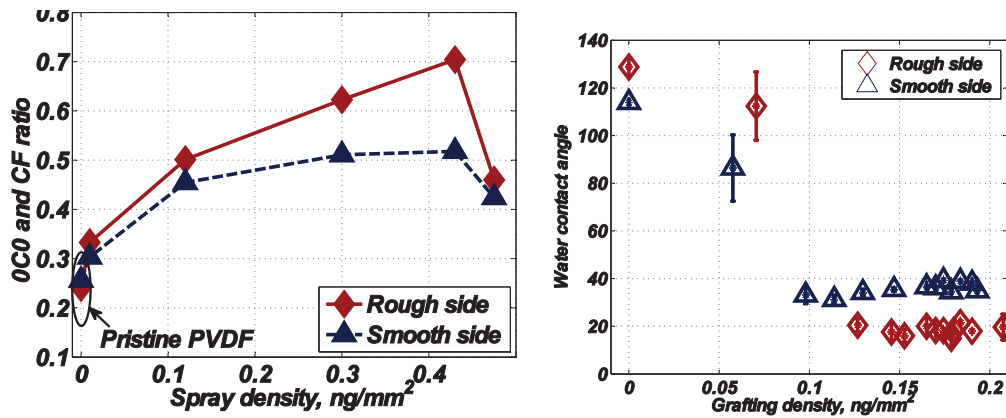


Fig. 2.12. (a) Ratio of integrated OCO and CF peaks of pristine (indicated with an arrow) and functionalized PVDF membranes versus sprayed amount of precursor (PEGMA) (blue \diamond - rough side, red \triangle - smooth side) and (b) Water contact angle of pristine PVDF (grafting density = 0 ng/mm²) and PVDF-graft-PEGMA membranes at different grafting densities. (c) Topographic AFM measurements of the cross-sectional profiles of membranes with different grafting densities for the two sides.

suggesting that except the upper surface of the membrane, reaction is mostly restricted to a very thin layer.

Grafting depth

Even though increasing *SD* and *GD* does not seem to significantly influence the morphology of the membrane (especially on the smooth side) nor the wettability, the grafting density is still slightly increasing above $> 0.07 \text{ ng/mm}^2$. *PEG* and *PEGMA* are good wetting agents and are immediately adsorbed on *PVDF* membrane. Compared to water, their aqueous solutions spread easier (*WCA* are $53.3 \pm 2.3^\circ$ and $39.3 \pm 2.8^\circ$ for 10 vol% solution on rough and smooth sides of *PVDF*) and are infiltrated in its pores. Therefore, if during spraying *PEGMA* reaches the surface with a small amount of residual solvent it is likely to diffuse to a certain depth. Since Ar plasma fills the pores of the membrane and is even further accelerated by biasing, the depth of the plasma induced graft polymerization will be influenced by spraying parameters.

Different grafting densities were obtained by varying the distance of the spray coater and the volume of the sprayed *PEGMA* solution. The functionalization depth, estimated by *EDX*, versus grafting density is shown in *Fig. 2.13*. The thickness of the grafting depth is increasing with *GD* up to about $30 \mu\text{m}$. However, at higher grafting densities ($> 0.16 \text{ ng/mm}^2$) it seems to reach the saturation level and after 0.18 ng/mm^2 even starts to decrease. This corroborates with our earlier assumption that due to a fast *PEGMA* polymerisation on the outer surface of the membrane, plasma diffusion deeper into *PVDF* pores is restricted. Furthermore, a small difference might be observed for the mixing depth on the rough and smooth sides of the membrane - on the smooth side, it saturates at a lower depth. This again agrees with our assumption of the influence of the coverage on plasma diffusion, *i.e.* a smoother surface means a smaller surface area and a higher actual grafting density for the same amount of *PEGMA*. Subsequently this could lead to a faster reduction of the pore size.

Based on these results we suggest that two mechanisms compete during Ar plasma induced graft polymerization: (1) plasma diffusion in *PVDF*, that results in a large grafting depth and thin *PVDF-graft-PEGMA* layers along the pores and (2) cross-polymerisation of *PEGMA* on the upper surface, that may cause a dense coverage and limit the plasma diffusion to smaller depths.

2.3 Conclusion

In summary, we demonstrated a technique for the fabrication of hybrid hydrophilic-hydrophobic-hydrophilic *PVDF* membranes using argon plasma induced surface functionalisation with *PEGMA*. We showed that the membrane functionalization could be limited by both: (1) blocking the pore accessibility to plasma by filling the pores with viscous liquid and (2) depositing the reaction precursor on only the surface. The later one can be achieved by the optimized deposition of the *PEGMA* aqueous solution. The simplified fabrication scheme is summarized in *Fig. 2.14*.

We also showed that even a small grafting density leads to a fast coverage of the upper surface and a significant decrease of the water contact angle from 130° to about 20° .

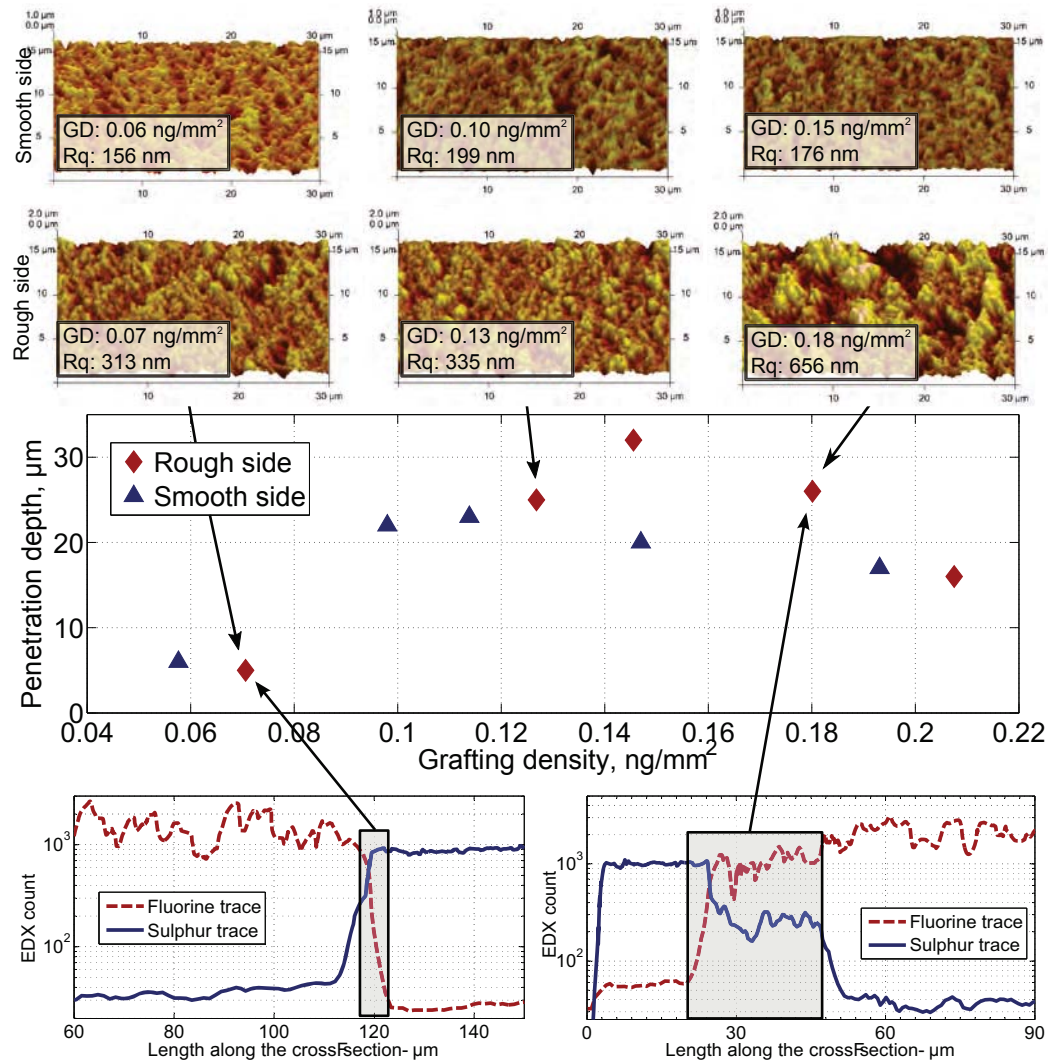


Fig. 2.13. (Bottom) EDX line scans for sulphur (blue full line) and fluorine (red dashed line) along the cross-sections of *PEDOT:PSS/PVDF-graft-PEGMA* with the *GD* indicated with the arrows. (Centre) The length of the depth of mixing versus the grafting density (*GD*) plotted separately for *PEDOT:PSS* deposited on the smooth side (blue \triangle) and the rough side (red \diamond) of *PVDF-graft-PEGMA*. (Top) AFM images of the rough and smooth surfaces of the *PVDF-graft-PEGMA* membranes with different grafting densities (*GD*). Grafting density and the roughness are indicated in the legends.

The grafting efficiency is slightly influenced by the morphology of the substrate as smoother surfaces lead to smaller grafting densities. This could be a consequence of a very fast reaction, leading to a fast polymerization on the surface that subsequently could block the membrane pores to plasma penetration. Finally, the deposition depth of the reaction precursor can be tuned by varying spray coating parameters. We show that by changing the spray gun distance or the volume of the precursor, hybrid PVDF membranes of various hydrophilic layer thicknesses (ranging from 5 μm to 40 μm) can be obtained.

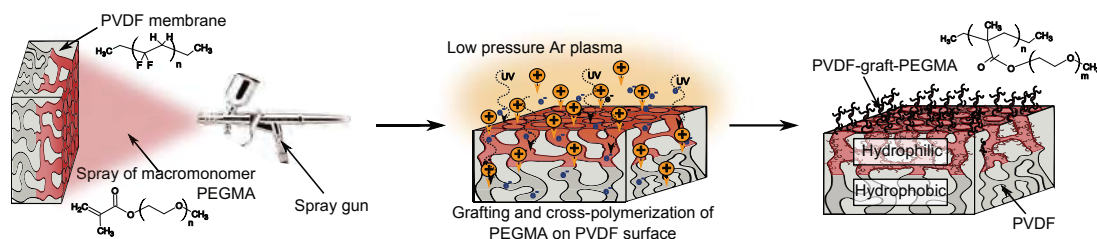


Fig. 2.14. Functionalization of PVDF membranes: deposition of reaction precursor (PEGMA) by spray coating only on the surface of the membrane and argon plasma induced grafting to PVDF backbone leading to hybrid hydrophilic-hydrophobic membranes.

2.3.1 Future work

- The exact mechanism explaining the impact of spray coating parameters on the deposition depth was not investigated. Due to complexity of both: spray coating and polymer diffusion in porous media, rather complicated models are needed. PEGMA could diffuse into the pores until mono-layer coverage is formed, as well as its amount could be gradually decreasing. In any case it leads to a sufficient decrease in the water contact angle that allows PEDOT:PSS infiltration in the pores, leading to a sharp interface.
- It is possible to obtain thicker interfaces, by changing spray coating parameters. A larger spraying distance, leads to significantly larger interfacial layers up to 60 μm in thickness (not discussed in the chapter). This is probably related to PEGMA diffusion phenomena during spray coating, that is difficult to predict and is worth further investigations.
- The polymerization kinetics is another challenging topic. Even though we observed competition between etching, degradation and polymerization at larger grafting times (from minutes to hours), neither etching nor polymerization rates were studied. As etching and degradation are slower processes, by decreasing the polymerization time these effects were minimized in our study. Nevertheless, 15 s is a short time for plasma process, leading to relatively unstable irradiation. This subsequently might cause irregularities between different batches. In our case, spray coating was most difficult to reproduce (due to the use of a basic spray-gun) and was causing largest deviations for the same conditions (as can be seen in Fig. 2.11: black diamonds represent the same spray coating conditions), but in case of an automated spray, increased plasma times might be necessary to assure reproducibility.

- The functionalization depth was measured by indirect method (*EDX*) and results might be influenced by diffusion of *PEDOT:PSS* and its composition (will be discussed in *Chapter 3*). Therefore more direct observations of chemical structure across the thickness, e.g. X-ray photoelectron spectroscopy (*XPS*) analysis, would be interesting in order to confirm our previous statements.
- Hybrid membranes were fabricated with potential application in conducting polymer actuators. Nevertheless, essential mechanical characterizations were not performed in order to ensure that grafting does not change mechanical properties. Even though plasma irradiation is usually limited to several angstroms and should not damage bulk *PVDF*, densely cross-linked *PEGMA* on its surface could restrict its flexibility. Furthermore, functionalization can also influence ionic conductivity of the membrane that has not been measured either.

PEDOT:PSS and PVDF membrane: adhesion versus infiltration

Contents

3.1	Introduction	36
3.1.1	Adhesion between polymers	37
3.1.2	Polymer adsorption on the surface out of solution	39
3.2	Adhesion between <i>PEDOT:PSS</i> and <i>PVDF</i>	40
3.2.1	Adhesion evaluation method	40
3.2.2	Adhesion between pristine <i>PVDF</i> and <i>PEDOT:PSS</i>	41
3.2.3	Effect of the infiltration on the poly(3,4-ethylenedioxythiophene) polystyrene sulfonate (<i>PEDOT:PSS</i>)-membrane adhesion	45
3.2.4	Effect of the polyvinylidene fluoride (<i>PVDF</i>) surface damage on adhesion	47
3.3	Adhesion between <i>PEDOT:PSS</i> and <i>PVDF-graft-PEGMA</i>	48
3.3.1	Influence of surface roughness	50
3.3.2	Influence of coating by physisorption	50
3.4	Comments on infiltration of <i>PEDOT:PSS</i>	53
3.5	Conclusion	56
3.5.1	Future work	56

The reliability of ionic polymer based actuators is one of the features limiting their use as devices. Not only are they hardly reproducible in identical manner [241], their performance is also largely influenced by the environment conditions, the degradation of the membrane and the electrodes, the evaporation or leakage of the electrolyte, the poor interface *etc.* As earlier works on ionic artificial muscles were mainly limited to actuation in liquid electrolyte, the influence of temperature and humidity had a minor role on actuation performance. Nevertheless, newer devices are being developed for applications in ambient environment and information regarding temperature and humidity conditions of testing is still missing. Only recently more detailed studies addressing this issue were reported [281, 313, 314, 388]. If actuators are operating in air, evaporation of the solvent is another challenge. A major breakthrough in the development of actuators was the discovery of ionic liquids used as an electrolyte. Ionic liquids prolong the lifetime of the actuators by several orders of magnitude but at the expense of decreased performances [29, 369]. Due to their larger electrochemical window, reactions degrading polymers are also less likely, further extending the lifetime of conducting polymer based actuators [29, 241].

Both, the influence of the environment and the solvent evaporation could be alternatively solved by the encapsulation of the device. Various coatings were tested for this purpose [192, 223, 382], but coatings increase the passive stiffness of the material and furthermore, add another layer in the device that often deteriorate due to delamination. Delamination of layers constituting an actuator is a common problem in ionic polymer-metal composites (*IPMCs*) [314]. Conducting polymer actuators can be made by electro-polymerization on the chemically synthesized substrate that creates an interfacial layer between the membrane and the electrode. Layers remain adhered for thousands of cycles, but adverse percolations between the electrodes are often created [104, 368, 369]. Alternatively, the actuators are electropolymerized on gold used as a substrate. Unfortunately, 50% of such actuators were shown to completely delaminate after less than 3000 cycles [241] and surface roughening methods are required to prevent it.

We developed hybrid *PVDF-graft-PEGMA* membranes in order to improve adhesion between the *PEDOT:PSS* electrodes and the *PVDF* membrane. Nevertheless, having similar chemical nature is not always sufficient to make two polymers adhere to each other. In this chapter we discuss interactions between polymer materials that influence their interface strength. As required for our application, we are mostly concerned with the special case when one of the materials is a polymer membrane and the other one is a solvent-casted polymer film. As infiltration to the membrane is also mostly dependent on the chemical nature of materials, the implications of these processes will also be shortly discussed. Finally, we suggest several rules that need to be followed in order to achieve a strong interface between *PEDOT:PSS* and *PVDF* and to avoid partial short circuits.

3.1 Introduction

Adhesion is a process of the attachment of a substance to the surface of the another substance. It can also be defined as a force that is required to separate two surfaces. The inter-atomic and intermolecular interactions causing adhesion cannot be explained with one unifying mechanism. Nevertheless, understanding it is of growing importance, especially for the applications in the automotive and aerospace industries as well as in the field of the biomedical engineering. Mechanisms that resist the separation of two solids were reviewed by Jon *et al* as follows [161].

- Van der Waals - the weak interactions between permanent or induced dipoles. They are rarely observed in the macroscopic solids as they require a large area of intimate contact.
- Covalent - stronger connections, but as for the physical van der Waals bonds, it requires the proximity and the reactivity of solids that is unlikely in macro-scale.
- Capillary bridge formed by the liquid in between can also be used to join two solids.

- Direct mechanical interlocking - the connection formed by inserting a screw in between two solids. Hook-and-loop, Velcro type of adhesives as well as pressure based adhesion when particular shape slides and gets locked in the gaps are also considered as a direct interlocking.
- Suction or vacuum gripping is an adhesion resulting from the pressure difference of a hermetically sealed volume with respect to the surroundings.
- Electrostatic adhesion is based on Coulomb attraction of opposite charges. It is limited to solids in which charges can be induced.
- Magnetic forces is another mechanism that is a characteristic of a material.
- (Inter)diffusion mechanism is possible between two polymers with the mobile backbone chains. It will be discussed in more details later in the chapter.

3.1.1 Adhesion between polymers

Rarely, a single mechanism plays role in the adhesion. Furthermore, only few of the mechanisms mentioned above are playing role in joining two polymers. The most important of them are: (1) covalent bonding (*Fig. 3.1a*), (2) thermodynamic interactions (*Fig. 3.1b*), (3) (inter)diffusion of polymer chains (*Fig. 3.1c*) and (4) mechanical interlocking (*Fig. 3.1d*). In our case, the later one does not only deal with the impact of roughness but is also important for explaining the adhesion in porous materials.

Chemical bonding

The formation of covalent bonds¹ (*Fig. 3.1a*) between two polymers could lead to a very strong adhesion. It requires the surface activation, that could be provided by plasma or chemical treatments as well as the intimate contact between two surfaces. For example, covalent bonding is often used in order to connect two polydimethylsiloxane (*PDMS*) films. Activated surfaces are being cross-linked by siloxane bonds (Si-O-Si) that lead to adhesion strength of up to 700 kPa [96]. Nevertheless there are several drawbacks of the chemical bonding. It needs a close contact and the activation that is usually unstable and therefore two materials need to be brought together immediately. Furthermore, the choice of the materials that could form bonds is also relatively limited. Finally, excessive chemical bonding could lead to a change in the mechanical properties of polymers that consequently decrease the adhesion strength [15].

Physisorption

Adhesion by van der Waals forces also requires a close contact with a gap of around 1 nm . Ensuring this proximity in macro-scale is difficult due to surface defects, cracks, dust, roughness, *etc.* Nevertheless, van der Waals forces are playing a key role in understanding adhesion between liquid and solids. It is also important for spontaneous adsorption from the solution as well as for ensuring wetting when one of the polymers is deposited in a liquid state. These circumstances will be further discussed later in the chapter.

¹ $153 - 614 \text{ kJmol}^{-1}$ for single or double bonds

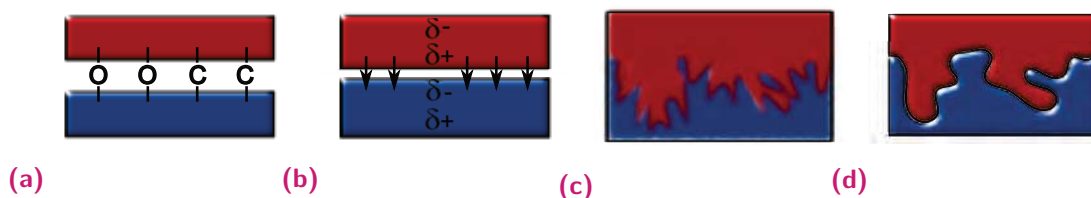


Fig. 3.1. Illustration of different mechanisms playing important role in the adhesion of two polymer solids: (a) formation of a covalent bond, (b) van der Waals interactions, (c) interdiffusion of the polymer chains during welding, (d) direct mechanical interlocking.

Interdiffusion of polymers

The second strongest interface that could be formed in between two polymers is their interdiffusion. When materials are pressed against each other in a melted state, the boundary between them could be removed *Fig. 3.1c*. For joining two polymer solids, the welding² is usually required and the miscibility and mobility of the polymers determine the diffusion rate. Unfortunately, most of the polymers are incompatible in nature and would display repulsive interactions, unless e.g. hydrogen bonding, reduces them. Even then diffusion requires solutions, melts, or temperatures above the polymer glass transition³.

Many studies linked the width of the interdiffusion with the mechanical strength of the interface [251, 68]. The width of the interdiffusion, determined by the mobility of the polymer chains, depends on their chain length, entanglement (degree of polymerization), side groups, *etc.* [71, 197, 251, 276]. Therefore, surface damage by plasma, as well as polymer chain scission and polymer grafted are often used as adhesion enhancers [71, 251, 276]. The interfacial entanglement was shown to be another important factor determining the adhesion strength [68, 122]. In both, the miscibility of the polymer is an essential requirement.

When immiscible polymers are joined, the interfacial tension leads to some interdiffusion, usually in order of up to 30 Å [166]. For comparison, entanglements in a polymer bulk are of the order of 90 Å. Therefore, low interdiffusion with small interfacial entanglements leads to low interfacial fracture energy⁴ (about 20 Jm^{-2}) and the interface fails through chain pullout [122].

Substantially larger interdiffusion widths and entanglements can be achieved for the miscible polymers. They are proportional to the fourth root of contact time therefore the annealing time is an important parameter determining interface strength. Depending on the polymers used, the formed interface could exceed the mechanical strength of the polymer itself. Therefore, tensile failure could be caused by (1) chain pullout for weak interfaces, (2) crazing⁵ and (3) chain scissions [122].

² melting surfaces of the material, joining them and cooling down. Surface can be melted by heating, friction during rubbing at high frequency and ultrasound.

³ for amorphous polymers, a temperature region where the polymer transitions from a hard, glassy material to a soft, rubbery material

⁴ the amount of external work per unit area required to propagate a crack across the interface

⁵ formation of an interpenetrating microvoids and small fibrils that elongate and break when tensile load is applied

Mechanical interlocking

Surface roughness should normally decrease the adhesion strength as it prevents close contact between polymers. Nevertheless, if materials that can be easily contoured are used (rubber-like, liquid materials that solidify afterwards, *etc.*), the adhesion strength is often improved. Two mechanisms are often used to explain this phenomenon. First of all it could be a consequence of a higher contact area and a stronger chemical or physical bonding. On the other hand, microscopic features can be pushed into the gaps of the other material. This would subsequently serve for the direct mechanical interlocking and could increase the adhesion [15, 161].

Good contour-ability or viscoelasticity needs to be ensured in order to lock materials by mechanical coupling. Nevertheless, when a material is being deposited in a liquid state, the interlocking due to the surface roughness is more likely. In this case, a close contact between the liquid and the solid needs to be ensured thus the wettability of the surface plays a crucial role. Another specific case relevant for our application is a deposition of a liquid that subsequently solidifies in the pores of the membrane. After solidification, the hook-and-loop system of two interconnected solids is created and the adhesion strength is dependent on the breakdown strength of the materials themselves.

3.1.2 Polymer adsorption on the surface out of solution

So far we have mostly introduced the adhesion mechanisms between two solid polymers. Nevertheless, for many practical applications (protective coatings, glues, paints, *etc.*), a coating layer is being deposited from a diluted solution on the solid surface. Therefore, deposition method and subsequently interactions between the solution, adsorbed layer and solid surface may influence adhesion strength.

A polymer from the dilute solution is often adsorbed on even weakly attractive surfaces. The adsorbed and the polymer in the solution are in equilibrium (continuous adsorption and relaxation) when sticking forces (such as hydrogen, ionic bonding *etc.*) are not available. Nevertheless, if a free surface area is available, even for a weak attractive forces adsorption of polymer chains is often faster than equilibration [332]. That subsequently leads to the formation of a monolayer and a full surface coverage. Constrained mobility of polymer chains in a monolayer produces essentially irreversible structures.

In general, adsorption on a surface proceeds in the following steps. (1) First, the polymer is transported to the surface, usually by diffusion. Then as a result of surface-polymer interactions (2) adsorption to random free surface areas takes place. This is followed by (3) reorientation and spreading of the polymer leading to even stronger interaction and irreversibility. Finally, once the surface is covered, (4) multilayers start to be formed, whose strength depends on the polymer-polymer and polymer-solvent interactions. Adsorption from solution is often used for building polyelectrolyte films by layer-by-layer deposition [51] but in general is limited to the formation of monolayers. Nevertheless, the interaction of it with surface is important in determining the overall adhesion between films fabricated by solution-casting, spraying, spin-coating, *etc.*

Material	Surface tension	PEDOT:PSS on PVDF rough	PEDOT:PSS on PVDF smooth	Water on PVDF rough	Water on PVDF smooth
PEDOT:PSS	70.3 mN/m				
PVDF	72.8 mN/m	CA: 132	CA: 116	WCA: 129	WCA: 114
Water	71.9 mN/m				

Fig. 3.2. Measured (for *PEDOT:PSS* and water) or reported (for *PVDF*) surface tension and pictures of the contact angle measurements between water, *PEDOT:PSS* and *PVDF*.

3.2 Adhesion between *PEDOT:PSS* and *PVDF*

In this chapter we present the results of our study concerning the adhesion between the *PVDF* membrane and the *PEDOT:PSS* films deposited by solvent casting. The combination of adhesion and failure mechanisms will be discussed simultaneously in order to explain the observed occurrences, *i.e.* hook-and-loop mechanical interlocking due to infiltration and film formation in the pores of the membrane; polymer adsorption from the solution and interactions with hydrophobic and mobile grafted hydrophilic surfaces; mechanical properties of the polymer causing interface failure *etc.*

In our case, initial stage of an interaction of the materials is the deposition of the diluted polymer solution on the membrane surface. Many adhesion mechanisms require an intimate contact between materials, *i.e.* good wetting. The surface tension of the liquid (γ_L) and its contact angle (with a perfectly flat substrate) can be used to estimate the spreading coefficient using Young-Dupré equation:

$$S = \gamma_L(\cos\Theta - 1) \quad (3.1)$$

Positive wetting parameter S means complete, while negative - partial wetting. Initial contact angle does not necessarily represent the adhesion strength between a subsequently formed polymer film and the substrate. Nevertheless, it is an indicator of a poor wetting and immiscibility of the polymers that subsequently lead to small interdiffusion width.

PVDF is one of the polymers with the lowest surface energy of 25 mN m^{-1} . Its hydrophobicity is mainly determined by the fluorocarbons on the surface leading to fewer van der Waals interaction sites (in comparison to hydrocarbons) [75]. Therefore, water contact angle (*WCA*) on *PVDF* is close to 130° as shown in *Fig. 3.2*. *PEDOT:PSS* aqueous solutions have a high surface tension of 70.2 mN m^{-1} that is similar to the one of pure water (at 25°C). High surface tension and large water contact angle in both cases lead to negative spreading coefficient. The condition of the intimate contact between materials is not satisfied and interdiffusion of polymer chains is highly unlikely. Therefore, poor adhesion can be expected.

3.2.1 Adhesion evaluation method

Several quantitative methods could be used in order to determine the adhesion strength between materials. Including but not limited to (1) peeling tests, when a force is

measured during the peeling off two solids from one another under a fixed peeling angle and rate; (2) torque test allowing calculations of shear stress; (3) scratch or nanoindentation test, when a fine tip is dragged on the surface under an increasing load, leading to information on delamination force, *etc.* [15, 215]. Nevertheless, plastic deformation of the membrane, its porosity as well as mechanical properties of *PEDOT:PSS* films make these methods inapplicable, especially in a quantitative matter. Therefore, for characterization of adhesion, qualitative cross-cut Scotch™ tape peeling test (similar to ISO 2409 : 2013 recommendations) was performed.

3 ml of *PEDOT:PSS* solution with various compositions were deposited on *PVDF* membranes by solvent casting and dried overnight or as indicated. A *PEDOT:PSS* film (10 – 50 μm depending on the infiltration depth and the density of the film) was formed. Then two series of parallel cuts cross-angled to each other in order to obtain a pattern of 25 similar squares were cut on the surface using a surgical scalpel. The cutting force was controlled so that grid is cut through the *PEDOT:PSS* film but does not slice the *PVDF* membrane. The membrane was then attached to a more solid surface and a Scotch™ tape (with adhesion indicator⁶) was adhered. Then the adhesive tape was slowly removed by hand, pulling the adhesive tape up at 90° angle. *PEDOT:PSS* remaining on the adhesive tape as well as on the *PVDF* membrane were then evaluated. Tests were performed on several cut grids and in the following pictures the worse adhesion case is shown. This 'pass-fail' evaluation procedure was previously used and validated by Liu *at al.* [241, 193]. More detailed sample preparation is described in Appendix A.3.1.

3.2.2 Adhesion between pristine *PVDF* and *PEDOT:PSS*

Due to the low free surface energy *PVDF* and *PEDOT:PSS* are known for their weak adhesion with other materials [140, 95, 9]. In aqueous solutions, *PEDOT:PSS* forms core/shell structure where polystyrene sulfonate (*PSS*) insulating layer is outside and conducting poly(3,4-ethylenedioxythiophene) (*PEDOT*) chains are inside the nanoparticle [215]. This causes low conductivity of as-prepared films [298]. Furthermore, the *PSS* insulating layer is highly hydrated and a water boundary is created not only between *PEDOT:PSS* particles but also in between *PVDF* surface and *PEDOT:PSS* as illustrated in Fig. 3.4a [238]. This has two implications: (1) the films formed from

⁶ the color of a Scotch™ tape changes from white to translucent when tape is well adhered

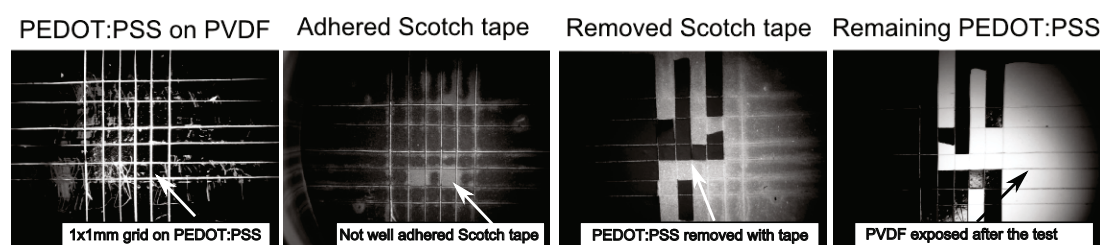


Fig. 3.3. Steps of adhesion evaluation process (from left to right): grid of 25 squares cut on the *PEDOT:PSS* surface until *PVDF* membrane; Scotch™ applied on the grid and indication of good adhesion; picture of the Scotch™ tape after it was removed from the film; picture of the *PVDF* membrane and the remaining *PEDOT:PSS* film after adhesive tape was removed.

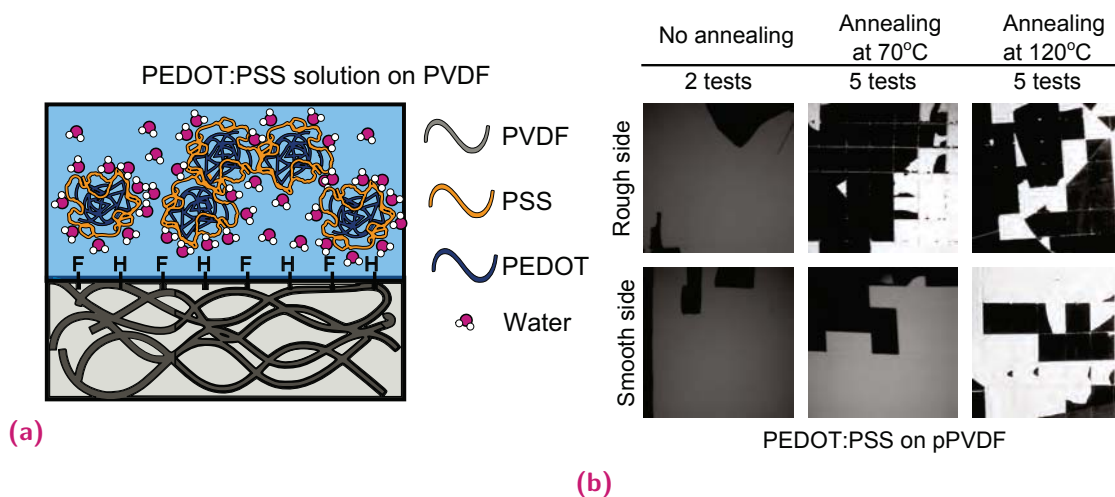


Fig. 3.4. (a) Illustration of *PEDOT:PSS* core/shell structured nanoparticles in aqueous solution with *PEDOT* chains in the core (blue) and *PSS* around (yellow). The hydration shell on *PSS* presumably prevents the polymer adsorption on the *PVDF* (grey) surface. (b) Pictures of the remaining *PEDOT:PSS* films (black) on the *PVDF* membrane (white) surface (rough and smooth) after adhesion tests. The annealing condition and the number of tests performed before taking the picture is indicated above.

such dispersions are brittle and fragile at low humidity due to the lack of entanglement of the polymers⁷ [215]; (2) hydration shell is also likely to prevent the spontaneous polymer adsorption on the *PVDF* surface thus high annealing temperatures might be needed in order to make it evaporate.

In order to prove this assumption, the influence of humidity and residual water on the adhesion was investigated. Adhesion tests were performed on *PEDOT:PSS* films after each drying step: (1) at room temperature for 24 hours (no annealing), (2) in the oven at 70°C for 2 hours and (3) after a thermal annealing step of 15 minutes at 120°C. Even though at 120°C most of the water is removed from the *PEDOT:PSS* film, its hygroscopic nature causes immediate reabsorption as soon as the film is exposed to the air and room temperature⁸. Nevertheless we assume that annealing causes smaller amounts of residual water in the film and even less of it at the interface between *PVDF* and *PEDOT:PSS*.

The results of the adhesion tests indicating the influence of the residual water in the *PEDOT:PSS* film on the adhesion to pristine *PVDF* membrane (*pPVDF*) are shown in Fig. 3.4b. Due to the difference of roughness of the two sides of the membrane (Section 2.2.2) adhesion was tested on both sides and the effect of roughness was also considered. Nevertheless, if high amounts of residual water are present (no annealing), *PEDOT:PSS* layer is completely removed from the *pPVDF* with only two applications of the adhesive tape test. In this case the adhesion strength is independent

⁷ This was also observed in our experiments as *PEDOT:PSS* film forms multiple cracks during thermal annealing.

⁸ This can be observed with a simple experiment as follows. Once exposed to 120°C due to evaporation of water *PEDOT:PSS* film contracts and causes the rolling of the *PEDOT:PSS-PVDF* bilayer into a tube like structure. Nevertheless, immediately after the exposure to room temperature and humidity the tube un-rolls forming slightly stressed (bended) bilayer. If the bilayer is flattened by hand, *PEDOT:PSS* film cracks.

on the film roughness. This is in corroboration with the previous assumption that the hydration shell is not removed during drying at room temperature and possibly remains in between *PEDOT:PSS* and *PVDF*.

Nevertheless, after annealing at relatively low temperature (70°C) the interfacial water layer seems to be removed. Not only adhesion improves (significantly larger amount of *PEDOT:PSS* remains on the *pPVDF*) but the influence of the surface roughness starts to play a role. More of *PEDOT:PSS* is removed from the smooth side of the membrane. The effect of the roughness is even more visible after thermal annealing at 120°C - significantly larger area of the *PEDOT:PSS* film remains on the rough side of the *pPVDF*. As the influence on adhesion due to the surface roughness is debatable (Section 3.1.1) it could be both, due to an increased area of interaction and a larger number of van der Waals bonds between two materials or due to mechanical interlocking in the more frequent and deep corrugations of the membrane surface.

Adhesion between *pPVDF* and *PEG-PEDOT*

It was shown that even after solution casting of *PEDOT:PSS* films, its core/shell structure remains intact, and often leads to the brittleness of the film [215]. Therefore pristine *PEDOT:PSS* films are rarely used. Furthermore, *PSS* is an insulating polymer and the core/shell structure in the shell leads to larger distances between conducting *PEDOT* grains. This consequently leads to a low conductivity of the film. Various secondary doping and post-treatment methods were suggested in order to destroy nanoparticle structure, improve the connectivity of the *PEDOT* cores and subsequently the conductivity of the *PEDOT:PSS* film [5, 90, 146, 264, 298, 402]. The most common additives are polar organic solvents with high boiling point. It is thought that polar molecules bind to *PSS* and force *PEDOT* to rearrange [264, 298]. Furthermore, these kinds of additives often decrease the surface tension of the aqueous solutions leading to an increased wetting of the hydrophobic substrates [140]. Both, destroyed core/shell structure and better wetting could be advantageous as it could lead to adsorption of *PEDOT:PSS* and adhesion to *PVDF*.

In most of our experiments we use poly(ethylene glycol) of $M_r - 400$ (*PEG400*) as a secondary dopant to *PEDOT:PSS* (*PEDOT:PSS* with *PEG* as secondary dopant (*PEG-PEDOT*)). Small amounts of *PEG400* (up to 2 vol%) increase the conductivity of *PEDOT* thin films from 0.3 S/cm to about 800 S/cm . This effect is attributed to the breaking of *PEDOT:PSS* core/shell structure [264]. Secondary dopants that have similar core/shell structure breaking effect, were also reported to decrease the elastic modulus and increase the elongation at break of *PEDOT:PSS* films [47, 148, 228, 329]. Therefore, 1 vol% *PEG400* does not only increase conductivity of *PEDOT:PSS* (as discussed in Section 5.2.2), it also lead to formation of continuous unbroken film even after thermal annealing. The illustration showing likely *PEG-PEDOT* structure in solution is shown in Fig. 3.5a.

The effect of *PEG400* on adhesion to *pPVDF* is shown in Fig. 3.5b. The results are very similar to the ones obtained with pristine *PEDOT:PSS*. The *PEG-PEDOT* film is easily removed in case of a large quantity of residual water (no annealing) and the influence of the surface roughness is even more pronounced after thermal annealing (at

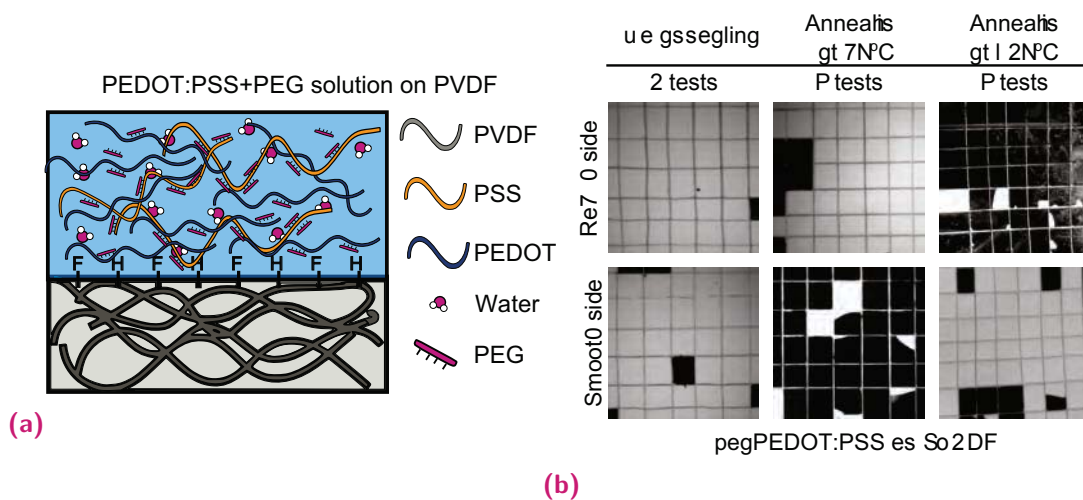


Fig. 3.5. (a) Illustration of the likely *PEDOT:PSS* structure in the aqueous solution with *PEG400* as an additive. *PEG400* (pink) forms hydrogen bonds with both *PEDOT* (blue) and *PSS* (yellow) partially removing the nanoparticle organisation. Presumably adsorption of polymer chains is more likely in this configuration. (b) Pictures of the remaining *PEG-PEDOT* films (black) on the *pPVDF* membrane (white) surface (rough and smooth) after the adhesion tests. The annealing condition and the number of tests performed before taking the picture is indicated above.

120°C). Nearly no *PEG-PEDOT* is removed from the rough side of the *PVDF* membrane. The reasons behind the apparently better adhesion of *PEDOT:PSS* on the smooth side of the *PVDF* after annealing at 70°C are harder to interpret and were not further investigated.

PEDOT:PSS/PVDF adhesion needs to be strong enough to sustain a certain amount of stress induced at their interface, especially during mechanical cycling or actuation [241]. Furthermore, during actuation, the electrolyte will be moving from one material to the other therefore the interface needs to be strong enough to allow the presence of the liquid. Finally, due to the absorption of the ionic liquid, *PVDF* membrane might expand inducing stresses due to different expansion rates. As shown in Fig. 3.6a (Test II), once the membrane and *PEG-PEDOT* sandwich is put into the ionic liquid, *PEG-PEDOT* is completely removed even from the rough side of the membrane. If the film was not washed away during incubation, only one adhesion test was needed to remove it.

To sum up, aqueous solutions of *PEDOT:PSS* or *PEG-PEDOT* have high surface tension leading to a low wetting and weak interactions with hydrophobic *pPVDF*. Large contact angle also prevents the penetration of the solution into the pores of the *PVDF* membrane and the film is formed only on the upper part of the membrane (Fig. 3.6b). This allowed us to observe the influence of the surface morphology on the adhesion. As we showed, a rougher surface leads to slightly better adhesion, especially when the core/shell structure of *PEDOT:PSS* is broken. On the other hand, the residual water in the *PEDOT:PSS* film is likely to form a barrier layer between *PVDF* and the polymer film and the incomplete drying was shown to drastically reduce the adhesion.

In order to use the *PVDF/PEDOT:PSS* sandwich for the fabrication of actuators, significantly stronger adhesion needs to be ensured. Several adhesion improvement methods could be considered such as: (1) improving the wetting of *PVDF* by decreasing the

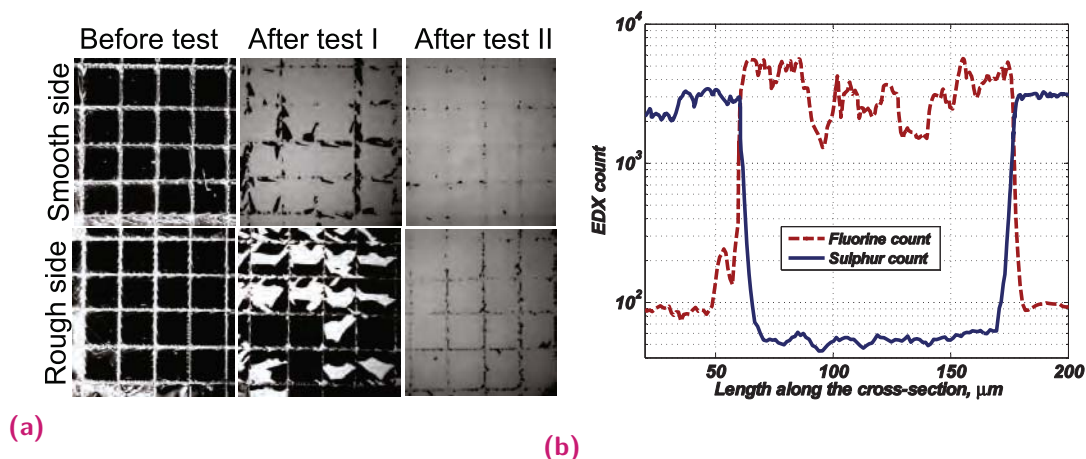


Fig. 3.6. (a) Pictures of the remaining PEG-PEDOT films (black) on the pPVDF membrane (white) surface (rough and smooth) after the adhesion test in a dry state (test I) and after incubation in ionic liquid for 24 hours (test II). (b) Energy-dispersive X-ray spectroscopy (EDX) scan along the cross-section of the pegPEDOT/pPVDF/pegPEDOT trilayer. The fluorine trace (signature of pPVDF) is shown in red (full line) and sulphur trace (signature of PEG-PEDOT) in blue (dashed line)

surface tension of the PEDOT:PSS solution; (2) modifying the surface of the PVDF membrane by the oxidation or plasma induced damage in order to improve the mobility of the PVDF chains; (3) functionalizing PVDF with the hydrophilic moieties in order to create hydrogen bonding interactions and possibly allow interdiffusion with the more mobile grafted chains.

3.2.3 Effect of the infiltration on the PEDOT:PSS-membrane adhesion

Not only polyethylene glycol (PEG) and other polar high boiling point solvents are used to enhance conductivity of PEDOT:PSS films. Surfactants such as Triton-X100 [372], Zonyl fluorosurfactant [329], etc. [229, 329, 416] have similar effect. Furthermore, surfactants significantly reduce surface tension of aqueous solution. Sufficiently low surface tension (γ_{Lc}) of a casted solution causes the wetting of the membrane and penetration of it through the pores [111]. If infiltrated, PEDOT:PSS film would be formed in the pores of the membrane and outside. That could cause a direct mechanical interlocking. Two experiments were used to test the importance of mechanical interlocking on the adhesion.

The critical surface tension value (γ_{Lc}) for pPVDF (pore size of 100 nm, porosity 70%) was estimated by the 'penetrating drop method' (Appendix A.3.2) and is about 35 mN/m [111]. We used a small amount (1 vol%) of nonionic surfactant Triton X-100 to decrease the surface tension of PEDOT:PSS to 18.8 mN/m leading to a contact angle of a few degrees and a nearly immediate infiltration of PEDOT:PSS in the pores of the membrane. The infiltrated PEDOT:PSS can be seen on the back side of the membrane in Fig. 3.7a.

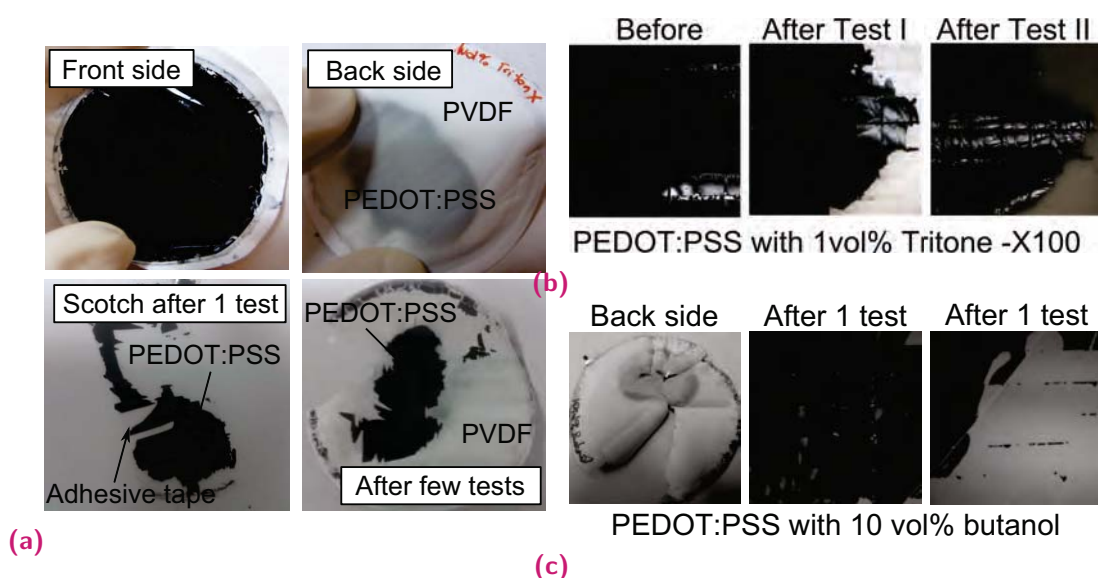


Fig. 3.7. (a) Pictures of *PEDOT:PSS* (with 1 vol% Triton X – 100) film deposited by solvent casting on *pPVDF*. Top: front and back sides after deposition and drying, bottom: adhesive tape after one adhesion test showing that most of *PEDOT:PSS* remained on the tape and the front side of the *PVDF* membrane after several application of adhesive tape showing that only at areas where *PEDOT:PSS* penetrated through the membrane adhesion is strong. (b) Adhesion test with a cut grid: Test I - after 5 applications of adhesive tape in a dry state; Test II - after incubation in ionic liquid for 24 hours and another 5 applications of adhesive tape. (c) Equivalent test performed on *PVDF-PEDOT:PSS* (diluted with 10vol% of *i*-butanol) sandwich showing that only at the penetration through area adhesion is strong.

As shown in Fig. 3.7a-3.7b, only good wetting and partial infiltration do not improve adhesion between *PEDOT:PSS* and the membrane. *PEDOT:PSS* film is easily removed with one Scotch™ tape from nearly all areas of the membrane. Darker areas on the membrane after the test indicate that *PEDOT:PSS* was infiltrated in the pores to a certain depth and remained in the pores after the test. On the other hand, interface at the area where *PEDOT:PSS* penetrated through (clearly visible on the back side of the membrane) was sufficiently strong to last 5 Scotch™ adhesion tests even after incubation in ionic liquid for 24 hours (Test I and II in Fig. 3.7b). This is a clear indication of the effect of mechanical interlocking on adhesion strength. Nevertheless, it seems that sufficiently deep interface formed by formation of well interconnected *PEDOT:PSS* film is necessary for the strong adhesion. The influence of the infiltration is discussed again in Section 3.4.

Another material that was used to decrease surface tension of *PEDOT:PSS* solution was *i*-butanol. Butanol as other alcohols was also shown to increase conductivity of *PEDOT:PSS* films, most likely by washing out excess of *PSS* [5, 402]. The film formation and the adhesion results are identical to the ones obtained with the films treated with *Triton X-100* as shown in Fig. 3.7c. Only in the area where *PEDOT:PSS* is deeply infiltrated in the membrane the interface is strong (Fig. 3.7c picture in the middle) while lower infiltration depth leads to the delamination after one test (3rd picture in Fig. 3.7c). Nevertheless, just as in the case of *Triton X-100* after the test, the darker areas on the membrane were visible, showing that some *PEDOT:PSS* remains in the

membrane. The fact that membrane is easily fractured (during handling as shown in Fig. 3.7c) also suggests that some *PEDOT:PSS* remains in the pores and that the butanol is removed from the *PEDOT:PSS* films leading to its brittleness⁹.

To sum up, decreasing surface tension of *PEDOT:PSS* solution, leads to infiltration of *PEDOT:PSS* into the pores of the membrane. During evaporation of the solvent, *PEDOT:PSS* film is formed, mechanically interlocked in the pores of the membranes. It seems that if sufficient interlocking area (or volume) is provided, strong interface can be ensured and the result are similar when the surfactant remains in the film after drying (boiling point of *Triton X-100* is 270°C) or when it is removed (as is likely in the case of butanol). Nevertheless, forming trilayer films with this strategy is inapplicable for our purpose as the infiltration area is not homogeneous and its width would be difficult to control.

3.2.4 Effect of the *PVDF* surface damage on adhesion

One of the most common adhesion improvement methods is a surface damage by plasma. Several factors are attributed to the improved adhesion, *i.e* the increased surface roughness [194], scission of the polymer backbone and generation of shorter more mobile layers [71, 251], the addition of hydrophilic moieties and consequent hydrogen bonding [308]. *PVDF* is a semi-crystalline polymer, meaning that due to its highly ordered and dense structure movements of the polymer chains are restricted even above its glass transition temperature (−41 °C). Therefore even if proximate contact is established, interdiffusion of *PVDF* with another polymer is very unlikely [238] and is one of the reasons of its weak adhesion with other materials.

Despite its chemical stability, *PVDF* surface can be damaged and chemically activated by ultraviolet (*UV*) and plasma (Section 2.1.1). Induced radicals, oxygen species or cleavage of *PVDF* backbone and improved mobility of the chains could therefore improve the adhesion strength with *PEG-PEDOT*. Nevertheless, as shown in Fig. 3.8a, *PEG-PEDOT* is relatively easily removed from the *PVDF* surface that was treated by *UV*/ozone for 1 hour (exact modification procedure and characterization provided in Appendix A.3.1). Similar results are obtained by depositing *PEG-PEDOT* on the membrane treated for 15 seconds with Ar plasma (Fig. 3.8b) and most of *PEDOT:PSS* is removed with one Scotch™ test. Moreover, white traces was visible on the adhesive tape after the second test in areas where the tape was adhered to the membrane itself as shown in Fig. 3.8c (dark grey area as pictures are grey-scale). It was previously reported that plasma damage and creation of mobile layers on the polymer surface may have negative effects on adhesion, if these layers are too thick [71]. It seems that for clean *PVDF* membranes, even 15 seconds of Ar plasma irradiation creates *PVDF* layer that is weakly attached to the bulk of the rest of the polymer chains and is easily removed.

⁹ During drying *PEDOT:PSS* contracts exerting mechanical stresses on the substrate. Depending on the substrate it can be compensated by substrates deformation (rolling into the tube if deposited on a non-fixed *PVDF* or cracking of the *PEDOT:PSS* film if it is not supported by secondary dopants) [98]. At low relative humidity and without additives with plasticization effects, *PEDOT:PSS* forms very brittle films. In our experiment, the film was not supported during drying and *PVDF* was fractured during the attempt to unroll it

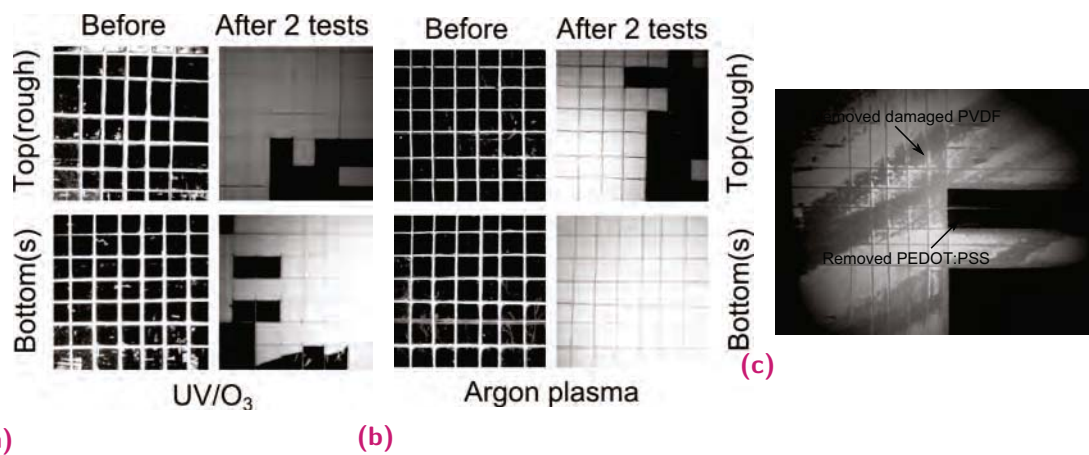


Fig. 3.8. (a) Pictures of the remaining PEG-PEDOT films (black) on *p*PVDF membrane (white) surface (rough and smooth) after the adhesion test in a dry state. Number of performed peeling tests and PVDF modification methods are indicated above and below the picture respectively. (b) Picture of the adhesive tape taken after the second adhesion test on Ar plasma damaged PVDF. PEDOT:PSS removed during the test is indicated with the arrow (black). The darker area indicated with another arrow, shows PVDF membrane layer removed during the test.

3.3 Adhesion between PEDOT:PSS and PVDF-graft-PEGMA

As discussed in *Section 2.1* surface graft polymerization is another way to introduce short mobile polymer chains on the surface of PVDF. It was reported that introduction of mobile chains on the smooth hydrophobic surfaces improve adhesion between two of them, as mobile chains get entangled [49]. Grafting can also add chemically active moieties that would subsequently adjoin polymers by covalent or ionic bonding [230]. Compared to ionic interactions, mechanical interlocking was shown to contribute little to adhesion [230]. However, even with no ionic interactions, grafting acrylic acid on various substrates significantly improve adhesion with materials deposited on them [366].

The polymerized poly(ethylene glycol) methyl ether methacrylate (PEGMA) on the PVDF surface provides both, the miscibility due to its hydrophilicity and the mobility of shorter polymer chains. The improved wetting of PVDF-graft-PEGMA membrane (*m*PVDF) by PEDOT:PSS is shown in *Fig. 3.9*. The adhesion improvement after solvent evaporation can also be expected due to stronger intermolecular forces (hydrogen bonding). Moreover, the interdiffusion of PEDOT:PSS with *graf*-PEGMA can also take place as *graf*-PEGMA is mobile and hydrated in aqueous solutions [49, 176, 44]. Finally, because of the functionalization to certain depth of the membrane, the infiltration of PEDOT:PSS can be expected. That could possibly add strength to the interface due to the direct mechanical interlocking.

The adhesion improvement between PEDOT:PSS secondary doped with polyethylene oxide (PEO) ($M_r - 100000$) and PVDF modified with PEGMA by photoinduced grafting was already mentioned by Ikushima *et al* [148]. They achieved a mixing depth of several microns that was enough to adjoin the layers for the fabrication of actuators.

Material	Surface tension	PEDOT:PSS on PVDF		PEDOT:PSS on mPVDF	
		rough	smooth	rough	smooth
PEDOT:PSS (with PEG400)	61.9 mN/m				
mPVDF	unknown				
PVDF	72.8 mN/m	CA: 136	CA: 115	CA: 23	CA: 28

Fig. 3.9. (Table) Measured surface tension of PEG-PEDOT (1 vol%) and (pictures) contact angle measurements of PEG-PEDOT on pristine (pPVDF) and modified (mPVDF) membranes.

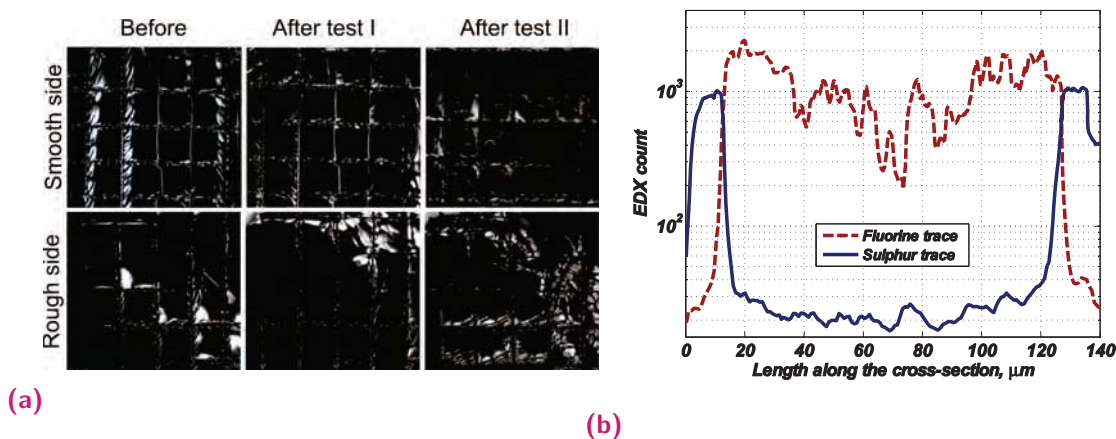


Fig. 3.10. Qualitative adhesion test of PVDF and PVDF-graft-PEGMA membranes and PEDOT:PSS. Pictures are taken before, after 5 Scotch™ Tape peeling tests (Test I) and 5 more peeling tests after incubation in ionic liquid for 48 hours (Test II)

Adhesion tests on mPVDF membranes prepared as discussed in Section 2.2.3 are shown in Fig. 3.10a. Even low density (grafting density (GD) - 0.07 ng/mm^2) of mPVDF leads to significantly improved adhesion strength¹⁰. PEDOT:PSS film remains on mPVDF membrane surface after tests in a dry state (Test I) and is not influenced by initial roughness of the membrane (smooth and rough sides). Furthermore, even after immersion in ionic liquid for 24 hours and subsequent adhesion tests (Test II) PEDOT:PSS remained on mPVDF. In fact the time of incubation in ionic liquid does not influence the adhesion strength, as PEDOT:PSS/mPVDF/PEDOT:PSS trilayers remain intact even after a year in a liquid. Furthermore, interface did not fail after as produced trilayers were actuated to strain of 1% for tens of thousands cycles (discussed in Section 4.4.1) and at excessive strain that was artificially induced[340].

A GD of about 0.07 ng/mm^2 creates an interfacial layer of only a few micrometers as shown in Fig. 3.10b. In fact, the EDX scans of PEDOT:PSS deposited on the pPVDF show very similar mixing depth profile (Fig. 3.6b). Nevertheless, as PEDOT:PSS wets the surface of mPVDF and infiltrates in pores, the contact area should be significantly larger. Moreover, if infiltrated for a few microns, a PEDOT:PSS film is formed in the pores and outside that could influence adhesion by direct mechanical interlocking. In order to test the importance of the mechanical interlocking on adhesion, non-porous PVDF films were functionalized.

¹⁰ Adhesion tests of PEG-PEDOT on mPVDF of larger grafting densities and larger mixing depths were also done and provided identical results in these testing conditions.

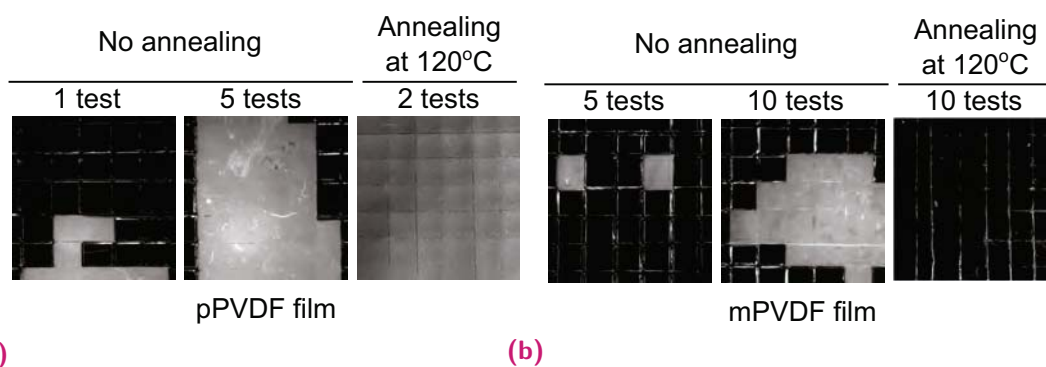


Fig. 3.11. Adhesion tests of *PEDOT:PSS* (with 1 vol% *PEG400*) and flat *PVDF* films in a dry state. Annealing condition and the number of adhesive tape applications is indicated above each picture. Type of the film is indicated below (*mPVDF* - functionalized film, *pPVDF* - pristine film).

3.3.1 Influence of surface roughness

Due to the various factors playing a role in adhesion, exact mechanism cannot be determined. Nevertheless, the influence of the surface roughness and mechanical interlocking in the pores can be eliminated by depositing *PEDOT:PSS* on a smooth *PVDF* film. *PVDF* film was produced by heating pristine *PVDF* membrane on a hot plate above its melting point 180°C and cooling it down. *PVDF* film was then functionalized in the same way as membranes that leads to a grafting density of $0.04 \pm 0.01 \text{ ng/mm}^2$ and subsequently decreased water contact angle from 82.16 ± 7 to 56.3 ± 2 ¹¹ (more detail fabrication procedure is presented in *Appendix A.3.1*). Adhesion tests on such pristine (*pPVDF*) and modified (*mPVDF*) films are shown in *Fig. 3.11*.

Nevertheless, water contact angle on flat *PVDF* film is lower and smoothness should improve contact between polymers, adhesion seems to be worse (*Fig. 3.11a*) and most of the grid squares are removed with 5 Scotch™ tests independent of the annealing temperature. On the other hand, *PVDF* grafting seem to lead to better adhesion and even after 10 tests *PEDOT:PSS* film remain on *mPVDF* film. Nevertheless, the adhesion is slightly worse if the film is not well dried (no annealing) and some grid squares are removed. The results corroborate with our previous discussion in *Section 3.3* that for *mPVDF*, a large interfacial layer is not necessary since hydrogen bonding and polymer entanglement are sufficient for strong interface. Furthermore, after immersion in ionic liquid for 48 hours, most of the *PEDOT:PSS* film was removed with a single Scotch™ adhesion test as shown in *Fig. B.2*. Even though hydrogen bonding and polymer entanglement improve the interfacial strength, certain depth of the mixing depth is still needed in order to ensure good interface that can withstand electrochemomechanical cycling.

3.3.2 Influence of coating by physisorption

Due to their slightly hydrophobic nature, materials such as glycerol, ethylene glycol, *PEG* readily adsorb on the pore walls of *PVDF*. They are also used as a modification

¹¹ The lower *WCA* of the melted *PVDF* film again shows the importance of the surface roughness on the contact angle.

Material	Surface tension	Contact angle with pPVDF		PEDOT:PSS on PVDF treated with PEG	
		Smooth side	Rough side	rough	smooth
PEG	44.7 mN/m	infiltrates	infiltrates		
PEDOT:PSS	70.2 mN/m	119.0±5+%	134.6±2.9	CA: 28	CA: 38
+ 1 vol% PEG	61.9 mN/m	114.0±1.9	128.8±3.5		
+ 2 vol% PEG	60.3 mN/m	114.4±2.3	132.8±2.1		
+ 5 vol% PEG	59.3 mN/m	111.6±1.5	129.3±2.7		
+ 10 vol% PEG	not measured	110.6±5+%	127.5±1.9		

Fig. 3.12. Measured surface tension of *PEDOT:PSS* solutions with different *PEG400* volume concentrations and their contact angle with pristine *PVDF* membrane. Contact angle of *PEDOT:PSS* and *PVDF* membrane that was *a priori* infiltrated with *PEG* is shown on the right.

method in order to increase the water flux [238, 175]. *PEG* is not a surfactant and does not decrease the surface tension below the critical value and the contact angle with *pPVDF* remains large as shown in Fig. 3.12. Nevertheless, due its amphiphilic nature it adsorbs on the surface of the hydrophobic *PVDF* membranes. Therefore, if excess of the *PEG* is present in the *PEDOT:PSS* solution, part of it will not be forming hydrogen bonding with *PEDOT* and *PSS* and will be freely dissolved in water. According to Mengistie *et al* [264] more than 2 vol% of *PEG400* in *PEDOT:PSS* solution does not influence the conductivity of the thin film and even decreases it. Therefore, we assume that only up to this amount, *PEG400* would be attached to *PEDOT* and *PSS* by hydrogen bonding. Furthermore, the excess of it, is then available for adsorption on the surface.

PEG400 adsorbed on *PVDF* would hydrophilize the walls of *PVDF* membrane. This could then cause *PEDOT:PSS* infiltration in the membrane to a certain depth. The contact angle of *PEDOT:PSS* on the *PVDF* membrane treated with *PEG* (by putting a drop of *PEG* and letting it adsorb) is shown in Fig. 3.12 confirming this assumption.

3 ml of *PEDOT:PSS* having 5 vol% or 3 vol% of *PEG400* were deposited on *pPVDF* and *mPVDF* (Appendix A.3.1). The *EDX* scans along the cross-sections of the trilayers with *pPVDF* are shown in Fig. 3.13a-3.13b. Even with 2 vol% *PEG* the amount of *PEDOT:PSS* along the cross-section is above the noise level¹². Moreover, 5 vol% lead to nearly filling of the pores and high sulphur content along the cross-section. The infiltration is also visible in the membrane pictures after the adhesion test. Due to the pores filled with *PEDOT:PSS* the membrane remains black leading to much lower contrast in the pictures. The infiltration is not so visible in the case of 2 vol% *PEG400* and we assume that *PEDOT:PSS* only cover the walls of the pores.

Regardless of the amount of the *PEG* excess, infiltration through the membrane does not improve the adhesion as shown in Fig. 3.13c-3.13d. *PEDOT:PSS* film is removed from membranes with only 2 Scotch™ tests. On the other hand, it is not clear if the interface failure is due to the weakened interactions between the film and the membrane or if it is a consequence of the altered *PEDOT:PSS* mechanical properties and a lack of the entanglement between the polymer chains. As *PEDOT:PSS* is being removed square by square and the film does not fall apart at other locations, the first possibility is more likely.

¹² the fluorine signal 'outside' the membrane

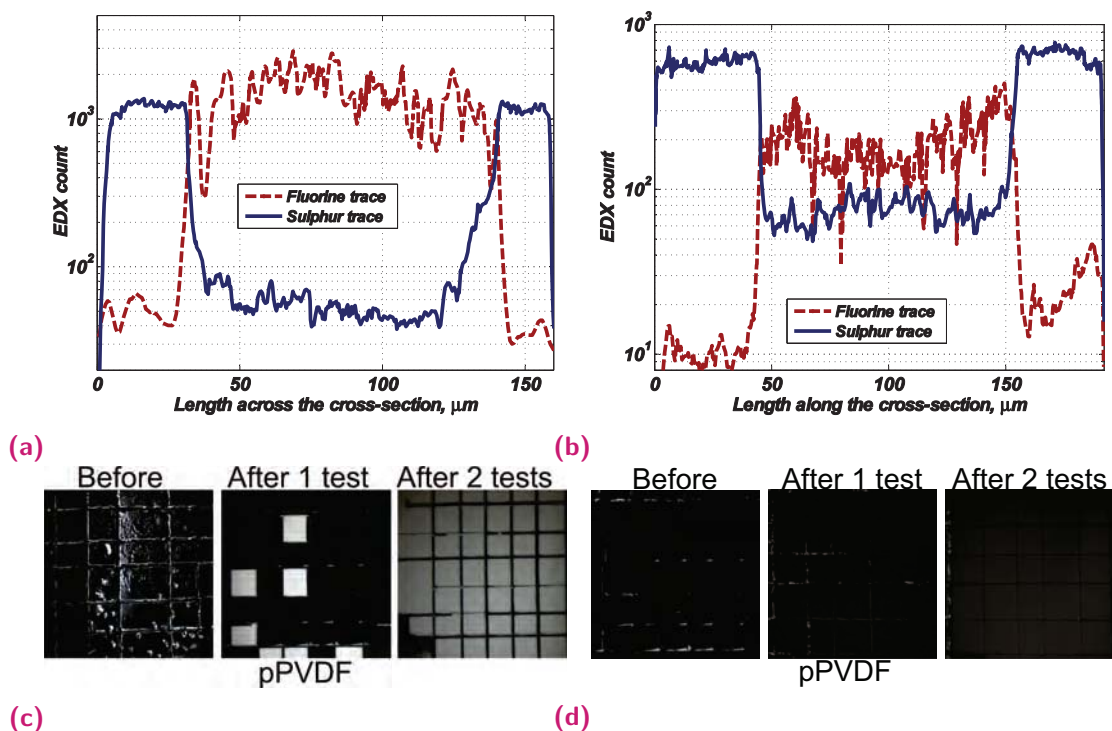


Fig. 3.13. EDX line scans for fluorine (red) and sulphur (blue) traces along the cross-section of the trilayers PEDOT:PSS/pPVDF/PEDOT:PSS ((a)-(b)) and adhesion tests of the PEDOT:PSS film deposited on the rough side of the membrane ((c)-(d)). For (a) and (c) PEDOT:PSS is secondary doped with 2 vol% PEG400, for (b) and (d) with 5 vol% PEG400.

Equivalent results were obtained for *m*PVDF as shown in Fig. 3.13c-3.13d. Excess of secondary dopant (*PEG*) lead to significantly worse adhesion to the film and PEDOT:PSS is removed with 2 Scotch™ tests. The EDX scans show similar results. In case of the lower *PEG* concentration (2 vol%) step distribution of the PEDOT:PSS across the cross-section can be seen as shown in Fig. 3.14a. High PEDOT:PSS content on each outer side of the membrane (20 μm) corresponds to the PVDF-graft-PEGMA length (*GD* of 0.103 ± 0.05 ng/mm²). The area in between shows lower but still visible PEDOT:PSS trace. Just as in case of *p*PVDF, when larger excess of PEG400 is used, PEDOT:PSS is homogeneously distributed along the cross-section (Fig. 3.14b) and the hydrophilicity of the membrane does not matter.

It is likely that the thickness of the layer of *PEG* adsorbed on the PVDF membrane is in the same order of magnitude as the thickness of the graft-PEGMA layer. This would explain the lack of adhesion between PEG-PEDOT and *m*PVDF with access of *PEG* in solution. *PEG* adsorbs on the membrane before the evaporation of the solvent, and remains on the surface after the thermal annealing. Therefore during solvent evaporation PEDOT:PSS settles on the surface of the *PEG* adsorbed layer and does not reach the PVDF-graft-PEGMA as illustrated in Fig. C.16. As multilayer of adsorbed *PEG* is in a state of a viscous liquid, there is no entanglement of polymers and interface fails at the level of *PEG* layer. Nevertheless, these results are based on qualitative tests and quantitative measurements are needed to confirm this assumption.

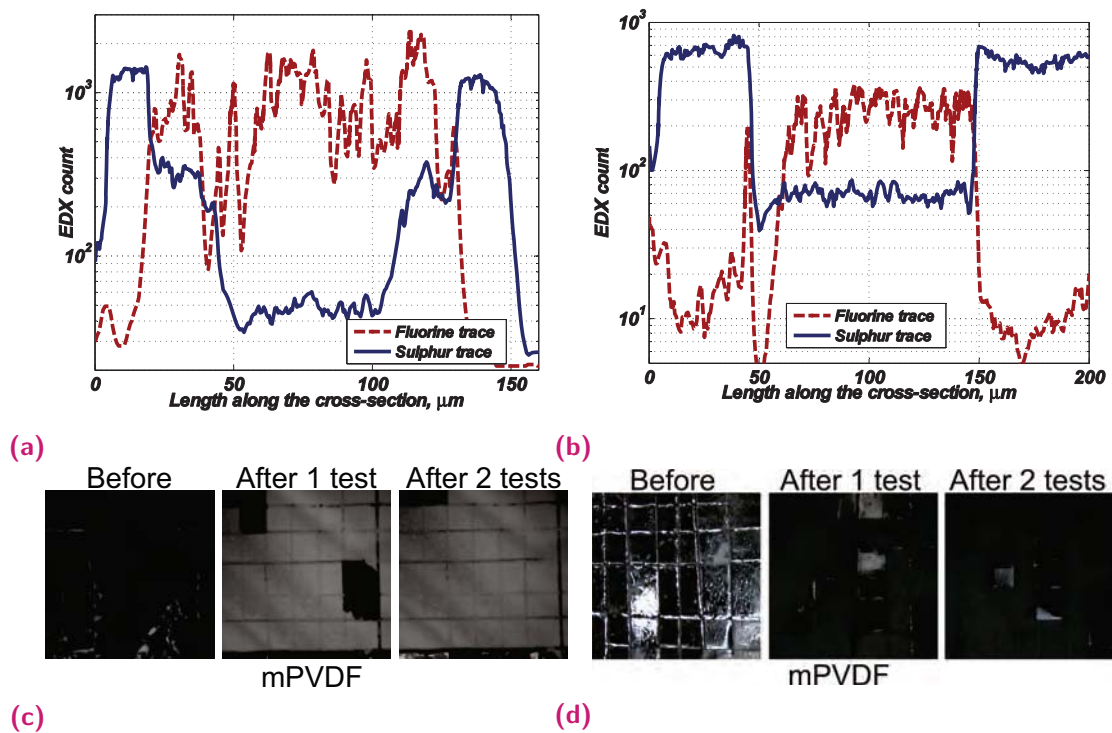


Fig. 3.14. EDX line scans for fluorine (red) and sulphur (blue) traces along the cross-section of the trilayers PEDOT:PSS/PVDF-graft-PEG/PEDOT:PSS (a)-(b) and adhesion tests of the PEDOT:PSS film deposited on the rough side of the functionalized membrane (c)-(d) For (a) and (c) PEDOT:PSS is secondary doped with 2 vol% PEG400, for (b) and (d) with 5 vol% PEG400.

3.4 Comments on infiltration of PEDOT:PSS

As mentioned previously, sufficiently low surface tension (γ_{Lc}) of the solution causes the wetting (WCA of 0°) of the hydrophobic membrane and the liquid penetrates into the membrane pores [111]. This process is mainly influenced by the pressure difference across the membrane and can be described by the Laplace equation:

$$\Delta P = -\frac{2B\gamma_{Lc}\cos\Theta}{r_{max}} \quad (3.2)$$

where ΔP is a liquid entry pressure (LEP) - maximum liquid feed pressure a membrane can withstand without getting wet. Θ is a contact angle between the membrane and the liquid and B and r_{max} are the pore geometry coefficient (1 for cylindrical pores) and the maximum pore size respectively. For PVDF membrane (pore size $0.22 \mu m$) the mean¹³ wetting surface tension is about $34 mN/m$ [121]. With the more simple method (Section A.3.2 we estimated that the critical surface tension of the PVDF membranes we used ($0.1 \mu m$) is also about $35 mN/m$. Nevertheless, the value of the critical surface tension was shown to be largely influenced by the composition of the solution. It depends on both, the class of organic solutes and on their molecular weight [111, 121, 184]. For example, a higher critical surface tension was measured for the

¹³ Calculated using several different water/alcohol solutions. The liquid surface tension was varied by changing the alcohol-water molar ratio [121]

carboxylic acid solution in comparison to the water-alcohol mixtures for the same membranes. Moreover, the molecular weight of the molecule and its concentration also matter. Larger molecular weights and larger concentrations increase the γ_{Lc} (or lower critical entry pressure). The effect of infiltration when surface tension is decreased was observed when surfactants (discussed later) or butanol were added to solution (Fig. 3.7).

Surfactants adsorb on the surface only if their concentration in the solution is above the critical micelles concentration (cmc)¹⁴. The dynamics of spreading of the complex solutions, *i.e.* with polymers and surfactants, is important for painting and coating applications but are not yet well studied [35]. The major process determining the spreading of an aqueous surfactant solution on hydrophobic surface and its penetration into porous media is the adsorption of surfactant molecules onto a surface in front of the moving three-phase contact line (solution, solid, air). Subsequently the surface in front of the drop is partially hydrophilised and causes spontaneous spreading [219, 246]. This phenomenon is known as autophilic effect [210, 268] but exact mechanism of how a surfactant molecule is transferred in front of the moving three-phase contact line is debatable. Moreover, the mechanisms behind slow spreading that would follow autophilization are also under investigation (reviewed by [219, 268]).

The spreading and imbibition of surfactant solution in porous media follows the same principles [219]. Surfactants such as *Tween-20*, cover the entire membrane surface and even when the membrane is previously fouled with proteins [246, 282]. In fact preferential adsorption of surfactants from the solution was observed when performing filtration of protein solutions [255, 282] and also during oil/water separation [203]. In addition to the physiochemical properties of the solid and the surfactant, the process in this case is also dependent on the pore size [352] and roughness in the meso and nanoscales [239].

The cmc of *Triton-X100* is 0.22 – 0.24 mM . In our experiments much higher concentration of 17 mM was used, therefore it can be assumed that large amount of surfactant micelles in solution are available for adsorption. The effect of surfactants on infiltration of *PEDOT:PSS* aqueous solutions in the hydrophobic *PVDF* membranes was shown in Section 3.2.3. Nevertheless, our study case is more complex than previously reported. In addition to surfactant, *PEDOT:PSS* makes the solution a non-Newtonian fluid [140, 141]. Furthermore, the evaporation of the solvent also influences wetting and spreading [35] rates. Therefore, only a few observations will be presented without an attempt to provide a consistent explanation. The understanding and modelling of transport phenomenon of such a complex solutions merits further investigation.

In addition to the penetration of liquids described by Laplace equation and imbibition driven by surfactant adsorption, a third process needs to be introduced in order to better understand the infiltration observed in our previous experiments. That is the capillary flow driven by the hydrophobic interactions. It is mostly studied in the context of oil/water separation. Separation of solution using porous membranes is a widely

¹⁴ cmc is a concentration of surfactants above which micelles form. Addition of surfactant above cmc only increase the number of micelles and does not significantly change the surface tension.

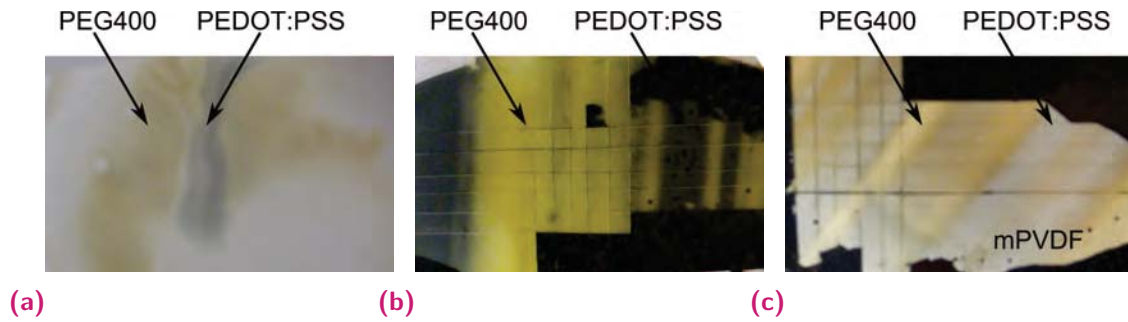


Fig. 3.15. (a) Back side of the membrane 24 hours after deposition of pegPEDOT (with 5 vol% PEG400). Penetrated PEG400 is visible as yellow and PEDOT:PSS as black marks. (b) PEDOT:PSS/pPVDF/PEDOT:PSS (with 5 vol% PEG400) trilayer after upper PEDOT:PSS layer is removed. The part of the PVDF membrane filled with mainly PEG400 is visible in yellow, part infiltrated with PEDOT:PSS is visible as black. (c) PEDOT:PSS/mPVDF/PEDOT:PSS (with 2 vol% PEG400) trilayer after upper PEDOT:PSS layer is removed. Yellowish surface shows mainly PEG400 on the PVDF (pores not completely filled - membrane is not translucent), black areas probably correspond to PEDOT:PSS infiltrated mPVDF.

used practice. In most of the cases, water is recovered as a permeate and molecules of a certain size remain on the surface of the membrane or adsorbed on the pores [299]. Nevertheless, hydrophobic membranes can also be used for selective oil/water emulsion separation by absorbing hydrophobic liquid [227]. When hydrophobic membrane is exposed to water/oil mixture, oil droplets attach to the membrane surface. Depending on the physiochemical properties of both, the membrane and the solution, the droplets can then de-attach or penetrate into the membrane pores due to capillary forces [203]. If large amounts of oil are accumulated on the surface, their flow can even be described by Hagen-Poiseuille equation¹⁵ [203]:

$$J = \frac{\epsilon \Delta p r^2}{8 \tau \mu \sigma} \quad (3.3)$$

where J is the permeation flux, Δp is the pressure drop across the membrane, ϵ , r , τ , σ are the membrane porosity, largest pore size, tortuosity and thickness respectively. Even though PEG is not a very hydrophobic molecule, it has amphiphilic properties that drives its adsorption on hydrophobic surfaces [42, 357, 418]. In a way, hydrophobic capillary infiltration could be observed when large excess of PEG was used in PEDOT:PSS solutions (5 vol% discussed in Section 3.3.2). Pores could be completely impregnated with PEG, preventing even PEDOT:PSS to diffuse into. In Fig. 3.15b, taken after PEDOT:PSS upper layer was removed from the PVDF surface as discussed in Section 3.3.2, the yellow areas seen on the membrane correspond to mainly PEG in the membrane pores, while darker areas show presence of PEDOT:PSS. The amount of PEDOT:PSS along the cross-section at that part was not estimated. Furthermore, larger amount of PEG penetrated through the membrane is seen in Fig. 3.15a. Images suggest that PEG is being adsorbed on the surface of the membrane before PEDOT:PSS. The presence of PEDOT:PSS in the pores filled with PEG could then be the consequence of the solubility of PEDOT:PSS in PEG.

¹⁵ used to determine the pressure drop of a constant viscosity fluid exhibiting laminar flow through a rigid pipe

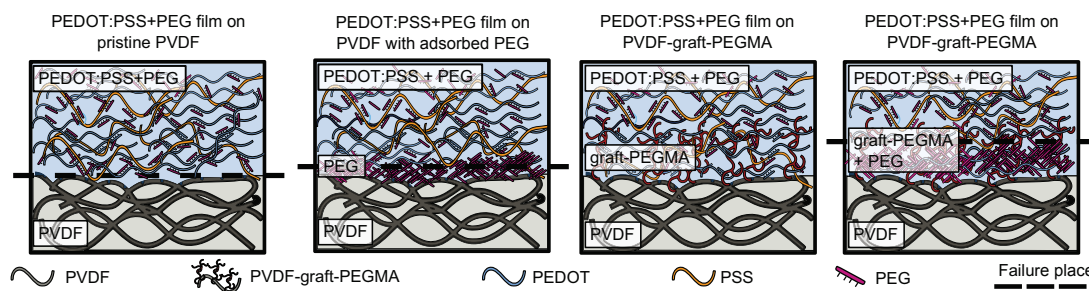


Fig. 3.16. Schematic drawing of different *PVDF* functionalisation methods and their influence on adhesion with *PEDOT:PSS*

3.5 Conclusion

A summary of these results is represented in Fig. C.16. We showed that direct mechanical interlocking that is a result of infiltrated and solidified *PEDOT:PSS* film in the pores of the membrane is one of the ways to ensure good adhesion between those two materials. Another way to join *PEDOT:PSS* and *PVDF* was shown to be hydrophilization of *PVDF* surface by *graft-PEGMA*. Adhesion just by entanglement or hydrogen bonding with graft-polymer (as was tested on a smooth substrate) is strong enough to pass adhesive tape test in a dry state. In case of porous substrate, it allows infiltration of *PEDOT:PSS* in the pores of the membrane. Furthermore, in this case only a few micrometers of mixing depth are needed for strong adhesion. We also showed that in both cases, mechanical interlocking and graft-functionalization, proximate interaction between materials need to be ensured. Water, or any other mobile coating in between two materials-to-be-joined lead to facile delamination. In these conditions, neither infiltration through the membrane nor *PVDF-graft-PEGMA* aid the adhesion.

Both, adhesion and mass transport through hydrophobic membranes is influenced by the physiochemical properties of materials. Therefore, both processes need to be taken into account when designing bilayer or trilayer structures with membranes. The infiltration of the aqueous polymer solution into the membrane pores occur on hydrophilic membranes, when surface tension of the solution is low enough or when oily, hydrophobic materials are used. This limits the choice of the secondary dopants - surfactants and even slightly hydrophobic molecules are likely to cause infiltration of *PEDOT:PSS*.

3.5.1 Future work

- Understanding adhesion between materials as well as wetting and spreading of solutions is an ongoing research topic with many unanswered questions [35, 161]. Materials that are needed for our purpose bring even larger complexity to the system. First of all, many factors influencing adhesion, *i.e.* roughness, mechanical interlocking, are debatable. It is not surprising, that quantitative data regarding adhesion on membranes is not yet available. Nevertheless, the growing membrane technology requires possibilities to strongly attach other materials on their surface and it becomes essential to better understand the interactions at

their interface. Therefore, methods to quantify the adhesion on the membrane as a substrate need to be developed and validated. Then, the influence of surface morphologies (such as we have in case of *pPVDF*) could be studied and explained.

- We were using functionalized membranes, whose exact surface structure (branching of graft-polymer, cross-polymerization *etc.*) is unknown. Furthermore, we did not provide the mechanism that would explain improved adhesion between *PEDOT:PSS* and *graft-PEGMA*. Hydrogen bonding, interdiffusion of polymer chains, entanglement of polymers possibly have a different importance in creating strong interfaces. Explaining these processes at the interface would be notable for the choice of the graft-process conditions. By tuning the polymer grafting, needed morphology could be obtained further improving the adhesion between the materials.
- It was mentioned that there are several mechanisms for the failure of the interface. In our case, mostly breakdown of the polymer film, leaving part of *PEDOT:PSS* in the pores was observed. When *PVDF-graft-PEGMA* was used some *PEDOT:PSS* could remain on the surface (noticeably darker areas) and in this case, it could be due to both chain pullout or crazing. Nevertheless, the surfaces of the materials after the adhesion tests were not investigated thoroughly. Therefore, the failure mechanisms remain unknown. Understanding the interface failure mechanisms could be another way to improve the adhesion strength between the materials.
- Another important factor that was not discussed in this chapter is the influence of the mechanical properties of the *PEDOT:PSS* on the adhesion. We mentioned that adding secondary dopants change the mechanical properties. Brittle fracture of *PEDOT:PSS* could be observed when butanol, ethylene glycol and *PEG400* (after thermal annealing) was used. Nevertheless, in other cases, removal square-by-square was observed showing more plastic behaviour. Finally, when excess of *PEG400* was used (5 vol%) *PEDOT:PSS* film was not well formed and it could be easily removed by scratching. Conditions separating influence of the mechanical properties and the additives to *PEDOT:PSS* was not separated, *i.e.* it remains unanswered if having a *PEG* layer at the interface, but well interconnected and plastic *PEDOT:PSS* film mechanically interlocked in the pores of the membrane, would cause delamination.
- Finally, spreading and wetting of complex liquids such as polymer solution with surfactants is even a less studied process. Only surfactants in aqueous solution or only non-Newtonian fluid (such as *PEDOT:PSS* aqueous solution) already pose a debate in understanding the mechanism of spreading. Having mixture of both, makes the system hardly predictable. Here we presented several cases of the *PEDOT:PSS* mixtures used on the *PVDF* membrane. We also shortly discussed possible mechanisms leading to its spreading and infiltration in the pores. Nevertheless, our observations create more questions than answers. A great extend of work still needs to be done in order to fully understand the kinetics and dynamics of the processes causing infiltration of complex fluids in the membranes. More-

over, even more research is needed in order to establish methods for controlling such processes.

PEDOT:PSS/mPVDF/ionic liquid actuators

Contents

4.1	Introduction	60
4.1.1	Volume change in the conducting polymer based actuators	61
4.1.2	PEDOT:PSS in ionic liquid	64
4.2	Fabrication	64
4.2.1	State-of-the-art	64
4.2.2	PEDOT:PSS/mPVDF/PEDOT:PSS actuators by drop casting	66
4.3	Characterization of PEDOT:PSS based actuators	68
4.3.1	Long time performance	73
4.4	The importance of a good adhesion	76
4.4.1	Lifetime	76
4.4.2	Performance	78
4.5	Influence of the mixing depth on actuators performance	79
4.6	Towards actuator performance improvement by altering <i>PEDOT:PSS</i>	83
4.6.1	Post-treatment of PEDOT:PSS	84
4.7	Conclusions	87
4.7.1	Future work	88

Compared to other kinds of artificial muscles, conducting polymer actuators (CPAs) have fair advantage in biomedical applications or when continuous position control is needed [345]. Generally, they are fast to respond (in seconds), require low voltages (up to 2 V), they are lightweight and compliant. As was shown in *Chapter 1 Fig. 1.1a*, they can produce large stain and stress and work in electrolytes or biological fluids [76, 150]. CPAs can be exploited as free-standing (single film submerged in liquid electrolyte) or bilayer and trilayer actuators. In the free-standing polymer films, volumetric expansion can be measured directly [261], and out-of-plane strain is usually used to characterize the process. Nevertheless, for practical applications bending actuators are usually used that take advantage of much higher in-plane strains¹. In order to achieve bending motion, an electromechanically active conducting polymer is laminated with an inactive substrate creating bilayer or trilayer structures. During volumetric expansion of the polymer, stress gradient is generated at the interface subsequently leading to bending. Bilayer structures are the most often studied, but as their operation requires a counter

¹Highest reported CPAs strain (in-plane) of 33.5 % were measured of a free-standing polypyrrole film immersed in LiTFSI/PC/H₂O solution [135, 136]

electrode, trilayer devices are more suitable for applications². In our work, only trilayer CPAs will be discussed.

Actuators performance largely depends on the mechanical properties of the passive layer in between the electrodes. Various materials could be used for that purpose such as flexible solid films, porous membranes [117, 171, 368, 369], soft gels or polymer electrolytes [61, 105, 295, 327, 422]. Another advantage of the trilayer actuator structures is that the passive support could be used as an electrolyte storing layer (membranes impregnated with the liquid), that subsequently allows actuation in air³. In addition to the mechanical flexibility, the passive layer should provide good adhesion, good ionic conductivity and prevent percolation of the electrodes. Therefore, the hybrid membranes developed as described in the previous chapter are expected to have advantage compared to conventional polyvinylidene fluoride (PVDF) membranes.

In this chapter we will firstly introduce the working principle of the conducting polymer based actuators. The mechanism of the electro-chemo-mechanical actuation of the polypyrrole (PPy) based actuators is already extensively studied. That is not the case for poly(3,4-ethylenedioxythiophene) polystyrene sulfonate (PEDOT:PSS) based actuators. Therefore, we will introduce and characterise performance of the CPAs using the experimental results obtained with PEDOT:PSS trilayer actuators in 1-ethyl-3-methylimidazolium bis(trifluoromethanesulfonyl)imide (*emimTFSI*) ionic liquid. In the second part of the chapter, we will also show the importance of the good adhesion to the lifetime and performance of the actuators. Finally, in the last part of the chapter we will demonstrate the amendment to our fabrication method that could significantly improve the performance of the actuator in terms of strain, speed and creep.

4.1 Introduction

The use of the polyacetylene and polyaniline (PANi) for actuators, especially having in mind biomedical applications is rather limited⁴. Polypyrrole is probably the most used conducting polymer for applications in CPAs. During oxidation it can produce volumetric swelling of typically 2 – 3% that can subsequently produce mechanical work. Compared to others, polypyrrole based actuators produce largest displacements and forces [116, 369] and maximum electrochemical strains of up to 29% [135, 136]. Factors influencing the performance of PPy based actuators are also well understood. Despite the complexity, several electro-chemo-mechanical actuation models were developed [92, 289] leading to sophisticated feed-forward [391, 392] and feed-back [406] based control attempts.

²In trilayer configuration, working-electrode is connected to one side of a film and counter-electrode to another. The electric potential leads to the simultaneous oxidation and reduction of two sides.

³Due to the solvent evaporation, conventional electrolytes were reported to limit the lifetime of the devices, therefore more and more often they are being replaced by ionic liquids (ILs) [13, 29, 89, 243, 386]. ILs are the salts of the large, poorly coordinated ions that are in a liquid state below 100°C or at room temperature. As we are also interested in 'in-air' applications, all the measurements reported in this chapter were done using room temperature ionic liquid.

⁴Conductivity of the polyacetylene is unstable in air and PANi is electroactive in only acidic solutions [347].

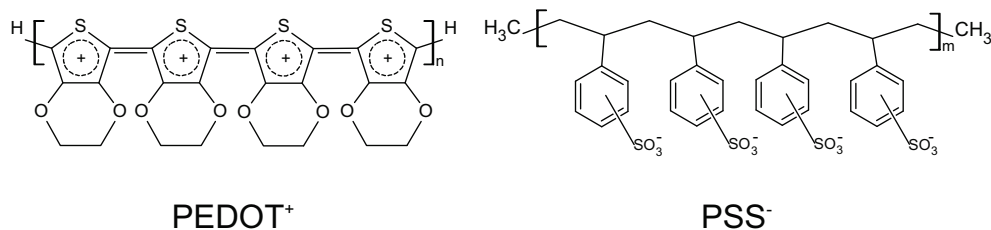


Fig. 4.1. Chemical structure of poly(3,4-ethylenedioxythiophene) (*PEDOT*) and polystyrene sulfonate (*PSS*)

The main disadvantage of polypyrrole as an electrode material is its electrical conductivity, that decreases by 2 – 3 orders of magnitude in the reduced state. That means that only small part of the film can be active (as over-reduction is irreversible) and electrochemical creep during actuation is expectable [171]. Furthermore, *PPy* films are usually very rigid leading to low ion diffusion speed and slow actuation rates [296, 369]. Therefore, use of polythiophene derivatives as electrodes is now considered.

The chemical formula of poly(3,4-ethylenedioxythiophene) (*PEDOT*) and one of its possible counterions - polystyrene sulfonate (*PSS*) are shown in *Fig. 4.1*. The performance of the actuators based on *PEDOT* in comparison to *PPy* are still hard to make. Significantly less research is done in order to optimise its synthesis (except [183]) and doping conditions for applications in *CPAs*. Nevertheless, similar strains and strain rates are expected [369]. *PEDOT* is a well known polymer for its chemical, electrochemical (in doped state) and thermal stability as well as for its high electrical conductivity that could reach up to 2000 Scm^{-1} [263]. Furthermore, when doped with the immobile anions (*DBS*, *PSS*, *etc.*) its softness and porosity lead to a better ion diffusion and consequently faster actuation [296, 369, 411]. Therefore, *PEDOT* could eventually emerge as an advantageous alternative to conventional *CPAs* electrodes.

4.1.1 Volume change in the conducting polymer based actuators

The use of the conducting polymers as actuators is based on the linear dimensional changes during their electrochemical doping and dedoping process, *i.e.* the change of the polymer oxidation state is balanced by the flux of ions from the electrolyte leading to the volume changes. There are several simultaneous and subsequent processes involved in changing the electrochemical state of the conjugated polymer as illustrated in *Fig. 4.2a*. They could be split into: (1) the charge and (2) mass transport (*Fig. 4.2a*) and (3) the conformational changes of the polymer (*Fig. 4.2b*). Nevertheless, the sequence of the events is convoluted and still debatable. For example the charge transfer in the polymer happens only if the counter-ion is present to balance it. At the same time, conformational changes of the polymer, altered by the change in the electronic structure, are needed in order to create free space for the ion ingress. These processes will be further discussed assuming that they are non-instantaneous.

Charge transport

In its oxidised state (such as created during the synthesis), *PEDOT:PSS* is heavily p-

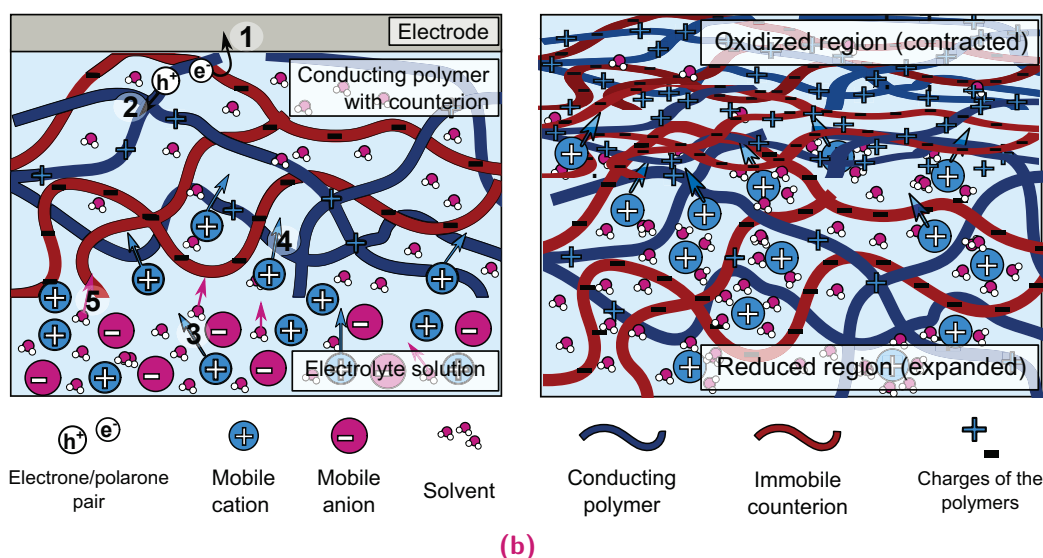


Fig. 4.2. (a) Schematic illustration of the basic processes that are taking place during the volumetric expansion. ① electrons are removed from the polymer chain; ② created polarons are propagating along the polymer chains and created polymer conformation changes; ③-④ cations move through the electrolyte, across the interface and between polymer chains and also opens channels in the polymer, ⑤ if present, solvent molecules can enter the polymer film as a solvation shell of the ions or due to the osmotic pressure. (b) The polymer structure in the oxidized and reduced states. Due to the net charge induced conformation changes and due to the presence of the ions and the solvent, the reduced state is more open. On the other hand, oxidized state is more compact, contains less water and impedes ions mobility.

doped⁵ and the charge is delocalized along the conjugated π bonds (Fig. 4.1) making the polymer electrically conductive⁶. Both, the charge in the polymer backbone and the induced lattice distortion, named polarons or bipolarons⁷, are participating in the charge transfer process by both drift (also known as migration, due to an electric field) and diffusion (due to a concentration gradient) [393] (① in Fig. 4.2a).

The intrinsic conductivity represents the conduction process along a conjugated chain. Nevertheless, macroscopic charge transport in *PEDOT:PSS* films requires 'hopping' between polymer chains that is usually a rate limiting step. Because of this, the composition and the morphology of the polymer film might have a significant influence on the charge transfer (will be shortly discussed later in Chapter 5) [97]. Furthermore, as the electronic structure of the polymer is altered the polymer backbones undergoes conformational changes (Fig. 4.2b) [52, 234, 297] that can also influence the conductivity of the film.

Mass transport

Ion transport is considered to be the dominant factor responsible for the volume changes

⁵one positive charge per 3-4 thiophene rings

⁶The electrical conductivity of the uncharged conducting polymer is 10 – 12 orders of magnitude lower than charged, therefore it is important to ensure that the polymer is not over-reduced. When electric field is applied, the polymer chains become only slightly more or less oxidized, but remain positively charged. Over-reduction would create irreversibly insulating films.

⁷Singly charged cation radicals at the polymer chain coupled with local deformations and two charged defects that usually exist at higher charging levels.

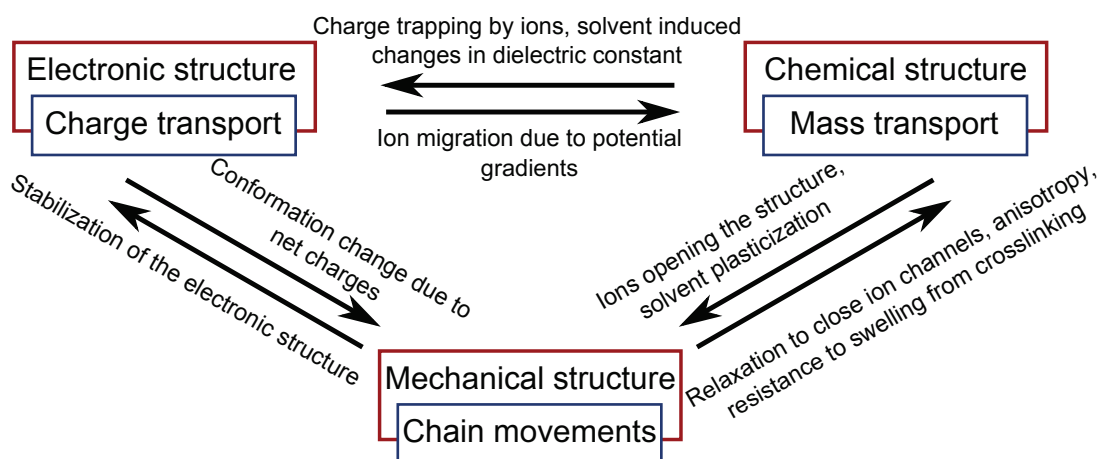


Fig. 4.3. Illustration of the interrelations between the processes during the actuation. After the synthesis and deposition, polymers have different mechanical, chemical and electrical properties. These properties are further altered by the electrical signal and lead to the change of the oxidation state. This subsequently results in particular strain, stress, expansion speed and efficiency. *Adapted from [316].*

in the conducting polymers. During the redox process, ions from the electrolyte or the ionic liquid cross the interface and drift (dominant process) or diffuse through the polymer film in order to maintain the charge neutrality (*Fig. 4.2a*). A more complete volumetric expansion mechanism needs to take into account the doping of the conducting polymer, the size and mobility of the anion and cation in the electrolyte and the solvent [119]. This leads to three expansion possibilities: (1) if the cation is large and unable to enter polymer film, during oxidation the anion will move to balance the charge causing expansion. Nevertheless, if (2) polymer is doped with a large immobile anion, cation will move to balance the charge and the film will expand during reduction. In case when both ions have a comparable mobility, 'salt draining' can occur, *i.e.* the neutral pairs of ions could form and move out from the polymer, leading to a decrease of expansion [343].

Ions in the electrolyte are usually solvated and their actual volume and mobility depend on the solvation shell. Therefore some kind of the solvent can be critical in determining the mobile species. Furthermore, osmotic effects, that lead to solvent molecules moving in and out of the polymer (5) in *Fig. 4.2a*) were also shown to play significant role in actuation [26].

Polymer conformation changes

Finally, even though the flux of ions to and from the material is considered to be the primary mechanism for producing deformation, conformational changes in the polymer could also play a role [52]. Those changes are mostly related to the reconfigured carbon-carbon bond length and angle, electrostatic repulsions between the chains because of the net charges and the stretch of the polymer chains by inserted ion and solvent molecules [297, 296].

To sum up, *Fig. 4.3* represents some of the relations between the charge, mass transport and the conformational chain movements. These processes dependent on the material

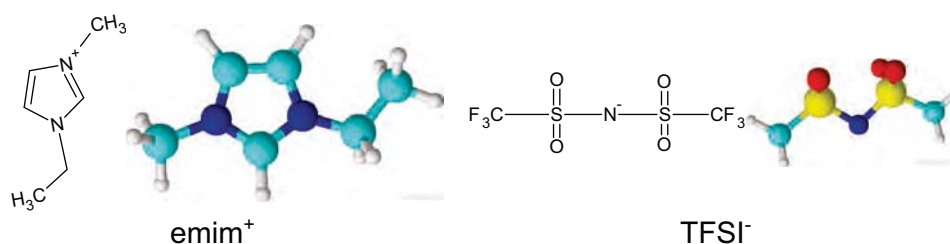


Fig. 4.4. Chemical and 3D structures of the ionic liquid 1-Ethyl-3-methylimidazolium bis(trifluoromethanesulfonyl)imide (*emimTFSI*)

properties, actuation and cycling conditions and affect the performance of the actuators in terms of strain, speed, stress and efficiency in a complex and still not fully understood way.

4.1.2 PEDOT:PSS in ionic liquid

In our work we are using *PEDOT* that is doped with large immobile anion (*PSS*) during its synthesis (chemical structures are shown in *Fig. 4.1*). Furthermore, we will only consider the actuation in air achieved by using ionic liquid (*emimTFSI*) as the mobile ions (*Fig. 4.4*). In this case the ideal process during doping/dedoping cycling is redox of the $PEDOT^+$ and the ingress and egress of $emim^+$:



Nevertheless, as in the ionic liquid anion and cation and relatively similar in size, *i.e.* the volume of the *emim* and *TFSI* are 157.66 \AA^3 and 224.39 \AA^3 respectively [112] egress of both ions can occur simultaneously [369]:



The dominant process will eventually depend on the polymer properties, *i.e.* its material and structure, geometry, electrolyte, as well as on the cycling conditions, cycling history and the environment.

4.2 Fabrication

4.2.1 State-of-the-art

Due to the low solubility of the conducting polymers, they have to be synthesized directly on the substrate in order to produce *CPAs*⁸. Only the surfactant-stabilised aqueous solutions of the polyaniline nanofibers [242] and *PEDOT:PSS* are feasible. Compared to the chemical synthesis, electropolymerisation is preferred as it is a better controlled

⁸The earliest fabrication attempts were mostly developed using lamination or gluing of a free-standing conducting polymer film to the substrate. Nevertheless, in this case, the strong proximity required for the strong interface between materials is hard to ensure leading to a lifetime of a few cycles. Gluing layers create additional barrier at the interface that might drastically increase the resistance of the ion transfer across the interface

process that leads to a better quality and conductivity of the polymer. Subsequently, actuators fabricated with the electropolymerized electrodes were shown to lead to significantly better actuation strains [116].

Electropolymerization requires a conducting substrate. It can be provided in two ways: (1) deposition of a thin conductive metal layer, *e.g.* gold or platinum, on the membrane ([117, 147, 350] *etc.*) or (2) chemical synthesis of a thin *PPy* or *PEDOT* layer on the membrane [368, 369]. In addition to providing a substrate, the metal layer between the membrane and conducting polymer also ensures good and stable electrical conductivity and low voltage drop along the electrode. Nevertheless, the metal - polymer interface is often very weak and does not sustain mechanical cycling [241]. On the other hand, during the chemical synthesis of the *PPy* or *PEDOT*, an interfacial layer between the membrane and the polymer is created ensuring the good adhesion. The interaction between the chemically and electrochemically synthesized layers was also shown to be stable [369, 411]. Nevertheless, chemical synthesis is harder to control and might lead to percolation of electrodes and occasional short circuits [104].

Chemically synthesized *CPAs* were also reported, such as *PPy* synthesized on polyurethane [61] or on silk fibroin [322]. Nevertheless, actuators were poorly performing in terms of the lifetime and strain. The most established technique employing chemically synthesized conducting polymers was suggested by Vidal *et al.*, who used interpenetrated polymer networks (*IPNs*) as a matrix for polymerisation reaction. Like that, *PEDOT* is gradually distributed along the *IPNs* leading to the pseudotrilayer actuators that are stable for millions of cycles [104, 105, 310, 311, 385, 386]. Nevertheless, too large amounts of conducting polymer lead to large currents between electrodes or even non-functional devices [104].

PEDOT:PSS

Chemically synthesized *PEDOT* doped with *PSS* forms the gelled particles that are dispersible in water. Therefore, several solution based *CPAs* fabrication methods were suggested. The first *PEDOT:PSS* trilayer bending actuator produced by simple casting of *PEDOT:PSS* commercially available solution was reported by Ikushima *et al.* [148]. They ensured good adhesion between *PVDF* and *PEDOT:PSS* by modifying the *PVDF* membrane and using *PEO* as a secondary dopant. Fabricated micro autofocus lenses were able to lift weight of 24 *mg* for millions of cycles. Similarly, Kim *et al.*, deposited *PEDOT:PSS* on freeze-dried bacterial cellulose by dipping and drying [193] and Okuzaki *et al.*, used polyurethane/ionic liquid composite membranes with sticky *PEDOT:PSS/xylitol* to produce actuators by simple drop-casting [228, 295].

Despite the advantages provided by a simple processability of *PEDOT:PSS*, the maximum produced strain of casted *CPAs* is less than 0.3% [295]. This is at least 10 times lower than that of other conductive polymer based actuators. One of the explanation to this poor performance could be the electrochemical stability of *PEDOT:PSS*. In comparison to *PPy* actuators that are usually driven by less than 1 *V*, voltages higher than 1.5 *V* are required to observe signs of reduction [295]. Even then, it is suggested that the actuation is based on the double layer charging rather than the redox reaction. On the other hand, membranes used for such fabrication have significantly lower ionic conductivity

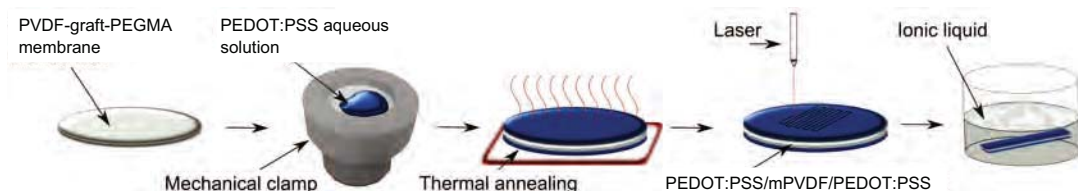


Fig. 4.5. Illustration of a fabrication process flow for a solvent casted actuators. Hybrid *PVDF-graft-PEGMA* (*mPVDF*) membranes are clamped mechanically in an aluminium holder and *PEDOT:PSS* aqueous solution (secondary doped) is deposited by drop-casting. After drying at room temperature, the clamp is reversed and the procedure is repeated for the another side of the actuator in order to produce the trilayer. Membrane with *PEDOT:PSS* on both sides is then dried in the oven at 70°C for 2 hours. 1.5 mm x 2 cm rectangular actuators are then cut by a laser, actuators are thermally annealed at 120°C (not shown) and are incubated in ionic liquid for 10 – 120 minutes.

that also influences the performance. For example, the ionic conductivity of *emimTFSI* in *PVDF* is 19.4 mS/cm while in polyurethane is significantly lower, 0.9 μS/cm [295, 369]. Therefore, it is likely that the performance can be significantly improved if *PVDF* membranes are used with the same electrodes.

4.2.2 PEDOT:PSS/mPVDF/PEDOT:PSS actuators by drop casting

A schematic illustration of the process that we used for the fabrication of the actuators with the hybrid *PVDF/PVDF-graft-PEGMA* membranes is shown in Fig. 4.5. In most of the cases (unless indicated differently) functionalized *PVDF* membranes were used with spraying density (*SD*) of $0.9 \pm 0.1 \text{ ng/mm}^2$ and grafting density (*GD*) of $0.14 \pm 0.02 \text{ ng/mm}^2$ produced as specified in Section A.4.1. This corresponds to the width of an hydrophilic part of about 20 μm and 40 μm for the smooth and the rough side respectively, as shown in Fig. 4.6. After preparation, membranes were dried and fixed in a ∅45 mm aluminium clamp in order to hold the stress caused by drying of *PEDOT:PSS*. 3 ml of 1.3 wt% aqueous solution of *PEDOT:PSS* was then drop casted on the membrane. In order to increase its electrical conductivity and mechanical properties prior to the deposition, *PEDOT:PSS* was secondarily doped with 1 vol% poly(ethylene glycol) of *Mr* – 400 (*PEG400*) (unless indicated differently). Membranes with solvent casted *PEDOT:PSS* were then dried at clean-room temperature (20°C) and humidity in UV limited environment for at least 12 hours. This procedure was then repeated for the other side in order to obtain trilayers. Finally, in order to decrease the amount of residual water, membranes were then dried for 2 hours at 70°C.

Actuator were cut into 2 mm x 1.5 cm rectangles by CO₂ laser and each was thermally annealed at 120°C for 2 hours. Before each measurement, actuators were kept in *emimTFSI* ionic liquid for 3 – 120 minutes. About 20 actuators were cut from one membrane, 8 from half of the membrane (when post treatment conditions were tested). One actuator from each batch was taken and broken under liquid nitrogen for mixing depth measurements, others were used for electrochemical, and electromechanical characterization (Appendix A.4.2).

Structure of the actuator

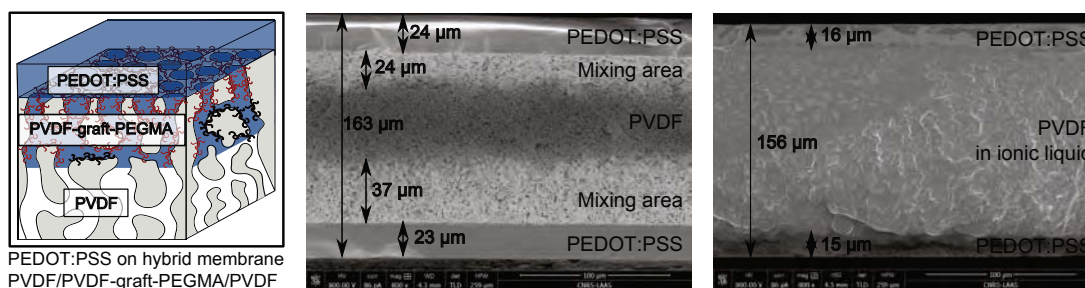


Fig. 4.6. Scheme of the interface and the mixing depth (penetration depth) of *PEDOT:PSS* and *PVDF-graft-PEGMA* and the *SEM* images of the cross-sections of the *PEDOT:PSS/mPVDF/PEDOT:PSS* trilayers before the immersion in the ionic liquid and after the immersion (2 hours). Different actuators fabricated on the membranes with $GD - 0.22 \pm 0.03$ were used for the measurements.

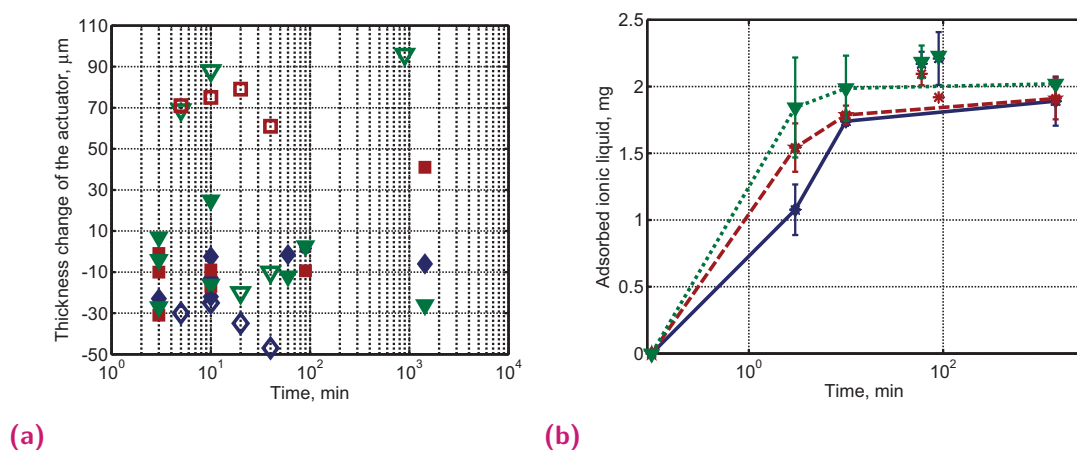


Fig. 4.7. (a) Difference of the thickness of the actuators and (b) increase in the actuators weight after different times of incubation in *emimTFSI*. Actuators produced on the membranes with GD 0.16 ± 0.003 , 0.11 ± 0.002 and 0.046 ± 0.018 ng/mm^2 were corresponding to mixing depths of $< 5 \mu m$ (green dotted line), $30 \mu m$ (blue line) and $25 \mu m$ (red dashed line) respectively. Thickness measurements done after incubation in *ILs* and 5 mins cycling with 2 V square wave at 200 *mHz* are indicated with open markers.

scanning electron microscopy (*SEM*) images of the cross-sections of a typical actuator before immersion in ionic liquid and after are shown in *Fig. 4.6*. The thickness of *PEDOT:PSS* electrodes outside the membrane depends on the mixing depth and *PEDOT:PSS* density and larger mixing depth leads to thinner electrodes. When needed for calculations, the thickness of the actuators and electrodes in a dry state estimated from *SEM* images was used.

Interestingly, once immersed in ionic liquid, the thickness of the trilayer decreases as shown in *Fig. 4.6*. A noticeable decrease is also observed for *PEDOT:PSS* electrodes. A thickness decrease was also measured by mechanical profilometer (as in *Section A.4.2*) as shown in *Fig. 4.7a*. Even though the error of the measurement is very high, negative change in the thickness of the actuator is observed in most of the cases.

The amount of the adsorbed ionic liquid is plotted in *Fig. 4.7b*. Ionic liquid is nearly immediately absorbed to *PVDF* and the weight of the actuator increases only slightly after more than 10 minutes. Adsorption rate seems to be influenced by the trilayer

structure: actuators with larger mixing depth (MD) (blue), adsorb less liquid than actuators with small MD in the same time. It indicates that ionic liquid is initially being adsorbed by *PVDF* membrane and not by *PEDOT:PSS* that is known to repel *ILs* [14]. As *PEDOT:PSS* fills the pores of *PVDF*, larger MD means smaller free volume of *PVDF* that can accommodate *emimTFSI*.

Nevertheless, it was observed that the thickness of the actuator is increasing after large incubations (more than 24 hours) as well as when actuators are cycled between the incubations. This could be explained as partial irreversibility of cycling and permanent accumulation of the ionic liquid in *PEDOT:PSS* [261] or as conformational changes of the *PEDOT:PSS* structure (also discussed in *Section 4.1.1*). Unfortunately, the method for the thickness measurement is not precise enough to draw any sophisticated conclusion.

4.3 Characterization of *PEDOT:PSS* based actuators

The processes involved in the volume changes in conducting polymers during their redox reactions are extensively studied. The most common studied polymer in this case is polypyrrole (*PPy*) secondarily doped with immobile anion (*DBS*) during its synthesis. Nevertheless, the ion transport and volume expansion of the *PEDOT:PSS* is barely studied. Even though it is expected to behave in a similar manner, slight differences might exist due to the different electrical and mechanical properties of the material. In the subsequent chapter, we will use current understanding of the actuation mechanisms of *PPy(DBS)* based actuators in order to explain the behaviour of *PEDOT:PSS* in ionic liquid.

Characterization measurements were mostly done with trilayer actuator (*PEDOT:PSS/mPVDF/PEDOT:PSS*) clamped at one end. The actuators were cycling by applying a potential waveform between two electrodes and the response was recorded by recording the video of the bending or by laser displacement sensor (*Section A.4.2*). The change in the displacement was then extracted from the video and is also shown in *Fig. 4.8a*. The transferred current was simultaneously measured and was used for calculations of the dissipated power (*Fig. 4.8b*) and transferred charge (*Fig. 4.9c*).

Strain

Using displacement and curvature in order to characterize the performance of the actuator is rather trivial as they do not take into account the dimensions of the actuators. Therefore, the actuators bending is more often expressed as strain. In the context of artificial muscles, strain is defined as a displacement normalized by the original material length in the direction of actuation [249]. It can be measured by direct means of free-standing polymer films⁹ or indirectly using bending beam theory. Sugino *et al.* suggested

⁹Due to their microstructure most of the polymers are anisotropic. Therefore, in-plane and out-of-plane strains can be used to characterize the expansion. Only in-plane strains cause the bending of the bilayer or trilayer structures

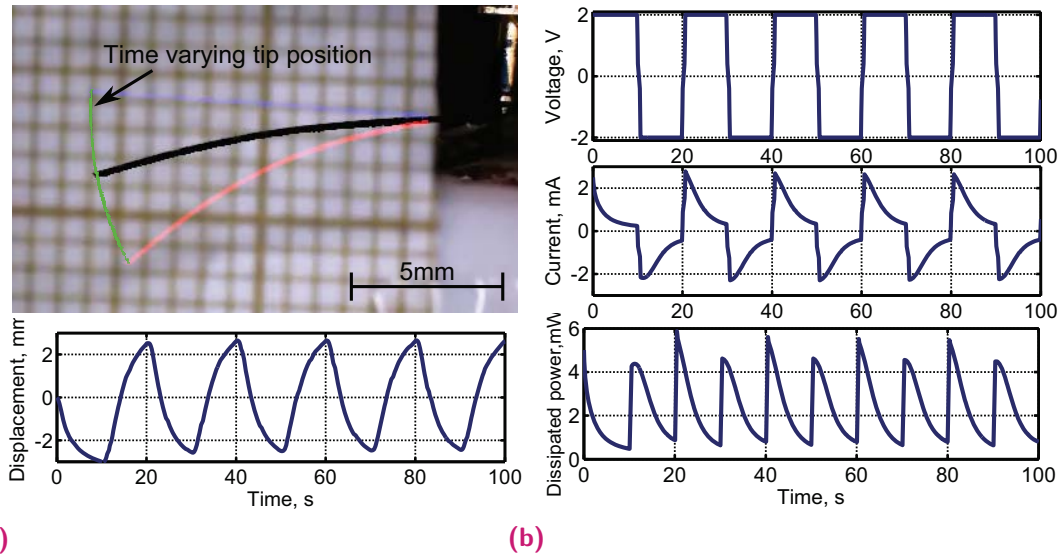


Fig. 4.8. (a) Merged images of the actuator at its extremities during actuation applying square wave with frequency of 50 mHz and 2.0 V amplitude. Blue and red actuators show its maximum and minimum displacement position, green dots show the tip position calculated from recorded videos. Actuator displacement profile in time is shown in the figure below. Actuator is bending towards the negative electrode. (b) Applied voltage, current and power dissipation measured during the actuation.

an equation to evaluate the difference in strain (ϵ) during bending of the actuator [356]:

$$\epsilon = \frac{2DW}{L^2 + D^2}, \quad (4.3)$$

where L , W are the length and the thickness of the actuator and D is the measured displacement. Even though it is based on a simplified geometrical model assuming low displacements, it is viable for our measurements.

Due to the mechanisms other than ion transport involved in volume expansion, irreversible expansion (creeping) is often observed. Irreversible expansion is indicated in *Fig. 4.9a* and will be discussed in *Section 4.3.1*. In our measurements we will mostly consider the "active strain" as the difference between the maximum peak strain and the following minimum strain of each voltage cycle (shown in *Fig. 4.9a* as $\Delta\epsilon_{max}$).

Strain rate

Another important characteristic of the actuator is its speed. A strain rate is one of the ways to express it. As shown in *Fig. 4.9a* it is the average change in strain per unit time during an actuator stroke [249]. Nevertheless, the strain rate expressed like this is highly dependent on the actuation frequency. The speed of the actuation is not constant and its bending significantly slows down once about 70% of the maximum strain is reached. Therefore, sometimes for comparison purposes we will be using the maximum speed of expansion that is calculated at each time interval ($\delta\epsilon/\delta t$ and shown in *Fig. 4.9b*).

PPy based actuators typically have strain rates of approximately $1\text{ \%}/\text{sec}$. The strain rate is mostly limited by how quickly ions can move through the polymer film. Therefore,

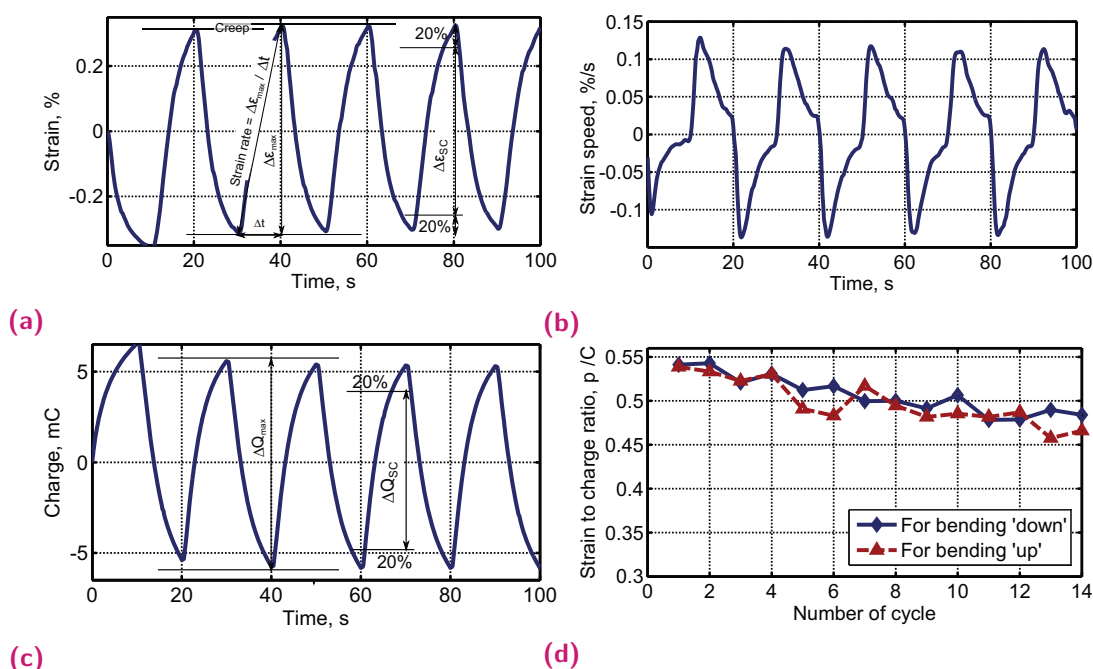


Fig. 4.9. (a) Actuator bending profile shown as calculated strain versus time. Strain is calculated using Equation 4.3 for every point detected during video processing. Min to max strain ($\Delta\epsilon_{max}$) is defined as strain difference between extremities during one actuation period (T), strain rate is a ratio of ($\Delta\epsilon_{max}$) and $T/2$. (b) The speed of the actuator is calculated at every point as $\delta\epsilon/\delta t$. (c) Transferred charge calculated from the measured current during the actuation. The measures are equivalent to (a). (d) Strain to charge ratio calculated for each period separately for an actuator moving towards the positive ('up') and negative ('down') electrodes. The $\Delta\epsilon_{SC}$ and ΔQ_{SC} used for calculation are shown in (a).

size of the ion, the microstructure of the polymer and history of the cycling have large influence on the speed of actuation [261, 316]. Another implication of the diffusion model is that it takes more time to diffuse deeper into the film and the full depth might not be reachable. Nevertheless the training the maximum expansion limit is usually not observed even for thin polymer films [261]. The strain and speed profiles of the prolonged actuation at 2–10 mHz that exhibit very slow expansion after 10 s are shown in Fig. B.3-B.4b.

Strain-to-charge ratio

In general the volume change of the actuator is directly proportional to the injected charge [250]:

$$\epsilon = \alpha \frac{Q}{V}, \quad (4.4)$$

where, ϵ is the strain, Q is the injected charge, α is the strain-to-charge density ratio and V is the volume of the polymer. A good CPA has a high strain-to-charge density ratio, meaning that little energy is needed to produce high strains. Typical values for strain-to-charge ratio for the polypyrrole are in the order of $\pm 10^{-10} \text{ C/m}^3$. It relates the specific material properties, *i.e.* polymer elastic modulus, conductivity, capacitance anisotropy, ion size, solvent, to actuator performance. Even though it is often used as a constant, it might be time varying as polymer properties were shown to be cycling and history dependent.

Another challenge for determining the strain-to-charge density ratio in practise, is the estimation of the injected charge within the polymer. The charge calculated as the integral of the transferred current as shown in *Fig. 4.9c* is a combination of: (1) a Faraday current and charge stored in a bulk capacitance, (2) a capacitive current used for the double-layer capacitance on the polymer surface¹⁰, (3) electrochemical reactions other than polymer charging, conductivity of the electrolyte and the currents between the electrodes.

Different components contributing to the current can be partly identified in *Fig. 4.8b*. The spike of the current once voltage step is applied is probably due to the fast double layer charging. It will also determine the initial speed of bending as creating an electric double layer requires redistribution of ions at the solution-surface interface. The fast charging is then followed by the slower Faraday reactions. Depending on the conditions, redox reaction can be limited by either: the electrical conductivity of the polymer or the diffusion rate of the ions. In any case the slow charge/discharge can be considered to be a signature of the redox process. Finally, the residual current that is not visible in *Fig. 4.8b* but is noticeable during the actuation at lower frequencies (*Fig. B.4c-B.4d*) is a consequence of the side reactions and leakage currents.

Nevertheless, the ratio of the transferred charge to produced strain can still be used for comparison of different actuators. In this case, the ratio should not be considered as a constant as both, the properties of the actuator as well as the transferred charge depends on cycling history and can be influenced by environment. In addition, in our case we cannot determine the exact volume of the polymer due to the mixing depth and unknown density of the films. Therefore, we will use the strain-to-transferred-charge ratio (*STC*) calculated as

$$STC = \frac{\Delta\epsilon_{SC}}{\Delta Q_{SC}} \quad (4.5)$$

where $\Delta\epsilon_{SC}$ and ΔQ_{SC} are strain and transferred charge difference during 60% of the cycle as illustrated in *Fig. 4.9*.

Mechanical and electrical properties of the polymer are different in the oxidised and reduced states [261, 316] and it can induce asymmetry in expansion and contraction (further discussed in *Section 4.3.1*). Therefore, the *STC* was calculated separately for upward and downward bending as shown in *Fig. 4.9d*. In the following sections we will use *STC* in order to (1) compare the efficiency of the actuators produced in different conditions and (2) track and compare the stability of the actuation in time.

Double-layer versus bulk capacitance

As soon as a voltage is applied to the polymer film, a electrochemical double layer at the polymer surface will be created. If the capacitance is assumed to be independent of the voltage, the charge accumulated at the interface will be directly proportional to the applied voltage. Formation of the double-layer is the initial step before diffusion of ions into (out of) the polymer bulk that subsequently cause its swelling (shrinking). In most of the cases, the double layer capacitance is negligible compared to the polymer

¹⁰usually negligible in comparison to the bulk charge

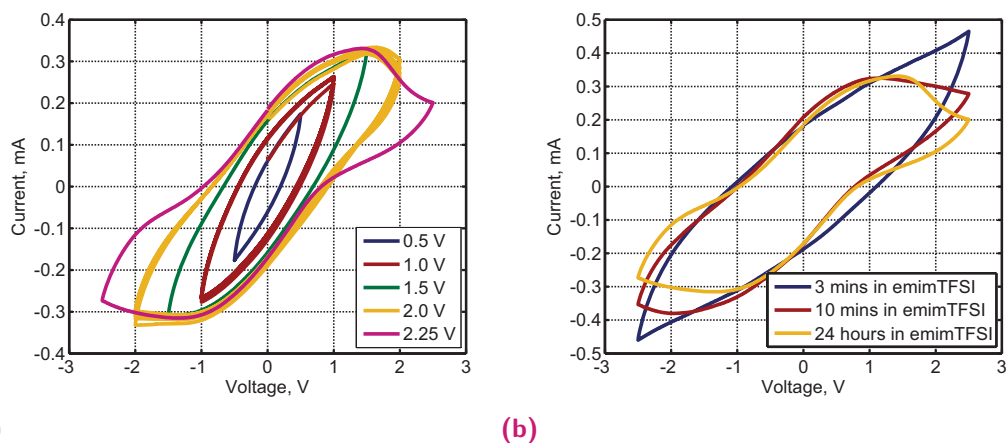


Fig. 4.10. Cyclic voltammograms of the *PEDOT:PSS/mPVDF/ILs* trilayer actuators in air recorded in two electrode set-up (100 mV/s scan rate) (a) measured up to different voltages 5 consequent cycles are shown for cyclic voltammetry (CV) up to 1 V and 2 V showing the stability in time. (b) CV of the *PEDOT:PSS/mPVDF/ILs* actuators after different incubation in ionic liquid times.

bulk [249]. Nevertheless, it might play significant role in *PEDOT:PSS* based actuators [295].

PEDOT:PSS films do not easily swell in ionic liquid and are in general very compact compared to *PPy* [124, 369]. Therefore the ingress of the ions from the double layer to the polymer bulk, the diffusion in between the polymer chains and subsequently the redox processes are slow. As reported by Okuzaki *et al.*, and also seen in our CV in Fig. 4.10a, potentials larger than 1.5 V and slow scan rates are required in order to notice a redox behaviour.

On the other hand, *PEDOT:PSS* blended with polyethylene oxide (*PEO*) was shown to form more porous and open film and have subsequently lower ionic resistance [124]. Ikushima *et al.* also used *PEO* as a secondary dopant in fabrication of trilayer actuators [148]. *PEG400* that was used throughout our experiments is expected to have similar effect to *PEO*. As shown in the CV voltammograms in Fig. B.6a-B.6b, the pseudocapacitance is significantly larger and the redox peaks are more pronounced if larger amounts of *PEG400* are used. Unfortunately, in our case, the use of *PEG400* is restricted to 1vol% in order to ensure good adhesion. Longer incubation in ionic liquid could also slightly influence the structure of the *PEDOT:PSS* film. Even though we have shown that the amount of adsorbed ionic liquid does not change after more than 3 minutes, redox behaviour is facilitated with longer incubation times as shown in Fig. B.5a, Fig. 4.10a-4.10b.

Finally, redox reactions and polymer swelling are the main drawbacks of the conducting-polymer based supercapacitors [349]. First of all, the redox reactions are slow reducing the power of the device; secondly, they are often partially irreversible and cause the degradation of the polymer properties (the change in structure due to the ingress and egress of ions was discussed in Section 4.1.1). This can also be observed in Fig. 4.10a and B.5a, where cycling at voltages below 1.5 V does not change the capacitance, but it

is gradually decreasing with every slow cycle above 2 V. The long term implications of such processes are discussed in the following section.

4.3.1 Long time performance

Lifetime is an important characteristic for many devices. In case of artificial muscles, lifetime often depends on the frequency of actuation, *i.e.* strain difference, and could be, e.g. 10^5 at 3 Hz, 10^3 at 1 Hz and even lower at lower frequencies [247]. Two main processes limiting the lifetime of the conducting polymer actuators are: (1) degradation of the polymer or decomposition of the electrolyte under electrochemical cycling and (2) delamination of the electrodes from the membrane due to stresses at the interface [17, 241]. The higher electrochemical window of ionic liquids reduces the degradation effect [29, 243]. Furthermore, their non-volatility enable longer actuation in air [295, 386]. Nevertheless, the delamination of layers constituting an actuator is still a common problem. When conducting polymers are synthesized directly on the membrane, the produced interfacial layer prevails for thousands of cycles but adverse partial connections between electrodes are often created [104, 368, 369]. When the actuators are electropolymerized on gold as a substrate, surface roughening methods are required to prevent fast delamination [241]. In most of the cases actuators fail gradually due to fatigue during the actuation or due to spontaneous self-degradation as shown in Fig. 4.11b and Fig. 4.11c-4.11d respectively and also reviewed by Punning *et al.* [313]. Gradual degradation is observed and reported most often and could be due to fatigue of the polymer, *i.e.* change in the mechanical properties, chemical degradation of the material, receding electrolyte¹¹ or irreversible redox reactions and reduction in the charge transfer [247, 313, 314, 322, 388].

The ageing of actuators can also occur spontaneously as shown as in Fig. 4.11c-4.11d. In this case, the actuator was cycled for 6 hours until a stable displacement was achieved and then left in air for another 20 hours. The significant decrease from 4 mm of min-to-max displacement to 3 mm can be seen. This could be a consequence of the receded amount of ionic liquid, degradation of the polymer in air¹², influence of the change in environment etc. The properties of the polymer based electrodes are sensitive to the environment (mechanical and electrical conductivity) and the influence of humidity and temperature to the actuation performance can be expected. This case will be discussed later in the chapter.

¹¹Even though ionic liquids are not volatile, they could leak out from the actuator near the electrodes due to the mechanical deformations

¹²It was reported that PEDOT:PSS could irreversibly degrade if exposed to the UV and oxygen or higher temperature [97, 387]. Therefore, small decay in its conductivity is likely even at ambient environment.

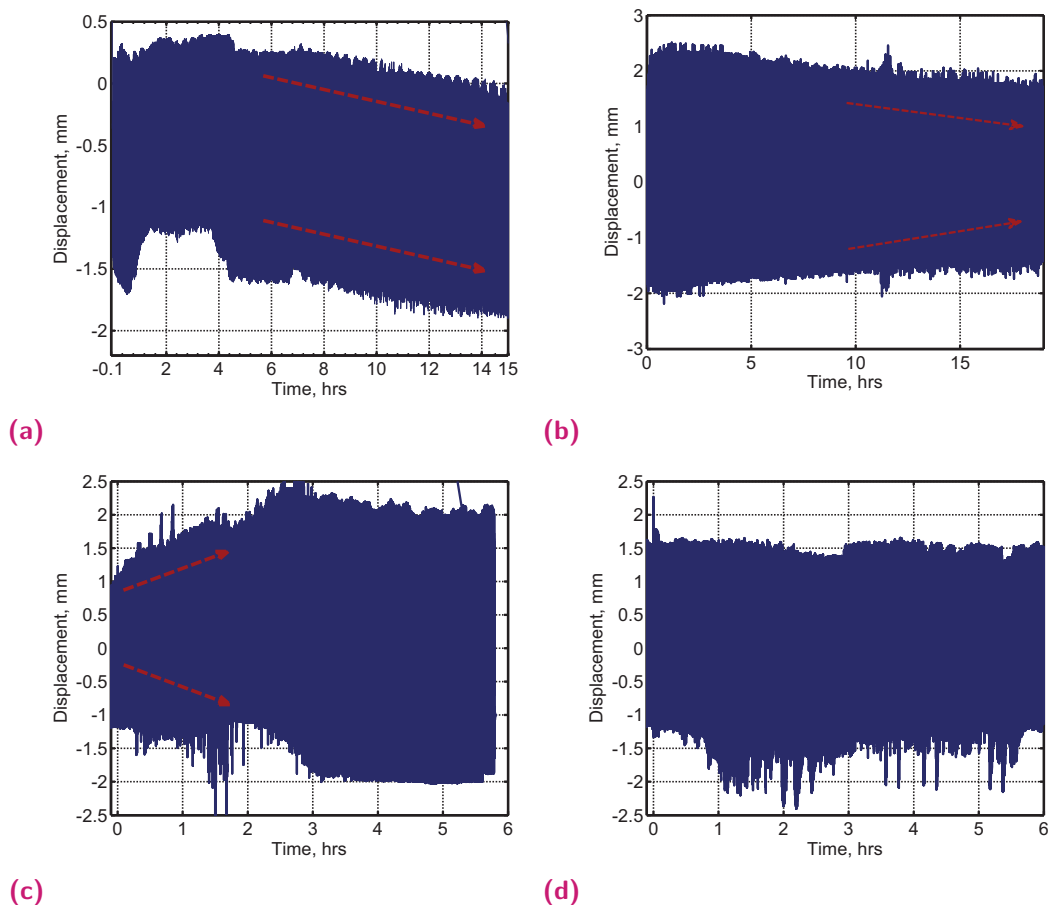


Fig. 4.11. (a) Actuation displacement profile of the *PEDOT:PSS/mPVDF/PEDOT:PSS* trilayer cycled in air with 2 V square wave with 100 *mHz* frequency. Significant creeping (indicated with red arrows) can be observed after 6 actuation hours. (b) Gradual decrease in the actuators displacement after 2 hours of actuation. Actuated with 1.5 V voltage sine wave with 50 *mHz* frequency. (c) Training effect (red arrows) shown during cycling of the actuator with 2 V square wave with 50 *mHz* frequency. The actuation profile of the same actuator after 20 hours in a static position is shown in (d)

Creep

The actuation is largely cycling-history dependent and there are two main effects related to the actuator itself that can competitively affect the performance: (1) irreversible expansion and (2) training effect [261, 376].

Irreversible expansion in the beginning of the actuation is shown in *Fig. 4.9a* and *B.7*. It is suggested by Melling *et al.*, that the primary source of irreversible expansion is solvent swelling that is further increased by cycling [261]. Cycling opens the polymer matrix so that with each cycle ions diffuse faster and therefore deeper into the film. It also allows irreversible accommodation of more solvent if present [171, 261, 297, 394]. We observed similar effect during our rough thickness measurements - even though only incubation in ionic liquid contracts the trilayer, cycling in between immersions has opposite effect and the film continuously swells (*Fig. 4.7a*). This might be surprising as there is no solvent in ionic liquid. Nevertheless, both ionic liquids and *PEDOT:PSS* are

hygroscopic materials and could absorb water from the environment. This water could subsequently accumulate in the polymer film.

Another mechanism possibly contributing to the irreversible expansion is the unbalanced charging as characterized by Kaneto *et al.* [172, 171, 376]. Both faster actuation rate during reduction [261] and during oxidation [346] were previously observed. It is attributed to the higher electronic conductivity in the oxidised state and to the higher ion conductivity because of the more expanded, open and swollen polymer. In any case, if the charges are not balanced by the end of an actuation cycle, this would induce accumulation of the ions in the films [171].

These effects are mostly relevant for free-standing conducting polymer films and bilayer actuators. In case of a trilayer structure, both electrodes are reversibly oxidized and reduced. Therefore the accumulation of ions should be equivalent on both sides. Nevertheless, if the electrodes are slightly asymmetrical¹³ this could cause differences in irreversible expansion and creep-like behaviour in the long term. It could be one of the explanations of the observed creeping shown in *Fig. 4.11a*. Another example of the obvious creeping once one of the electrodes gets damaged is provided in *Fig. B.8*.

'Kick-in' effect

Another effect shown in *Fig. 4.11c* is the improvement of the actuators performance in time. The change of the structure during the initial cycles, does not only cause irreversible expansion but also opens the channels between the polymer chains that facilitates the motion of the ions [261]. Polymer conformational changes as well as incorporated solvent (adsorbed water) and ions, increase the chain mobility, decrease the elastic modulus and facilitates the ion conductivity in the film. Therefore the speed of actuation can increase with each cycle [261]. It would also lead to continuously increasing the area of the polymer that is more open and to higher strains. Once maximum open area or ionic conductivity is reached, the actuation should stabilize (*Fig. 4.11c*). The time needed for training is mostly dependent on the fabrication and the environment conditions that could affect the morphology. As shown in *Fig. 4.11b* and *4.11c*, several cycles or several hours of cycling might be needed. One of the factors influencing the time needed for the 'kick-in' is the incubation time in the electrolyte. Often the electrochemical 'warming-up' in the electrolyte is performed to make sure that the film is fully swollen [257, 316].

Hysteresis

As previously mentioned, the oxidation and reduction processes in the conducting polymer electrodes are not symmetric. Reduced state of the polymer is less electronically conducting. In addition, if swollen with ions, the polymer morphology is disrupted so that increased interchain distance reduce the conductivity even further [393]. On the other hand, the less compact structure allows faster ion motion within the polymer [261]. It was also observed that the ion expulsion happens more quickly than ion incorporation [393]. In general the difference in the speed of the actuation creates hysteresis and is dependent on the morphology of the polymer and cycling conditions.

¹³In our case, due to asymmetry of the membrane and different grafting depth, mixing depth on both sides might vary, changing the electrical and electrochemical properties of two electrodes.

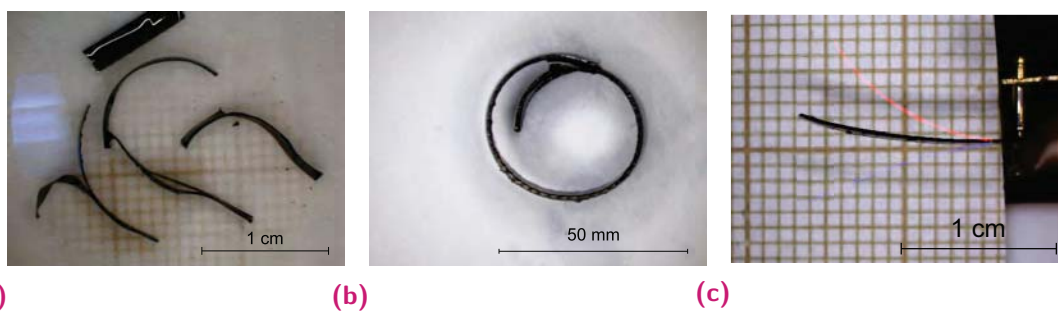


Fig. 4.12. (a) Picture of *PEDOT:PSS/pPVDF/PEDOT:PSS* actuators just after immersion in ionic liquid: adhesion is not strong enough and layers separate. If part of the *PEDOT:PSS* remain on the membrane, different expansion coefficients of the materials are causing bending and twisting of the rectangular. (b) Picture of *PEDOT:PSS/mPVDF* bilayer after immersion in ionic liquid: adhesion between materials is strong enough and due to difference in expansion of each material, bilayer rolls into a cylinder. Nevertheless, adhesion is strong enough to sustain the stress at the interface. (c) Merged images of the trilayer actuator with a strong adhesion between layer at initial position (black) and at extremities during actuation (red and blue). Actuated with 2 V, 10 mHz square voltage wave.

Hysteresis was observed in most of the cases during characterization of the trilayer actuators made of *PEDOT:PSS/mPVDF/PEDOT:PSS* that we were working on. One example of that can be seen in Fig. 4.9b. As in the case of the creep, the asymmetry of the actuator is probably playing role in creating hysteresis. Many small differences might contribute to such behaviour, *i.e.* the thickness of the electrode, the mixing depth, electrical conductivity etc. Unfortunately, the electrochemical characterization versus the inert reference electrode was not performed in our studies and definite reasons behind this difference cannot be identified.

4.4 The importance of a good adhesion

The difficulties encountered during fabrication of the actuators by solvent casting *PEDOT:PSS* were discussed previously (Chapter 3). As reported by Ikushima et al, *PEDOT:PSS* deposited on pristine *PVDF* delaminates nearly immediately. The deformation of the actuator due to the poor adhesion between layers that can be caused by simply immersing the structure in ionic liquid is shown in Fig. 4.12a-4.12c. On the other hand, the functionalized membranes lead to the adhesion that can sustain large strains as shown in Fig. 4.12b. Moreover, actuators can be made that can be cycled for more than 10^4 cycles at 0.1 Hz (more than 150 hours) with no signs of delamination (Fig. 4.13a).

4.4.1 Lifetime

In Fig. 4.13a, actuators with a large grafting density and large interfacial layer (*MD* 25 μ m) (A25), low grafting density and small interfacial layer (*MD* - 5 μ m) (A5) and produced on pristine *PVDF* membrane (*pPVDF*) (AP) are compared. In order to fabricate functional actuators on pristine *PVDF*, a 5 vol% PEG400 in *PEDOT:PSS* was used, causing penetration of *PEDOT:PSS* through the membrane and resulting in a significantly

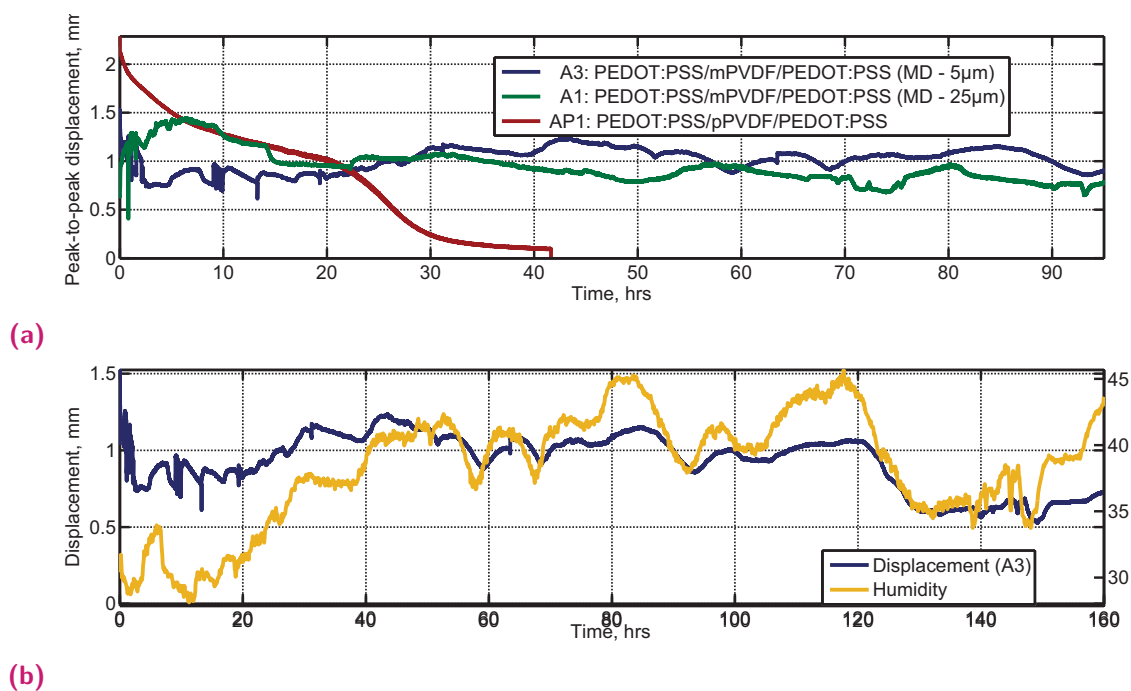


Fig. 4.13. (a) Lifetime measurement of actuators produced with hybrid PVDF-graft-PEGMA (mPVDF) and pristine membranes (PVDF). The mixing depth between *PEDOT:PSS* and *mPVDF* is indicated in the legend. (b) Amplitude of the displacement for *PEDOT:PSS*/PVDF-graft-PEG/*PEDOT:PSS* with MD of $5\mu\text{m}$ based actuator in ionic liquid (blue) and the change in the humidity of the environment (yellow).

higher current between electrodes. The resistance between electrodes of *AP* is 6 orders of magnitude lower than for *A5* and *A25*, $0.36\ \Omega$ vs $0.16\ \text{M}\Omega$, leading to a large power dissipation during actuation (further discussed in *Section 4.5*). The penetration through allowed sufficient adhesion between layers to sustain adsorption of $2.2\ \text{mg}$ of *emimTFSI* ionic liquid without delamination.

Once a voltage is applied ($1.5\ \text{V}$ sine wave, $0.1\ \text{Hz}$ frequency) the *AP* actuator displacement amplitude is continuously decreasing and the actuator stops responding after less than 50 hours of actuation. Meanwhile, actuators with even very small mixing depth ($5\ \mu\text{m}$) and stronger adhesion, remain active for more than 100 hours with no significant decrease in displacement amplitude and no signs of delamination.

Small variations of the amplitude can still be observed. As mentioned previously, actuators performance might be influenced by the ambient environment, especially because *PEDOT:PSS* and ionic liquids are hygroscopic materials that can easily absorb water. Displacement and humidity of the environment during actuation of *A3* actuator are shown in *Fig. 4.13b*. Humidity can influence strain of the actuator in two ways: (1) water can be absorbed and desorbed due to the passive, *i.e.* Joule, heating and (2) adsorbed water can change *PEDOT:PSS* microstructure and consequently its mechanical and electrical properties[364, 423]. On the other hand, the actuation was shown to be humidity dependent even in the actuators that do not use *PEDOT:PSS* based electrodes[281]. It was explained by the hygroscopicity of the ionic liquids. In agreement

with results published by Must *et al*, at relatively low frequency and this humidity range, actuation amplitude is larger when humidity is higher [281].

Despite the quite significant variation in the actuation amplitude, cycling is reversible and humidity does not cause permanent damage to actuators. On the other hand, if the position of the actuator needs to be controlled, the humidity should be monitored and the control algorithms should be adjusted accordingly¹⁴.

4.4.2 Performance

The working mechanism of the conducting polymer based actuators is considered to be one of the best understood among the artificial muscles. Various electro-chemo-mechanical models exist explaining the action [92, 144, 178, 339, 392]. Nevertheless, most of the models are based on approximations such as infinite conductivity of the electrodes, negligible double layer capacitance, perfect interface *etc*. In reality the performance of the actuators often varies significantly among different fabrication batches [241], is highly dependent on the environment conditions [281, 313, 314, 388] and can be hardly tuned by just varying one of the parameters.

Performance of ionic *EAP* artificial muscles depend on a wide range of parameters that were briefly summarized by Madden *et al* [249]. Mechanical and electrochemical properties of electrode material, such as elastic modulus, density, electrical and ionic conductivity, membranes elastic modulus, porosity, ionic conductivity are only few to mention. Furthermore, the performance of the actuator is also highly influenced by the geometry of the device, where thickness of both the electrode and the insulating membrane play their role [261, 274] and were shown to be influenced by three dimensional patterning [6].

In order to identify the most crucial parameters affecting the performance of the actuators various devices were tested. Actuators were fabricated from four membranes prepared with the same grafting conditions (*SD* - $0.98 \pm 0.2 \text{ ng/mm}^2$, *GD* - $0.06 \pm 0.01 \text{ ng/mm}^2$). Then half of the each membrane was post-treated (separate cases of post-treatment will be discussed further in the chapter) leading to eight different kinds of actuators. The performance of the 2 – 4 actuators of each kind is shown in *Fig. 4.14*. Furthermore, the displacement and the current amplitude (distance from the minimum to maximum per cycle) plotted versus the resistance of the electrodes, resistance between the electrodes, the weight of the actuator and the amount of the adsorbed ionic liquid, is provided in *Fig. B.10a-B.10f*. Even though scattered data clusters could be identified for the different fabrication batches, no clear influence of any of the mentioned parameters could be determined.

The main identified reason behind the variation of the performance is shown in *Fig. 4.14c*. In order to have functional actuators good interface on both sides of the membrane and symmetrical actuators are needed. Poor interface between layers or high asymmetry causes bending, twisting and other deformed shapes once actuators is

¹⁴The displacement profile of the same actuator and the humidity shown in Appendix B *Fig. B.9* suggest that creeping of the actuator is much larger problem to control in comparison to the effect of the environment

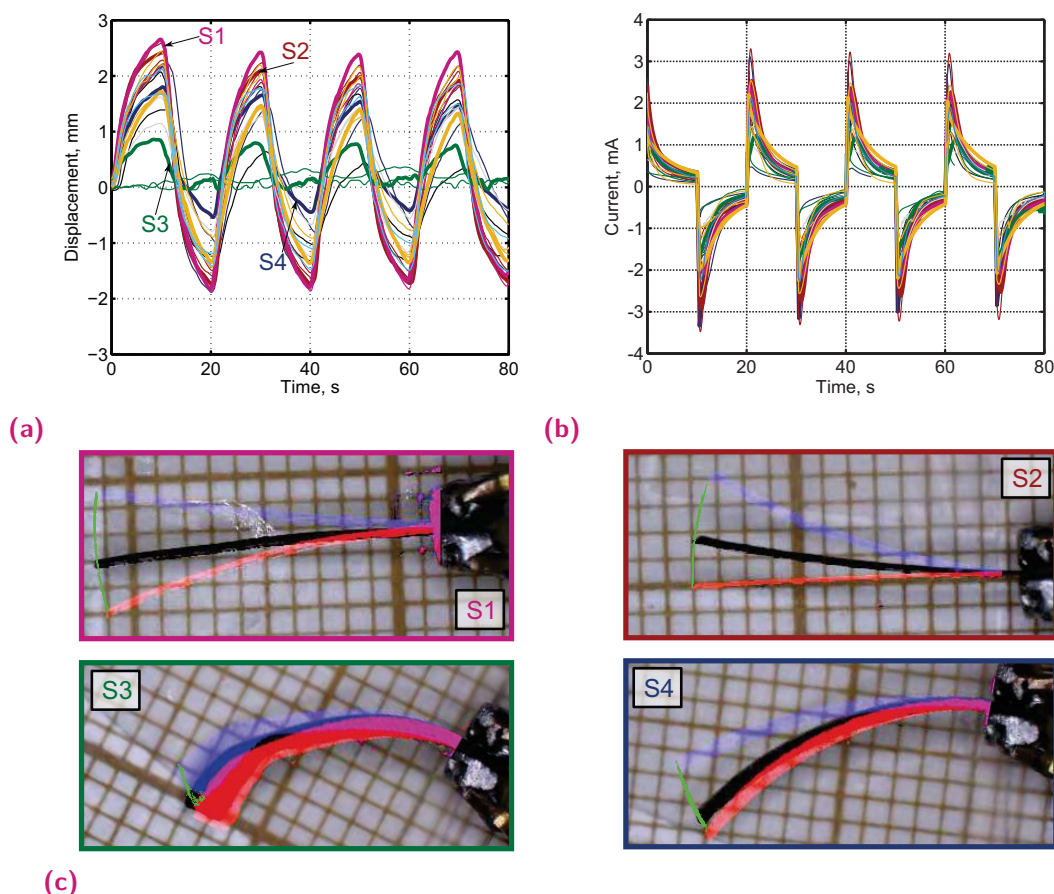


Fig. 4.14. (a) Displacement and (b) current versus time of various actuators made with or without post-treatment from four different membranes. Actuators made with the equivalent fabrication procedure are represented by the same colour. Performance versus other parameters of the same actuators are plotted in Fig. B.10, special cases shown with a thicker line, correspond to the filled markers. (c) Merged images of the several actuators at the initial (black) and extremities during actuation (red and blue). All measurements were recorded during actuation by 1.5 V and 50 mHz square wave.

put into the ionic liquid. Extreme cases of such deformation when *PEDOT:PSS* is adhered on only one side were also shown in Fig. 4.12a-4.12b. Even though unnoticeable visually, the observed bending of the actuator in ionic liquid, can be used as an early sign of the poor interface at least on one side and consequently the poor performance (S3 and S4 shown in Fig. 4.14c). For all the future performance comparison, only actuators that showed symmetrical structure were used (such as S1 and S2 in Fig. 4.14c).

4.5 Influence of the mixing depth on actuators performance

Even very small mixing depth is enough for ensuring long term adhesion. Nevertheless, the morphology of the actuator, and presumably its properties, changes with the mixing depth. We have already suggested that the slight difference in *MD* of two electrodes might influence the performance in a long term as the impact accumulates. It is

Tab. 4.1. Geometry and electrical properties of actuators

	$h_{dry}^b, \mu\text{m}$	$h_{el}^d, \mu\text{m}$	$h_{int}^e, \mu\text{m}$	w_{act}^f, mg	w_{IL}^g, mg	$R_{el}^h, k\Omega$
A5	123 ± 3.7	20/19	19/27	3.75 ± 0.21	1.9 ± 0.2	$4.9/2.4 \pm 0.6$
A30	117 ± 5.5	23/19	28/30	3.75 ± 0.22	2.0 ± 0.1	$3.7/2.2 \pm 0.3$
A25	129 ± 3.7	25/20	5-20	3.75 ± 0.15	2.1 ± 0.2	$2.5/1.2 \pm 0.3$
AP	129 ± 17	36/43	-	6.89 ± 1.4	2.25 ± 0.1	$0.9/0.8 \pm 0.08$

^b Thickness of dry membrane; ^d PEDOT:PSS electrode thickness; ^e Thickness of interfacial layer; ^f Weight of dry actuator; ^g Weight of absorbed emimTFSI; ^h Resistance of the electrodes.

interesting to try identifying the reasons behind it or at least to determine if large or small mixing depth is preferable.

The goal of our work was to develop membranes that would allow good adhesion and will ensure a good insulating layer between the electrodes. Meanwhile, the actuators with semi-trilayer structure and gradually dispersed conducting material in the polymer matrix are being successfully used [104, 386]. The differences in the actuator performance of actuators with *MD* of $30 \mu\text{m}$ (A30), $5 \mu\text{m}$ ¹⁵ (A5) and actuator fabricated on pristine PVDF but with excess of the PEG400 (AP) were compared. In the last case, PEDOT:PSS is present in all the pores of the membrane connecting the electrodes. The summary of the geometry and electrical properties of these actuators is shown in Table 4.1.

The first difference among different actuators that can be observed, from the given electrical properties is the resistance of the electrode. It increases with the length of the interfacial layer (measured as in Appendix A.4.2). It is likely that PEDOT:PSS in the pores of the membrane, does not form a good path for electrical conductivity (discussed further in Section 5.2.2). It would explain the higher resistance for A25 (large interface) in comparison to A5 (small interface), $2.4 \pm 0.6 k\Omega$ and $1.2 \pm 0.3 k\Omega$ respectively, and also the difference for the two sides of the actuator, $4.9 k\Omega$ and $2.4 k\Omega$. As a consequence of a lower resistance, the voltage drop along the electrodes is probably lower and therefore, the double-layer voltage is higher. As can be seen in Fig. 4.15b, the peak-to-peak current (corresponding to double-layer charging) is highest for electrodes with higher conductivity and equivalent tendency is observed for actuators with different mixing depths as shown in Appendix B Fig. B.11a-B.11b (the peak-to-peak current is highest for lowest *MD* and the difference is increasing with the applied voltage.)

The initial bending of the actuator seems to be driven by the double-layer charging as shown in the Fig. 4.15c - the higher conductivity of the electrodes leads to the sharper increase in strain (nearly $0.2 \%/s$ for AP actuator). Alternatively, the faster bending in actuators with the larger mixing depth might as well be due to the smaller

¹⁵The value is just indicative of a small mixing depth. The SEM images of the cross-section showing that the *MD* is not homogeneous and in most of the cases hard to measure are shown in Appendix B Fig. B.12

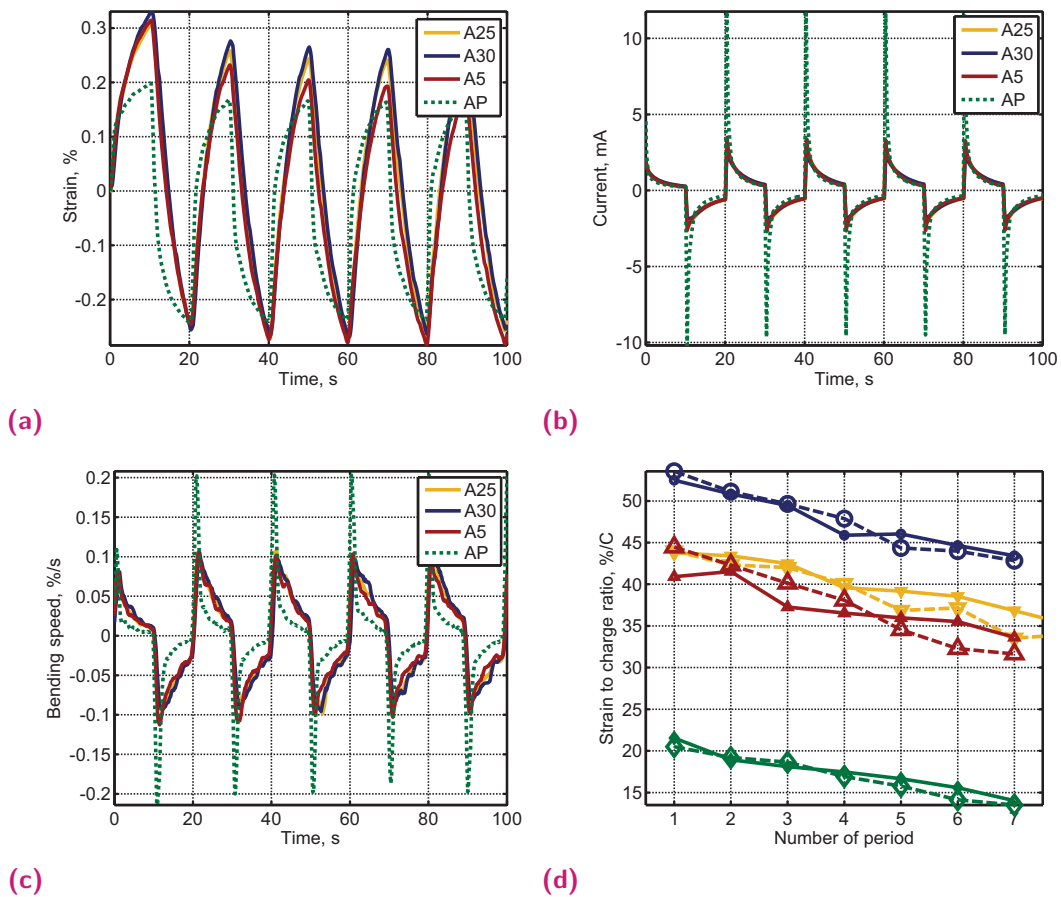


Fig. 4.15. (a) Strain and (b) transferred current and (c) bending speed profiles of the actuators having a different mixing depth (indicated in the legend as a number, *AP* - semi-trilayer with percolated electrodes (green dotted line)). 2.0 V square voltage wave at 50 mHz was used for actuation. (d) Calculated strain-to-transferred charge ratio for each cycle for different actuators (colors correspond to the legends in (a)-(c)). The ratio calculated for motion and upwards and downwards is plotted separately as dotted and full lines.

distance between the electrodes¹⁶ that would reduce the ion diffusion path and increase the speed [258] as well as increase the strain due to the thinner passive layer [6]. Nevertheless, as the double-layer charging is instantaneous, the subsequent bending and slowly decreasing current is most likely due to the ingress of the ions in the polymer film as a result of the redox reactions. At this point, the process is not any more limited by the electrical conductivity of the polymer electrodes and the profiles of the transferred current and bending speed are very similar for all (A5-30) actuators. In fact, ingress of ions seem to be slower for the A5 actuator leading to slightly lower maximum strain at a given frequency (50 *mHz*). Interestingly, this difference appears only when higher than 1.5 V is used for actuation as shown in Fig. 4.16a. 1.5 V corresponds to the appearance of the redox reactions (Fig. 4.10a). It seems that despite the lower electrical conductivity, the structure of PEDOT:PSS in the pores of the membrane may favour the electrochemical reactions.

Differently from the actuators with the insulating layer, AP actuator slows down significantly after the initial spike and does not reach the strain of A30 or A5. In fact, when actuated at the lower frequencies, back relaxation is observed after a few seconds as shown in Fig. B.12a¹⁷. Even though the current seems to come back to nearly zero, it is likely that the charge used at this time is being dissipated due to the conducting paths in between two electrodes¹⁸ and is not used to charge the polymer bulk. Very low pseudo-capacitance and no redox behaviour is observed in CV voltammograms either (Fig. B.12b) confirming that the bending is governed by double-layer charging. Overall, AP, A30 and A5 needs similar amount of power per cycle (44.48, 37.49 and 36.9 *mW* respectively) but the *STC* ratio is significantly smaller for AP actuator as shown in Fig. 4.15d.

A slightly different behaviour is observed when rather low conductivity PEDOT:PSS (doped with 1 *vol%* PEG400) connects the electrodes. This is the case, when PEDOT:PSS is deposited on the PVDF membrane that is functionalized through all its depth (Fig. B.12d). Despite the lack of the passive layer, the actuator bends when a voltage is applied (Fig. B.12d) and furthermore, the current comes back to nearly zero. After the study of the semi-interpenetrated networks with different amounts of the conducting polymer, Festin *et al* concluded that the conducting polymer percolations are cut out during the swelling [104]. In our case, membranes do not swell. Lack of the short circuit between the electrodes could be explained by in general low conductivity of the PEDOT:PSS in the membrane that should be below 9 *S/cm* (Chapter 5 Fig. 5.7f). Also, in contradiction to [104], the electrical resistance decreases when actuators are put into the ionic liquid (Fig. B.13a) to about 0.2 Ω and very similar resistance value was obtained along the electrodes (0.3 – 0.5 Ω). The conductivity of the ionic liquid itself

¹⁶Assuming that the electrolyte-electrode interface is in the membrane at the end of the mixing depth and the double layer is forming at that point, the distance between the electrodes would be about 80, 70 and 60 μm for A5, A25 and A30 actuators respectively.

¹⁷One of the possible explanation for the back relaxation in our case, could be the 'salt-draining' at the polymer-electrolyte interface. As the ions at the double-layer do not ingress into the polymer, large cation concentration gradient is created along the membrane. In a longer time, the anion could diffuse to reduce the gradient.

¹⁸The measured resistance between AP electrodes in a dry state is 0.4 Ω and in A5-A30 actuators is 6 orders of magnitude higher - 0.2 $M\Omega$

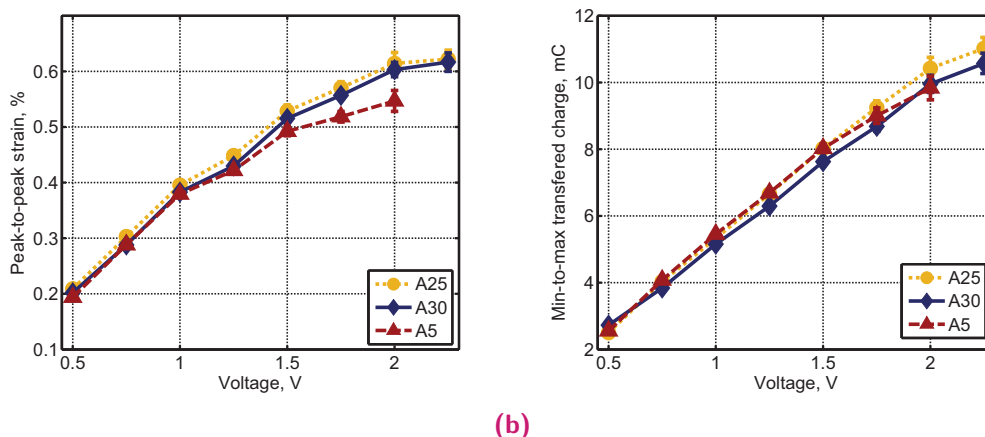


Fig. 4.16. (a) Peak-to-peak strain and (b) transferred charge for actuators with different mixing depth at different voltages.

(9 mS/cm [415]) is too low to explain this decrease in resistance. It is possible that incubation in ionic liquid wash out the *PSS* and improve the electrical conductivity of *PEDOT*. The *PEDOT:PSS* conductivity could be improved by several orders of magnitude with addition of imidazolium ionic liquids [16, 90, 237].

To sum up, the influence of the mixing depth on the actuators performance is rather complex and needs further investigation. First of all, the electrical conductivity in the pores of the membranes is low and therefore percolations might not necessary cause a short circuit. On the other hand, large surface area of *PEDOT:PSS* in the pores might favour the electrochemical reactions. Furthermore, the larger mixing depth leads to smaller passive membrane layer that subsequently leads to decreased ion diffusion distance and faster actuation. On the other hand, we also observed that having redox reactions lead to the faster degradation of the actuators performance. Therefore, appropriate fabrication conditions should be chosen if actuators producing small strain but having a long lifetime (no redox) or actuators with a large strain and stable position are needed.

4.6 Towards actuator performance improvement by altering *PEDOT:PSS*

Using aqueous solution of *PEDOT:PSS* as the conducting polymer for ionic actuators is a relatively new idea. Nevertheless, the possibility to produce actuators by simple drop-casting is interesting as it allows tuning of several parameters. We have already discussed the influence of the difference mixing depth. We also mentioned that *PEDOT:PSS* properties and subsequently actuators morphology and performance change with different amounts of *PEG400*. There are dozens of other substitutes that were reported to influence electrical and mechanical properties of *PEDOT:PSS* (Section 5.2.2), *i.e.* ionic and non-ionic surfactants [416, 229, 101], carbon nanotubes (*CNTs*) [10, 410, 413], ionic liquids [90], low melting point compounds [194, 285, 264]. Not only electrical conductivity is improved with secondary doping but also the redox behaviour

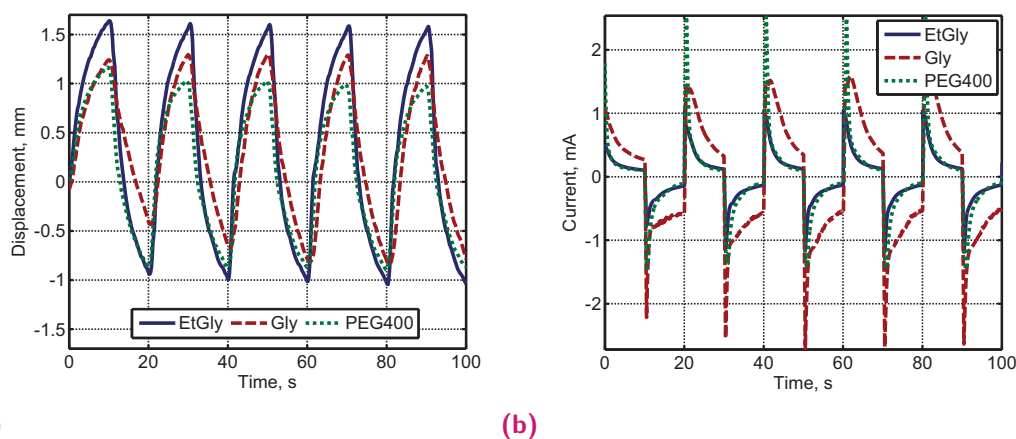


Fig. 4.17. (a) Bending and (b) transferred current profiles of the actuators with *PEDOT:PSS* electrodes that were secondary doped with 1 vol% of ethylene glycol (blue full line), glycerol (red dashed line) and standard PEG400 (green dotted line). 1.5 V square voltage wave at 50 mHz was used for actuation.

[302]. Simple drop casting based fabrication could be used to tune the mechanical, electrical and electrochemical properties of *PEDOT:PSS* electrodes toward the optimized conditions for applications in mind.

Example of such possibility is shown in Fig. 4.17 where performance of the actuators secondary doped with 1 vol% of glycerol, 1 vol% ethylene glycol and 1 vol% of PEG400 are compared. The thoughtful investigation of the mechanical, electrical and electrochemical properties of such electrodes still need to be conducted, but the significant differences, especially in the transferred current profile, can be seen. Glycerol doped *PEDOT:PSS* is reported to improve the electrical conductivity as well as to lower the work function that subsequently improves the charge transfer [348]. Improved conductivity is seen as large current peak corresponding to the double-layer charging and a relatively large charge transfer after a few seconds that is attributed to polymer bulk charging. On the other hand, ethylene glycol and polyethylene glycol have similar effect on the morphology of the *PEDOT:PSS* [264] and their current transfer profiles are therefore very similar (the difference in the initial current peak is probably the result of the conductivity difference as shown in Fig. 5.7e-5.7f). Nevertheless, the *PEDOT:PSS* with ethylene glycol as secondary dopant (*EG-PEDOT*) actuators show largest and fastest displacement and the smallest transferred current. This is probably due to the significantly thinner actuators¹⁹.

4.6.1 Post-treatment of *PEDOT:PSS*

Even though numerous, the choice of the secondary dopant in *PEDOT:PSS* is limited as discussed in Chapter 3. Alternatively, several post-treatment methods were suggested to improve *PEDOT:PSS* properties, *i.e.* drop-cast or bath treatment with water, methanol,

¹⁹The thickness of the actuator depends on the mixing depth and the density of *PEDOT:PSS* that consequently determines the thickness of *PEDOT:PSS* electrodes above the membrane. The density of *PEDOT:PSS* is largely dependent on its composition and it seems that secondary doping with ethylene glycol lead to very thin electrodes in comparison to doping with glycerol or PEGs

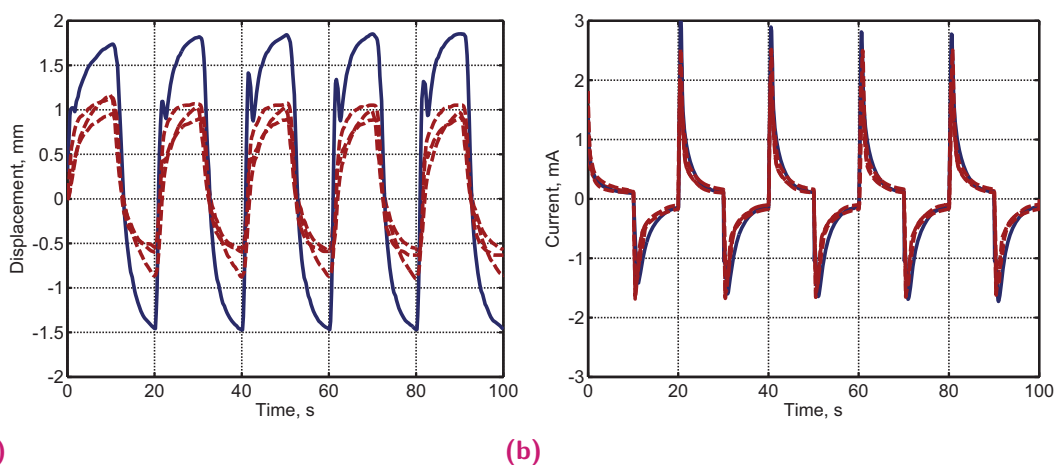


Fig. 4.18. (a) Bending and (b) transferred current profiles of the standard (red dashed line) actuators and actuators treated with sprayed sodium dodecyl sulfate (*SDS*) (blue full line). 1.5 V square voltage wave at 50 *mHz* was used for actuation.

ethanol, ethylene glycol, organic and inorganic acids (reviewed by [359]). Nevertheless, in most of the cases, post-treatment methods were performed to thin *PEDOT:PSS* layers (tens of nanometers) and similar attempts to improve properties of thick *PEDOT:PSS* led to the destruction of the film due to cracking²⁰.

Alternatively, post-treatment could be limited to only thin upper part of the electrode by spray-coating. For example, anionic surfactants such as *SDS* are used to enhance *PEDOT:PSS* conductivity [101]. Nevertheless, if added to the aqueous solution before drop casting, it would lead to the percolation of the electrodes. The effect of a post-treatment on the deposited and dried *PEDOT:PSS* with small amounts of sprayed surfactant is shown in Fig. 4.3 (fabrication method is provided in Section A.4.3). Post-treatment with *SDS* significantly improves the strain and bending speed with nearly the same amount of the transferred charge. Nevertheless, the amount of *SDS* needs to be carefully controlled as it could diffuse from the upper surface through *PEDOT:PSS* to the membrane-electrode interface leading to poor adhesion and infiltration as discussed in Chapter 3²¹.

CNT carpets for creep reduction

Carbon nanotubes have been widely used to increase the conductivity, robustness and the stiffness of the polymer matrix [110, 273, 373]. In addition, incorporation of carbon nanomaterials in actuators was shown to increase the accessibility of the Faradaic capacitance of the conducting polymer, the electrical conductivity and to consequently

²⁰Most of the proposed methods are based on the removal of the insulating *PSS* layer from the surface of the polymer film. It is understandable that such action would lead to volume change of the film, that in our case, caused cracking of the *PEDOT:PSS* layer. Washing with methanol and ethanol were tested with our actuators.

²¹In depth experiments still need to be performed, but the preliminary results suggest that a large amounts of the sprayed surfactant reached the electrode-membrane interface, and diffused further into the pores of the membrane. In a longer term this led to the percolation of the electrodes and delamination as suggested by Energy-dispersive X-ray spectroscopy (*EDX*) sulphur scan along the cross-section of *PEDOT:PSS/mPVDF/PEDOT:PSS* trilayer without and with treatment with *CNT/SDS* mixture. Delamination of layers for similar actuators was observed after immersion in ionic liquid a few weeks after fabrication.

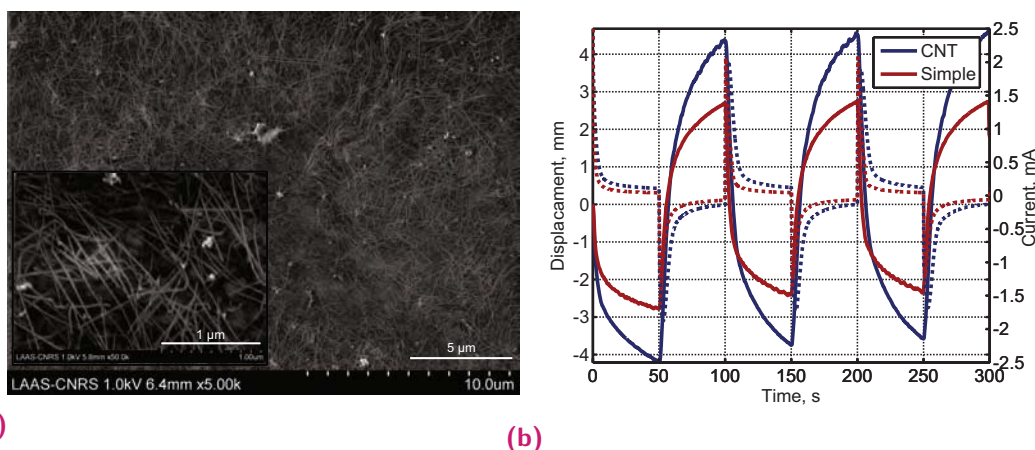


Fig. 4.19. (a) SEM image of the *PEDOT:PSS* electrode surface with sprayed *CNTs* carpet. (b) Displacement (solid line) and transferred current (dashed line) profiles of the actuators with (blue) and without (red) carbon nanotube carpet. Actuation with the square voltage wave of $\pm 2V$ and 10 mHz was used for actuation.

increases actuators stroke and work per cycle [180, 309, 365, 379, 421]. Furthermore, just as in batteries, incorporation of the *CNTs* increases the redox reversibility and significantly reduces creep [99, 110, 365].

Nevertheless, one of the biggest challenges for using these composites is the solubility of carbon materials [351]. Only small amounts of the more conductive, non-oxidised carbon nanotubes or graphene can be homogeneously dispersed in the polymer solutions [410, 413]. Higher concentrations lead to the formation of aggregates. When incorporated during the electropolymerization [379], the concentration of carbon nanotubes is difficult to control. Other fabrication methods, *i.e.* layer-by-layer deposition [421], drop casting [365], soaking [309], that would allow to increase the *CNTs* amount in the polymer actuators were also suggested, but they also require soluble and easily processable *CNTs*. *CNTs* incorporation methods in *PPy* are introduced and discussed in more details in the thesis [309].

We suggest to use spray coating as a carbon nanotube deposition method [27, 168]. In this way, large amounts of *CNTs* can be deposited only on the upper surface of the conducting polymer (shown in Fig. 4.19a). Preliminary experiments showed that such *CNTs* carpets could significantly improve the actuators performance as shown in Fig. 4.19b. The electrical conductivity of the electrodes is only slightly improved (3 S/cm to $3,5\text{ S/cm}$ without and with *CNTs* respectively) and as *CNTs* are present only on the upper surface, strain increases due to the increasing double layer charge is also unlikely. Therefore, the performance improvement is most likely due to the increased accessibility of the Faradaic capacitance of *PEDOT:PSS* itself - *CV* voltammograms showing much larger pseudocapacitance and more pronounced redox peaks are shown in Fig. B.14.

As reported in previous *CNTs*-conducting polymer composite studies, improved cycle reversibility and creep reduction are major advantages of using carbon nanotubes in actuators. The significance of it is demonstrated in Fig. 4.20a where the time needed to

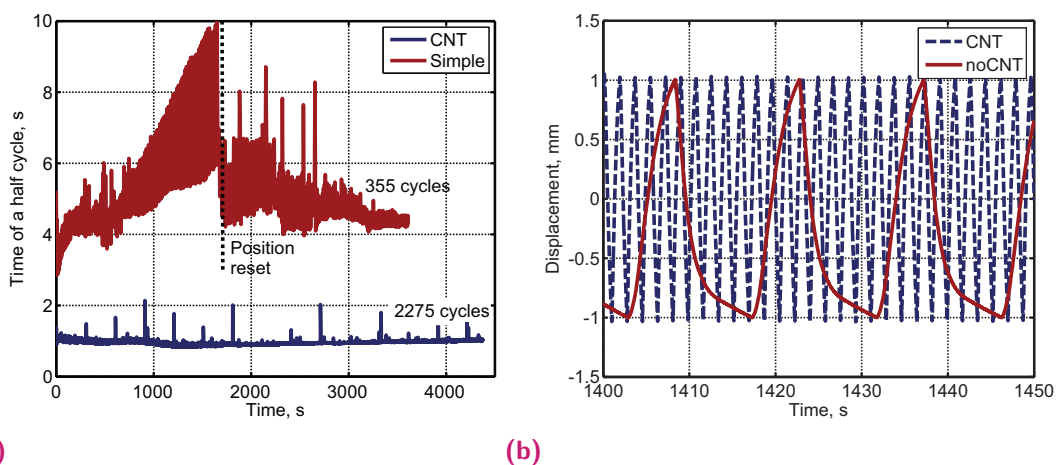


Fig. 4.20. (a) The change in the actuation frequency in time for the *CNTs* (blue) and simple (red) actuators measured as a time needed to move from/to ± 1 mm. ± 1.5 V was used to change the direction of bending as soon as the actuator tip reached set value. For actuator without *CNTs* the value was reset to $+1.2 - -0.8$ mm due to the large creeping (shown as dotted line). (b) Bending profiles in time for actuators with (blue dotted line) and without (red line) *CNTs* carpet. The voltage polarity (± 1.5 V) was changed everytime the actuator reach the set ± 1 mm value.

reach ± 1 mm is plotted in time and the bending profiles are compared in Fig. 4.20b (Characterization set up is provided in Section A.4.2). The difference in time needed to move the actuator upwards or downwards appears in Fig. 4.20a as a filled area. Due to the creep, after about 1500 s it takes about 6 s for the actuator to go one direction and more than 10 s to move back (at this point the position was set to 0.8 – 1.2mm). On the other hand, actuators treated with *CNTs* remained fast (about 2 s per cycle) and with relatively symmetrical bending profile for more than 2000 cycles. This is a very promising improvement if actuators were to be used for cyclic positioning.

The effect of *CNTs* on the actuation performance is similar to previously reported [99, 110, 180, 365, 421]. Nevertheless, in our case, in order to spray *CNTs*, their suspension in water is needed that is stabilized by surfactant. Therefore, further work is needed in order to separate the possible effects of surfactant and *CNTs* on performance (compared in Fig. B.15).

4.7 Conclusions

We presented fast, simple and versatile fabrication technique for conducting polymer based actuators. Drop casting of *PEDOT:PSS* on modified *PVDF-graft-PEGMA* membrane (*mPVDF*) membranes allows fabrication of devices with various properties, *i.e.* the length of the mixing depth, thickness of the electrodes, intake of ionic liquid, composition of electrode. The use of hybrid *PVDF* membranes, significantly improves the adhesion strength allowing large lifetime actuation in air for more than 150 hours and 50000 cycles. Furthermore, the performance was shown to be robust against humidity in the environment. Actuators were also capable of producing strains higher than 0.6% (at 2 mHz frequency) (Fig. B.16), that are highest reported for *PEDOT:PSS* aqueous solution based actuators [193, 295]. Finally, due to its simplicity, our fabrication method

could also be a tool to study and better understand important factors influencing actuation. We have also shortly introduced the preliminary results towards improving the performance of the actuators by spraying single wall carbon nanotubes on *PEDOT:PSS* surface. It seems that *CNTs* could improve the electrochemical activity of *PEDOT:PSS* that could further increase the strain (to 0.5% (at 2 V 10 mHz)) and significantly reduce creeping.

4.7.1 Future work

In this chapter the use of hybrid *PVDF/PVDF-graft-PEGMA* membranes were validated for fabrication of actuators with *PEDOT:PSS* conducting polymer electrodes. Even though some actuators with different structures were compared and possible working mechanisms were suggested, a extensive work need to be done to better characterize and understand the performance.

- In order to better understand the influence of the mixing depth on the actuators performance, electrochemical characterization (CV and electrochemical impedance spectroscopy) of *PEDOT:PSS* on the membrane should be performed in three electrode cell set-up. This could lead to better understanding of the complex charge and mass transport phenomenon at the interfaces formed in the pores. Understanding of such processes is essential for the electro-mechanical modelling of the actuation as well as for the optimization of the performance.
- As discussed in *Chapter 2*, functionalization leads to a slightly asymmetrical membranes. We showed here that this might cause the difference in the electrochemo-mechanical properties of *PEDOT:PSS* that subsequently affect the actuation reversibility. Even though in most of the cases, these effects are not observable in short term, they might accumulate in time. One of the solutions to improve the long time performance could be the optimization of the grafting. On the other hand, asymmetrical actuation signal could also be used, if the influence of the mixing depth on the performance could be accurately estimated.
- In general, the morphology leading to the best actuators performance was not optimized in our work. In addition to the optimal mixing depth, the thickness of the electrodes, the incubation in ionic liquid time, the thermal annealing procedure *etc.* could be adjusted in order to improve needed parameters, *i.e.* speed of actuation, maximum strain, power consumption *etc.*
- The mechanical properties of *PEDOT:PSS* electrodes, that influence the ionic conductivity in the film is probably the most critical parameter. In our case, when aqueous *PEDOT:PSS* solution is used, they can be easily tuned by pre- or post-treatment of the film with secondary dopants and other compounds. We have shown that *PEDOT:PSS* composition could alter performance of the actuator. Nevertheless, much more work needs to be done not only to optimize the composition of the electrodes, but also to understand the mechanisms behind it.

- The main parameter for the actuators used in this work was the strain of the actuator in a trilayer configuration. Nevertheless, the produced stress and force are equally important for most of the applications. Characterization of the actuators in terms of blocking force and stress needs to be performed and optimized.
- We have also showed that *CNTs* could be used to improve the performance of the actuator. Nevertheless, the fabrication parameters that leads to the improved performance but that does not affect the adhesion strength of the actuators need to be found. The use of *CNTs* could have a tremendous impact on improvement of the devices and their easier control.
- Finally, for the applications of the conducting polymer actuators better electro-chemo-mechanical models are needed, that could lead to sophisticated feed-forward control. On the other hand, integrated sensing could be implemented that would allow feed-back control without bulky external displacement sensors. The internal sensing using *PEDOT* trilayers was already suggested [104], but its realization is still at the embryonic stage.

Towards inkjet printed artificial muscles

Contents

5.1	Introduction	91
5.1.1	Generation of droplets	91
5.1.2	Drop-substrate interaction and solidification	94
5.1.3	Inkjet of conductive polymers	94
5.2	Printing PEDOT:PSS on PVDF membrane	95
5.2.1	Ink-substrate interaction	95
5.2.2	Ink composition	99
5.3	Printing and characterisation of actuators	103
5.4	Conclusion	105
5.4.1	Future work	106

5.1 Introduction

In order to push the technology of soft actuators from the laboratory bench to the production plant, large scale fabrication methods are needed. One of the most likely solutions is inkjet printing. Inkjet printing is a non-contact direct printing technique¹ that is considered to be one of the key technologies for defined polymer deposition. Furthermore, it is a low cost, high speed and high precision technique. It also allows printing of several functional inks in parallel giving way to material and shape patterning and could be used in linear arrays for high throughput fabrication. This technology has many promising applications including printing of displays [57, 88], plastic electronics [21, 173], solar cells [100, 145, 361], soldering [137], biosensors [202], tissue engineering [73, 328] *etc.* There are three process steps that need to be understood in order to achieve full potential of inkjet printing: (1) generation, ejection and flight of droplet; (2) positioning, impact and interaction of droplet with the substrate; (3) drying and solidification of the product.

5.1.1 Generation of droplets

Ink-jet printing could be used in 2 modes: continuous or drop-on-demand (*DoD*) mode. In the continuous mode the ink is being pumped through the nozzle and due to the imposed periodic perturbation, uniformly sized and spaced droplets are being generated

¹It does not require masks nor stencils

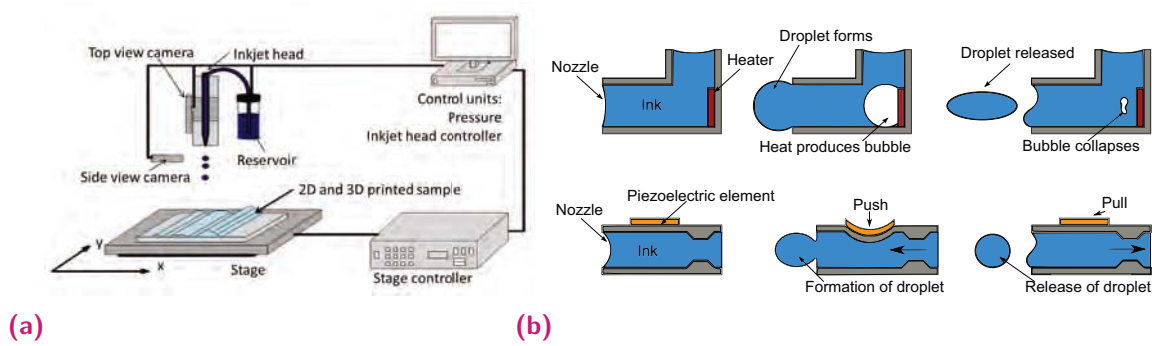


Fig. 5.1. (a) Schematic diagram of a drop-on-demand inkjet printer. (b) The schematic cycle of drop ejection in (above) thermal (rapid expansion and collapse of the bubble) and (below) piezoelectric (by direct mechanical deformation at typically $1 - 20 \text{ kHz}$) inkjet drop-on-demand printing.

(based on the Rayleigh-Tomotika instability). The unwanted drops are then deflected by the electric field and, if possible, recycled. Continuous mode is mainly used for high-speed (drop generation rates $20 - 60 \text{ kHz}$, drop velocity $> 10 \text{ m.s}^{-1}$) and low precision (drop size of approximately $100 \mu\text{m}$) applications and will not be further discussed.

Drop-on-demand mode (Fig. 5.1a) has less restrictions on the ink properties and is superior due to the higher placement accuracy and smaller droplet size ($20 - 50 \mu\text{m}$). In this mode, the printer nozzle is manually located above the desired position and droplets are ejected when needed by using thermally or piezo-electrically generated pressure pulses (Fig. 5.1b). Even though droplet size is mostly dependent on the size of the nozzle, controlling pressure pulses allows limited control of its size and ejection velocity and is a crucial know-how in order to form stable drop ejection [85].

Ink requirements

The crucial aspect of the inkjet printing is the physical properties of the ink, especially its viscosity, density and surface tension. Appropriate ink composition is required not only for printability, but also for a good accuracy and resolution. Physics and fluid mechanics of jetting is a complex process and is usually approximated and characterised by Fromm equation [113]:

$$Z = \frac{N_{Re}}{(N_{We})^{1/2}} = \frac{(\alpha\rho\gamma)^{1/2}}{\eta} \quad (5.1)$$

where $N_{Re} = \alpha\rho\nu/\eta$ is the Reynolds number (ratio of inertial and viscous forces), $N_{We} = \alpha\rho\nu^2/\gamma$ is the Weber number (ratio between inertial and capillary forces), ρ , γ , η are the density, surface tension and viscosity of the ink respectively, ν is velocity and α is the length of the printing orifice. The value of the dimensionless Z number, that permits printing of the fluid was determined by computational fluid dynamics to be between 1 and 10 [320]. On the other hand, more recent experimental studies based on *in-situ* monitoring of drop formation redefined the printable range to be between $Z = 4$ and $Z = 14$ [156]. It was shown that liquids having low Z values are unable to form a droplet due to the viscous dissipation. Meanwhile, high Z values lead to the

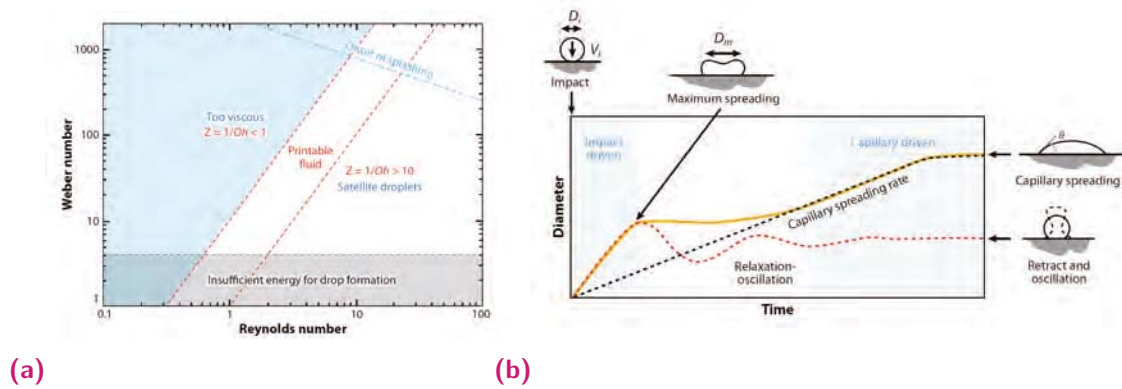


Fig. 5.2. (a) Illustration of the range of the fluid properties that allows *DoD* inkjet printing. (b) Equations plotted in a coordinate system defined by the Reynolds and Weber numbers. (c) Schematic illustration of the sequence of the events that occur after droplet impact an a substrate. Reprinted from [85].

formation of a long-lived filament between the nozzle and the droplet or large number of satellite drops that degrade printing resolution.

In general, viscosity determines the velocity and the amount of the fluid ejected². In order to allow ejection of the droplet it should be bellow 20 mPa s . On the other hand surface tension is determining the shape of the droplet and in order to obtain spheroids it should range from 30 mN/m to 350 mN/m [120]. Ejection velocity will also influence the splashing on the surface and for the flat, smooth surfaces the product $We^{1/2} Re^{1/4}$ should remain about 50. All these parameters were summarised by [85] and are shown in Fig. 5.2a.

Other factors influencing printing performance are wetting of the nozzle by the fluid³ and the particle size in the solution. Intuitively, large particles⁴ would often cause clogging. On the other hand, presence of the smaller particles was shown to lead to the entrapment of the air bubbles in the nozzle and asymmetric jet formations [167]. Furthermore, particles could also influence formation of satellites and filament breakup.

Printing polymers

Limited solubility and miscibility and high viscosity make the polymer printing a challenging task. Therefore only very dilute solutions of long chain polymers and low volumes of particles are normally printable. Furthermore, polymers in the ink influence the drop and filament formation. These processes were shown to be dependent on the polymer rheological properties, *i.e.* structure, molecular weight, concentration. The main observed difference in comparison to Newtonian ink is the increased breakup length, meaning that after the jetting, solution does not break into the drops that remain connected by long threads. These threads are thinning with increasing distance and

²In order to be ejected, drop needs to overcome fluid/air surface tension at the nozzle that leads to the minimum ejection velocity [120]: $v_{min} = \left(\frac{4\gamma}{\rho d_n}\right)^{1/2}$

³Too low contact angle would lead to formation of spray.

⁴Depends on the nozzle diameter, for $30 \mu\text{m}$ nozzle $> 20 \mu\text{m}$.

eventually break, but at much larger distances [127]. The main rheological parameter characterising this behaviour is elongation viscosity⁵. Mun *et al.* showed that in solutions with similar density, viscosity and surface tension, the breakup behaviour differed depending on the concentration and molecular weight of the polymer and the breakup length increases with increasing molecular weight (above M_W 300000) and concentration [279].

5.1.2 Drop-substrate interaction and solidification

For most of the applications, the ejected drop is reaching the substrate in the liquid state and consequent phase change occurs (by solvent evaporation, chemical reaction etc) leading to solid final product. The liquid drop will be on the substrate for a finite time, allowing liquid-solid interaction. Due to the low density, surface tension, diameter and the length scales ($2 - 3 \text{ mm}$) gravitational forces (in order of 10^{-14} J) can be neglected and inertial and capillary forces are dominant. Schematic illustration showing sequence of events occurring after the impact is shown in Fig. 5.2b. Initial events ($< 1 \mu\text{s}$), such as impact driven spreading and oscillations are determined by viscosity of the fluid [331]. At the later stages ($0.1 - 1 \text{ ms}$), capillary forces start to dominate and the final drop size is mostly dependent on its volume and contact angle.

On flat and smooth substrates the contact angle and the volume are determining the resolution of printing (typically about $30 \mu\text{m}$). Nevertheless, if needed, several chemical [335, 342, 389] or mechanical [139, 254] surface patterning methods were suggested in order to produce features smaller than $5 \mu\text{m}$. If a porous substrate is used, as in our case, another parameter needs to be taken into account, *i.e.* infiltration speed. Factors influencing penetration of liquid through the membrane were more extensively discussed in Chapter 3.4. Here we will only add, that for small droplets of $30 - 60 \mu\text{m}$ and porosities of $0.07 - 0.17 \mu\text{m}$ infiltration times are in range of $100 - 500 \text{ ms}$. This means that liquid begins to recede due to infiltration only when the spreading stops [142] and this process is likely to be dependent on the chemical nature of the porous substrate.

The last step influencing morphology of the deposited spot is its solidification. In most of the cases it is based on drying. Formation of a coffee stain, *i.e.* aggregation of solute at the initial contact line [82], is one of the well known resolution limitations associated with inkjet printing. Several methods were used to reduce this effect, such as enhanced vapour pressure of environment, more complex solvents, phase change flow depletion *etc.* [85], but they mostly rely on implying even more limitations on printable ink.

5.1.3 Inkjet of conductive polymers

Inkjet printing of conductive polymers is challenging due to their small solubility and miscibility. Furthermore, for most of the applications, good conductivity and adherence to substrate is required that increase requirements for the ink and its rheological properties. Very often additives to the solvent are used in order to adjust rheological and surface energy characteristics, same additives can also have beneficial effects

⁵The resistance of the fluid to stretching motion.

on solvent-polymer compatibility and interaction. For example, ethylene glycol in poly(3,4-ethylenedioxythiophene) polystyrene sulfonate (*PEDOT:PSS*) does not only affects viscosity and surface tension, but also significantly increases its conductivity and changes the water solubility of the film [140, 235].

Even though other conductive polymers such as polyaniline were shown to be possible to print by synthesizing their nanoparticle dispersions [277], *PEDOT:PSS* is the only commercially available conducting polymer that is extensively used in flexible and printed electronics [21, 174, 221]. The main challenge remains in increasing its electrical conductivity and various ink formulations were suggested as well as pre- and post-treatment strategies [100, 195, 221, 232, 400, 403]. The most common additives are: (1) *DMSO* [79, 400], that facilitates the charge transport by aligning poly(3,4-ethylenedioxythiophene) (*PEDOT*) chains and coarsening of *PEDOT:PSS* grains; (2) glycerol [100, 401], that increases conductivity as dimethyl sulfoxide (*DMSO*) and is also used to tune the viscosity of the ink and (3) various surfactants [140, 400], usually used for easier adjustment of the surface tension and elongation viscosity. In addition to improved conductivity and fluid properties, very often additives are also used to improve interaction between the printed *PEDOT:PSS* and the substrate [232].

Interaction between *PEDOT:PSS* and the substrate is another critical aspect of printed electronics. Most of the substrates are hydrophobic plastics *i.e.* polyethylene terephthalate *PET* [21], polyvinylpyrrolidone (*PVP*) [221], polyimide [174], or glass [118], therefore hydrophilic *PEDOT:PSS* aggregates making it difficult to define patterns. Unsurprisingly, it also leads to poor adhesion [9]. Therefore, various surface treatments are often performed before inkjet printing in order to improve pattern resolution [254, 407] and conductivity of the layer.

5.2 Printing *PEDOT:PSS* on PVDF membrane

Even though printing of *PEDOT:PSS* is a commonly used technique, the knowledge of the influence of the additives on drop and film formation is very vague. Even less is known about inkjet printing of polymers on porous substrate. Angelo *et al* observed penetration of *PEDOT:PSS* based ink into photo paper, that was used as a substrate and discussed influence of the penetration depth to conductivity [9]. Nevertheless, no studies regarding mechanisms of this behaviour were yet done and to our knowledge, printing of *PEDOT:PSS* on polyvinylidene fluoride (*PVDF*) filtration membranes was not yet reported.

5.2.1 Ink-substrate interaction

In addition to the normal model explaining interactions between the ink and the substrate, that considers only impact and capillary driven spreading, we need to take into account roughness, porosity and chemical nature of the membrane. Even though jetted droplets are 50 times larger than the size of the pores (50 μm vs 100 nm), the ink is a very diluted polymer solution (1.3 $\text{wt}\%$) leading to only very thin layer of polymer being deposited per droplet. This can be observed in atomic force microscopy (*AFM*)

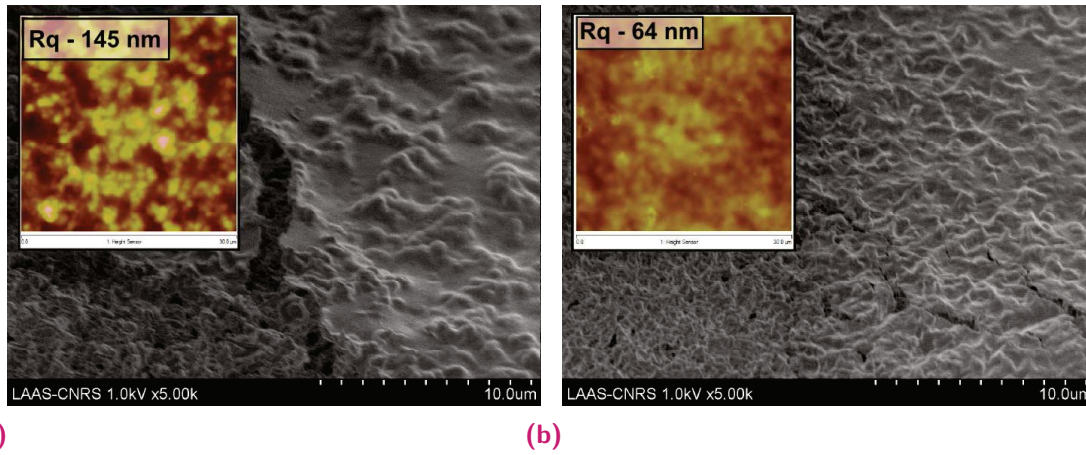


Fig. 5.3. SEM of PEDOT:PSS layer printed on (a) rough and (b) smooth side of the PVDF membrane at the printing borderline. Inset: AFM surface scan of the PEDOT:PSS printed on each side of the membrane.

and scanning electron microscopy (SEM) images shown in Fig. 5.3, where PEDOT:PSS seems to cover roughness of PVDF membrane. The roughness of the membranes only slightly decreases after printing: from 252 nm to 145 nm (for rough side of PVDF and PEDOT:PSS printed on PVDF respectively) and from 158 nm to 64 nm on the smooth side of PVDF.

It can be expected that roughness of the membrane disrupts the conductive paths between PEDOT:PSS grains. That should lead to lower conductivity in comparison to the thin films deposited on glass. Assuming thickness of 0.5 μm (as roughly estimated by AFM (Appendix B Fig. B.17)) conductivity of pristine PEDOT:PSS printed with a 40 x 40 μm printing resolution on hydrophobic membrane are 2.7 Scm^{-1} and 3.0 Scm^{-1} for rough and smooth sides respectively. As the thickness of PEDOT:PSS is very similar to the roughness of the membrane it cannot be accurately estimated. Therefore, comparison of conductivities with external sources is hard to make. The influence of the printing resolution on the measured conductivity is shown in Fig. A.5b. Reported value for lower resolution printing (50 x 50 μm with 60 μm droplet size leading to 400 nm thickness) of pristine PEDOT:PSS on glass is 0.1 Scm^{-1} [403] - 30 times lower than estimated in our experiments. Because of the approximate thickness, only qualitative comparison of ink composition to the conductivity of the film will be made. On the other hand, surface roughness is expected to play minor role on conductivity if more than one layer of PEDOT:PSS is printed.

Mechanical properties of PEDOT:PSS were reported to be very dependent on the thickness of the film. For example, it was evaluated that the elastic modulus of thin PEDOT:PSS films (500 nm) might be twice as much as of thicker ones (25 μm) - 6 - 7 GPa - 2.8 GPa respectively [214]. In our case, printing pristine PEDOT:PSS led to extremely brittle thin films, that formed numerous cracks while handling as shown in Fig. 5.4a. Furthermore, as discussed in the Chapter 3, adhesion and infiltration of PEDOT:PSS also need to be taken into account when printing actuators. As shown in Fig. 5.4b, just as for the drop casted films, a thicker layer of inkjet printed PEDOT:PSS easily detaches from the membrane, and trilayer actuator delaminates as soon as put in

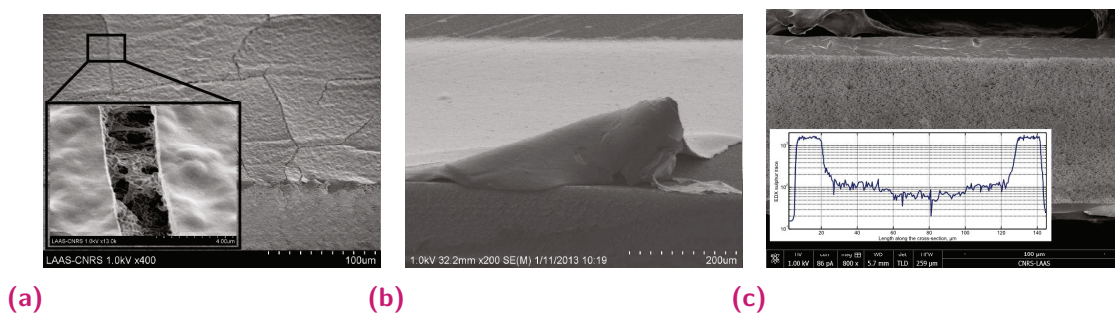


Fig. 5.4. (a) SEM of one pure PEDOT:PSS layer printed on PVDF membrane cracked after drying, (b) SEM of 10 PEDOT:PSS layer having 10 vol% glycerol printed on PVDF membrane showing easy delamination caused by handling and (c) SEM image of the cross-section of PEDOT:PSS/PVDF/PEDOT:PSS trilayer, when surfactant (1 vol% Triton-X100) was added to PEDOT:PSS ink. *Inset:* EDX line scan along the cross-section, indicating PEDOT:PSS abundance through the PVDF membrane.

the liquid. Equivalently, if surfactants are being used, *i.e.* *Triton-X100*, PEDOT:PSS ink penetrates through the membrane, percolating the electrodes as shown in Fig. 5.4c.

Therefore, in addition to established requirements for ink that allows good jetting, secondary dopants need to be used in order to increase the conductivity of the ink and to improve mechanical properties of the thin films. Furthermore, the surface tension of the ink needs to be monitored in order to prevent infiltration while assuring good adhesion. In contrast to previous discussion in Chapter 3, gravitational forces exerted by a drop are low and the pressure of the ink on the membrane is negligible, therefore the impact and capillary forces are dominant in ink-substrate interaction.

As water is used as a solvent and printing is done keeping the sample holder at room temperature, the evaporation of the solvent is slow (for 50 μm water drop on flight could take several seconds) [143]. Furthermore, interference of two neighbouring droplets increases evaporation time even further [198] leading to, in our case, still wet films after tens of minutes of printing. That gives sufficient time window for capillary forces to drive the outward spreading of the droplet as well as infiltration into the pores of the membrane. Thus, when PEDOT:PSS is printed on hydrophilic PVDF or surfactants decreasing surface tension are used (such as *Triton-X100* leading to surface tension lower than 15 mN/m), ink covers all the pores of the membrane (Fig. 5.4c).

Due to low evaporation time and high printing resolution (40 x 40 μm and 50 μm initial droplet size), evaluation of a single droplet drying is not relevant. In our case, droplets merge on the surface before drying and form a macroscopic pattern. Initial phase of impact and capillary driven spreading of the liquid solution can be characterized by the contact angle between the materials and is mostly dependent on the material properties. On the other hand final film formation will depend on several other effects that play role during drying. Such effects include, evaporation of the solvent and the recession or pinning of the contact line, outward flow of the polymer within the liquid film, that often creates coffee ring effect (Fig. 5.5a) [82], Marangoni effect⁶, that leads to films with flatter profiles (Fig. 5.5b) [170] and, in our case, infiltration rate (Fig. 5.5e).

⁶the flow towards the centre due to surface tension gradients

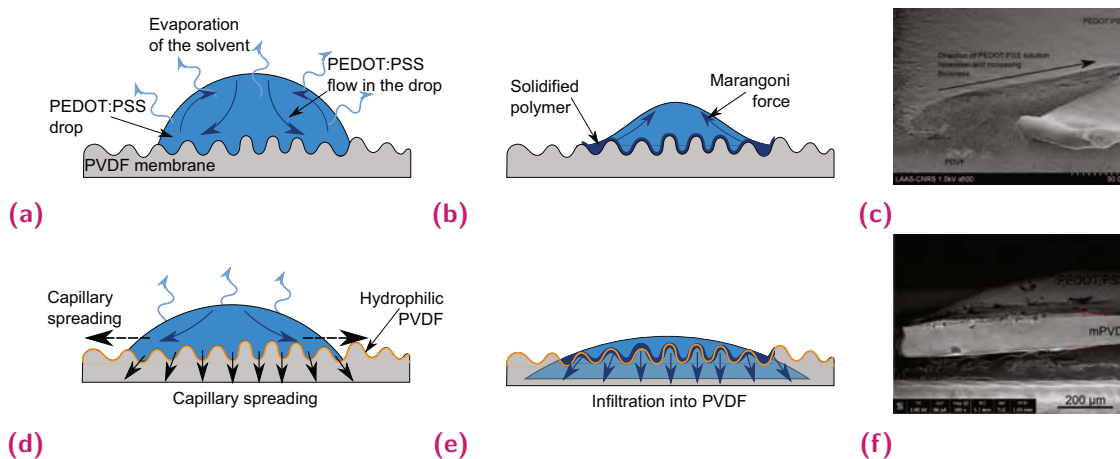


Fig. 5.5. Schematic illustration of some substrate-ink interactions, when (a)-(b) hydrophobic or (d)-(e) hydrophilic membrane is used as a substrate. SEM pictures of *PEDOT:PSS* printed on the (c) hydrophobic and (f) hydrophilic *PVDF* membranes.

Detailed analysis of the underlying mechanisms was not carried out in our work, but several relevant observations can be mentioned. In the case of printing *PEDOT:PSS* on the hydrophobic *PVDF* membrane, the infiltration is negligible and the contact line is not pinned and is receding when drying. Nevertheless, this behaviour does not lead to the formation of the coffee ring. Due to the viscosity of *PEDOT:PSS* receding line leaves part of the film behind, as previously explained by Kajiya *et al* [170]. Subsequently, the thickness of the polymer film is gradually increasing as shown in Fig. 5.5c. The roughness of the surface seems to play role in this behaviour, as for smooth surface the formed dried film profile is more gradual than for rough side (shown in Fig. 5.3. If thicker *PEDOT:PSS* films are printed on the modified *PVDF*, infiltration should compete with recession. The change in thickness on the edge of the printed film is shown in Fig. 5.5f. Another interesting phenomenon, observed after printing surfactant-free *PEDOT:PSS* on the hydrophilic *PVDF* membranes is the large surface diffusion. Traces of *PEDOT:PSS* can be observed few millimetres away from the initial deposition place as shown in Fig. 5.6a-5.6b. Even more impressive is the formation of two rings with different quantities of *PEDOT:PSS* as shown in Fig. 5.6b. Enlarged SEM images of the membrane surface at different distance from the printed pattern are shown in Fig. 5.6c-5.6f. *PEDOT:PSS* covers the pores of *PVDF* and, at least within the limits of the first ring, the length of the *PEDOT:PSS* diffusion into the pores correspond to the functionalization length of *PVDF* membrane (Fig. 5.6g): sulphur traces few micrometers in depth are visible on the surface of the membrane even where it was not printed. Furthermore, as shown in SEM images, the amount of *PEDOT:PSS* seems to be quite homogeneous within a ring - *PVDF* surface looks very similar close to the printed pattern and further away (Fig. 5.6c-5.6d).

This phenomenon was not observed neither when *PEDOT:PSS* was printed on hydrophobic *PVDF* nor when surfactant (*Triton-X100*) was used to facilitate the jetting. Even though extensive studies were not performed, it is clear that hydrophilic functionalization of the surface is causing this behaviour. It would be interesting to link the size of the rings to the morphology of the functionalized membrane. When *Triton-X100* is used

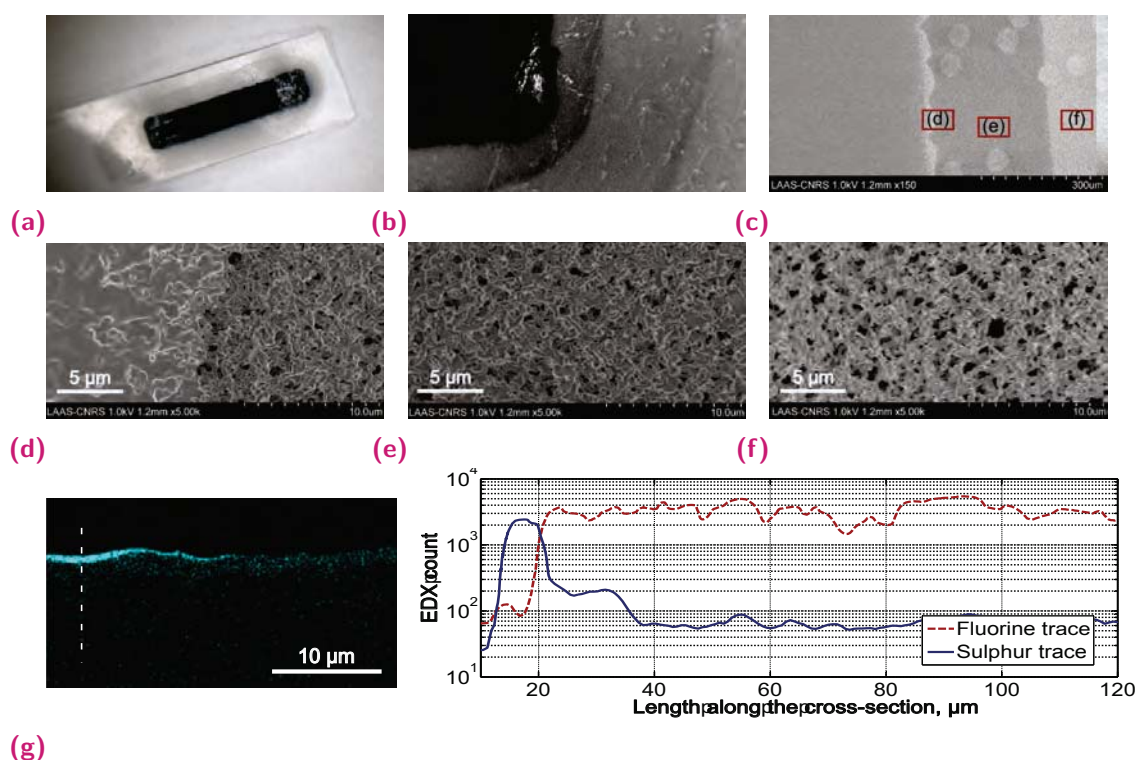


Fig. 5.6. (a) Picture of the *PEDOT:PSS* electrodes printed on *PVDF* membrane and *PEDOT:PSS* 'ring' on the surface after incubation in the ionic liquid. (b) Picture of the same actuator before immersion in ionic liquid showing two rings formed by *PEDOT:PSS* spreading on the surface. (c) SEM image of the edge of the printed actuator and the 'ring' (satellite droplets are also seen around the actuator (lighter rounds)), (d)-(f) shows enlarged areas of the membrane and different amounts of *PEDOT:PSS* on the surface. (e) EDX area and line scans along the cross-section of 10 layers of *PEDOT:PSS* printed on *PVDF-graft-PEGMA* membrane (*mPVDF*). Sulphur trace is shown in blue. The approximate place of the line scan is indicated with the white dashed line.

as a surfactant, functionalization of the membrane does not influence the distribution of *PEDOT:PSS* in the membrane. Diffusion of *PEDOT:PSS* in that case seems to be driven by surfactant and is more anisotropic towards vertical infiltration⁷. Observed surface diffusion means that high resolution patterns will not be feasible with our materials. Nevertheless, it is possible that such a small amount of *PEDOT:PSS* on only the surface of the membrane would not significantly influence the behaviour of the actuators. This and further questions are the subjects of a future study.

5.2.2 Ink composition

Conductivity

Thermal and solvent annealing play important role in determining the conductivity and mechanical properties of inkjet printed *PEDOT:PSS* thin films [146, 264, 403]. Nevertheless, secondary additives and temperature annealing do not only effect the

⁷Nevertheless, the Energy-dispersive X-ray spectroscopy (EDX) area scan at the edge of the pattern was not taken. The statement is based on the EDX line scan, that does not show larger amount of *PEDOT:PSS* in the hydrophilized pores and SEM images at the edge of the printing, where *PEDOT:PSS* is not as visible as in Fig. 5.6d.

morphology of the polymer but might as well influence the polymer-substrate interactions. Study on the conductivity of *PEDOT:PSS* printed on porous substrates has not yet been reported. In order to make a good choice for a composition of the ink, the conductivity of *PEDOT:PSS* with various secondary dopants was measured as illustrated in Fig. 5.7a. Lines of *PEDOT:PSS* with various secondary dopants were printed in between two sputtered gold electrodes on the pristine or functionalized *PVDF* membrane. Conductivity was subsequently calculated from measured resistance in between the electrodes, assuming that the thickness of the film is the same in all cases ($0.5 \mu\text{m}$). (More detailed set-up is provided in Appendix A.5). *PEDOT:PSS* with glycerol as secondary dopant (*G-PEDOT*) [213], *PEDOT:PSS* with ethylene glycol as secondary dopant (*EG-PEDOT*) [195, 293] and *PEDOT:PSS* with *PEG* as secondary dopant (*PEG-PEDOT*) [264] were tested.

The conductivity of printed films shows similar behaviour as previously reported. Ethylene glycol is significantly improving conductivity of *PEDOT:PSS* film at lower concentration (up to 4 vol%) and conductivity does not significantly change for higher ethylene glycol concentrations as shown in Fig. 5.7b [195, 396]. Nevertheless, measured highest conductivity is nearly 20 times lower than reported by Kim et al (700 S/cm vs 40 S/cm). On the contrary, the conductivity of *G-PEDOT* increases with increased concentration of glycerol but thermal annealing is required for the effect to take place (as shown in Fig. 5.7c). As in case of *EG-PEDOT*, in comparison to printed on glass thin films *PEDOT:PSS* doped with glycerol also shows conductivity several times lower than reported [403].

One significant difference between previously reported *PEDOT:PSS* conductivity studies and our results is the effect of thermal annealing on conductivity. It is commonly accepted, that conductivity increases after thermal annealing [146, 264, 403, 423]. Nevertheless, in our case, a slight decrease is observed for most of the polymer compositions⁸ even after short thermal annealing times (30 minutes at $80-100^\circ\text{C}$) Fig. 5.7b-5.7d. Furthermore the conductivity is further decreasing with increased annealing time.

The porous substrate used in our conductivity studies is probably the explanation of such observations. As previously mentioned and shown in Fig. 5.7b the conductivity of the thin film is dependent on the roughness of the membrane and is generally about 10 S/cm lower for *PEDOT:PSS* deposited on the rough side. The infiltration of *PEDOT:PSS* to the pores of the membrane is expected to decrease the conductivity of the polymer even further (also discussed in Section 4.5). Nevertheless, thermally driven infiltration should be thermodynamically unfavourable due to the immiscibility of *PEDOT:PSS* and *PVDF*. As shown in Fig. 5.7d, thermal annealing has no observable effect on the conductivity of the pristine *PEDOT:PSS* film printed on hydrophobic *PVDF*. Nevertheless, glycerol is an amphiphilic molecule that can adsorb on hydrophobic surface and subsequently favour the infiltration of *PEDOT:PSS*. Infiltration of *PEDOT:PSS* to the pores of the membrane when large amounts of glycerol are used could explain the divergence from the reported conductivity (black dashed line) observed for amounts larger than 10 vol%. Even though, it should be proven with infiltration studies, 10 vol% of glycerol in *PEDOT:PSS* could be the threshold value for formation of interfacial layer.

⁸Except initial thermal annealing step of thin films of *G-PEDOT*

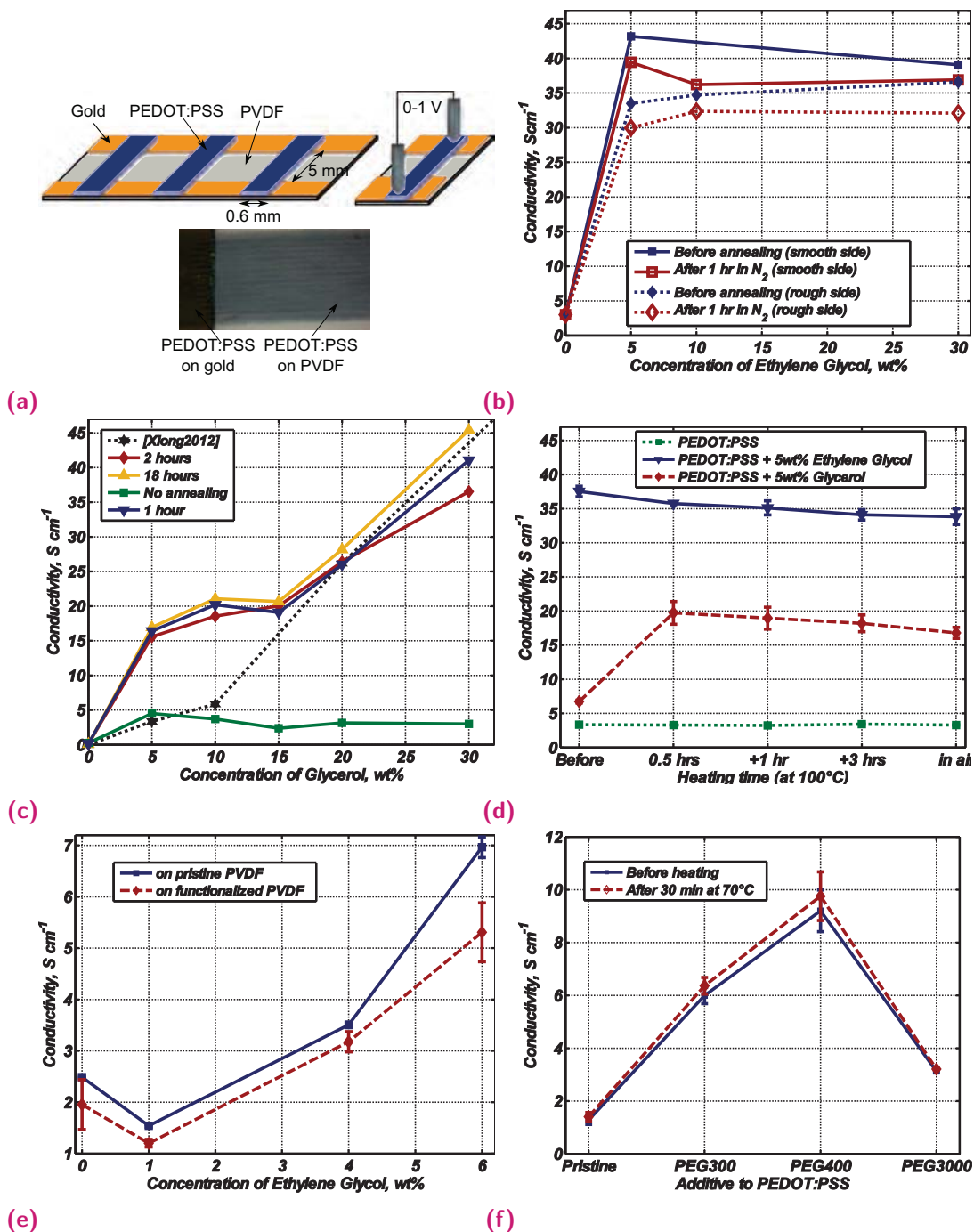


Fig. 5.7. (a) Schematic illustration of the set-up for conductivity measurement. 10 lines of PEDOT:PSS with $40 \times 40 \mu\text{m}$ resolution were printed on the PVDF membrane in between two sputtered gold electrodes. Picture of the printed film on the membrane and the electrode is shown below. The lines were cut and the resistance of the electrodes was measured. The conductivity was calculated assuming dimensions of $0.6 \text{ mm} \times 5 \text{ mm} \times 500 \text{ nm}$. Conductivity of PEDOT:PSS secondary doped with different amounts of (b) ethylene glycol or (c) glycerol before and after thermal annealing. Annealing conditions are indicated in the legend. Films were printed on the smooth side of pristine PVDF membrane (pPVDF) unless indicated differently. Conductivity of G-PEDOT reported by [403] is plotted as a black dotted line. (d) Summarized influence of thermal annealing on conductivity of PEDOT (green dotted line) EG-PEDOT (red dashed line) and G-PEDOT (blue line). (e) EG-PEDOT with 5 vol% of Triton-X100 printed on the pristine (blue line) and functionalized (red dashed line) PVDF membrane. (f) Conductivity of PEDOT secondary doped with 1 vol% of PEG of different molecular weights and printed on functionalized PVDF membrane. Thermal annealing conditions are indicated in the legend.

Fig. 5.7e and 5.7f also support the idea that measured conductivity decreases if *PEDOT:PSS* is infiltrated into *PVDF*. Fig 5.7e shows conductivity measurement of *PEDOT:PSS* with ethylene glycol and with 5 vol% of surfactant (*Triton-X100*) printed on pristine and functionalized *PVDF* membrane (*mPVDF*). As estimation of thickness is difficult due to small amounts⁹, the thickness of 500 nm was used for calculation for comparison with previous results. In this case, for the same ethylene glycol concentration conductivity is 10 times lower than in Fig. 5.7b. This value is further decreased if a functionalized *PVDF* membrane is used. Infiltration facilitated by the hydrophilic *PVDF* membrane leads to a larger interfacial layer and, in this case, lower conductivity of the printed polymer layer. Similar conductivity values were obtained for printing 1 vol% of *PEG-PEDOT mPVDF* membranes. As previously reported, conductivity enhancement with polyethylene glycol (*PEG*) in comparison to ethylene glycol is generally higher, but when printed on hydrophilic membranes, we obtained 70 times lower than reported conductivities, 9 S/cm vs 650 S/cm for 1 vol% poly(ethylene glycol) of $M_r = 400$ (*PEG400*) [264].

The conductivity enhancement mechanisms of *PEDOT:PSS* are not yet fully understood therefore effect of heating can not be easily explained. The temperature influence correspond to the reported one in a way that thermal annealing significantly enhance *G-PEDOT* conductivity [403], but do not significantly change *EG-PEDOT* [235]. In our case, as relatively low temperatures were used the influence of the evaporation of the additives is negligible¹⁰ and the reorganisation of *PEDOT* and polystyrene sulfonate (*PSS*) is also unlikely [423]. Therefore the decrease in conductivity is most likely due to the infiltration of *PEDOT:PSS* into *PVDF* that is facilitated by secondary dopants. Contrary, the conductivity of *PEG-PEDOT* printed on *mPVDF* increases after thermal annealing. Probably, lower mobility of *PEG* in comparison to ethylene glycol prevents it from infiltration in the pores and, therefore, the infiltration depth is limited to functionalization and is independent of temperature. Thus, slight conductivity increase after the thermal annealing could be due to the evaporation of residual water from *PEDOT:PSS* film [423].

To sum up, the conductivity of *PEDOT:PSS* thin films printed on porous substrate is tens of times lower than on flat substrates. We showed that in our case, the infiltration in the pores of the membrane is the main cause of low conductivity. Therefore, addition of surfactants, that are often used to improve conductivity, significantly reduce it. Furthermore, thermal annealing can also have double effect on conductivity. If facilitated by amphiphilic additives, thermal annealing could increase the mixing depth. On the other hand, if the infiltration is prevented, thermal annealing could help to improve the conductivity probably by removing residual water from the film.

Liquid properties

One of the parameters determining the jetting stability is the diameter of the nozzle (see Eq.5.1). The nozzle was changed in between different experiments but once the possibility to use surfactants was declined due to the risk of percolation, 30 μm was

⁹The thickness of the printed films is on the same order of magnitude as the roughness of the membrane. Therefore, it is impossible to detect the edge by *AFM* or mechanical profilometer.

¹⁰boiling point of ethylene glycol and glycerol are 197°C and 290°C respectively

Tab. 5.1. Physical properties of PEDOT:PSS inks

PEDOT:PSS additive	Density, g/ml	Surface tension, mN/m	Viscosity, $_{a}$ $mPas$	Z^b
pristine	1	66.7	15	2.98
5 vol% EG	1	69.0	8.2	7.16
5 vol% glycerol	1.01		17.5	
1 vol% PEG400	1	45.2	12.7	2.90
1 vol% PEG400 +1 vol% Triton-X100	1.01	18.8	12.5	1.91

^a Measured at 25°C. ^a For calculations α value of 30 μm was used. It corresponds to the diameter of nozzle that was used for printing latest actuators.

chosen as most suitable one. The Z values of different *PEDOT:PSS* inks are shown in Table 5.1. Only *PEDOT:PSS* with ethylene glycol as secondary dopant (*EG-PEDOT*) has a Z value larger than 4, that should theoretically lead to stable jetting. In order to print inks discussed in previous section, larger nozzle or variation of the temperature of the nozzle were used to adjust viscosity of the ink. For example, if 50 μm nozzle is used, Z value for pristine *PEDOT:PSS* is 3.85. It can be further increase to above 5 if temperature is used to decrease the viscosity. Nevertheless, even if theoretically acceptable, jetting of pristine *PEDOT:PSS* is still often unstable. In addition to temperature, the waveform and driving voltage had to be optimised for each solution. Variation of these parameters could also have some influence¹¹ to the quality of the deposited film¹¹ Nevertheless, probably due to the non-Newtonian fluid properties of *PEDOT:PSS* as well as its particle-like tertiary structure in water, stable jetting is a very challenging task.

As printing actuators should be not only be material but also time efficient process, the ink satisfying previously mentioned requirements and allowing reliable jetting was chosen. Using ethylene glycol as secondary dopant improves the conductivity and mechanical properties of the film and does not facilitate the infiltration and subsequent electrode percolation. Furthermore, it allows relatively stable jetting ($Z = 7.16$)¹². Therefore, *PEDOT:PSS* secondary doped with 5 vol% of ethylene glycol was chosen for further preliminary experiments and actuator fabrication by inkjet printing (unless specified differently).

5.3 Printing and characterisation of actuators

For characterisation purpose, rectangular actuators were produced by inkjet printing small 1.5 x 8 mm^2 rectangular *PEDOT:PSS* actuators were printed on *PVDF* membrane as shown in Fig. 5.8a. Then actuators with a size 2x15 mm^2 were cut by hand (Fig. 5.6a). 2 different actuators with $0.27 \pm 0.13 mg$ ¹³ and $0.42 \pm 0.06 mg$ of

¹¹For example, due to the change of the shape of the waveform used for jetting, *PEDOT:PSS* film weighting 0.18 mg and 0.36 mg were obtained (10 layers of *PEG-PEDOT* printed in a pattern of 0.8 x 5 mm on *mPVDF*).

¹²Some satellite drops were still formed during printing *EG-PEDOT* as can be seen in Fig. 5.6c

¹³Large error is most likely due to the change of the waveform that was used for jetting.

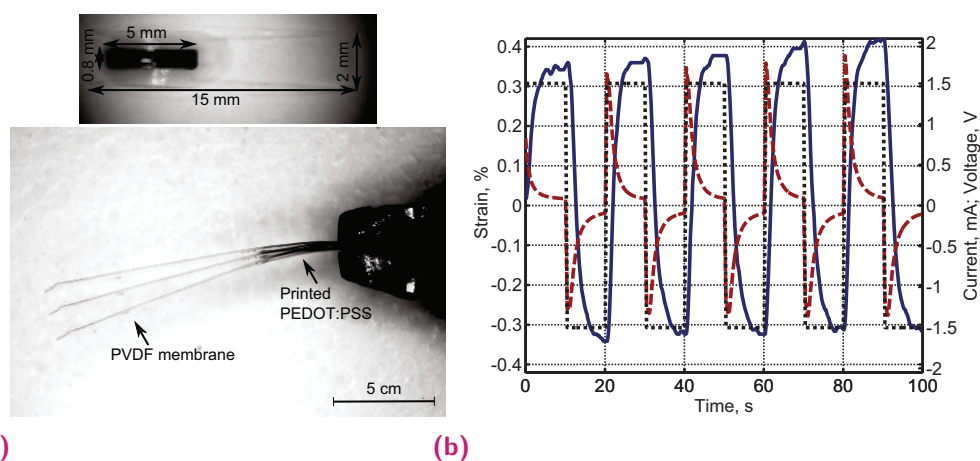


Fig. 5.8. (a) Merged images of the actuator at its initial position and extremities during the actuation with 1.5 V square wave at 50 mHz. The position of printed *PEDOT:PSS* is indicated with arrows. Dimensions of used actuator (2x15 mm) and printed *PEDOT:PSS* layer (0.8x5 mm) are shown above. (b) Displacement (blue line) and transferred current (red dashed line) profiles of printed actuator (10 layers, 0.36 mg) during actuation. The voltage waveform used is shown as black dotted line.

EG-PEDOT were printed on 3.19 ± 0.006 mg of *PVDF* membrane. After thermal annealing *PVDF* was impregnated with 4.5 ± 0.06 mg of ionic liquid and were immediately used for characterization (Appendix A.4.1). Notably, *PEDOT:PSS* does not impede the adsorption of ionic liquid (0.45 ± 0.09 mg were adsorbed by empty *mPVDF* membrane of the same size) and more than double amount of 1-ethyl-3-methylimidazolium bis(trifluoromethanesulfonyl)imide (*emimTFSI*) is adsorbed in comparison to drop-casted actuators (Fig. 4.7b). The amount of adsorbed ionic liquid was suggested to be the strain limiting factor [104] and possibility to increase the amount of ionic liquid available could be another advantage of inkjet printing.

Electrical conductivity measurements of dry printed *EG-PEDOT* are shown in Fig. B.13b. As mentioned, ethylene glycol does not cause the infiltration of *PEDOT:PSS* into the membrane and the resistance between the electrodes of inkjet printed actuators is higher than 1 GΩ. On the other hand, even relatively small amounts of *EG-PEDOT* are printed that are partially infiltrated in the pores of the membrane as shown in Fig. 5.6g (for 10 layers printed) the conductivity of the electrodes is quite high - 9.4 ± 2.3 S/cm and 27.0 ± 6.9 S/cm¹⁴.

The displacement and transferred current profiles of printed actuators are shown in Fig. 5.8b¹⁵. Significantly smaller actuators of only 0.36 mg are able to produce peak-to-peak strain of more than 0.6% that subsequently moves much longer impregnated *PVDF* membrane of 8.30 mg. Merged images of the maximum displacements during the

¹⁴Conductivity calculated assuming 10 μm thickness independently of number of layers printed and dimensions of 0.8 x 5 mm². Furthermore, conductivities for both sides were averaged even though there is a notable difference that is most likely caused by asymmetry of the membranes and infiltration depth. Finally, the conductivity of the film is proportional to the amount of *PEDOT:PSS* printed as can be seen in Fig. B.13b.

¹⁵Actuator that showed the best performance is represented - with 10 layers (0.36 mg) of printed *PEDOT:PSS* and with 4.6 mg of *emimTFSI* adsorbed. Total mass of the actuator is 8.15 mg.

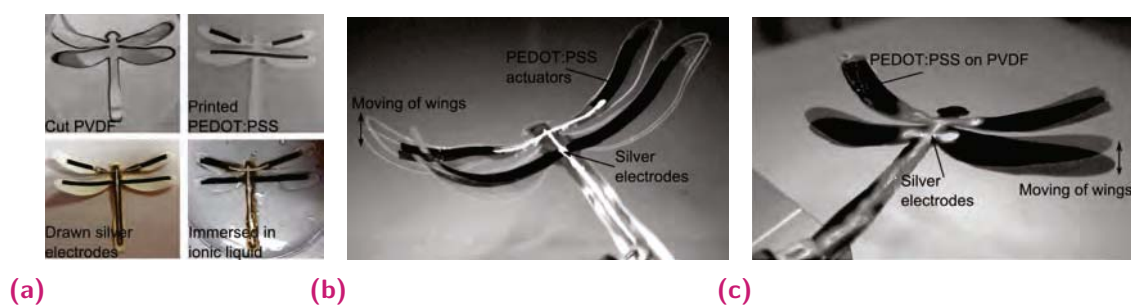


Fig. 5.9. (a) Fabrication steps for printed actuators: (1) *PVDF* membrane of wanted shape is cut; (2) *PEDOT:PSS* rectangular actuators were printed on each side of the membrane in the place where actuation was desired; (3) silver paste electrodes are drawn to connect different electrodes; (4) *PVDF* is impregnated with ionic liquid. Merged images of two actuation positions (+/− 2 V at 1 Hz) of dragonfly with (b) printed actuators and (c) actuators produced by drop casting and cutting.

actuation with 1.5 V square wave at 50 mHz is shown in Fig. 5.8a. Differently from the actuators described in Chapter 4 bending of the actuators nearly stop after few seconds (Fig. B.18a). This might be a consequence of the very thin electrodes and their small volume ($< 10 \mu\text{m}$) - full film oxidation/reduction of full film might possibly be reached. As actuators are asymmetrical (as was shown by electrical conductivity measurements), this could also explain observed rather large electrochemical creep (Fig. B.18b). If large fraction of the total volume is being irreversibly reduced during each cycle and if this process is asymmetrical for two electrodes, charge accumulation could happen on one side, causing only partly reversible cycling. This assumption still needs to be confirmed with lifetime measurements.

5.4 Conclusion

One of the advantages of inkjet printing for fabrication of soft actuators, is that it can be used to pattern and actuate various shapes in material efficient manner. Example of this is shown in Fig. 5.9. The same motion, of moving wings of the 2D dragonfly-shaped membrane was produced by fabricating device (1) by drop casting (Fig. 5.9c), when all the shape is used as a trilayer (6 ml of *PEDOT:PSS* solution required), and (2) by inkjet printing, where only $0.2 \times 1 \text{ cm}^2$ actuators were printed for each wing (using less than 0.5 ml of ink). In addition to (1) possibility to actuate various complex shapes, other possible advantages include: (2) printing complex shapes, such as spirals, U-shape etc; (3) ink patterning that allows printing parts of the actuator with different mechanical and electrical properties; (4) printing various other components of the actuators, e.g. electrodes, connections. Furthermore, inkjet printing can be scalable meaning that large quantities of identical devices can be easily produced.

In this chapter we introduced challenges that need to be overcome when printing conducting polymer on porous membranes. First of all, as for all non-Newtonian fluids and nano-particle solutions, stable satellite-free jetting needs to be obtained. It is especially challenging as the choice of the additives that are often used to tune fluid properties is limited by membrane-liquid interactions. Even if the gravitational forces

of the droplet are neglected, solutions containing surfactant are infiltrated in the pores of the membrane. Another challenge is the spreading of the ink on the surface of the hydrophilic membrane. In most of the cases, this phenomenon will limit the printing resolution of the actuators.

We have also fabricated first inkjet printed conducting polymer based actuators. Even very thin ($10\ \mu\text{m}$), printed *PEDOT:PSS* electrodes were able to produce large strains (0.3%) and subsequently move larger structures. This has huge potential as a low-cost, material efficient and up-scalable alternative fabrication technique.

5.4.1 Future work

Most of the challenges of inkjet printing were already discussed in this chapter. As for drop-casted actuators, asymmetry of the functionalization introduces asymmetrical bending. It seems that for inkjet printed actuators the difference in the reversibility of the performance is even more pronounced, probably due to the lower polymer volume. Another specific challenge to inkjet printing is alignment of the electrodes. Even though, designed non-alignment could possibly allow generation of different than bending motions (*e.g.* torque), for most basic bending actuators it might have adverse effects.

In general, inkjet printing is a very promising and powerful fabrication method and in this thesis we have just demonstrated the proof of concept of using it for printing actuators. Jetting optimization for stable, satellite-free printing needs to be performed and a large range of additives needs to be tested in order to optimize the ink composition. Furthermore, the influence of the geometry of devices (thickness, aspect ratio, *etc.*) should be investigated and could also lead to the improvement of performance. In a later study material patterning could be considered if several suitable ink compositions were found. In this way, actuators with varying electrical and mechanical properties could be printed, that could subsequently lead to different motions. Due to availability of inks, not only actuator itself, but also its connections could be printed (carbon nanotubes (*CNTs*), Ag and other metal nanoparticles *etc.*). Furthermore, it could also be used for post-treatment in order to enhance the performance of the actuators (instead of spraying, *CNTs* can also be printed on the surface of the electrode).

Finally, full characterization of the actuators was not performed. Voltage and frequency response of actuators should be determined as well as they should be characterized in terms of the stress and blocking force. That should provide more insights on overall advantages of the inkjet printed actuators.

Summary of scientific contributions and closing remarks

This thesis work was focused on the development of the fabrication technique for conducting polymer based actuators. To our best knowledge, the first artificial muscles based on poly(3,4-ethylenedioxythiophene) polystyrene sulfonate (*PEDOT:PSS*) conducting polymer inkjet printed on porous polyvinylidene fluoride (*PVDF*) membrane were demonstrated. Inkjet printing is a known fabrication method, nevertheless, it is challenging when complex fluid solutions are concerned. Overcoming technical challenges brought by the especially complex interactions between the porous membranes and the conducting polymer solution required in-depth understanding of those interactions. This led to several scientific contributions that are:

- Partly identified requirements for the composition of the polymer solution, membrane surface and fabrication conditions that lead to a strong adhesion between the formed polymer film and the membrane. Adhesion between materials was demonstrated to be an essential requirement in order to fabricate the actuators; it was also shown to play important role in the performance of the device and especially its lifetime. The work presented here proved that large infiltration into the membrane area can strongly bond materials that have different chemical nature. Furthermore, it was also demonstrated that small infiltration depth is sufficient if *graft*-polymer of similar chemical nature with short mobile chains is present at the interface. Several factors influencing this interaction were determined, e.g. the necessity of a proximate contact that is not hindered by the presence of water or other mobile molecules at the interface.
- A developed fabrication method for hybrid hydrophilic/hydrophobic/hydrophilic *PVDF* ultrafiltration membranes with the possibility to tune the thickness of each layer. Commercially available hydrophobic membranes were partly functionalized on their outer surfaces by Ar plasma induced *graft*-polymerization. In order to prevent the functionalization in the pores of the membrane, spray coating was used in a novel way for the deposition of the reaction precursor. The way to partially control the infiltration of the reaction precursor in the pores of the membrane was described and hybrid membranes with different levels of hydrophilization were demonstrated.
- Demonstration of the influence of the surface morphology of commercially available *PVDF* membranes on the deposition efficiency of sprayed polymer solution, consequent grafting reaction and adhesion. As pristine *PVDF* membranes have different surface roughnesses, the influence of it on membrane - solution interactions was studied and partly identified.

- The infiltration of complex polymer solutions in the porous membrane was discussed in the context of artificial muscles. Even though imbibition in the porous media is a widely occurring phenomenon, it was never discussed in this context. Partial explanations were provided that can be used as a guide for selecting appropriate polymer compositions when infiltration is required or needs to be avoided.
- Fabrication of conducting polymer based actuators with different areas of the infiltration in the membrane was developed. Furthermore, up to now highest produced strain of solvent casted *PEDOT:PSS* based actuators was demonstrated with a huge potential for further improvements through *PEDOT:PSS* composition optimization and post-treatments.
- Finally, *PEDOT:PSS* composition that allows stable jetting and strong membrane-polymer interaction was identified and used for inkjet printing prototype soft actuators. The possibility of low cost and material efficient fabrication of actuators operating in air was demonstrated.

6.1 Future Work

Using *PEDOT:PSS* aqueous solution for fabrication of conducting polymer actuators (*CPAs*) is a relatively new idea. It provides a wide range of possibilities for tuning electrical and mechanical properties of conducting polymer that could push further the understanding of electro-chemo-mechanical actuation. Furthermore, it could potentially increase currently very low efficiency of *CPAs*. Therefore, actuators using *PEDOT:PSS* pre- or post-treated with various secondary dopants and additives merit further investigation. Furthermore, the possibility to tune the infiltration depth of the conducting polymer in the membrane allows fabrication of actuators with different morphologies. That subsequently provides means to study the influence of the mixing depth on the performance of the actuators. In our work, these questions were only shortly introduced, but a thorough electrochemical characterization is needed in order to provide a sophisticated conclusion. In general, performance of the actuators was very poorly characterized in our work. In addition to electrochemical, extensive mechanical characterization needs to be performed. In this way performance of the actuators could be optimized not only for displacement, but also for produced stress.

Investigation of the performance enhancement by post-treatment of the actuators by carbon based nanomaterials, *i.e.* carbon nanotubes (*CNTs*), is also being carried out in our group. In this thesis, only preliminary results of this work were presented and process optimization and thorough characterization needs to be performed. Creep reduction and improved redox reversibility by *CNTs* were already reported [99, 110, 365] and some explanations to improved actuator performance were provided [309]. Versatility of fabrication by drop-casting as well as spray coating allows variation of many electro-chemo-mechanical properties of actuators that could bring further understanding of the actuation processes. *CNTs* are only one of many nanomaterials that are used to enhance properties of polymer composites [209, 351]. The use of

nanoporous carbide-derived carbon [379] and graphene [231] was already reported for applications in actuators. As spray coating bypasses the solubility in the polymer limitation, deposition of various other *CNTs* and graphene derivatives could be tested. Finally, it was also reported that the orientation and alignment of carbon nanotubes could influence performance of artificial muscles [421]. Deposition of *CNTs* by spray coating creates carpet of a randomly oriented *CNTs*. Even though spray coating is simple and versatile fabrication technique, other *CNTs* deposition and, potentially, alignment methods should be tested.

The goal of this thesis was to enable the fabrication of conducting polymer actuators by inkjet printing. Nevertheless only prototype actuators were fabricated providing only the proof-of-concept of such fabrication alternative. Optimization of the process and complete electro-chemo-mechanical characterization of inkjet printed actuators still need to be done. In addition to being a material efficient process, inkjet printing also allows material and shape patterning. Once optimized, actuators of various shapes could be produced and used for generation of the complex motions. Furthermore, wide range of materials could possibly be printed producing various functional devices or their components. Therefore, printing the conducting polymer is only the first step and the process could be further expanded by adding post-treatment of printed actuator, e.g. printing *CNTs* [50, 205, 333, 380], printing electrical wires and connections between the electrodes, e.g. silver nanowires [106, 169, 283], or printing strain gauges [8, 40, 59, 69, 325, 330]. The later possibility is especially interesting as it could allow one step fabrication of the actuator and the integrated sensor for closed-loop control. Several inkjet printed strain sensors, including sensors based on *PEDOT:PSS* [40, 69, 325], were reported and could be potentially adopted.

Having actuators with integrated strain or force feed-back possibility has been a goal for many research groups [54, 103, 104, 164, 315]. Nevertheless, thorough investigation of the dynamic behaviour of the actuator needs to be characterized using reliable external sensory feed-back before integrated sensors are implemented. Extensive modeling, simulation and control studies were already performed for polypyrrole (*PPy*) based actuators (detailed in PhD thesis of [250], [36] and [165]) [102, 391, 406]. We are currently working on the identification of the empirical transfer function models of *PEDOT:PSS* based actuators. As *PEDOT:PSS* actuators are nearly not electrochemically active at low voltages and are mostly driven by double layer charging, deviations from *PPy* based models might exist. Finally, significant change in actuators behaviour in time was presented in this thesis. Means to predict and estimate long term response should be studied and the control algorithms that could efficiently compensate the deterioration in performance developed.

Bibliography

- [1] Michel A Aegerter, Jörg Puetz, Guido Gasparro, and Naji Al-Dahoudi. „Versatile wet deposition techniques for functional oxide coatings“. In: *Optical Materials* 26.2 (2004), pp. 155–162 (cit. on p. 28).
- [2] Yumi Ahn, Hyungjin Lee, Donghwa Lee, and Youngu Lee. „Highly Conductive and Flexible Silver Nanowire-Based Microelectrodes on Biocompatible Hydrogel“. In: *ACS applied materials & interfaces* 6.21 (2014), pp. 18401–18407 (cit. on p. 5).
- [3] S Akbari and HR Shea. „Microfabrication and characterization of an array of dielectric elastomer actuators generating uniaxial strain to stretch individual cells“. In: *Journal of Micromechanics and Microengineering* 22.4 (2012), p. 045020 (cit. on p. 10).
- [4] Barbar Akle and Donald J Leo. „Electromechanical transduction in multilayer ionic transducers“. In: *Smart materials and structures* 13.5 (2004), p. 1081 (cit. on p. 6).
- [5] Desalegn Alemu, Hung-Yu Wei, Kuo-Chuan Ho, and Chih-Wei Chu. „Highly conductive PEDOT: PSS electrode by simple film treatment with methanol for ITO-free polymer solar cells“. In: *Energy & environmental science* 5.11 (2012), pp. 9662–9671 (cit. on pp. 43, 46).
- [6] Gursel Alici, Brian Mui, and Chris Cook. „Bending modeling and its experimental verification for conducting polymer actuators dedicated to manipulation applications“. In: *Sensors and Actuators A: Physical* 126.2 (2006), pp. 396–404 (cit. on pp. 78, 82).
- [7] Ali E Aliev, Jiyoung Oh, Mikhail E Kozlov, et al. „Giant-stroke, superelastic carbon nanotube aerogel muscles“. In: *science* 323.5921 (2009), pp. 1575–1578 (cit. on p. 5).
- [8] Bruno Ando and Salvatore Baglio. „All-inkjet printed strain sensors“. In: *Sensors Journal, IEEE* 13.12 (2013), pp. 4874–4879 (cit. on pp. 11, 109, 169).
- [9] Peter D Angelo and Ramin R Farnood. „Poly (3, 4-ethylenedioxythiophene): poly (styrene sulfonate) inkjet inks doped with carbon nanotubes and a polar solvent: the effect of formulation and adhesion on conductivity“. In: *Journal of Adhesion Science and Technology* 24.3 (2010), pp. 643–659 (cit. on pp. 41, 95).
- [10] Dennis Antiohos, Glenn Folkes, Peter Sherrell, et al. „Compositional effects of PEDOT-PSS/single walled carbon nanotube films on supercapacitor device performance“. In: *Journal of Materials Chemistry* 21.40 (2011), pp. 15987–15994 (cit. on p. 83).
- [11] O Araromi, Alexandre Poulin, Samuel Rosset, et al. „Thin-film dielectric elastomer sensors to measure the contraction force of smooth muscle cells“. In: *SPIE Smart Structures and Materials+ Nondestructive Evaluation and Health Monitoring*. International Society for Optics and Photonics. 2015, 94300Z–94300Z (cit. on p. 10).

- [12] Oluwaseun Araromi, Irina Gavrilovich, Jun Shintake, et al. „Rollable multisegment dielectric elastomer minimum energy structures for a deployable microsatellite gripper“. In: *Mechatronics, IEEE/ASME Transactions on* 20.1 (2015), pp. 438–446 (cit. on p. 9).
- [13] Michel Armand, Frank Endres, Douglas R MacFarlane, Hiroyuki Ohno, and Bruno Scrosati. „Ionic-liquid materials for the electrochemical challenges of the future“. In: *Nature materials* 8.8 (2009), pp. 621–629 (cit. on pp. 60, 169).
- [14] Kinji Asaka and Hidenori Okuzaki. *Soft Actuators: Materials, Modeling, Applications, and Future Perspectives*. Springer, 2014 (cit. on p. 68).
- [15] Firas Awaja, Michael Gilbert, Georgina Kelly, Bronwyn Fox, and Paul J Pigram. „Adhesion of polymers“. In: *Progress in polymer science* 34.9 (2009), pp. 948–968 (cit. on pp. 37, 39, 41, 177).
- [16] Chantal Badre, Ludovic Marquant, Ahmed M Alsayed, and Lawrence A Hough. „Highly Conductive Poly (3, 4-ethylenedioxythiophene): Poly (styrenesulfonate) Films Using 1-Ethyl-3-methylimidazolium Tetracyanoborate Ionic Liquid“. In: *Advanced Functional Materials* 22.13 (2012), pp. 2723–2727 (cit. on p. 83).
- [17] Yoseph Bar-Cohen. „Electroactive polymers as artificial muscles: A review“. In: *Journal of Spacecraft and Rockets* 39.6 (2002), pp. 822–827 (cit. on pp. 73, 182).
- [18] JN Barisci, GG Wallace, DR MacFarlane, and RH Baughman. „Investigation of ionic liquids as electrolytes for carbon nanotube electrodes“. In: *Electrochemistry communications* 6.1 (2004), pp. 22–27 (cit. on p. 7).
- [19] Joao Barramba, Joao Silva, and PJ Costa Branco. „Evaluation of dielectric gel coating for encapsulation of ionic polymer–metal composite (IPMC) actuators“. In: *Sensors and Actuators A: Physical* 140.2 (2007), pp. 232–238 (cit. on p. 6).
- [20] University of Basel. *Nano-Tera Project: SmartSphincter*. 2007 (cit. on p. 10).
- [21] Laura Basiricò, Piero Cosseddu, Beatrice Fraboni, and Annalisa Bonfiglio. „Inkjet printing of transparent, flexible, organic transistors“. In: *Thin Solid Films* 520.4 (Dec. 2011), pp. 1291–1294 (cit. on pp. 91, 95, 167).
- [22] Maria Bassil, Judy AL Moussawel, Michael Ibrahim, Georges Azzi, and Mario El Tahchi. „Electrospinning of highly aligned and covalently cross-linked hydrogel microfibers“. In: *Journal of Applied Polymer Science* 131.22 (2014) (cit. on pp. 5, 165).
- [23] Ray H Baughman, Changxing Cui, Anvar A Zakhidov, et al. „Carbon nanotube actuators“. In: *Science* 284.5418 (1999), pp. 1340–1344 (cit. on pp. 5, 7, 165).
- [24] RH Baughman. „Conducting polymer artificial muscles“. In: *Synthetic metals* 78.3 (1996), pp. 339–353 (cit. on pp. 5, 165).
- [25] Priya Bawa, Viness Pillay, Yahya E Choonara, and Lisa C du Toit. „Stimuli-responsive polymers and their applications in drug delivery“. In: *Biomedical Materials* 4.2 (2009), p. 022001 (cit. on p. 5).
- [26] Lasse Bay, Torben Jacobsen, Steen Skaarup, and Keld West. „Mechanism of actuation in conducting polymers: osmotic expansion“. In: *The Journal of Physical Chemistry B* 105.36 (2001), pp. 8492–8497 (cit. on p. 63).

- [27] Amélie Bédurier, Florent Seichepine, Emmanuel Flahaut, and Christophe Vieu. „A simple and versatile micro contact printing method for generating carbon nanotubes patterns on various substrates“. In: *Microelectronic Engineering* 97 (2012), pp. 301–305 (cit. on p. 86).
- [28] Marc Behl, Karl Kratz, Ulrich Noechel, Tilman Sauter, and Andreas Lendlein. „Temperature-memory polymer actuators“. In: *Proceedings of the National Academy of Sciences* 110.31 (2013), pp. 12555–12559 (cit. on pp. 2, 165).
- [29] Matthew D Bennett and Donald J Leo. „Ionic liquids as stable solvents for ionic polymer transducers“. In: *Sensors and Actuators A: Physical* 115.1 (2004), pp. 79–90 (cit. on pp. 6, 35, 60, 73, 169).
- [30] Euclides Alexandre Bernardelli, Marcio Mafra, Ana Maria Maliska, Thierry Belmonte, and Aloisio Nelmo Klein. „Influence of neutral and charged species on the plasma degradation of the stearic acid“. In: *Materials Research* 16.2 (2013), pp. 385–391 (cit. on p. 20).
- [31] Thomas Berthelot, Xuan Tuan Le, Pascale Jégou, et al. „Photoactivated surface grafting from PVDF surfaces“. In: *Applied Surface Science* 257.22 (2011), pp. 9473–9479 (cit. on pp. 16, 20, 172).
- [32] Qiuyan Bi, Qian Li, Ye Tian, Yakai Lin, and Xiaolin Wang. „Hydrophilic modification of poly (vinylidene fluoride) membrane with poly (vinyl pyrrolidone) via a cross-linking reaction“. In: *Journal of Applied Polymer Science* 127.1 (2013), pp. 394–401 (cit. on p. 14).
- [33] J Biener, A Wittstock, LA Zepeda-Ruiz, et al. „Surface-chemistry-driven actuation in nanoporous gold“. In: *Nature materials* 8.1 (2009), pp. 47–51 (cit. on p. 8).
- [34] J-PL Bigue and J-S Plante. „Experimental study of dielectric elastomer actuator energy conversion efficiency“. In: *Mechatronics, IEEE/ASME Transactions on* 18.1 (2013), pp. 169–177 (cit. on pp. 4, 165).
- [35] Daniel Bonn, Jens Eggers, Joseph Indekeu, Jacques Meunier, and Etienne Rolley. „Wetting and spreading“. In: *Reviews of modern physics* 81.2 (2009), p. 739 (cit. on pp. 54, 56).
- [36] Thomas Alan Bowers. „Modeling, simulation, and control of a polypyrrole-based conducting polymer actuator“. PhD thesis. Massachusetts Institute of Technology, 2004 (cit. on p. 109).
- [37] Paul Brochu and Qibing Pei. *Advances in dielectric elastomers for actuators and artificial muscles*. 2010 (cit. on pp. 4, 5, 165).
- [38] Etienne Cabane, Xiaoyan Zhang, Karolina Langowska, Cornelia G. Palivan, and Wolfgang Meier. „Stimuli-Responsive Polymers and Their Applications in Nanomedicine“. In: *Biointerphases* 7.1, 9 (2012), pp. – (cit. on p. 5).
- [39] Tao Cai, Rong Wang, Wen Jing Yang, et al. „Multi-functionalization of poly (vinylidene fluoride) membranes via combined “grafting from” and “grafting to” approaches“. In: *Soft Matter* 7.23 (2011), pp. 11133–11143 (cit. on p. 14).
- [40] Paul Calvert, Deepak Duggal, Prabir Patra, Animesh Agrawal, and Amit Sawhney. „Conducting polymer and conducting composite strain sensors on textiles“. In: *Molecular Crystals and Liquid Crystals* 484.1 (2008), pp. 291–657 (cit. on pp. 11, 109, 169).

- [41] F. Cellini, A. Grillo, and M. Porfiri. „Ionic polymer metal composites with polypyrrole-silver electrodes“. In: *Applied Physics Letters* 106.13, 131902 (2015), pp. – (cit. on p. 6).
- [42] CY Chang, WT Tsai, CH Ing, and CF Chang. „Adsorption of polyethylene glycol (PEG) from aqueous solution onto hydrophobic zeolite“. In: *Journal of colloid and interface science* 260.2 (2003), pp. 273–279 (cit. on p. 55).
- [43] Longfei Chang, Kinji Asaka, Zicai Zhu, et al. „Effects of surface roughening on the mass transport and mechanical properties of ionic polymer-metal composite“. In: *Journal of Applied Physics* 115.24 (2014), p. 244901 (cit. on p. 6).
- [44] Yung Chang, Yu-Ju Shih, Chao-Yin Ko, et al. „Hemocompatibility of poly (vinylidene fluoride) membrane grafted with network-like and brush-like antifouling layer controlled via plasma-induced surface PEGylation“. In: *Langmuir* 27.9 (2011), pp. 5445–5455 (cit. on pp. 19, 20, 23, 48, 172).
- [45] Yung Chang, Yu-Ju Shih, Ruoh-Chyu Ruaan, et al. „Preparation of poly (vinylidene fluoride) microfiltration membrane with uniform surface-copolymerized poly (ethylene glycol) methacrylate and improvement of blood compatibility“. In: *Journal of Membrane Science* 309.1 (2008), pp. 165–174 (cit. on pp. 16, 19, 20, 172).
- [46] Yung Chang, Chao-Yin Ko, Yu-Ju Shih, et al. „Surface grafting control of PEGylated poly (vinylidene fluoride) antifouling membrane via surface-initiated radical graft copolymerization“. In: *Journal of Membrane Science* 345.1 (2009), pp. 160–169 (cit. on pp. 16, 17, 19, 20, 23, 172).
- [47] Chang-hsiu Chen, Anna Torrents, Lawrence Kulinsky, et al. „Mechanical characterizations of cast Poly (3, 4-ethylenedioxythiophene): Poly (styrenesulfonate)/Polyvinyl Alcohol thin films“. In: *Synthetic Metals* 161.21 (2011), pp. 2259–2267 (cit. on pp. 43, 168).
- [48] Chien-Chun Chen, Wen-Pin Shih, Pei-Zen Chang, et al. „Onion artificial muscles“. In: *Applied Physics Letters* 106.18, 183702 (2015), pp. – (cit. on p. 8).
- [49] Ko-Shao Chen, Yoshikimi Uyama, and Yoshito Ikada. „Adhesive interaction between polymer surfaces grafted with water-soluble polymer chains“. In: *Langmuir* 10.4 (1994), pp. 1319–1322 (cit. on p. 48).
- [50] Pochiang Chen, Haitian Chen, Jing Qiu, and Chongwu Zhou. „Inkjet printing of single-walled carbon nanotube/RuO₂ nanowire supercapacitors on cloth fabrics and flexible substrates“. In: *Nano Research* 3.8 (2010), pp. 594–603 (cit. on p. 109).
- [51] Wei Chen and Thomas J McCarthy. „Layer-by-layer deposition: a tool for polymer surface modification“. In: *Macromolecules* 30.1 (1997), pp. 78–86 (cit. on p. 39).
- [52] Xiwen Chen, Ke-Zhao Xing, and Olle Inganäs. „Electrochemically induced volume changes in poly (3, 4-ethylenedioxythiophene)“. In: *Chemistry of materials* 8.10 (1996), pp. 2439–2443 (cit. on pp. 62, 63).
- [53] Zheng Chen, Tae I Um, and Hilary Bart-Smith. „A novel fabrication of ionic polymer-metal composite membrane actuator capable of 3-dimensional kinematic motions“. In: *Sensors and Actuators A: Physical* 168.1 (2011), pp. 131–139 (cit. on pp. 6, 166).
- [54] Zheng Chen, Ki-Yong Kwon, and Xiaobo Tan. „Integrated IPMC/PVDF sensory actuator and its validation in feedback control“. In: *Sensors and Actuators A: Physical* 144.2 (2008), pp. 231–241 (cit. on p. 109).

- [55] Zheng Chen, Hilary Bart-Smith, and Xiaobo Tan. „IPMC-Actuated Robotic Fish“. English. In: *Robot Fish*. Ed. by Ruxu Du, Zheng Li, Kamal Youcef-Toumi, and Pablo Valdivia y Alvarado. Springer Tracts in Mechanical Engineering. Springer Berlin Heidelberg, 2015, pp. 219–253 (cit. on p. 9).
- [56] Chuan Cheng and Alfonso H. W. Ngan. „Reversible Electrochemical Actuation of Metallic Nanohoneycombs Induced by Pseudocapacitive Redox Processes“. In: *ACS Nano* 9.4 (2015). PMID: 25758028, pp. 3984–3995 (cit. on p. 8).
- [57] Ziyong Cheng, Rubo Xing, Zhiyao Hou, Shanshan Huang, and Jun Lin. „Patterning of light-emitting YVO₄: Eu³⁺ thin films via inkjet printing“. In: *The Journal of Physical Chemistry C* 114.21 (2010), pp. 9883–9888 (cit. on p. 91).
- [58] Sadiqali Cheruthazhekatt, Mirko Černák, Pavel Slavíček, and Josef Havel. „Gas plasmas and plasma modified materials in medicine“. In: *Journal of Applied Biomedicine* 8.2 (2010), pp. 55–66 (cit. on p. 20).
- [59] Alessandro Chiolerio, Ignazio Roppolo, and Marco Sangermano. „Radical diffusion engineering: Tailored nanocomposite materials for piezoresistive inkjet printed strain measurement“. In: *RSC Advances* 3.10 (2013), pp. 3446–3452 (cit. on p. 109).
- [60] HR Choi, KM Jung, JC Koo, and JD Nam. „Robotic applications of artificial muscle actuators“. In: *Electroactive Polymers for Robotic Applications*. Springer, 2007, pp. 49–90 (cit. on pp. 1, 164).
- [61] Hwa-Jeong Choi, Young-Min Song, Ildoo Chung, Kwang-Sun Ryu, and Nam-Ju Jo. „Conducting polymer actuator based on chemically deposited polypyrrole and polyurethane-based solid polymer electrolyte working in air“. In: *Smart Materials and Structures* 18.2 (2009), p. 024006 (cit. on pp. 60, 65).
- [62] Jeong-Gil Choi, DD Do, and HD Do. „Surface diffusion of adsorbed molecules in porous media: Monolayer, multilayer, and capillary condensation regimes“. In: *Industrial & engineering chemistry research* 40.19 (2001), pp. 4005–4031 (cit. on p. 28).
- [63] Seung Tae Choi, Jeong Yub Lee, Jong Oh Kwon, Seungwan Lee, and Woonbae Kim. „Varifocal liquid-filled microlens operated by an electroactive polymer actuator“. In: *Optics letters* 36.10 (2011), pp. 1920–1922 (cit. on p. 4).
- [64] Yong-Jin Choi, Seung-Hyeon Moon, Takeo Yamaguchi, and Shin-Ichi Nakao. „New morphological control for thick, porous membranes with a plasma graft-filling polymerization“. In: *Journal of Polymer Science Part A: Polymer Chemistry* 41.9 (2003), pp. 1216–1224 (cit. on pp. 19, 20, 22, 23).
- [65] Patrick Chouinard and Jean-Sébastien Plante. „Bistable antagonistic dielectric elastomer actuators for binary robotics and mechatronics“. In: *Mechatronics, IEEE/ASME Transactions on* 17.5 (2012), pp. 857–865 (cit. on p. 9).
- [66] Chen-Kuei Chung, PK Fung, YZ Hong, et al. „A novel fabrication of ionic polymer-metal composites (IPMC) actuator with silver nano-powders“. In: *Sensors and Actuators B: Chemical* 117.2 (2006), pp. 367–375 (cit. on p. 6).
- [67] Eyal Cohen and Amos Ophir. „Irradiation-induced grafting of poly (vinylidene fluoride)-graft-poly (styrene sulfonic acid) for the preparation of planar and tube-shaped air-drying membranes“. In: *Journal of Applied Polymer Science* 126.2 (2012), pp. 442–451 (cit. on p. 16).

- [68] Phillip J Cole, Robert F Cook, and Christopher W Macosko. „Adhesion between immiscible polymers correlated with interfacial entanglements“. In: *Macromolecules* 36.8 (2003), pp. 2808–2815 (cit. on p. 38).
- [69] Vítor Correia, C Caparros, C Casellas, et al. „Development of inkjet printed strain sensors“. In: *Smart Materials and Structures* 22.10 (2013), p. 105028 (cit. on pp. 11, 109, 169).
- [70] SR Coulson, IS Woodward, JPS Badyal, SA Brewer, and C Willis. „Ultralow surface energy plasma polymer films“. In: *Chemistry of materials* 12.7 (2000), pp. 2031–2038 (cit. on p. 19).
- [71] Linying Cui, Alpama N Ranade, Marvi A Matos, Geraud Dubois, and Reinhold H Dauskardt. „Improved adhesion of dense silica coatings on polymers by atmospheric plasma pre-treatment“. In: *ACS applied materials & interfaces* 5.17 (2013), pp. 8495–8504 (cit. on pp. 38, 47).
- [72] Edward Lansing Cussler. *Diffusion: mass transfer in fluid systems*. Cambridge university press, 2009 (cit. on p. 23).
- [73] Amer B Dababneh and Ibrahim T Ozbolat. „Bioprinting Technology: A Current State-of-the-Art Review“. In: *Journal of Manufacturing Science and Engineering* 136.6 (2014), p. 061016 (cit. on p. 91).
- [74] Frank Daerden and Dirk Lefeber. „Pneumatic artificial muscles: actuators for robotics and automation“. In: *European journal of mechanical and environmental engineering* 47.1 (2002), pp. 11–21 (cit. on pp. 2, 164).
- [75] Vishwanath H Dalvi and Peter J Rossky. „Molecular origins of fluorocarbon hydrophobicity“. In: *Proceedings of the National Academy of Sciences* 107.31 (2010), pp. 13603–13607 (cit. on p. 40).
- [76] Eugene Dariush Daneshvar and Elisabeth Smela. „Characterization of conjugated polymer actuation under cerebral physiological conditions.“ In: *Advanced healthcare materials* 3.7 (July 2014), pp. 1026–35 (cit. on pp. 10, 59).
- [77] Tim R Dargaville, Mathias C Celina, Julie M Elliott, et al. *Characterization, performance and optimization of PVDF as a piezoelectric film for advanced space mirror concepts*. Sandia National Laboratories, 2005 (cit. on p. 9).
- [78] Tim R Dargaville, Graeme A George, David JT Hill, and Andrew K Whittaker. „High energy radiation grafting of fluoropolymers“. In: *Progress in Polymer Science* 28.9 (2003), pp. 1355–1376 (cit. on p. 16).
- [79] Anna De Girolamo Del Mauro, Rosita Diana, Immacolata Angelica Grimaldi, et al. „Polymer solar cells with inkjet-printed doped-PEDOT: PSS anode“. In: *Polymer Composites* 34.9 (2013), pp. 1493–1499 (cit. on pp. 95, 167).
- [80] Viviana De Luca, Paolo Digiamberardino, Giovanna Di Pasquale, et al. „Ionic electroactive polymer metal composites: Fabricating, modeling, and applications of postsilicon smart devices“. In: *Journal of Polymer Science Part B: Polymer Physics* 51.9 (2013), pp. 699–734 (cit. on p. 6).
- [81] Michaël De Volder and Dominiek Reynaerts. „Pneumatic and hydraulic microactuators: a review“. In: *Journal of Micromechanics and microengineering* 20.4 (2010), p. 043001 (cit. on pp. 2, 164).

- [82] Robert D Deegan, Olgica Bakajin, Todd F Dupont, et al. „Capillary flow as the cause of ring stains from dried liquid drops“. In: *Nature* 389.6653 (1997), pp. 827–829 (cit. on pp. 94, 97).
- [83] Remi Delille, Mario Urdaneta, Kuangwen Hsieh, and Elisabeth Smela. „Compliant electrodes based on platinum salt reduction in a urethane matrix“. In: *Smart Materials and Structures* 16.2 (2007), S272 (cit. on p. 4).
- [84] Jianping Deng, Lifu Wang, Lianying Liu, and Wantai Yang. „Developments and new applications of UV-induced surface graft polymerizations“. In: *Progress in Polymer Science* 34.2 (2009), pp. 156–193 (cit. on p. 16).
- [85] Brian Derby. „Inkjet printing of functional and structural materials: fluid property requirements, feature stability, and resolution“. In: *Annual Review of Materials Research* 40 (2010), pp. 395–414 (cit. on pp. 92–94).
- [86] Eric Detsi, Sergey Punzhin, Jiancun Rao, Patrick R Onck, and Jeff Th M De Hosson. „Enhanced strain in functional nanoporous gold with a dual microscopic length scale structure“. In: *Acs Nano* 6.5 (2012), pp. 3734–3744 (cit. on p. 8).
- [87] Eric Detsi, Marc Sanchez Selles, Patrick R Onck, and Jeff Th M De Hosson. „Nanoporous silver as electrochemical actuator“. In: *Scripta Materialia* 69.2 (2013), pp. 195–198 (cit. on p. 8).
- [88] JF Dijkstra, PC Duineveld, MJJ Hack, et al. „Precision ink jet printing of polymer light emitting displays“. In: *Journal of Materials Chemistry* 17.6 (2007), pp. 511–522 (cit. on p. 91).
- [89] Jie Ding, Dezhi Zhou, Geoffrey Spinks, et al. „Use of ionic liquids as electrolytes in electromechanical actuator systems based on inherently conducting polymers“. In: *Chemistry of materials* 15.12 (2003), pp. 2392–2398 (cit. on pp. 60, 169).
- [90] Markus Döbbelin, Rebeca Marcilla, Maitane Salsamendi, et al. „Influence of ionic liquids on the electrical conductivity and morphology of PEDOT: PSS films“. In: *Chemistry of materials* 19.9 (2007), pp. 2147–2149 (cit. on pp. 43, 83).
- [91] Artjom Doring, Wolfgang Birnbaum, and Dirk Kuckling. „Responsive hydrogels—structurally and dimensionally optimized smart frameworks for applications in catalysis, micro-system technology and material science“. In: *Chemical Society reviews* 42.17 (2013), 7391–7420 (cit. on p. 5).
- [92] Ping Du, Xi Lin, and Xin Zhang. „A multilayer bending model for conducting polymer actuators“. In: *Sensors and Actuators A: Physical* 163.1 (Sept. 2010), pp. 240–246 (cit. on pp. 60, 78).
- [93] Philippe Dubois, Samuel Rosset, Sander Koster, et al. „Microactuators based on ion implanted dielectric electroactive polymer (EAP) membranes“. In: *Sensors and actuators A: Physical* 130 (2006), pp. 147–154 (cit. on p. 4).
- [94] Mariana D Duca, Carmina L Plosceanu, and Tatiana Pop. „Surface modifications of polyvinylidene fluoride (PVDF) under rf Ar plasma“. In: *Polymer Degradation and Stability* 61.1 (1998), pp. 65–72 (cit. on pp. 20, 171).
- [95] Stephanie R Dupont, Mark Oliver, Frederik C Krebs, and Reinhold H Dauskardt. „Inter-layer adhesion in roll-to-roll processed flexible inverted polymer solar cells“. In: *Solar Energy Materials and Solar Cells* 97 (2012), pp. 171–175 (cit. on p. 41).

- [96] Mark A Eddings, Michael A Johnson, and Bruce K Gale. „Determining the optimal PDMS–PDMS bonding technique for microfluidic devices“. In: *Journal of Micromechanics and Microengineering* 18.6 (2008), p. 067001 (cit. on p. 37).
- [97] Andreas Elschner, Stephan Kirchmeyer, Wilfried Lovenich, Udo Merker, and Knud Reuter. *PEDOT: principles and applications of an intrinsically conductive polymer*. CRC Press, 2010 (cit. on pp. 62, 73).
- [98] Andreas Elschner, Wilfried Lovenich, Aloys Eiling, and John Bayley. *White Paper ITO Alternative Solution Deposited Clevios PEDOT PSS materials for transparent conductive applications*. 2012 (cit. on p. 47).
- [99] Morinobu Endo, Michael S Strano, and Pulickel M Ajayan. „Potential applications of carbon nanotubes“. In: *Carbon nanotubes*. Springer, 2008, pp. 13–62 (cit. on pp. 86, 87, 108).
- [100] Seung Hun Eom, S Senthilarasu, Periyayya Uthirakumar, et al. „Polymer solar cells based on inkjet-printed PEDOT: PSS layer“. In: *Organic Electronics* 10.3 (2009), pp. 536–542 (cit. on pp. 91, 95, 167).
- [101] Benhu Fan, Yijie Xia, and Jianyong Ouyang. „Novel ways to significantly enhance the conductivity of transparent PEDOT: PSS“. In: *SPIE Photonic Devices+ Applications*. International Society for Optics and Photonics. 2009, 74151Q–74151Q (cit. on pp. 83, 85).
- [102] Yang Fang, Xiaobo Tan, and Gürsel Alici. „Robust adaptive control of conjugated polymer actuators“. In: *Control Systems Technology, IEEE Transactions on* 16.4 (2008), pp. 600–612 (cit. on pp. 9, 109).
- [103] Guo-Hua Feng and Wei-Lun Huang. „A self-strain feedback tuning-fork-shaped ionic polymer metal composite clamping actuator with soft matter elasticity-detecting capability for biomedical applications“. In: *Materials Science and Engineering: C* 45 (2014), pp. 241–249 (cit. on pp. 6, 109, 166).
- [104] Nicolas Festin, Cedric Plesse, Patrick Pirim, Claude Chevrot, and Frédéric Vidal. „Electroactive Interpenetrating Polymer Networks actuators and strain sensors: Fabrication, position control and sensing properties“. In: *Sensors and Actuators B: Chemical* 193 (2014), pp. 82–88 (cit. on pp. 36, 65, 73, 80, 82, 89, 104, 109, 180).
- [105] Nicolas Festin, Ali Maziz, Cédric Plesse, et al. „Robust solid polymer electrolyte for conducting IPN actuators“. In: *Smart Materials and Structures* 22.10 (2013), p. 104005 (cit. on pp. 60, 65).
- [106] David J Finn, Mustafa Lotya, and Jonathan N Coleman. „Inkjet Printing of Silver Nanowire Networks“. In: *ACS applied materials & interfaces* 7.17 (2015), pp. 9254–9261 (cit. on p. 109).
- [107] Emmanuel Flahaut, Revathi Bacsá, Alain Peigney, and Christophe Laurent. „Gram-scale CCVD synthesis of double-walled carbon nanotubes“. In: *Chemical Communications* 12 (2003), pp. 1442–1443 (cit. on p. 144).
- [108] Renate Förch, Anye N Chifen, Angelique Bousquet, et al. „Recent and Expected Roles of Plasma-Polymerized Films for Biomedical Applications“. In: *Chemical Vapor Deposition* 13.6-7 (2007), pp. 280–294 (cit. on p. 20).
- [109] Stefan Ford, Gary Macias, and Ron Lumia. „Single active finger IPMC microgripper“. In: *Smart Materials and Structures* 24.2 (2015), p. 025015 (cit. on pp. 6, 166).

- [110] Elzbieta Frackowiak and Francois Beguin. „Carbon materials for the electrochemical storage of energy in capacitors“. In: *Carbon* 39.6 (2001), pp. 937–950 (cit. on pp. 85–87, 108).
- [111] ACM Franken, JAM Nolten, MHV Mulder, D Bargeman, and CA Smolders. „Wetting criteria for the applicability of membrane distillation“. In: *Journal of Membrane Science* 33.3 (1987), pp. 315–328 (cit. on pp. 45, 53, 147).
- [112] Andrey I Frolov, Kathleen Kirchner, Tom Kirchner, and Maxim V Fedorov. „Molecular-scale insights into the mechanisms of ionic liquids interactions with carbon nanotubes“. In: *Faraday discussions* 154 (2012), pp. 235–247 (cit. on p. 64).
- [113] Jacob E Fromm. „Numerical calculation of the fluid dynamics of drop-on-demand jets“. In: *IBM Journal of Research and Development* 28.3 (1984), pp. 322–333 (cit. on p. 92).
- [114] Takanori Fukushima, Kinji Asaka, Atsuko Kosaka, and Takuzo Aida. „Fully Plastic Actuator through Layer-by-Layer Casting with Ionic-Liquid-Based Bucky Gel“. In: *Angewandte Chemie* 117.16 (Apr. 2005), pp. 2462–2465 (cit. on p. 7).
- [115] Takanori Fukushima, Atsuko Kosaka, Yoji Ishimura, et al. „Molecular Ordering of Organic Molten Salts Triggered by Single-Walled Carbon Nanotubes“. In: *Science* 300.5628 (2003), pp. 2072–2074. eprint: <http://www.sciencemag.org/content/300/5628/2072.full.pdf> (cit. on p. 7).
- [116] Babita Gaihre, Syed Ashraf, Geoffrey M Spinks, Peter C Innis, and Gordon G Wallace. „Comparative displacement study of bilayer actuators comprising of conducting polymers, fabricated from polypyrrole, poly (3, 4-ethylenedioxythiophene) or poly (3, 4-propylenedioxythiophene)“. In: *Sensors and Actuators A: Physical* 193 (2013), pp. 48–53 (cit. on pp. 60, 65).
- [117] Babita Gaihre, Gursel Alici, Geoffrey M Spinks, and Julie M Cairney. „Synthesis and performance evaluation of thin film PPy-PVDF multilayer electroactive polymer actuators“. In: *Sensors and Actuators A: Physical* 165.2 (2011), pp. 321–328 (cit. on pp. 60, 65).
- [118] Yulia Galagan, Erica W.C. Coenen, Sami Sabik, et al. „Evaluation of ink-jet printed current collecting grids and busbars for ITO-free organic solar cells“. In: *Solar Energy Materials and Solar Cells* 104 (Sept. 2012), pp. 32–38 (cit. on p. 95).
- [119] MR Gandhi, P Murray, GM Spinks, and GG Wallace. „Mechanism of electromechanical actuation in polypyrrole“. In: *Synthetic Metals* 73.3 (1995), pp. 247–256 (cit. on p. 63).
- [120] B-J de Gans, Paul C Duineveld, and Ulrich S Schubert. „Inkjet printing of polymers: state of the art and future developments“. In: *Advanced materials* 16.3 (2004), pp. 203–213 (cit. on pp. 11, 93, 169).
- [121] María del Carmen García-Payo, María Amparo Izquierdo-Gil, and Cristóbal Fernández-Pineda. „Wetting study of hydrophobic membranes via liquid entry pressure measurements with aqueous alcohol solutions“. In: *Journal of colloid and interface science* 230.2 (2000), pp. 420–431 (cit. on p. 53).
- [122] Ting Ge, Gary S Grest, and Mark O Robbins. „Tensile Fracture of Welded Polymer Interfaces: Miscibility, Entanglements, and Crazing“. In: *Macromolecules* 47.19 (2014), pp. 6982–6989 (cit. on p. 38).

- [123] Amy Gelmi, Jiabin Zhang, Artur Cieslar-Pobuda, et al. „Electroactive polymer scaffolds for cardiac tissue engineering“. In: *SPIE Smart Structures and Materials+ Nondestructive Evaluation and Health Monitoring*. International Society for Optics and Photonics. 2015, 94301T–94301T (cit. on p. 10).
- [124] Soumyadeb Ghosh and Olle Inganäs. „Networks of electron-conducting polymer in matrices of ion-conducting polymers applications to fast electrodes“. In: *Electrochemical and solid-state letters* 3.5 (2000), pp. 213–215 (cit. on p. 72).
- [125] PJ Glazer, M van Erp, A Embrechts, SG Lemay, and E Mendes. „Role of pH gradients in the actuation of electro-responsive polyelectrolyte gels“. In: *Soft Matter* 8.16 (2012), pp. 4421–4426 (cit. on p. 5).
- [126] Julie Melissa Goddard and JH Hotchkiss. „Polymer surface modification for the attachment of bioactive compounds“. In: *Progress in polymer science* 32.7 (2007), pp. 698–725 (cit. on p. 20).
- [127] Michael Goldin, Joseph Yerushalmi, Robert Pfeffer, and Reuel Shinnar. „Breakup of a laminar capillary jet of a viscoelastic fluid“. In: *Journal of Fluid Mechanics* 38.04 (1969), pp. 689–711 (cit. on p. 94).
- [128] Benjamin Gorissen, Radu Donose, Dominiek Reynaerts, and Michaël De Volder. „Flexible pneumatic micro-actuators: analysis and production“. In: *Procedia Engineering* 25 (2011), pp. 681–684 (cit. on p. 2).
- [129] Benjamin Gorissen, Takuya Chishiro, Shuhei Shimomura, et al. „Flexible pneumatic twisting actuators and their application to tilting micromirrors“. In: *Sensors and Actuators A: Physical* 216 (2014), pp. 426–431 (cit. on p. 2).
- [130] Malgorzata Graca, Jeroen HH Bongaerts, Jason R Stokes, and Steve Granick. „Friction and adsorption of aqueous polyoxyethylene (Tween) surfactants at hydrophobic surfaces“. In: *Journal of colloid and interface science* 315.2 (2007), pp. 662–670 (cit. on p. 15).
- [131] Nathalie K Guimard, Natalia Gomez, and Christine E Schmidt. „Conducting polymers in biomedical engineering“. In: *Progress in Polymer Science* 32.8 (2007), pp. 876–921 (cit. on pp. 1, 164).
- [132] L Guzman, R Celva, A Miotello, et al. „Polymer surface modification by ion implantation and reactive deposition of transparent films“. In: *Surface and Coatings Technology* 103 (1998), pp. 375–379 (cit. on p. 19).
- [133] David M Haddleton, Carl Waterson, and Peter J Derrick. „Comment: A simple, low-cost, air-spray method for improved sample preparation for matrix-assisted laser desorption/ionisation mass spectrometry of derivatised poly (ethylene glycol)“. In: *European Mass Spectrometry* 4 (1998), pp. 203–208 (cit. on p. 24).
- [134] Carter S Haines, Márcio D Lima, Na Li, et al. „Artificial muscles from fishing line and sewing thread“. In: *science* 343.6173 (2014), pp. 868–872 (cit. on pp. 2, 4, 10, 165).
- [135] Susumu Hara, Tetsuji Zama, Wataru Takashima, and Keiichi Kaneto. „Artificial muscles based on polypyrrole actuators with large strain and stress induced electrically“. In: *Polymer journal* 36.2 (2004), pp. 151–161 (cit. on pp. 59, 60).

- [136] Susumu Hara, Tetsuji Zama, Wataru Takashima, and Keiichi Kaneto. „Free-standing gel-like polypyrrole actuators doped with bis (perfluoroalkylsulfonyl) imide exhibiting extremely large strain“. In: *Smart Materials and Structures* 14.6 (2005), p. 1501 (cit. on pp. 59, 60).
- [137] Donald J Hayes, David B Wallace, and W Royall Cox. „MicroJet printing of solder and polymers for multi-chip modules and chip-scale packages“. In: *Proceedings-SPIE the International Society for Optical Engineering*. Citeseer. 1999, pp. 242–247 (cit. on p. 91).
- [138] Qingsong He, Min Yu, Xu Yang, Kwang Jin Kim, and Zhendong Dai. „An ionic electro-active actuator made with graphene film electrode, chitosan and ionic liquid“. In: *Smart Materials and Structures* 24.6 (June 2015), p. 065026 (cit. on p. 6).
- [139] Chris E Hendriks, Patrick J Smith, Jolke Perelaer, Antje MJ Van den Berg, and Ulrich S Schubert. „“Invisible” Silver Tracks Produced by Combining Hot-Embossing and Inkjet Printing“. In: *Advanced Functional Materials* 18.7 (2008), pp. 1031–1038 (cit. on p. 94).
- [140] Stephen D Hoath, Sungjune Jung, Wen-Kai Hsiao, and Ian M Hutchings. „How PEDOT: PSS solutions produce satellite-free inkjets“. In: *Organic Electronics* 13.12 (2012), pp. 3259–3262 (cit. on pp. 41, 43, 54, 95, 168).
- [141] Stephen D Hoath, Wen-Kai Hsiao, Graham D Martin, et al. „Oscillations of aqueous PEDOT: PSS fluid droplets and the properties of complex fluids in drop-on-demand inkjet printing“. In: *Journal of Non-Newtonian Fluid Mechanics* (2015) (cit. on p. 54).
- [142] Richard K Holman, Michael J Cima, Scott A Uhland, and Emanuel Sachs. „Spreading and infiltration of inkjet-printed polymer solution droplets on a porous substrate“. In: *Journal of colloid and interface science* 249.2 (2002), pp. 432–440 (cit. on p. 94).
- [143] HJ Holterman. *Kinetics and evaporation of water drops in air*. Vol. 2012. IMAG Wageningen, 2003 (cit. on p. 97).
- [144] Wangyujue Hong, Catherine Meis, James R. Heflin, and Reza Montazami. „Evidence of counterion migration in ionic polymer actuators via investigation of electromechanical performance“. In: *Sensors and Actuators B: Chemical* 205.0 (2014), pp. 371–376 (cit. on pp. 6, 78, 166).
- [145] Claudia N Hoth, Pavel Schilinsky, Stelios A Choulis, and Christoph J Brabec. „Printing highly efficient organic solar cells“. In: *Nano letters* 8.9 (2008), pp. 2806–2813 (cit. on p. 91).
- [146] J Huang, PF Miller, JC De Mello, AJ De Mello, and DDC Bradley. „Influence of thermal treatment on the conductivity and morphology of PEDOT/PSS films“. In: *Synthetic Metals* 139.3 (2003), pp. 569–572 (cit. on pp. 43, 99, 100).
- [147] AS Hutchison, TW Lewis, SE Moulton, GM Spinks, and GG Wallace. „Development of polypyrrole-based electromechanical actuators“. In: *Synthetic Metals* 113.1 (2000), pp. 121–127 (cit. on p. 65).
- [148] Kimiya Ikushima, Stephen John, Atsushi Ono, and Sachio Nagamitsu. „PEDOT/PSS bending actuators for autofocus micro lens applications“. In: *Synthetic Metals* 160.17 (2010), pp. 1877–1883 (cit. on pp. 14, 16, 20, 43, 48, 65, 72, 168, 171).
- [149] Filip Ilievski, Aaron D Mazzeo, Robert F Shepherd, Xin Chen, and George M Whitesides. „Soft robotics for chemists“. In: *Angewandte Chemie* 123.8 (2011), pp. 1930–1935 (cit. on pp. 1, 2, 164).

- [150] Charlotte Immerstrand, Kajsa Holmgren-Peterson, K-E Magnusson, et al. „Conjugated-polymer micro-and milliactuators for biological applications“. In: *MRS bulletin* 27.06 (2002), pp. 461–464 (cit. on pp. 10, 59).
- [151] Abu Bin Imran, Takahiro Seki, and Yukikazu Takeoka. „Recent advances in hydrogels in terms of fast stimuli responsiveness and superior mechanical performance“. In: *Polymer journal* 42.11 (2010), pp. 839–851 (cit. on pp. 5, 165).
- [152] Jacob Israelachvili. „The different faces of poly (ethylene glycol)“. In: *Proceedings of the National Academy of Sciences* 94.16 (1997), pp. 8378–8379 (cit. on p. 23).
- [153] Edwin W. H. Jager, Olle Inganäs, and Ingemar Lundström. „Microrobots for Micrometer-Size Objects in Aqueous Media: Potential Tools for Single-Cell Manipulation“. In: *Science* 288.5475 (2000), pp. 2335–2338. eprint: <http://www.sciencemag.org/content/288/5475/2335.full.pdf> (cit. on p. 10).
- [154] Edwin WH Jager, Nirul Masurkar, Nnamdi Felix Nworah, et al. „Patterning and electrical interfacing of individually controllable conducting polymer microactuators“. In: *Sensors and Actuators B: Chemical* 183 (2013), pp. 283–289 (cit. on pp. 7, 166).
- [155] R K Jain, S Majumder, and A Dutta. „Microassembly by an IPMC-based flexible 4-bar mechanism“. In: *Smart Materials and Structures* 21.7 (2012), p. 075004 (cit. on p. 9).
- [156] Daehwan Jang, Dongjo Kim, and Jooho Moon. „Influence of Fluid Physical Properties on Ink-Jet Printability“. In: *Langmuir* 25.5 (2009), pp. 2629–2635 (cit. on p. 92).
- [157] C Jean-Mistral, A Sylvestre, S Basrour, and J-J Chaillout. „Dielectric properties of polyacrylate thick films used in sensors and actuators“. In: *Smart Materials and Structures* 19.7 (2010), p. 075019 (cit. on p. 4).
- [158] YongGang Jiang, Syohei Shiono, Hiroyuki Hamada, et al. „Reactive ion etching of poly (vinylidene fluoride-trifluoroethylene) copolymer for flexible piezoelectric devices“. In: *Chinese Science Bulletin* 58.17 (2013), pp. 2091–2094 (cit. on p. 18).
- [159] Hai-Jun Jin and Jörg Weissmüller. „A Material with Electrically Tunable Strength and Flow Stress“. In: *Science* 332.6034 (2011), pp. 1179–1182. eprint: <http://www.sciencemag.org/content/332/6034/1179.full.pdf> (cit. on p. 8).
- [160] Hai-Jun Jin, Xiao-Lan Wang, Smrutiranjana Parida, et al. „Nanoporous AuPt Alloys As Large Strain Electrochemical Actuators“. In: *Nano Letters* 10.1 (2010). PMID: 20000673, pp. 187–194 (cit. on p. 8).
- [161] Xin Jin, Lars Heepe, Jan Strueben, et al. „Challenges and Solutions for Joining Polymer Materials“. In: *Macromolecular rapid communications* 35.18 (2014), pp. 1551–1570 (cit. on pp. 36, 39, 56, 175).
- [162] Choonghee Jo, David Pugal, Il-Kwon Oh, Kwang J Kim, and Kinji Asaka. „Recent advances in ionic polymer–metal composite actuators and their modeling and applications“. In: *Progress in Polymer Science* 38.7 (2013), pp. 1037–1066 (cit. on pp. 5, 6, 165).
- [163] Stephen W John, Gursel Alici, and Christopher D Cook. „Inversion-based feedforward control of polypyrrole trilayer bender actuators“. In: *Mechatronics, IEEE/ASME Transactions on* 15.1 (2010), pp. 149–156 (cit. on p. 9).

- [164] Stephen W John, Gursel Alici, and Christopher D Cook. „Towards the position control of conducting polymer trilayer bending actuators with integrated feedback sensor“. In: *Advanced Intelligent Mechatronics, 2009. AIM 2009. IEEE/ASME International Conference on. IEEE. 2009*, pp. 65–70 (cit. on p. 109).
- [165] Stephen William John. „Modelling and control of conducting polymer actuators“. PhD thesis. University of Wollongong, 2008 (cit. on p. 109).
- [166] Richard AL Jones and Randal W Richards. *Polymers at surfaces and interfaces*. Cambridge University Press, 1999 (cit. on p. 38).
- [167] Jos de Jong, Gerrit de Bruin, Hans Reinten, et al. „Air entrapment in piezo-driven inkjet printheads“. In: *The Journal of the Acoustical Society of America* 120.3 (2006), pp. 1257–1265 (cit. on p. 93).
- [168] M Kaempgen, GS Duesberg, and S Roth. „Transparent carbon nanotube coatings“. In: *Applied Surface Science* 252.2 (2005), pp. 425–429 (cit. on p. 86).
- [169] Yung Ho Kahng, Min-Kang Kim, Jong-Hoon Lee, et al. „Highly conductive flexible transparent electrodes fabricated by combining graphene films and inkjet-printed silver grids“. In: *Solar Energy Materials and Solar Cells* 124 (2014), pp. 86–91 (cit. on p. 109).
- [170] Tadashi Kajiyama, Cecile Monteux, Tetsuharu Narita, Francois Lequeux, and Masao Doi. „Contact-Line Recession Leaving a Macroscopic Polymer Film in the Drying Droplets of Water- Poly (N, N-dimethylacrylamide)(PDMA) Solution“. In: *Langmuir* 25.12 (2009), pp. 6934–6939 (cit. on pp. 97, 98).
- [171] Keiichi Kaneto, Teruyuki Shinonome, Kazuo Tominaga, and Wataru Takashima. „Electrochemical creeping and actuation of polypyrrole in ionic liquid“. In: *Japanese Journal of Applied Physics* 50.9R (2011), p. 091601 (cit. on pp. 60, 61, 74, 75).
- [172] Keiichi Kaneto, Hiroataka Suematsu, and Kentaro Yamato. „Training effect and fatigue in polypyrrole-based artificial muscles“. In: *Bioinspiration & biomimetics* 3.3 (2008), p. 035005 (cit. on p. 75).
- [173] Boseok Kang, Wi Hyoung Lee, and Kilwon Cho. „Recent advances in organic transistor printing processes“. In: *ACS applied materials & interfaces* 5.7 (2013), pp. 2302–2315 (cit. on p. 91).
- [174] Byung Ju Kang, Chang Kyu Lee, and Je Hoon Oh. „All-inkjet-printed electrical components and circuit fabrication on a plastic substrate“. In: *Microelectronic Engineering* 97.4023 (Sept. 2012), pp. 251–254 (cit. on pp. 95, 167).
- [175] Guo-dong Kang and Yi-ming Cao. „Application and modification of poly (vinylidene fluoride)(PVDF) membranes—A review“. In: *Journal of Membrane Science* 463 (2014), pp. 145–165 (cit. on pp. 14, 15, 51).
- [176] Koichi Kato, Emiko Uchida, En-Tang Kang, Yoshikimi Uyama, and Yoshito Ikada. „Polymer surface with graft chains“. In: *Progress in Polymer Science* 28.2 (2003), pp. 209–259 (cit. on p. 48).
- [177] Satinderpal Kaur, Zuwei Ma, Renuga Gopal, et al. „Plasma-induced graft copolymerization of poly (methacrylic acid) on electrospun poly (vinylidene fluoride) nanofiber membrane“. In: *Langmuir* 23.26 (2007), pp. 13085–13092 (cit. on pp. 19, 20, 23).

- [178] Akif Kaynak, Chunhui Yang, Yang C Lim, and Abbas Kouzani. „Electrochemical fabrication and modelling of mechanical behavior of a tri-layer polymer actuator“. In: *Materials Chemistry and Physics* 125.1 (2011), pp. 113–117 (cit. on p. 78).
- [179] Alexandre Khaldi, Ali Maziz, Gursel Alici, Geoffrey M Spinks, and Edwin WH Jager. „Soft, flexible micromanipulators comprising polypyrrole trilayer microactuators“. In: *SPIE Smart Structures and Materials+ Nondestructive Evaluation and Health Monitoring*. International Society for Optics and Photonics. 2015, 94301R–94301R (cit. on p. 9).
- [180] Nazanin Khalili, Hani E Naguib, and Roy H Kwon. „On the geometrical and mechanical multi-aspect optimization of PPy/MWCNT actuators“. In: *SPIE Smart Structures and Materials+ Nondestructive Evaluation and Health Monitoring*. International Society for Optics and Photonics. 2014, 90561S–90561S (cit. on pp. 86, 87).
- [181] Ibrahim Sadek Khattab, Farzana Bandarkar, Mohammad Amin Abolghassemi Fakhree, and Abolghasem Jouyban. „Density, viscosity, and surface tension of water+ ethanol mixtures from 293 to 323K“. In: *Korean Journal of Chemical Engineering* 29.6 (2012), pp. 812–817 (cit. on p. 147).
- [182] Mohammad Mahdi Kheirikhah, Samaneh Rabiee, and Mohammad Ehsan Edalat. „A review of shape memory alloy actuators in robotics“. In: *RoboCup 2010: Robot Soccer World Cup XIV*. Springer, 2011, pp. 206–217 (cit. on p. 2).
- [183] Rudolf Kiefer, Daniel Georg Weis, Jadranka Travas-Sejdic, Gerald Urban, and Jürgen Heinze. „Effect of electrochemical synthesis conditions on deflection of PEDOT bilayers“. In: *Sensors and Actuators B: Chemical* 123.1 (2007), pp. 379–383 (cit. on p. 61).
- [184] Byoung-Sik Kim and Peter Harriott. „Critical entry pressure for liquids in hydrophobic membranes“. In: *Journal of Colloid and Interface Science* 115.1 (1987), pp. 1–8 (cit. on p. 53).
- [185] Byungkyu Kim, Deok-Ho Kim, Jaehoon Jung, and Jong-Oh Park. „A biomimetic undulatory tadpole robot using ionic polymer–metal composite actuators“. In: *Smart Materials and Structures* 14.6 (2005), p. 1579 (cit. on pp. 6, 166).
- [186] Jaehwan Kim, Jin-Han Jeon, Hyun-Jun Kim, Hyuneui Lim, and Il-Kwon Oh. „Durable and Water-Floatable Ionic Polymer Actuator with Hydrophobic and Asymmetrically Laser-Scribed Reduced Graphene Oxide Paper Electrodes“. In: *ACS Nano* 8.3 (2014). PMID: 24548279, pp. 2986–2997 (cit. on p. 6).
- [187] Kwang J Kim and Mohsen Shahinpoor. „A novel method of manufacturing three-dimensional ionic polymer–metal composites (IPMCs) biomimetic sensors, actuators and artificial muscles“. In: *Polymer* 43.3 (2002), pp. 797–802 (cit. on p. 6).
- [188] Kwang J Kim and Mohsen Shahinpoor. „Ionic polymer–metal composites: II. Manufacturing techniques“. In: *Smart Materials and Structures* 12.1 (2003), p. 65 (cit. on p. 6).
- [189] Onnuri Kim, Sung Yeon Kim, Byungrak Park, Woonbong Hwang, and Moon Jeong Park. „Factors Affecting Electromechanical Properties of Ionic Polymer Actuators Based on Ionic Liquid-Containing Sulfonated Block Copolymers“. In: *Macromolecules* 47.13 (2014), pp. 4357–4368. eprint: <http://dx.doi.org/10.1021/ma500869h> (cit. on p. 6).

- [190] Seong J Kim, David Pugal, Johnson Wong, Kwang J Kim, and Woosoon Yim. „A bio-inspired multi degree of freedom actuator based on a novel cylindrical ionic polymer–metal composite material“. In: *Robotics and Autonomous Systems* 62.1 (2014), pp. 53–60 (cit. on p. 9).
- [191] Seong Jun Kim, In Taek Lee, and Yong Hyup Kim. „Performance enhancement of IPMC actuator by plasma surface treatment“. In: *Smart materials and structures* 16.1 (2007), N6 (cit. on p. 6).
- [192] Seong Jun Kim, In Taek Lee, Ho-Young Lee, and Yong Hyup Kim. „Performance improvement of an ionic polymer–metal composite actuator by parylene thin film coating“. In: *Smart Materials and Structures* 15.6 (2006), p. 1540 (cit. on pp. 6, 36).
- [193] Si-Seup Kim, Jin-Han Jeon, Chang-Doo Kee, and Il-Kwon Oh. „Electro-active hybrid actuators based on freeze-dried bacterial cellulose and PEDOT: PSS“. In: *Smart Materials and Structures* 22.8 (2013), p. 085026 (cit. on pp. 13, 41, 65, 87, 170, 177).
- [194] Soo Hong Kim, Sun Woong Na, N-E Lee, Yun Woo Nam, and Young-Ho Kim. „Effect of surface roughness on the adhesion properties of Cu/Cr films on polyimide substrate treated by inductively coupled oxygen plasma“. In: *Surface and Coatings Technology* 200.7 (2005), pp. 2072–2079 (cit. on pp. 47, 83).
- [195] Yong Hyun Kim, Christoph Sachse, Michael L Machala, et al. „Highly conductive PEDOT: PSS electrode with optimized solvent and thermal post-treatment for ITO-free organic solar cells“. In: *Advanced Functional Materials* 21.6 (2011), pp. 1076–1081 (cit. on pp. 95, 100, 167).
- [196] Park Kiwon. „Characterization of the solvent evaporation effect on ionic polymer-metal composite sensors“. In: *Journal of Korean Physical Society* 59 (2011), p. 3401 (cit. on pp. 6, 166).
- [197] Jacob Klein. „Interdiffusion of Polymers“. In: *Science* 250.4981 (1990), pp. 640–646 (cit. on p. 38).
- [198] Masaru Kobayashi, Masato Makino, Tohru Okuzono, and Masao Doi. „Interference effects in the drying of polymer droplets on substrate“. In: *Journal of the Physical Society of Japan* 79.4 (2010), p. 044802 (cit. on p. 97).
- [199] Takuma Kobayashi and Masaki Omiya. „Deformation behaviors of ionic-polymer–metal composite actuator with palladium electrodes for various solvents, temperatures, and frequencies“. In: *Smart Materials and Structures* 21.10 (Oct. 2012), p. 105031 (cit. on p. 6).
- [200] Hilmar Koerner, Gary Price, Nathan A Pearce, Max Alexander, and Richard A Vaia. „Remotely actuated polymer nanocomposites—stress-recovery of carbon-nanotube-filled thermoplastic elastomers“. In: *Nature materials* 3.2 (2004), pp. 115–120 (cit. on pp. 2, 165).
- [201] Guggi Kofod, Peter Sommer-Larsen, Roy Kornbluh, and Ron Pelrine. „Actuation response of polyacrylate dielectric elastomers“. In: *Journal of intelligent material systems and structures* 14.12 (2003), pp. 787–793 (cit. on p. 4).
- [202] Nobutoshi Komuro, Shunsuke Takaki, Koji Suzuki, and Daniel Citterio. „Inkjet printed (bio) chemical sensing devices“. In: *Analytical and bioanalytical chemistry* 405.17 (2013), pp. 5785–5805 (cit. on p. 91).

- [203] J Kong and K Li. „Oil removal from oil-in-water emulsions using PVDF membranes“. In: *Separation and purification technology* 16.1 (1999), pp. 83–93 (cit. on pp. 54, 55).
- [204] Lirong Kong and Wei Chen. „Carbon Nanotube and Graphene-based Bioinspired Electrochemical Actuators“. In: *Advanced Materials* 26.7 (2014), pp. 1025–1043 (cit. on pp. 5, 165).
- [205] Krisztián Kordás, Tero Mustonen, Géza Tóth, et al. „Inkjet printing of electrically conductive patterns of carbon nanotubes“. In: *Small* 2.8-9 (2006), pp. 1021–1025 (cit. on p. 109).
- [206] Roy D Kornbluh, David S Flamm, Harsha Prahlad, et al. „Shape control of large lightweight mirrors with dielectric elastomer actuation“. In: *Smart Structures and Materials*. International Society for Optics and Photonics. 2003, pp. 143–158 (cit. on p. 9).
- [207] Roy D Kornbluh, Ron Pelrine, Harsha Prahlad, et al. „Stretching the Capabilities of Energy Harvesting: Electroactive Polymers Based on Dielectric Elastomers“. In: *Advances in Energy Harvesting Methods*. Springer, 2013, pp. 399–415 (cit. on p. 5).
- [208] Karl Kruusamäe, Andres Punning, Alvo Aabloo, and Kinji Asaka. „Self-Sensing Ionic Polymer Actuators: A Review“. In: *Actuators*. Vol. 4. 1. Multidisciplinary Digital Publishing Institute. 2015, pp. 17–38 (cit. on p. 10).
- [209] Tapas Kuilla, Sambhu Bhadra, Dahu Yao, et al. „Recent advances in graphene based polymer composites“. In: *Progress in polymer science* 35.11 (2010), pp. 1350–1375 (cit. on p. 108).
- [210] Nitin Kumar, Kalyani Varanasi, Robert D Tilton, and Stephen Garoff. „Surfactant self-assembly ahead of the contact line on a hydrophobic surface and its implications for wetting“. In: *Langmuir* 19.13 (2003), pp. 5366–5373 (cit. on p. 54).
- [211] O Kylian, A Choukourov, and H Biederman. „Nanostructured plasma polymers“. In: *Thin Solid Films* 548 (2013), pp. 1–17 (cit. on p. 17).
- [212] Vincent Labrot, Patrick De Kepper, Jacques Boissonade, István Szalai, and Fabienne Gauffre. „Wave patterns driven by chemomechanical instabilities in responsive gels“. In: *The Journal of Physical Chemistry B* 109.46 (2005), pp. 21476–21480 (cit. on p. 5).
- [213] SL Lai, MY Chan, MK Fung, CS Lee, and ST Lee. „Concentration effect of glycerol on the conductivity of PEDOT film and the device performance“. In: *Materials Science and Engineering: B* 104.1 (2003), pp. 26–30 (cit. on p. 100).
- [214] Udo Lang. „Experimental methods for evaluating the mechanical properties of thin layers of intrinsically conductive polymers“. PhD thesis. Eidgenössische Technische Hochschule ETH Zürich, 2008 (cit. on p. 96).
- [215] Udo Lang, Nicola Naujoks, and Jurg Dual. „Mechanical characterization of PEDOT: PSS thin films“. In: *Synthetic Metals* 159.5 (2009), pp. 473–479 (cit. on pp. 41–43, 167).
- [216] Levi G Ledgerwood, Steven Tinling, Craig Senders, et al. „Artificial muscle for reanimation of the paralyzed face: durability and biocompatibility in a gerbil model“. In: *Archives of facial plastic surgery* 14.6 (2012), pp. 413–418 (cit. on p. 10).
- [217] Jeongho Lee and Takuzo Aida. „Bucky gels for tailoring electroactive materials and devices: the composites of carbon materials with ionic liquids“. In: *Chem. Commun.* 47 (24 2011), pp. 6757–6762 (cit. on p. 7).

- [218] Kenneth KC Lee, Nigel R Munce, Tina Shoa, et al. „Fabrication and characterization of laser-micromachined polypyrrole-based artificial muscle actuated catheters“. In: *Sensors and Actuators A: Physical* 153.2 (2009), pp. 230–236 (cit. on p. 10).
- [219] KS Lee, N Ivanova, VM Starov, N Hilal, and V Dutschk. „Kinetics of wetting and spreading by aqueous surfactant solutions“. In: *Advances in colloid and interface science* 144.1 (2008), pp. 54–65 (cit. on p. 54).
- [220] Minyoung Lee, Young-Gwang Ko, Jae Baek Lee, et al. „Hydrophobization of silk fibroin nanofibrous membranes by fluorocarbon plasma treatment to modulate cell adhesion and proliferation behavior“. In: *Macromolecular Research* 22.7 (2014), pp. 746–752 (cit. on p. 19).
- [221] Myung-Won Lee, Mi-Young Lee, Jae-Cheol Choi, Jong-Seung Park, and Chung-Kun Song. „Fine patterning of glycerol-doped PEDOT:PSS on hydrophobic PVP dielectric with ink jet for source and drain electrode of OTFTs“. In: *Organic Electronics* 11.5 (May 2010), pp. 854–859 (cit. on pp. 95, 167).
- [222] Seunghwan Lee and Nicholas D Spencer. „Aqueous lubrication of polymers: influence of surface modification“. In: *Tribology International* 38.11 (2006), pp. 922–930 (cit. on p. 15).
- [223] Hong Lei, Wen Li, and Xiaobo Tan. „Encapsulation of ionic polymer-metal composite (IPMC) sensors with thick parylene: Fabrication process and characterization results“. In: *Sensors and Actuators A: Physical* 217 (2014), pp. 1–12 (cit. on pp. 6, 36).
- [224] Chunyu Li, Erik T. Thostenson, and Tsu-Wei Chou. „Sensors and actuators based on carbon nanotubes and their composites: A review“. In: *Composites Science and Technology* 68.6 (May 2008), pp. 1227–1249 (cit. on p. 7).
- [225] Hongbin Li, Wenying Shi, Yufeng Zhang, Rong Zhou, and Haixia Zhang. „Preparation of hydrophilic PVDF/PPTA blend membranes by in situ polycondensation and its application in the treatment of landfill leachate“. In: *Applied Surface Science* 346 (2015), pp. 134–146 (cit. on p. 14).
- [226] Qingwei Li, Changhong Liu, Yuan-Hua Lin, et al. „Large-Strain, Multiform Movements from Designable Electrothermal Actuators Based on Large Highly Anisotropic Carbon Nanotube Sheets“. In: *ACS Nano* 9.1 (2015). PMID: 25559661, pp. 409–418 (cit. on p. 8).
- [227] Xiong Li, Min Wang, Ce Wang, Cheng Cheng, and Xuefen Wang. „Facile Immobilization of Ag Nanocluster on Nanofibrous Membrane for Oil/Water Separation“. In: *ACS applied materials & interfaces* 6.17 (2014), pp. 15272–15282 (cit. on p. 55).
- [228] Yuechen Li, Ryo Tanigawa, and Hidenori Okuzaki. „Soft and flexible PEDOT/PSS films for applications to soft actuators“. In: *Smart Materials and Structures* 23.7 (2014), p. 074010 (cit. on pp. 43, 65, 168).
- [229] Zaifang Li, Wei Meng, Jinhui Tong, et al. „A nonionic surfactant simultaneously enhancing wetting property and electrical conductivity of PEDOT: PSS for vacuum-free organic solar cells“. In: *Solar Energy Materials and Solar Cells* 137 (2015), pp. 311–318 (cit. on pp. 45, 83).
- [230] Chang-Sheng Liang, Zhong-Fei Lv, Yang Bo, Jia-Yang Cui, and Shi-Ai Xu. „Effect of modified polypropylene on the interfacial bonding of polymer-aluminium laminated films“. In: *Materials & Design* (2015) (cit. on p. 48).

- [231] Jiajie Liang, Yanfei Xu, Yi Huang, et al. „Infrared-triggered actuators from graphene-based nanocomposites“. In: *The Journal of Physical Chemistry C* 113.22 (2009), pp. 9921–9927 (cit. on p. 109).
- [232] Jung Ah Lim, Jeong Ho Cho, Yeong Don Park, et al. „Solvent effect of inkjet printed source/drain electrodes on electrical properties of polymer thin-film transistors“. In: *Applied physics letters* 88.8 (2006), p. 082102 (cit. on pp. 95, 167).
- [233] Márcio D Lima, Na Li, Monica Jung De Andrade, et al. „Electrically, chemically, and photonically powered torsional and tensile actuation of hybrid carbon nanotube yarn muscles“. In: *Science* 338.6109 (2012), pp. 928–932 (cit. on pp. 2, 4, 10, 165).
- [234] Xi Lin, Ju Li, Elisabeth Smela, and Sidney Yip. „Polaron-induced conformation change in single polypyrrole chain: An intrinsic actuation mechanism“. In: *International Journal of Quantum Chemistry* 102.5 (2005), pp. 980–985 (cit. on p. 62).
- [235] Yow-Jon Lin, Wei-Shih Ni, and Jhe-You Lee. „Effect of incorporation of ethylene glycol into PEDOT: PSS on electron phonon coupling and conductivity“. In: *Journal of Applied Physics* 117.21 (2015), p. 215501 (cit. on pp. 95, 102).
- [236] Per Linse and Niklas Kallrot. „Polymer adsorption from bulk solution onto planar surfaces: effect of polymer flexibility and surface attraction in good solvent“. In: *Macromolecules* 43.4 (2010), pp. 2054–2068 (cit. on p. 24).
- [237] Congcong Liu, Jingkun Xu, Baoyang Lu, Ruirui Yue, and Fangfang Kong. „Simultaneous increases in electrical conductivity and Seebeck coefficient of PEDOT: PSS films by adding ionic liquids into a polymer solution“. In: *Journal of electronic materials* 41.4 (2012), pp. 639–645 (cit. on p. 83).
- [238] Fu Liu, N Awanis Hashim, Yutie Liu, MR Moghareh Abed, and K Li. „Progress in the production and modification of PVDF membranes“. In: *Journal of Membrane Science* 375.1 (2011), pp. 1–27 (cit. on pp. 14, 16, 41, 47, 51, 167).
- [239] Guodong Liu, Meiyun Zhang, Cathy Ridgway, and Patrick Gane. „Spontaneous Inertial Imbibition in Porous Media Using a Fractal Representation of Pore Wall Rugosity“. In: *Transport in porous media* 104.1 (2014), pp. 231–251 (cit. on p. 54).
- [240] Yang Liu, Caiyan Lu, Stephen Twigg, et al. „Direct observation of ion distributions near electrodes in ionic polymer actuators containing ionic liquids.“ In: *Scientific reports* 3.Mim (Jan. 2013), p. 973 (cit. on pp. 6, 166).
- [241] Yingkai Liu, Qi Gan, Shermeen Baig, and Elisabeth Smela. „Improving PPy adhesion by surface roughening“. In: *The Journal of Physical Chemistry C* 111.30 (2007), pp. 11329–11338 (cit. on pp. 35, 36, 41, 44, 65, 73, 78, 177, 182).
- [242] Wen Lu, Elisabeth Smela, Philip Adams, Guido Zuccarello, and Benjamin R Mattes. „Development of solid-in-hollow electrochemical linear actuators using highly conductive polyaniline“. In: *Chemistry of materials* 16.9 (2004), pp. 1615–1621 (cit. on p. 64).
- [243] Wen Lu, Andrei G Fadeev, Baohua Qi, et al. „Use of ionic liquids for π -conjugated polymer electrochemical devices“. In: *Science* 297.5583 (2002), pp. 983–987 (cit. on pp. 60, 73, 169).
- [244] Ron Lumia and Mohsen Shahinpoor. „IPMC microgripper research and development“. In: *Journal of Physics: Conference Series*. Vol. 127. 1. IOP Publishing. 2008, p. 012002 (cit. on p. 9).

- [245] Kevin Y Ma, Pakpong Chirarattananon, Sawyer B Fuller, and Robert J Wood. „Controlled flight of a biologically inspired, insect-scale robot“. In: *Science* 340.6132 (2013), pp. 603–607 (cit. on p. 9).
- [246] A Maartens, EP Jacobs, and P Swart. „UF of pulp and paper effluent: membrane fouling-prevention and cleaning“. In: *Journal of membrane science* 209.1 (2002), pp. 81–92 (cit. on p. 54).
- [247] John D Madden, Derek Rinderknecht, Patrick A Anquetil, and Ian W Hunter. „Creep and cycle life in polypyrrole actuators“. In: *Sensors and Actuators A: Physical* 133.1 (2007), pp. 210–217 (cit. on pp. 73, 182).
- [248] John DW Madden, Joseph N Barisci, Patrick A Anquetil, et al. „Fast carbon nanotube charging and actuation“. In: *Advanced Materials* 18.7 (2006), pp. 870–873 (cit. on p. 7).
- [249] Peter GA Madden, John DW Madden, Patrick Anquetil, Nathan Vandesteeg, and Ian W Hunter. „The relation of conducting polymer actuator material properties to performance“. In: *Oceanic Engineering, IEEE Journal of* 29.3 (2004), pp. 696–705 (cit. on pp. 3–5, 12, 68, 69, 72, 78, 164, 165).
- [250] Peter Geoffrey Alexander Madden. „Development and modeling of conducting polymer actuators and the fabrication of a conducting polymer based feedback loop“. PhD thesis. Massachusetts Institute of Technology, 2003 (cit. on pp. 70, 109).
- [251] Nobuo Maeda, Nianhuan Chen, Matthew Tirrell, and Jacob N Israelachvili. „Adhesion and friction mechanisms of polymer-on-polymer surfaces“. In: *Science* 297.5580 (2002), pp. 379–382 (cit. on pp. 38, 47).
- [252] Shingo Maeda, Yusuke Hara, Ryo Yoshida, and Shuji Hashimoto. „Active polymer gel actuators“. In: *International journal of molecular sciences* 11.1 (2010), pp. 52–66 (cit. on pp. 5, 165).
- [253] Luc Maffli, Samuel Rosset, Michele Ghilardi, Federico Carpi, and Herbert Shea. „Ultrafast All-Polymer Electrically Tunable Silicone Lenses“. In: *Advanced Functional Materials* 25.11 (2015), pp. 1656–1665 (cit. on p. 9).
- [254] Ankit Mahajan, Woo Jin Hyun, S Brett Walker, et al. „High-Resolution, High-Aspect Ratio Conductive Wires Embedded in Plastic Substrates“. In: *ACS applied materials & interfaces* 7.3 (2015), pp. 1841–1847 (cit. on pp. 94, 95).
- [255] Hanns-Christian Mahler, Franziska Huber, Ravuri SK Kishore, et al. „Adsorption behavior of a surfactant and a monoclonal antibody to sterilizing-grade filters“. In: *Journal of pharmaceutical sciences* 99.6 (2010), pp. 2620–2627 (cit. on p. 54).
- [256] Ramses V Martinez, Ana C Glavan, Christoph Keplinger, Alexis I Oyetibo, and George M Whitesides. „Soft actuators and robots that are resistant to mechanical damage“. In: *Advanced Functional Materials* 24.20 (2014), pp. 3003–3010 (cit. on p. 2).
- [257] Sean Maw, Elisabeth Smela, Ken Yoshida, Peter Sommer-Larsen, and Richard B Stein. „The effects of varying deposition current density on bending behaviour in PPy (DBS)-actuated bending beams“. In: *Sensors and Actuators A: Physical* 89.3 (2001), pp. 175–184 (cit. on p. 75).
- [258] Ali Maziz, Cedric Plesse, Caroline Soyer, et al. „Demonstrating kHz frequency actuation for conducting polymer microactuators“. In: *Advanced Functional Materials* 24.30 (2014), pp. 4851–4859 (cit. on p. 82).

- [259] Scott McGovern, Gursel Alici, Van-Tan Truong, and Geoffrey Spinks. „Finding NEMO (novel electromaterial muscle oscillator): a polypyrrole powered robotic fish with real-time wireless speed and directional control“. In: *Smart Materials and Structures* 18.9 (2009), p. 095009 (cit. on p. 9).
- [260] Michael A Meller, Matthew Bryant, and Ephrahim Garcia. „Reconsidering the McKibben muscle: Energetics, operating fluid, and bladder material“. In: *Journal of Intelligent Material Systems and Structures* 25.18 (2014), pp. 2276–2293 (cit. on p. 2).
- [261] Daniel Melling, Stephen Wilson, and Edwin WH Jager. „The effect of film thickness on polypyrrole actuation assessed using novel non-contact strain measurements“. In: *Smart Materials and Structures* 22.10 (2013), p. 104021 (cit. on pp. 59, 68, 70, 71, 74, 75, 78).
- [262] Jian-Qiang Meng, Chun-Lin Chen, Li-Ping Huang, Qi-Yun Du, and Yu-Feng Zhang. „Surface modification of PVDF membrane via AGET ATRP directly from the membrane surface“. In: *Applied Surface Science* 257.14 (2011), pp. 6282–6290 (cit. on p. 17).
- [263] Desalegn A Mengistie, Mohammed A Ibrahim, Pen-Cheng Wang, and Chih-Wei Chu. „Highly conductive PEDOT: PSS treated with formic acid for ITO-free polymer solar cells“. In: *ACS applied materials & interfaces* 6.4 (2014), pp. 2292–2299 (cit. on p. 61).
- [264] Desalegn Alemu Mengistie, Pen-Cheng Wang, and Chih-Wei Chu. „Effect of molecular weight of additives on the conductivity of PEDOT: PSS and efficiency for ITO-free organic solar cells“. In: *Journal of Materials Chemistry A* 1.34 (2013), pp. 9907–9915 (cit. on pp. 43, 51, 83, 84, 99, 100, 102).
- [265] Delphine Merche, Nicolas Vandencastele, and François Reniers. „Atmospheric plasmas for thin film deposition: A critical review“. In: *Thin Solid Films* 520.13 (2012), pp. 4219–4236 (cit. on p. 17).
- [266] Andrew Michelmores, David A Steele, Jason D Whittle, James W Bradley, and Robert D Short. „Nanoscale deposition of chemically functionalised films via plasma polymerisation“. In: *RSC Advances* 3.33 (2013), pp. 13540–13557 (cit. on p. 17).
- [267] Hirofumi Miki, G Matsui, M Kanda, and S Tsuchitani. „Fabrication of microstructure array directly on β -phase poly (vinylidene fluoride) thin film by O₂ reactive ion etching“. In: *Journal of Micromechanics and Microengineering* 25.3 (2015), p. 035026 (cit. on p. 18).
- [268] Andrew JB Milne and A Amirfazli. „Autophilic effect: wetting of hydrophobic surfaces by surfactant solutions“. In: *Langmuir* 26.7 (2009), pp. 4668–4674 (cit. on p. 54).
- [269] Tissaphern Mirfakhrai, John DW Madden, and Ray H Baughman. „Polymer artificial muscles“. In: *Materials today* 10.4 (2007), pp. 30–38 (cit. on pp. 3–5, 9, 12, 164, 165).
- [270] Seyed M Mirvakili, Alexey Pazukha, William Sikkema, et al. „Niobium nanowire yarns and their application as artificial muscles“. In: *Advanced Functional Materials* 23.35 (2013), pp. 4311–4316 (cit. on pp. 1, 2, 4, 163, 165).
- [271] AJM Moers, MFL De Volder, and Dominiek Reynaerts. „Integrated high pressure micro-hydraulic actuation and control for surgical instruments“. In: *Biomedical microdevices* 14.4 (2012), pp. 699–708 (cit. on p. 10).
- [272] Maryam Tavakol Moghadam, Geoffroy Lesage, Toraj Mohammadi, et al. „Improved antifouling properties of TiO₂/PVDF nanocomposite membranes in UV-coupled ultrafiltration“. In: *Journal of Applied Polymer Science* 132.21 (2015) (cit. on p. 15).

- [273] Mohammad Moniruzzaman and Karen I Winey. „Polymer nanocomposites containing carbon nanotubes“. In: *Macromolecules* 39.16 (2006), pp. 5194–5205 (cit. on p. 85).
- [274] Reza Montazami, Sheng Liu, Yang Liu, et al. „Thickness dependence of curvature, strain, and response time in ionic electroactive polymer actuators fabricated via layer-by-layer assembly“. In: *Journal of Applied Physics* 109.10 (2011), p. 104301 (cit. on p. 78).
- [275] Stephen A Morin, Yanina Shevchenko, Joshua Lessing, et al. „Using “Click-e-Bricks” to Make 3D Elastomeric Structures“. In: *Advanced Materials* 26.34 (2014), pp. 5991–5999 (cit. on p. 2).
- [276] Hiroshi Morita, Masamichi Yamada, Tetsuo Yamaguchi, and Masao Doi. „Molecular dynamics study of the adhesion between end-grafted polymer films“. In: *Polymer journal* 37.10 (2005), pp. 782–788 (cit. on p. 38).
- [277] Aoife Morrin, Orawan Ngamna, Eimer O’Malley, et al. „The fabrication and characterization of inkjet-printed polyaniline nanoparticle films“. In: *Electrochimica Acta* 53.16 (2008), pp. 5092–5099 (cit. on p. 95).
- [278] Bobak Mosadegh, Panagiotis Polygerinos, Christoph Keplinger, et al. „Pneumatic networks for soft robotics that actuate rapidly“. In: *Advanced Functional Materials* 24.15 (2014), pp. 2163–2170 (cit. on p. 2).
- [279] Robert P Mun, Jeffrey A Byars, and David V Boger. „The effects of polymer concentration and molecular weight on the breakup of laminar capillary jets“. In: *Journal of Non-Newtonian Fluid Mechanics* 74.1 (1998), pp. 285–297 (cit. on p. 94).
- [280] Indrek Must, Friedrich Kaasik, Inga Pöldsalu, et al. „Ionic and Capacitive Artificial Muscle for Biomimetic Soft Robotics“. In: *Advanced Engineering Materials* 17.1 (2015), pp. 84–94 (cit. on p. 9).
- [281] Indrek Must, Veiko Vunder, Friedrich Kaasik, et al. „Ionic liquid-based actuators working in air: The effect of ambient humidity“. In: *Sensors and Actuators B: Chemical* 202 (Oct. 2014), pp. 114–122 (cit. on pp. 35, 77, 78, 182).
- [282] Ronen Naim, Inna Levitsky, and Vitaly Gitis. „Surfactant cleaning of UF membranes fouled by proteins“. In: *Separation and Purification Technology* 94 (2012), pp. 39–43 (cit. on p. 54).
- [283] Keerthi G Nair, D Jayaseelan, and P Biji. „Direct-writing of circuit interconnects on cellulose paper using ultra-long, silver nanowires based conducting ink“. In: *RSC Advances* 5.93 (2015), pp. 76092–76100 (cit. on p. 109).
- [284] Satoshi Nakamaru, Shingo Maeda, Yusuke Hara, and Shuji Hashimoto. „Control of Autonomous Swelling- Deswelling Behavior for a Polymer Gel“. In: *The Journal of Physical Chemistry B* 113.14 (2009), pp. 4609–4613 (cit. on p. 5).
- [285] A Mantovani Nardes, Martijn Kemerink, MM De Kok, et al. „Conductivity, work function, and environmental stability of PEDOT: PSS thin films treated with sorbitol“. In: *Organic Electronics* 9.5 (2008), pp. 727–734 (cit. on p. 83).
- [286] Sia Nemat-Nasser. „Micromechanics of actuation of ionic polymer-metal composites“. In: *Journal of Applied Physics* 92.5 (2002), pp. 2899–2915 (cit. on pp. 6, 166).
- [287] Sia Nemat-Nasser and Jiang Yu Li. „Electromechanical response of ionic polymer-metal composites“. In: *Journal of Applied Physics* 87.7 (2000), pp. 3321–3331 (cit. on pp. 6, 166).

- [288] Sia Nemat-Nasser and Yongxian Wu. „Comparative experimental study of ionic polymer–metal composites with different backbone ionomers and in various cation forms“. In: *Journal of Applied Physics* 93.9 (2003), pp. 5255–5267 (cit. on p. 6).
- [289] Chuc Huu Nguyen, Gursel Alici, and Gordon G. Wallace. „Modelling trilayer conjugated polymer actuators for their sensorless position control“. In: *Sensors and Actuators A: Physical* 185 (Oct. 2012), pp. 82–91 (cit. on p. 60).
- [290] Xiaofan Niu, Xinguo Yang, Paul Brochu, et al. „Bistable Large-Strain Actuation of Interpenetrating Polymer Networks“. In: *Advanced Materials* 24.48 (2012), pp. 6513–6519 (cit. on p. 8).
- [291] Ch Oehr, M Müller, B Elkin, D Hegemann, and U Vohrer. „Plasma grafting—a method to obtain monofunctional surfaces“. In: *Surface and Coatings Technology* 116 (1999), pp. 25–35 (cit. on p. 19).
- [292] Hidenori Okuzaki and Keiichi Funasaka. „Electro-responsive polypyrrole film based on reversible sorption of water vapor“. In: *Synthetic metals* 108.2 (2000), pp. 127–131 (cit. on p. 8).
- [293] Hidenori Okuzaki, Yuko Harashina, and Hu Yan. „Highly conductive PEDOT/PSS microfibers fabricated by wet-spinning and dip-treatment in ethylene glycol“. In: *European Polymer Journal* 45.1 (2009), pp. 256–261 (cit. on p. 100).
- [294] Hidenori Okuzaki, Takayoshi Kuwabara, Keiichi Funasaka, and Tomooki Saido. „Humidity-Sensitive Polypyrrole Films for Electro-Active Polymer Actuators“. In: *Advanced Functional Materials* 23.36 (2013), pp. 4400–4407 (cit. on p. 8).
- [295] Hidenori Okuzaki, Satoshi Takagi, Fumiya Hishiki, and Ryo Tanigawa. „Ionic liquid/polyurethane/PEDOT: PSS composites for electro-active polymer actuators“. In: *Sensors and Actuators B: Chemical* 194 (2014), pp. 59–63 (cit. on pp. 13, 60, 65, 66, 72, 73, 87, 170, 182).
- [296] TF Otero and I Boyano. „Comparative study of conducting polymers by the ESCR model“. In: *The Journal of Physical Chemistry B* 107.28 (2003), pp. 6730–6738 (cit. on pp. 61, 63).
- [297] Toribio F Otero, Hans-Jürgen Grande, and Javier Rodríguez. „Reinterpretation of polypyrrole electrochemistry after consideration of conformational relaxation processes“. In: *The Journal of Physical Chemistry B* 101.19 (1997), pp. 3688–3697 (cit. on pp. 62, 63, 74).
- [298] Jianyong Ouyang. „“Secondary doping” methods to significantly enhance the conductivity of PEDOT: PSS for its application as transparent electrode of optoelectronic devices“. In: *Displays* 34.5 (2013), pp. 423–436 (cit. on pp. 41, 43, 167).
- [299] M Padaki, R Surya Murali, MS Abdullah, et al. „Membrane technology enhancement in oil–water separation. A review“. In: *Desalination* 357 (2015), pp. 197–207 (cit. on p. 55).
- [300] Viljar Palmre, Joel J Hubbard, Maxwell Fleming, et al. „An IPMC-enabled bio-inspired bending/twisting fin for underwater applications“. In: *Smart Materials and Structures* 22.1 (Jan. 2013), p. 014003 (cit. on pp. 6, 166).
- [301] Viljar Palmre, David Pugal, Kwang J Kim, et al. „Nanoothorn electrodes for ionic polymer-metal composite artificial muscles.“ In: *Scientific reports* 4 (Jan. 2014), p. 6176 (cit. on p. 6).

- [302] Han-Saem Park, Seo-Jin Ko, Jeong-Seok Park, Jin Young Kim, and Hyun-Kon Song. „Redox-active charge carriers of conducting polymers as a tuner of conductivity and its potential window“. In: *Scientific reports* 3 (2013) (cit. on p. 84).
- [303] Kiwon Park, Myung-Keun Yoon, Sangbok Lee, Jinho Choi, and Mano Thubrikar. „Effects of electrode degradation and solvent evaporation on the performance of ionic-polymer–metal composite sensors“. In: *Smart Materials and Structures* 19.7 (2010), p. 075002 (cit. on pp. 6, 166).
- [304] YW Park and N Inagaki. „Surface modification of poly (vinylidene fluoride) film by remote Ar, H₂, and O₂ plasmas“. In: *Polymer* 44.5 (2003), pp. 1569–1575 (cit. on pp. 16, 20, 171).
- [305] Qibing Pei, Marcus A Rosenthal, Ron Pelrine, Scott Stanford, and Roy D Kornbluh. „Multifunctional electroelastomer roll actuators and their application for biomimetic walking robots“. In: *Smart Structures and Materials*. International Society for Optics and Photonics. 2003, pp. 281–290 (cit. on p. 9).
- [306] Ron Pelrine, Roy Kornbluh, Jose Joseph, et al. „High-field deformation of elastomeric dielectrics for actuators“. In: *Materials Science and Engineering: C* 11.2 (2000), pp. 89–100 (cit. on p. 4).
- [307] Ron Pelrine, Roy Kornbluh, and Guggi Kofod. „High-Strain Actuator Materials Based on Dielectric Elastomers“. In: *Advanced Materials* 12.16 (2000), pp. 1223–1225 (cit. on p. 4).
- [308] Julien Petersen, Thierry Fouquet, Marc Michel, et al. „Enhanced adhesion over aluminum solid substrates by controlled atmospheric plasma deposition of amine-rich primers“. In: *ACS applied materials & interfaces* 4.2 (2012), pp. 1072–1079 (cit. on p. 47).
- [309] Priam Vasudevan Pillai. „Development and characterization of conducting polymer actuators“. PhD thesis. Massachusetts Institute of Technology, 2011 (cit. on pp. 86, 108).
- [310] C Plesse, A Khaldi, Q Wang, et al. „Polyethylene oxide–polytetrahydrofurane–PEDOT conducting interpenetrating polymer networks for high speed actuators“. In: *Smart Materials and Structures* 20.12 (2011), p. 124002 (cit. on p. 65).
- [311] Cédric Plesse, Frédéric Vidal, Hyacinthe Randriamahazaka, Dominique Teyssié, and Claude Chevrot. „Synthesis and characterization of conducting interpenetrating polymer networks for new actuators“. In: *Polymer* 46.18 (2005), pp. 7771–7778 (cit. on p. 65).
- [312] Andres Punning, Kwang J Kim, Viljar Palmre, et al. „Ionic electroactive polymer artificial muscles in space applications“. In: *Scientific reports* 4 (2014) (cit. on p. 9).
- [313] Andres Punning, Indrek Must, Inga Põldsalu, et al. „Lifetime measurements of ionic electroactive polymer actuators“. In: *Journal of Intelligent Material Systems and Structures* 25.18 (2014), pp. 2267–2275 (cit. on pp. 6, 10, 35, 73, 78).
- [314] Andres Punning, Indrek Must, Inga Põldsalu, et al. „Long-term degradation of the ionic electroactive polymer actuators“. In: *SPIE Smart Structures and Materials+ Nondestructive Evaluation and Health Monitoring*. International Society for Optics and Photonics. 2015, 94300S–94300S (cit. on pp. 35, 36, 73, 78).
- [315] Myoungcho Pyo, Clayton C Bohn, Elisabeth Smela, John R Reynolds, and Anthony B Brennan. „Direct strain measurement of polypyrrole actuators controlled by the polymer/gold interface“. In: *Chemistry of materials* 15.4 (2003), pp. 916–922 (cit. on p. 109).

- [316] Rachel Zimet Pytel. „Artificial muscle morphology: structure/property relationships in polypyrrole actuators“. PhD thesis. Massachusetts Institute of Technology, 2007 (cit. on pp. 63, 70, 71, 75).
- [317] A Rahimpour, SS Madaeni, S Zereshki, and Y Mansourpanah. „Preparation and characterization of modified nano-porous PVDF membrane with high antifouling property using UV photo-grafting“. In: *Applied Surface Science* 255.16 (2009), pp. 7455–7461 (cit. on pp. 16, 20, 172).
- [318] Saeid Rajabzadeh, Daichi Ogawa, Yoshikage Ohmukai, et al. „Preparation of a PVDF hollow fiber blend membrane via thermally induced phase separation (TIPS) method using new synthesized zwitterionic copolymer“. In: *Desalination and Water Treatment* ahead-of-print (2014), pp. 1–9 (cit. on p. 14).
- [319] D Rana and T Matsuura. „Surface modifications for antifouling membranes“. In: *Chemical reviews* 110.4 (2010), pp. 2448–2471 (cit. on p. 14).
- [320] N Reis and B Derby. „Ink jet deposition of ceramic suspensions: modeling and experiments of droplet formation“. In: *MRS proceedings*. Vol. 624. Cambridge Univ Press. 2000, p. 65 (cit. on p. 92).
- [321] Zhi Ren, Xiaofan Niu, Dustin Chen, Wei Hu, and Qibing Pei. „A new bistable electroactive polymer for prolonged cycle lifetime of refreshable Braille displays“. In: *SPIE Smart Structures and Materials+ Nondestructive Evaluation and Health Monitoring*. International Society for Optics and Photonics. 2014, pp. 905621–905621 (cit. on p. 8).
- [322] Isabella S Romero, Nathan P Bradshaw, Jesse D Larson, et al. „Biocompatible Electromechanical Actuators Composed of Silk-Conducting Polymer Composites“. In: *Advanced Functional Materials* 24.25 (2014), pp. 3866–3873 (cit. on pp. 65, 73).
- [323] Samuel Rosset and Herbert R Shea. „Flexible and stretchable electrodes for dielectric elastomer actuators“. In: *Applied Physics A* 110.2 (2013), pp. 281–307 (cit. on p. 4).
- [324] Siul Ruiz, Benjamin Mead, Viljar Palmre, Kwang J Kim, and Woosoon Yim. „A cylindrical ionic polymer-metal composite-based robotic catheter platform: modeling, design and control“. In: *Smart Materials and Structures* 24.1 (2015), p. 015007 (cit. on pp. 1, 6, 10, 164, 166).
- [325] Donghyeon Ryu, Frederick N Meyers, and Kenneth J Loh. „Inkjet-printed, flexible, and photoactive thin film strain sensors“. In: *Journal of Intelligent Material Systems and Structures* (2014), p. 1045389X14546653 (cit. on pp. 11, 109, 169).
- [326] R Samatham, KJ Kim, D Dogruer, et al. „Active polymers: an overview“. In: *Electroactive Polymers for Robotic Applications*. Springer, 2007, pp. 1–36 (cit. on p. 12).
- [327] JM Sansinena, V Olazabal, TF Otero, CN Polo Da Fonseca, and Marco-A De Paoli. „A solid state artificial muscle based on polypyrrole and a solid polymeric electrolyte working in air“. In: *Chemical Communications* 22 (1997), pp. 2217–2218 (cit. on p. 60).
- [328] Rachel Elizabeth Saunders and Brian Derby. „Inkjet printing biomaterials for tissue engineering: bioprinting“. In: *International Materials Reviews* 59.8 (2014), pp. 430–448 (cit. on p. 91).
- [329] Suchol Savagatrup, Esther Chan, Sandro M Renteria-Garcia, et al. „Plasticization of PEDOT: PSS by Common Additives for Mechanically Robust Organic Solar Cells and Wearable Sensors“. In: *Advanced Functional Materials* 25.3 (2015), pp. 427–436 (cit. on pp. 43, 45, 168).

- [330] Amit Sawhney, Animesh Agrawal, Te-Chen Lo, et al. „Soft-structured sensors and connectors by inkjet printing“. In: (2007) (cit. on pp. 11, 109, 169).
- [331] Stefano Schiaffino and Ain A Sonin. „Molten droplet deposition and solidification at low Weber numbers“. In: *Physics of Fluids (1994-present)* 9.11 (1997), pp. 3172–3187 (cit. on p. 94).
- [332] Hildegard M Schneider, Peter Frantz, and Steve Granick. „The bimodal energy landscape when polymers adsorb“. In: *Langmuir* 12.4 (1996), pp. 994–996 (cit. on p. 39).
- [333] Ethan B Secor and Mark C Hersam. „Emerging Carbon and Post-Carbon Nanomaterial Inks for Printed Electronics“. In: *The Journal of Physical Chemistry Letters* 6.4 (2015), pp. 620–626 (cit. on p. 109).
- [334] Florent Seichepine, Emmanuel Flahaut, and Christophe Vieu. „A simple and versatile method for statistical analysis of the electrical properties of individual double walled carbon nanotubes“. In: *Microelectronic Engineering* 88.7 (2011), pp. 1637–1639 (cit. on p. 144).
- [335] Christoph W Sele, Timothy von Werne, Richard H Friend, and Henning Sirringhaus. „Lithography-free, self-aligned inkjet printing with sub-hundred-nanometer resolution“. In: *Advanced Materials* 17.8 (2005), pp. 997–1001 (cit. on p. 94).
- [336] Mohsen Shahinpoor and Kwang J Kim. „Ionic polymer-metal composites: I. Fundamentals“. In: *Smart Materials and Structures* 10.4 (2001), p. 819 (cit. on p. 6).
- [337] Robert F Shepherd, Adam A Stokes, Rui Nunes, and George M Whitesides. „Soft machines that are resistant to puncture and that self seal“. In: *Advanced Materials* 25.46 (2013), pp. 6709–6713 (cit. on p. 2).
- [338] Jun Shintake, Samuel Rosset, Bryan Schubert, et al. „DEA for soft robotics: 1-gram actuator picks up a 60-gram egg“. In: *SPIE Smart Structures and Materials+ Nondestructive Evaluation and Health Monitoring*. International Society for Optics and Photonics. 2015, 94301S–94301S (cit. on p. 9).
- [339] Tina Shoa, Dan Sik Yoo, Konrad Walus, and John David W Madden. „A dynamic electromechanical model for electrochemically driven conducting polymer actuators“. In: *Mechatronics, IEEE/ASME Transactions on* 16.1 (2011), pp. 42–49 (cit. on p. 78).
- [340] Aiva Simate, Bertrand Tondu, Fabrice Mathieu, Philippe Souères, and Christian Bergaud. „Simple casting based fabrication of PEDOT: PSS-PVDF-ionic liquid soft actuators“. In: *SPIE Smart Structures and Materials+ Nondestructive Evaluation and Health Monitoring*. International Society for Optics and Photonics. 2015, 94301E–94301E (cit. on p. 49).
- [341] Kim Shyong Siow, Leanne Britcher, Sunil Kumar, and Hans J Griesser. „Plasma Methods for the Generation of Chemically Reactive Surfaces for Biomolecule Immobilization and Cell Colonization-A Review“. In: *Plasma processes and polymers* 3.6-7 (2006), pp. 392–418 (cit. on p. 19).
- [342] H Sirringhaus, T Kawase, RH Friend, et al. „High-resolution inkjet printing of all-polymer transistor circuits“. In: *Science* 290.5499 (2000), pp. 2123–2126 (cit. on p. 94).
- [343] Steen Skaarup, Lasse Bay, Kamal Vidanapathirana, et al. „Simultaneous anion and cation mobility in polypyrrole“. In: *Solid State Ionics* 159.1 (2003), pp. 143–147 (cit. on p. 63).

- [344] Michael J Skaug, Joshua N Mabry, and Daniel K Schwartz. „Single-Molecule Tracking of Polymer Surface Diffusion“. In: *Journal of the American Chemical Society* 136.4 (2013), pp. 1327–1332 (cit. on p. 24).
- [345] Elisabeth Smela. „Conjugated polymer actuators for biomedical applications“. In: *Otero* 7 (2003), p. 22 (cit. on pp. 7, 10, 59, 166).
- [346] Elisabeth Smela and Nikolaj Gadegaard. „Surprising volume change in PPy (DBS): an atomic force microscopy study“. In: *Advanced Materials* 11.11 (1999), pp. 953–957 (cit. on p. 75).
- [347] Elisabeth Smela, Wen Lu, and Benjamin R Mattes. „Polyaniline actuators: Part 1. PANI (AMPS) in hcl“. In: *Synthetic Metals* 151.1 (2005), pp. 25–42 (cit. on p. 60).
- [348] Henry J Snaith, Henry Kenrick, Marco Chiesa, and Richard H Friend. „Morphological and electronic consequences of modifications to the polymer anode ‘PEDOT: PSS’“. In: *Polymer* 46.8 (2005), pp. 2573–2578 (cit. on p. 84).
- [349] Graeme A Snook, Pon Kao, and Adam S Best. „Conducting-polymer-based supercapacitor devices and electrodes“. In: *Journal of Power Sources* 196.1 (2011), pp. 1–12 (cit. on p. 72).
- [350] Geoffrey M Spinks, Dezhi Zhou, Lu Liu, and Gordon G Wallace. „The amounts per cycle of polypyrrole electromechanical actuators“. In: *Smart materials and structures* 12.3 (2003), p. 468 (cit. on p. 65).
- [351] Zdenko Spitalsky, Dimitrios Tasis, Konstantinos Papagelis, and Costas Galiotis. „Carbon nanotube–polymer composites: chemistry, processing, mechanical and electrical properties“. In: *Progress in polymer science* 35.3 (2010), pp. 357–401 (cit. on pp. 86, 108).
- [352] Victor M Starov. „Surfactant solutions and porous substrates: spreading and imbibition“. In: *Advances in colloid and interface Science* 111.1 (2004), pp. 3–27 (cit. on p. 54).
- [353] Jason R Stokes, Lubica Macakova, Agnieszka Chojnicka-Paszun, Cornelis G de Kruif, and Harmen HJ de Jongh. „Lubrication, adsorption, and rheology of aqueous polysaccharide solutions“. In: *Langmuir* 27.7 (2011), pp. 3474–3484 (cit. on p. 15).
- [354] Matteo Stoppa and Alessandro Chiolerio. „Wearable electronics and smart textiles: a critical review“. In: *Sensors* 14.7 (2014), pp. 11957–11992 (cit. on p. 10).
- [355] Hristiyan Stoyanov, Paul Brochu, Xiaofan Niu, et al. „Long lifetime, fault-tolerant free-standing actuators based on a silicone dielectric elastomer and self-clearing carbon nanotube compliant electrodes“. In: *RSC Advances* 3.7 (2013), pp. 2272–2278 (cit. on p. 4).
- [356] Takushi Sugino, Kenji Kiyohara, Ichiroh Takeuchi, Ken Mukai, and Kinji Asaka. „Actuator properties of the complexes composed by carbon nanotube and ionic liquid: the effects of additives“. In: *Sensors and Actuators B: Chemical* 141.1 (2009), pp. 179–186 (cit. on pp. 69, 149).
- [357] Svetlana A Sukhishvili, Yan Chen, Joachim D Müller, et al. „Surface diffusion of poly (ethylene glycol)“. In: *Macromolecules* 35.5 (2002), pp. 1776–1784 (cit. on p. 55).
- [358] Haixiang Sun, Tiantian Wang, Yingying Zhou, Peng Li, and Ying Kong. „Synthesis of well-defined amphiphilic block copolymers via AGET ATRP used for hydrophilic modification of PVDF membrane“. In: *Journal of Applied Polymer Science* 132.24 (2015) (cit. on p. 14).

- [359] Kuan Sun, Shupeng Zhang, Pengcheng Li, et al. „Review on application of PEDOTs and PEDOT: PSS in energy conversion and storage devices“. In: *Journal of Materials Science: Materials in Electronics* (2015), pp. 1–25 (cit. on p. 85).
- [360] L Sun, WM Huang, CC Wang, et al. „Polymeric shape memory materials and actuators“. In: *Liquid Crystals* 41.3 (2014), pp. 277–289 (cit. on pp. 2, 165).
- [361] Youyi Sun, Yongji Zhang, Qing Liang, et al. „Solvent inkjet printing process for the fabrication of polymer solar cells“. In: *Rsc Advances* 3.30 (2013), pp. 11925–11934 (cit. on p. 91).
- [362] Karan Surana, Pramod K Singh, B Bhattacharya, CS Verma, and RM Mehra. „Synthesis of graphene oxide coated Nafion membrane for actuator application“. In: *Ceramics International* 41.3 (2015), pp. 5093–5099 (cit. on p. 7).
- [363] Karl Svennersten, Magnus Berggren, Agneta Richter-Dahlfors, and Edwin W. H. Jager. „Mechanical stimulation of epithelial cells using polypyrrole microactuators“. In: *Lab Chip* 11 (19 2011), pp. 3287–3293 (cit. on p. 10).
- [364] Silvia Taccola, Francesco Greco, Edoardo Sinibaldi, et al. „Toward a New Generation of Electrically Controllable Hygromorphic Soft Actuators“. In: *Advanced Materials* (2014) (cit. on pp. 8, 77, 182).
- [365] May Tahhan, Van-Tan Truong, Geoffrey M Spinks, and Gordon G Wallace. „Carbon nanotube and polyaniline composite actuators“. In: *Smart materials and structures* 12.4 (2003), p. 626 (cit. on pp. 86, 87, 108).
- [366] J Takahashi and A Hotta. „Adhesion enhancement of polyolefins by diamond like carbon coating and photografting polymerization“. In: *Diamond and Related Materials* 26 (2012), pp. 55–59 (cit. on pp. 20, 48).
- [367] GN Taylor and TM Wolf. „Oxygen plasma removal of thin polymer films“. In: *Polymer Engineering & Science* 20.16 (1980), pp. 1087–1092 (cit. on p. 18).
- [368] Rauno Temmer, Indrek Must, Friedrich Kaasik, Alvo Aabloo, and Tarmo Tamm. „Combined chemical and electrochemical synthesis methods for metal-free polypyrrole actuators“. In: *Sensors and Actuators B: Chemical* 166 (2012), pp. 411–418 (cit. on pp. 36, 60, 65, 73).
- [369] Rauno Temmer, Ali Maziz, Cédric Plesse, et al. „In search of better electroactive polymer actuator materials: PPy versus PEDOT versus PEDOT-PPy composites“. In: *Smart Materials and Structures* 22.10 (2013), p. 104006 (cit. on pp. 35, 36, 60, 61, 64–66, 72, 73, 170).
- [370] Naohiro Terasawa and Kinji Asaka. „Superior performance hybrid (electrostatic double-layer and faradaic capacitor) polymer actuators incorporating noble metal oxides and carbon black“. In: *Sensors and Actuators B: Chemical* 210 (Apr. 2015), pp. 748–755 (cit. on p. 7).
- [371] Naohiro Terasawa and Ichiroh Takeuchi. „Electrochemical and electromechanical properties of carbon black/carbon fiber composite polymer actuator with higher performance than single-walled carbon nanotube polymer actuator“. In: *Electrochimica Acta* 123 (Mar. 2014), pp. 340–345 (cit. on p. 7).

- [372] Tete Tevi, Shantonio W Saint Birch, Sylvia W Thomas, and Arash Takshi. „Effect of Triton X-100 on the double layer capacitance and conductivity of poly (3, 4-ethylenedioxythiophene): poly (styrenesulfonate)(PEDOT: PSS) films“. In: *Synthetic Metals* 191 (2014), pp. 59–65 (cit. on p. 45).
- [373] Erik T Thostenson, Zhifeng Ren, and Tsu-Wei Chou. „Advances in the science and technology of carbon nanotubes and their composites: a review“. In: *Composites science and technology* 61.13 (2001), pp. 1899–1912 (cit. on p. 85).
- [374] R Tiwari and E Garcia. „The state of understanding of ionic polymer metal composite architecture: a review“. In: *Smart Materials and Structures* 20.8 (2011), p. 083001 (cit. on pp. 5, 6, 165).
- [375] Michael T Tolley, Robert F Shepherd, Bobak Mosadegh, et al. „A resilient, untethered soft robot“. In: *Soft Robotics* 1.3 (2014), pp. 213–223 (cit. on p. 2).
- [376] Kazuo Tominaga, Hikaru Hashimoto, Wataru Takashima, and Keiichi Kaneto. „Training and shape retention in conducting polymer artificial muscles“. In: *Smart Materials and Structures* 20.12 (2011), p. 124005 (cit. on pp. 74, 75).
- [377] Bertrand Tondu. *Artificial muscles for humanoid robots*. na, 2007 (cit. on pp. 1, 9, 164).
- [378] Bertrand Tondu. „Modelling of the McKibben artificial muscle: A review“. In: *Journal of Intelligent Material Systems and Structures* 23.3 (2012), pp. 225–253 (cit. on p. 2).
- [379] Janno Torop, Alvo Aabloo, and Edwin WH Jager. „Novel actuators based on polypyrrole/carbide-derived carbon hybrid materials“. In: *Carbon* 80 (2014), pp. 387–395 (cit. on pp. 7, 86, 109).
- [380] Felice Torrisi, Tawfique Hasan, Weiping Wu, et al. „Inkjet-printed graphene electronics“. In: *Acs Nano* 6.4 (2012), pp. 2992–3006 (cit. on p. 109).
- [381] Piergiorgio Tozzi. „Artificial muscle: the human chimera is the future“. In: *Swiss Med Wkly* 141 (2011), w13311 (cit. on pp. 1, 164).
- [382] Shih-An Tsai, Hsiang-Chun Wei, and Guo-Dung J. Su. „Polydimethylsiloxane coating on an ionic polymer metallic composite for a tunable focusing mirror“. In: *Appl. Opt.* 51.35 (2012), pp. 8315–8323 (cit. on pp. 6, 36).
- [383] Meltem Tunckol, Jérôme Durand, and Philippe Serp. „Carbon nanomaterial–ionic liquid hybrids“. In: *Carbon* 50.12 (Oct. 2012), pp. 4303–4334 (cit. on p. 7).
- [384] Nicolas Vandencastele, Delphine Merche, and François Reniers. „XPS and contact angle study of N₂ and O₂ plasma-modified PTFE, PVDF and PVF surfaces“. In: *Surface and interface analysis* 38.4 (2006), pp. 526–530 (cit. on pp. 20, 171).
- [385] F Vidal, J-F Popp, C Plesse, C Chevrot, and D Teyssie. „Feasibility of conducting semi-interpenetrating networks based on a poly (ethylene oxide) network and poly (3, 4-ethylenedioxythiophene) in actuator design“. In: *Journal of applied polymer science* 90.13 (2003), pp. 3569–3577 (cit. on p. 65).
- [386] Frédéric Vidal, Cédric Plesse, Dominique Teyssié, and Claude Chevrot. „Long-life air working conducting semi-IPN/ionic liquid based actuator“. In: *Synthetic Metals* 142.1 (2004), pp. 287–291 (cit. on pp. 60, 65, 73, 80, 169, 182).
- [387] E Vitoratos, S Sakkopoulos, E Dalas, et al. „Thermal degradation mechanisms of PEDOT: PSS“. In: *Organic Electronics* 10.1 (2009), pp. 61–66 (cit. on p. 73).

- [388] V Vunder, A Punning, and A Aabloo. „Long-term response of ionic electroactive polymer actuators in variable ambient conditions“. In: *SPIE Smart Structures and Materials+ Nondestructive Evaluation and Health Monitoring*. International Society for Optics and Photonics. 2015, 94300R–94300R (cit. on pp. 35, 73, 78).
- [389] JZ Wang, ZH Zheng, HW Li, WTS Huck, and H Sirringhaus. „Dewetting of conducting polymer inkjet droplets on patterned surfaces“. In: *Nature materials* 3.3 (2004), pp. 171–176 (cit. on p. 94).
- [390] Peng Wang, KL Tan, ET Kang, and KG Neoh. „Plasma-induced immobilization of poly (ethylene glycol) onto poly (vinylidene fluoride) microporous membrane“. In: *Journal of Membrane Science* 195.1 (2002), pp. 103–114 (cit. on pp. 19–21, 23).
- [391] Xiangjiang Wang, Gursel Alici, and Chuc Huu Nguyen. „Adaptive sliding mode control of tri-layer conjugated polymer actuators“. In: *Smart Materials and Structures* 22.2 (2013), p. 025004 (cit. on pp. 60, 109).
- [392] Xiangjiang Wang, Gursel Alici, and Xiaobo Tan. „Modeling and inverse feedforward control for conducting polymer actuators with hysteresis“. In: *Smart Materials and Structures* 23.2 (2014), p. 025015 (cit. on pp. 60, 78).
- [393] Xuezheng Wang. *Understanding Actuation Mechanisms of Conjugated Polymer Actuators: Ion Transport*. ProQuest, 2007 (cit. on pp. 62, 75).
- [394] Xuezheng Wang and Elisabeth Smela. „Color and volume change in PPy (DBS)“. In: *The Journal of Physical Chemistry C* 113.1 (2008), pp. 359–368 (cit. on p. 74).
- [395] Youqi Wang, Changjie Sun, Eric Zhou, and Ji Su. „Deformation mechanisms of electrostrictive graft elastomer“. In: *Smart Materials and Structures* 13.6 (2004), p. 1407 (cit. on p. 4).
- [396] Qingshuo Wei, Masakazu Mukaida, Yasuhisa Naitoh, and Takao Ishida. „Morphological Change and Mobility Enhancement in PEDOT: PSS by Adding Co-solvents“. In: *Advanced materials* 25.20 (2013), pp. 2831–2836 (cit. on p. 100).
- [397] Florian M Weiss, Hans Deyhle, Gabor Kovacs, and Bert Müller. „Designing micro- and nanostructures for artificial urinary sphincters“. In: *SPIE Smart Structures and Materials+ Nondestructive Evaluation and Health Monitoring*. International Society for Optics and Photonics. 2012, 83400A–83400A (cit. on p. 10).
- [398] J. Weissmuller, R. N. Viswanath, D. Kramer, et al. „Charge-Induced Reversible Strain in a Metal“. In: *Science* 300.5617 (2003), pp. 312–315. eprint: <http://www.sciencemag.org/content/300/5617/312.full.pdf> (cit. on p. 8).
- [399] Robert N Wenzel. „Resistance of solid surfaces to wetting by water“. In: *Industrial & Engineering Chemistry* 28.8 (1936), pp. 988–994 (cit. on pp. 25, 29).
- [400] Peter Wilson, Constantina Lekakou, and John F. Watts. „A comparative assessment of surface microstructure and electrical conductivity dependence on co-solvent addition in spin coated and inkjet printed poly(3,4-ethylenedioxythiophene):polystyrene sulphonate (PEDOT:PSS)“. In: *Organic Electronics* 13.3 (Mar. 2012), pp. 409–418 (cit. on pp. 95, 167, 168).
- [401] Hongbin Wu, Jianhua Zou, Ding An, et al. „A new approach to efficiency enhancement of polymer light-emitting diodes by deposition of anode buffer layers in the presence of additives“. In: *Organic Electronics* 10.8 (Dec. 2009), pp. 1562–1570 (cit. on pp. 95, 167).

- [402] Yijie Xia and Jianyong Ouyang. „PEDOT: PSS films with significantly enhanced conductivities induced by preferential solvation with cosolvents and their application in polymer photovoltaic cells“. In: *Journal of Materials Chemistry* 21.13 (2011), pp. 4927–4936 (cit. on pp. 43, 46).
- [403] Zhaoting Xiong and Changqing Liu. „Optimization of inkjet printed PEDOT: PSS thin films through annealing processes“. In: *Organic Electronics* 13.9 (2012), pp. 1532–1540 (cit. on pp. 95, 96, 99–102, 167).
- [404] Xu Yan, Zhao Gang, Zhu Yuming, and Sun Zhuangzhi. „Morphology characterization and failure mechanism investigation of Ag-IPMC“. English. In: *Ionics* 21.4 (2015), pp. 1089–1094 (cit. on pp. 6, 166).
- [405] Takaichi Yanagida, Kazunori Adachi, and Taro Nakamura. „Development of Bellows-Type Artificial Rubber Muscle and Application to Peristaltic Crawling Endoscopic Robot“. In: *Journal ref: Journal of Robotics and Mechatronics* 25.4 (2013), pp. 748–754 (cit. on p. 10).
- [406] Qingyu Yao, Gursel Alici, and Geoffrey M Spinks. „Feedback control of tri-layer polymer actuators to improve their positioning ability and speed of response“. In: *Sensors and Actuators A: Physical* 144.1 (2008), pp. 176–184 (cit. on pp. 60, 109).
- [407] LP Yeo, BK Lok, QMP Nguyen, CW Lu, and YC Lam. „Selective surface modification of PET substrate for inkjet printing“. In: *The International Journal of Advanced Manufacturing Technology* 71.9-12 (2014), pp. 1749–1755 (cit. on p. 95).
- [408] S Yoshida, K Hagiwara, T Hasebe, and A Hotta. „Surface modification of polymers by plasma treatments for the enhancement of biocompatibility and controlled drug release“. In: *Surface and Coatings Technology* 233 (2013), pp. 99–107 (cit. on p. 20).
- [409] Zhibin Yu, Wei Yuan, Paul Brochu, et al. „Large-strain, rigid-to-rigid deformation of bistable electroactive polymers“. In: *Applied Physics Letters* 95.19 (2009), p. 192904 (cit. on p. 7).
- [410] Dong-Jin Yun, KiPyo Hong, Se hyun Kim, et al. „Multiwall carbon nanotube and poly (3, 4-ethylenedioxythiophene): polystyrene sulfonate (PEDOT: PSS) composite films for transistor and inverter devices“. In: *ACS applied materials & interfaces* 3.1 (2011), pp. 43–49 (cit. on pp. 83, 86).
- [411] Umer Lebbe Zainudeen, Mohamed Abdul Careem, and Steen Skaarup. „PEDOT and PPy conducting polymer bilayer and trilayer actuators“. In: *Sensors and Actuators B: Chemical* 134.2 (2008), pp. 467–470 (cit. on pp. 61, 65).
- [412] Jie Zhang, Zhiwei Wang, Xingran Zhang, Xiang Zheng, and Zhichao Wu. „Enhanced antifouling behaviours of polyvinylidene fluoride membrane modified through blending with nano-TiO₂/polyethylene glycol mixture“. In: *Applied Surface Science* 345 (2015), pp. 418–427 (cit. on p. 14).
- [413] Jing Zhang, Lian Gao, Jing Sun, et al. „Incorporation of single-walled carbon nanotubes with PEDOT/PSS in DMSO for the production of transparent conducting films“. In: *Diamond and Related Materials* 22 (2012), pp. 82–87 (cit. on pp. 83, 86).
- [414] Mei Zhang, Ken R Atkinson, and Ray H Baughman. „Multifunctional carbon nanotube yarns by downsizing an ancient technology“. In: *Science* 306.5700 (2004), pp. 1358–1361 (cit. on p. 2).

- [415] Suojiang Zhang, Ning Sun, Xuezhong He, Xingmei Lu, and Xiangping Zhang. „Physical properties of ionic liquids: database and evaluation“. In: *Journal of physical and chemical reference data* 35.4 (2006), pp. 1475–1517 (cit. on p. 83).
- [416] Wenfeng Zhang, Baofeng Zhao, Zhicai He, et al. „High-efficiency ITO-free polymer solar cells using highly conductive PEDOT: PSS/surfactant bilayer transparent anodes“. In: *Energy & Environmental Science* 6.6 (2013), pp. 1956–1964 (cit. on pp. 45, 83).
- [417] Zhiye Zhang and Michael Philen. „Review: Pressurized Artificial Muscles“. In: *Journal of Intelligent Material Systems and Structures* (2011), p. 1045389X11420592 (cit. on pp. 2, 164).
- [418] Jiang Zhao and Steve Granick. „How polymer surface diffusion depends on surface coverage“. In: *Macromolecules* 40.4 (2007), pp. 1243–1247 (cit. on pp. 24, 28, 55).
- [419] Jiang Zhao and Steve Granick. „Polymer lateral diffusion at the solid-liquid interface“. In: *Journal of the American Chemical Society* 126.20 (2004), pp. 6242–6243 (cit. on p. 28).
- [420] Zhi-Ping Zhao, Mei-Sheng Li, Ning Li, Ming-Xing Wang, and Yue Zhang. „Controllable modification of polymer membranes by long-distance and dynamic low-temperature plasma flow: AA grafting penetrated through electrospun PP fibrous membranes“. In: *Journal of Membrane Science* 440 (2013), pp. 9–19 (cit. on pp. 19, 20, 23).
- [421] Wen Zheng, Joselito M Razal, Philip G Whitten, et al. „Artificial muscles based on polypyrrole/carbon nanotube laminates“. In: *Advanced materials* 23.26 (2011), pp. 2966–2970 (cit. on pp. 86, 87, 109).
- [422] Dezhi Zhou, Geoffrey M Spinks, Gordon G Wallace, et al. „Solid state actuators based on polypyrrole and polymer-in-ionic liquid electrolytes“. In: *Electrochimica acta* 48.14 (2003), pp. 2355–2359 (cit. on p. 60).
- [423] Jian Zhou, Dalaver H Anjum, Long Chen, et al. „The temperature-dependent microstructure of PEDOT/PSS films: insights from morphological, mechanical and electrical analyses“. In: *Journal of Materials Chemistry C* 2.46 (2014), pp. 9903–9910 (cit. on pp. 77, 100, 102, 182).
- [424] Yuzhang Zhu, Dong Wang, Lei Jiang, and Jian Jin. „Recent progress in developing advanced membranes for emulsified oil/water separation“. In: *NPG Asia Materials* 6.5 (2014), e101 (cit. on p. 15).

Appendix 1: materials and experimental methods

Contents

A.1	Materials	143
A.1.1	Solutions	144
A.2	Chapter 2: Hybrid PVDF/PVDF-graft-PEGMA membranes	144
A.2.1	PEGMA deposition	144
A.2.2	Plasma irradiation	145
A.2.3	Characterization of PVDF membrane	146
A.3	Chapter 3: Adhesion	146
A.3.1	Fabrication of PVDF/PEDOT:PSS bilayers	146
A.3.2	Penetrating drop method	147
A.4	Chapter 4: PEDOT:PSS/mPVDF/ionic liquid actuators	148
A.4.1	Fabrication of actuators	148
A.4.2	Characterization of actuators	148
A.4.3	Post-treatment of actuators	150
A.5	Chapter 5: Towards inkjet printed artificial muscles	151
A.5.1	Ink preparation, printing and characterization	151
A.5.2	Printing and characterization of actuators	152

A.1 Materials

Millipore VVHP04700 Durapore Membrane Filter (hydrophobic, pore diameter of $0.1 \mu\text{m}$, thickness of $125 \mu\text{m}$ and 47mm in diameter) were bought from Merck Milipore Corp. PEDOT:PSS 1.3 wt% conductivity grade dispersion in water (483095 ALDRICH), having PEDOT and PSS ratio of 1:2.5 was bought from Sigma Aldrich. poly(ethylene glycol) of $M_r - 400$ (PEG400) (202398 ALDRICH) as well as polyethylene glycol (PEG) with average $M_n - 300$ and $M_n - 3000$ were used as a secondary dopant for PEDOT:PSS.. 1 vol% of PEG400 in PEDOT:PSS solution was prepared and kept at 4°C before use. poly(ethylene glycol) methyl ether methacrylate (PEGMA) (average $M_n - 526$) were also purchased from Sigma-Aldrich Inc. 10 vol% PEGMA solution in 10 vol% ethanol and water mixture was prepared and kept at room temperature before use. 1-ethyl-3-methylimidazolium bis(trifluoromethanesulfonyl)imide (*emimTFSI*) ionic liquid was bought from Solvionics (Im0208a). Other chemicals such as Triton X-100, i-butanol, ethylene glycol, glycerol, sodium dodecyl sulfate (SDS) were also received from Sigma Aldrich.

Double walled *CNTs* were synthesized in Cirimat-CNRS as reported in [107] and provided in water/SDS suspension. *CNTs* samples contained 77% of double walled *CNTs*, 18% of single-walled *CNTs* and 5% of triple-walled *CNTs* that have a length ranging between 1 and 10 μm and a diameter of 1.2 – 3.2 nm . They were shown to exhibit a metallic electrical behaviour [334].

A.1.1 Solutions

For preparing *PEDOT:PSS* inks and solutions for casting, required amounts of *PEDOT:PSS* water suspension and additives were mixed on the mechanical shaker at 300 rpm for at least 3 hours. If not used immediately, solutions were kept at 4°C.

For spraying 10 $\text{vol}\%$ *PEGMA* solution in azeotropic ethanol/water mixture (10 $\text{vol}\%$ unless indicated differently) was used. It was mixed on the mechanical shaker for 3 hours and kept in a dark place at room temperature until use.

0.1 $\text{wt}\%$ of *CNTs* and 1 $\text{wt}\%$ of *SDS* were dispersed in deionised water and separated using 150 W ultrasound (VibraCell 75042, Bioblock Scientific) in an ice bath for 30 mins . The suspension was then centrifuged (16000 rpm , 10 mins) and the supernatant was collected and the supernatant was collected. Prior to spray coating, all the suspensions were dispersed using pulsed ultrasound (5 sec on and 5 secs off) for 10 min at 150 W . For spraying *SDS*, its 1 $\text{wt}\%$ solution was prepared in deionised water.

A.2 Chapter 2: Hybrid PVDF/PVDF-graft-PEGMA membranes

A.2.1 PEGMA deposition

Section 2.2.1. For immobilization of *PEGMA* on the pores of the *PVDF* membrane, a pristine membrane was immersed into 10 $\text{vol}\%$ *PEGMA* in isopropanol solution and kept for 15 minutes (gently moving the dish in rotating motion by hand). $28.97 \pm 2.7\text{mg}$ of *PEGMA* per membrane were deposited. Membranes were drying in air for few minutes, until signs of the solvent were not visible and then in the oven for 1 hour at 70°C to remove residual isopropanol (keeping the side of the membrane that will be later exposed to plasma on top). The membranes were then cut in half and different sides of a half-membrane were used.

Section 2.2.2. For filling the pores of the membrane with *PEGMA*, the membrane was agitated at 300 rpm in a 100% *PEGMA* for 5 hours at room temperature. For deposition by spray coating (detailed procedure is explained further in the section), 30 drops of 5 $\text{vol}\%$ of *PEGMA* solution in water were sprayed keeping the minimum droplet size (nearly closed valve). The second side of the membrane was treated in the same way.

Section 2.2.3. 5 – 10 $\text{vol}\%$ *PEGMA* solution in water, ethanol or 10 $\text{vol}\%$ ethanol and water mixture was prepared by mixing solution on the mechanical shaker for at least 3 hours before use and kept at room temperature if needed to use later. *PVDF* membranes were dried at 70 °C for at least 1 hour and weighted. Spray coating was

done under the fume hood and in the glovebox (Captair Pyramid Glovebox) in order to prevent influence of air flow on spray direction. *PVDF* membranes were stick on metallic holder by adhesion or were stabilized by airflow from the spray-gun. *PEGMA* solution (5 – 10% in water, ethanol or water-ethanol mixtures) was spray coated on the surface of *PVDF* by Mecafer Ag4 airbrush (0.4 μm needle). Three valve position were set for droplet size control: '1', '2', '3', where '3' corresponds to approximately half a turn (no precise control of drop size is possible but the valve opening was maintained the same throughout different experiments). The membrane and the gun were fixed in one line and gun was slightly moved during the spray while keeping the distance constant. Optimization experiments were performed by changing distance, valve opening, pressure and solvent, spraying 0.5, 1.0 and 2 *ml* of *PEGMA* solution for each condition and calculating spraying efficiency (*SE*):

$$SE = \frac{w_{spray} - w_{ini}}{V_{sol}\phi_i\rho} \quad (A.1)$$

where, w_{ini} and w_{spray} are weight of the pristine and dried membrane with sprayed *PEGMA* respectively, V_{sol} , ϕ_i and ρ are volume of sprayed solution and volume concentration of *PEGMA* in solution and density of *PEGMA*.

After optimization experiments the valve opening controlling the droplet size was fixed at '2' valve position and 2 *kgf/cm³* pressure was used. In order to achieve different grafting densities the spray gun distance to the membrane was changed from 25 to 35 *cm* or different amounts (0.5-2.0 *ml*) were sprayed at 30 *cm*. For functionalization on both sides, membranes were kept in air for several minutes in between sprays. *PVDF* membranes were then dried in oven at 70 °C for 1 hour and weighted for spray density calculations (*SD*):

$$SD = \frac{w_{spray} - w_{ini}}{2\pi r^2} \quad (A.2)$$

where, w_{ini} and w_{spray} are weight of the pristine and dried membrane with sprayed *PEGMA* respectively, r is radius of the membrane (23.5 *mm*).

A.2.2 Plasma irradiation

Membranes coated with a dried *PEGMA* monomer layer were then treated by low-pressure plasma with argon flow rate of 5 *sccm*, input power of 10 *W* and 1 *W* bias (measured power of 5 *W* and 0.2 *W* bias), controlled by a 13.56 *MHz* RF generator (Aviza Technology Inc. OMEGA201). The low-pressure plasma treatment was operated at 50 *mTorr* after 1 *min* given for gas stabilization. If functionalization were needed on both sides, membranes were reversed and procedure repeated. After plasma treatment, the PEGylated *PVDF* membrane was kept in air for at least 72 hours to neutralise radicals on *PVDF* backbone. The non-reacted *PEGMA* monomer was removed by washing membranes in ultrasonic bath in water, ethanol and again in water for 1 hour each. The remaining solvent was removed by drying membranes in the oven of 70 °C for 2 hours. The membranes were weighted again for grafting density calculations:

$$GD = \frac{w_{graft} - w_{ini}}{2\pi r^2} \quad (A.3)$$

where, w_{ini} and w_{graft} are weight of the pristine and functionalized membranes respectively, r is radius of the membrane (23.5 mm).

Different plasma irradiation parameters were used in **Section 2.2.1**. The membranes were then functionalized by Ar plasma irradiation for 15-30 s with these plasma parameters: 5 W RF power, 0 bias power, pressure of 1 mTorr, Ar flow of 10 sccm. Furthermore, membranes were washed immediately after grafting in the ultrasound bath: 1 hour in water, 1 hour in methanol and 1 hour in water.

A.2.3 Characterization of PVDF membrane

Fourier transform infrared spectrophotometry (FT-IR) spectrophotometry in attenuated total reflectance ATR mode with GaSn crystal as reflection element (VERTX 70, Bruker Optics) was done for surface chemical characterization. 64 scans at a resolution of 4 cm^{-1} were averaged. The obtained spectrum were further used for numerical integration of peaks corresponding to OCO and CF bond vibrations from 1700 cm^{-1} to 1750 cm^{-1} and 1390 cm^{-1} to 1420 cm^{-1} respectively. The ratio of integrated peaks was used to characterise surface coverage by PVDF-graft-PEGMA of the membranes.

Water contact angle as well as contact angle measurements of various PEDOT:PSS solutions were performed at 25 °C temperature with Digidrop GBX Contact Angle Meter. At least 5 different measurements were performed for each side of the membrane and averaged.

Atomic force microscopy (AFM) of functionalized and pristine membranes was performed with Veeco-Dimension Icon AFM (Veeco) in a tapping mode using RTESP-300 AFM probes (resonance frequency of about 300 kHz) and the averaged roughness was calculated using the NanoScope Analysis software (Veeco).

Energy-dispersive X-ray spectroscopy (EDX) was performed on modified PVDF - PEDOT:PSS bilayers for the estimation of the mixing depth and subsequently the grafting depth. Modified PVDF membranes were fixed in a $\varnothing 45\text{ mm}$ aluminium clamp and 3 ml of PEDOT:PSS solution with 1 vol% PEG400 were drop casted. Then they were dried for 24 hours in air and 2 hours at 70 °C. Membranes were fractured in liquid N_2 in order to obtain clean cross-section. The distribution of sulphur (signature of PEDOT:PSS) and fluorine (signature of PVDF) were mapped by Energy-dispersive X-ray spectroscopy (EDX) spectrometer (Helios NanoLab 600i, accelerating voltage 5 kV, working distance 6 mm) in linear scan and map scan modes. The approximate length of the overlap of both signals was estimated visually.

A.3 Chapter 3: Adhesion

A.3.1 Fabrication of PVDF/PEDOT:PSS bilayers

For fabrication of PVDF/PEDOT:PSS bilayers needed for the adhesion testing, pristine or modified PVDF membranes were fixed in a $\varnothing 45\text{ mm}$ aluminium clamp. Then 3 ml of

PEDOT:PSS solution secondary doped with 1 vol% of *PEG400* was used for drop casting unless indicated differently. *PEDOT:PSS* was dried at room temperature for about 24 hours and for 2 hours at 70°C unless indicated differently. Variations of the fabrication procedure for each experiment are provided below.

Section 3.2.3. The *PEDOT:PSS* solutions were prepared as in Section A.1 but with 1 vol% of *Triton X-100* surfactant or with 10 vol% of *i*-butanol. *PEDOT:PSS* was then deposited on pristine *PVDF*.

Section 3.2.4. For damaging the surface of the *PVDF* membrane by Ar plasma, pristine *PVDF* membranes were exposed to irradiation as for grafting (Section A.2.1). Plasma irradiation did not significantly change the *WCA* that remained 113.2 ± 2.1 and 129.3 ± 1.9 for smooth and rough sides respectively. Also, as sputtering time (15 s) is low, the mass decrease was not observed either. Oppositely, slight increase was measured (about 0.1 mg) for both sides that could be due to the oxidation of the *PVDF*. UV/ozone is expected to be less effective in damaging *PVDF* than Ar plasma. In order to ensure the effect, pristine *PVDF* membranes were irradiated for 1 hour. *PEDOT:PSS* was deposited immediately and other membranes were used for *WCA* and weight measurements. After the treatment *WCA* remained 111.3 ± 1.5 and 121.9 ± 0.2 for smooth and rough sides respectively, but the weight decreased for about 0.42 and 0.26 mg for smooth and rough sides respectively.

Section 3.3.1. In order to produce flat *PVDF* film it was placed on the silicon wafer and on the hot plate heated to 170°C. In order to avoid the formation of air bubbles between the film and the wafer, a metal cylinder was used to apply pressure on the membrane while heating (several seconds). After melting, transparent *PVDF* film was formed. The silicon wafer was then removed from the hot plate and cooled down. The side of the *PVDF* film that was facing the wafer was used for functionalization in the same way as membranes (optimized spray coating, plasma grafting and washing). Grafting density of $0.04 \pm 0.01 \text{ ng/mm}^2$ was obtained and water contact angle (acsWCA) decreased from 82.16 ± 7 to 56.3 ± 2 .

Section 3.3.2. The *PEDOT:PSS* solutions were prepared as in Section A.1 but with 2 vol% or 5 vol% of *PEG* as a secondary dopant. The *PEDOT:PSS* was then deposited on both sides of the *pPVDF* membrane and on *mPVDF* (functionalized on both sides) as in Section A.4.1. *GD* of *mPVDF* used was $0.103 \pm 0.05 \text{ ng/mm}^2$. Surface tension of *PEDOT:PSS* solutions was measured as in Section A.5.1. For the water contact angle measurements shown in Fig. 3.12, the drop of *PEG400* was deposited on the *pPVDF* and allowed to adsorb. After the adsorption, the membrane became translucent. The excess of the *PEG* was removed from the surface of *PVDF* with filtration paper. The drop of pristine *PEDOT:PSS* was added and the contact angle was measured as for *WCA*.

A.3.2 Penetrating drop method

Critical surface tension was measured by penetrating drop method as verified by [111]. Water-ethanol azeotropic solutions with various ethanol ratios and consequently having surface tension varying from 72.10 mN/m to 22.00 mN/m [181] were used. A droplet of 4 μL was put on the pristine *PVDF* membrane and let to drain. The behaviour of

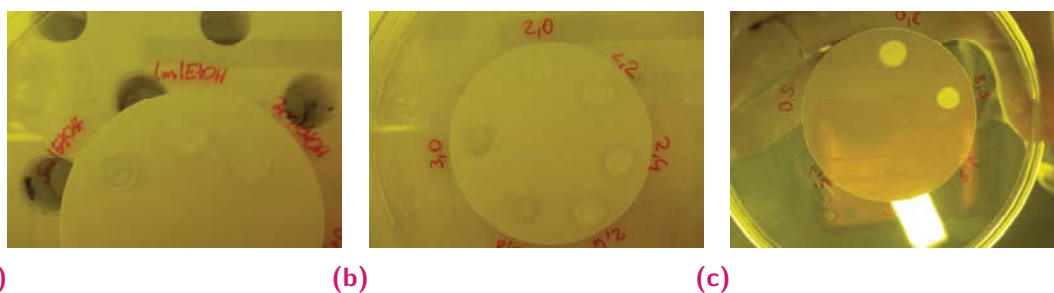


Fig. A.1. Pictures of drops of ethanol-water mixtures with different ratios (indicated next to the drop in red) on pristine PVDF membrane. (a) 1 – 3 vol%, (b) 2 – 3 vol%, (c) same as (b) but picture taken from below.

the droplet was observed in order to determine the minimum surface tension, at which the droplet did not spread nor penetrated in the membrane. Results of the experiment are shown in Fig. A.1.

A.4 Chapter 4: PEDOT:PSS/mPVDF/ionic liquid actuators

A.4.1 Fabrication of actuators

For the fabrication of actuators with different mixing depths, functionalized membranes were fabricated by spraying 2, 1.0 and 0.5 ml of PEGMA resulting in GD of approximately 0.15, 0.10 ng/mm^2 and 0.03 ng/mm^2 (GD of membranes used for fabrication of actuators are provided in labels of the figures). After drying they were fixed in a $\varnothing 45$ mm aluminium clamp and 3 ml of PEDOT:PSS, secondary doped with 1 vol% of PEG400, were drop-casted (if different, composition of PEDOT : PSS is provided in the text). Membranes were then dried in air in UV-reduced environment for at least 20 hours. The other side of the membrane was processed in the same way. Then membranes were thermally annealed in oven for 2 hours at 70 °C. 2 mm x 1.5 cm strips were cut by CO₂ laser (45 W power, 100 cm/s speed, 1000 Hz, Trotec FineMarker Hybrid). Each actuator was then weighted and its thickness measured. They were kept in *emimTFSI* for 1.5 hour before lifetime measurement experiments or 24 hours for strain characterisation. After soaking their weight and thickness were measured again.

A.4.2 Characterization of actuators

The **thickness** of dry and soaked actuators was measured by digimatic indicator (Mitutoyo Absolute) and also estimated from the scanning electron microscopy (SEM) pictures. SEM images of membranes and actuators were obtained using a Hitachi S – 4800 field emission scanning electron microscope (acceleration voltage 800 V, working distance of about 5 mm).

Resistance and conductivity of PEDOT:PSS was measured between two extremities of each electrode and between two electrodes, by applying 0.1 – 0.5 V voltage (with 0.01 V

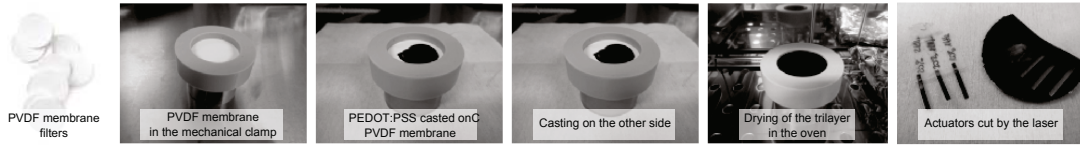


Fig. A.2. Pictures of the main fabrication steps of PEDOT:PSS/mPVDF/PEDOT:PSS actuators. Functionalized as in Section A.2 PVDF membranes were used. Membrane was then fixed in a metal mechanical clamp and 3 ml of PEDOT:PSS solution was drop casted on one side. After drying in air for about 24 hours, PEDOT:PSS was deposited and dried on the opposite side of the membrane. Then membrane with PEDOT:PSS on both sides was dried in oven at 70°C for 2 hours, occasionally reversing the clamp. After drying rectangular shaped actuators were cut with CO₂ laser. Actuators were immersed in ionic liquid before characterization (not shown).

increment) and measuring current, using Suss PA200 probe station and Agilent 4142B tester. Conductivity was then calculated assuming dimensions of 2 mm x 1.5 cm and the thickness measured by SEM not taking into account the PEDOT:PSS in the membrane as in Equation A.5.1.

For all **bending characterization** measurements, actuators were placed between two copper electrodes clamped at 1 – 2 mm from one end of the actuator. For bending measurements actuators were placed under Leica MZ-12 microscope (Leica Microsystems) with Digital Sight camera system (Nikon) as shown in Fig. A.3a. The square voltage wave with various amplitudes and frequencies was generated with Keithley 2450 sourcemeter. Bending was recorded at 100 frames per second, 640x480 resolution. After recording it was converted from raw to 5 frames per second 'mpeg4' encoded video in order to reduce its size. Videos there processed using Matlab Image processing toolbox to track the displacement of actuators tip. The strain was then calculated from tip displacement using formulas proposed by Sugino *et al* [356]:

$$\epsilon = \frac{2hd}{L^2 + d^2} \times 100\% \quad (\text{A.4})$$

where ϵ is strain in %, h , L and d are thickness, free length and displacement of the actuator respectively. Thickness of dry actuator, estimated by SEM, was used for calculations.

Cyclic voltammetry (CV) measurements were performed using Autolab potentiostat PGSTAT30 (Metrohm Autolab) coupled with NOVA 1.8 Software at room temperature (23 ± 1°C). Two electrode configuration was adopted (equivalent to the one used for bending characterization), in which two surfaces of PEDOT:PSS were working and reference electrodes. cyclic voltammetry (CV) measurements were performed at various voltages and scan rates as indicated in the labels of the figures.

Actuator bending for **lifetime measurements** was recorded by laser displacement sensor (optoNCDT 1302, MicroEpsilon) at the position of about 2 mm from the end of the actuator. All measurements were performed in the room temperature and humidity that were slightly varying. Actuation voltage was generated by Keithley 6221 waveform generator. For results shown in Fig. 4.11 the signal used for actuation is indicated in the label. For results discussed at Section 4.4.1 actuation with 1.5 V sine wave with 0.1 Hz frequency was performed.

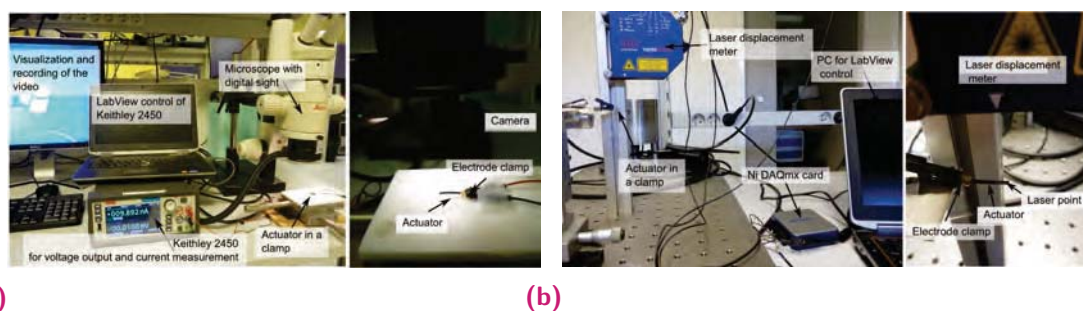


Fig. A.3. Picture of the experimental set-up used for bending characterization (a) by recording the bending and tracking the position of the tip and (b) by tracking bending using laser displacement meter.

For bending characterization shown in **Fig. 4.20**, laser displacement sensor (optoNCDT 1700, MicroEpsilon) was used connected to Ni-DAQmx card as shown in **Fig. A.3b**. Ni-DAQmx was also used for signal generation and current measurements. Displacement measured by laser was used as a feed-back in order to switch actuators position to 1 mm above or below the initial by changing polarity of applied voltage ($\pm 1.5 V$). The time needed to reach the set position was calculated for each cycle.

A.4.3 Post-treatment of actuators

For post-treatment of actuators with *CNTs* or *SDS*, functionalized *PVDF* membranes with grafting density (*GD*) of 0.14 ± 0.02 were used. *PEDOT:PSS* doped with 1 vol% of *PEG400* was drop-casted on both sides of the membrane as previously described. Trilayers were then cut in half and weighted. One half was used for further treatment and another used as a reference. The trilayer was attached on the glass slide, next to the silver electrodes as shown in **Fig. A.4a**. Silver electrodes were connected to the ohmmeter and the resistance between the electrodes was monitored during spraying. *CNTs* and *SDS* were sprayed using similar set-up as described in **Section A.2.1** (**Fig. A.4b**) with following parameters: nozzle of 0.2 mm and associate needle, pressure - 1.5 kgf/m², valve opening - 1.5 turn, distance - about 30 cm. Laser pointer was used for targeting and in order to ensure homogeneous spraying. *CNTs* were sprayed until the resistance between silver electrodes decreased to about 5 k Ω (for experiments in **Fig. 4.19**) or to 10 k Ω (for experiments in **Fig. 4.20**) corresponding to approximately 8 ml and 6 ml of *CNTs* solution respectively. After spray on one side, the membrane was dried under the fume hood at room temperature for 1 – 2 hours to make sure the surface of the trilayer is dry. The other side of the trilayer was treated in the same way. Actuators were cut and annealed as previously described in **Section A.4.1**.

For post-treatment with surfactant, *SDS* solution in water was sprayed. 6 ml of *SDS* were sprayed and actuators were fabricated in same conditions as *CNTs*.

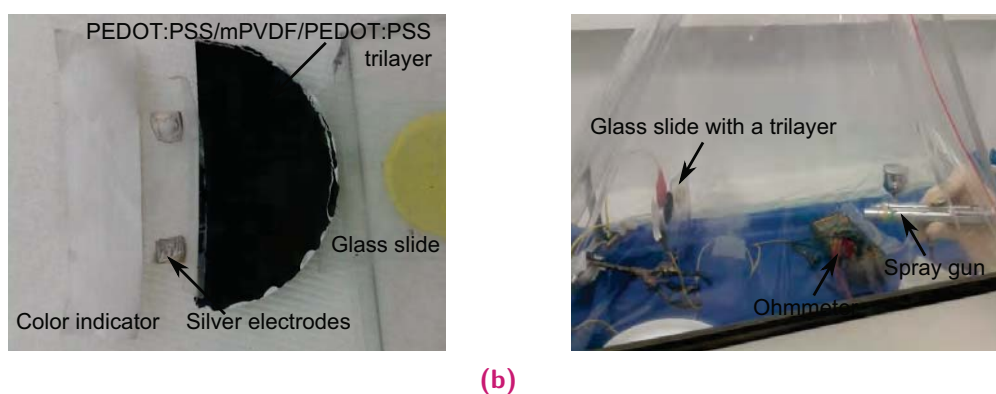


Fig. A.4. (a) Picture of *PEDOT:PSS/mPVDF/PEDOT:PSS* trilayer attached on the glass slides next to silver electrodes. (b) Picture of the set-up used for spraying carbon nanotubes.

A.5 Chapter 5: Towards inkjet printed artificial muscles

A.5.1 Ink preparation, printing and characterization

Inks were prepared by mixing *PEDOT:PSS* in a quantities provided in the text and mixing on mechanical shaker at 300 *rpm* for at least 3 hours. Before printing solutions were filtered with 5 μm polytetrafluoroethylene *PTFE* syringe filter. If needed prepared inks were stored in the fridge at 4°C.

Surface tension of the ink was measured by pendant drop test using Digidrop GBX Contact Angle Meter. **Viscosity** was measured using Anton Paar AMVn rolling ball viscometer. **Contact angle** was also measured using Digidrop GBX Contact Angle Meter.

The **ink-jet printing** was carried out using a Altadrop inkjet system (Altatech) with MicroFab electronics and software. Droplet ejection was first optimised to eliminate any satellites or deviation. The fluid were jetted at 21 – 25°C in DoD mode from a single-nozzle piezoelectric print-head (MicroFab) with a nominal exit diameter of 30 μm (unless indicated differently). The print-head was driven by a uni or bi-polar waveforms (the waveform was optimised for each printing and ink-composition in order to obtain stable jetting) with a range of driving voltages (20 *V* to 75 *V*), which resulted in drop speeds of about 5 *m/s*. Images of jets were formed with a CCD camera, using an automated stroboscopic illumination and data capture system.

For measuring **conductivity** of printed *PEDOT:PSS* with different additives, gold electrodes (300 *nm*) were deposited by sputtering on pristine and functionalized ($GD - 0.15 \text{ ng/mm}^2$) *PVDF* membranes using shadow masks. Then *PEDOT:PSS* wide lines were printed with both ends being on the electrodes. Then membrane was cut with scissors so that only one rectangular is per piece. Resistance between two probes was then measured using Suss *PA200* probe station and Agilent 4142*B* tester by applying 0 – 1 *V* voltage between two electrodes and measuring current. It was initially tested that measured resistance does not depend on the placement of the probes as long as

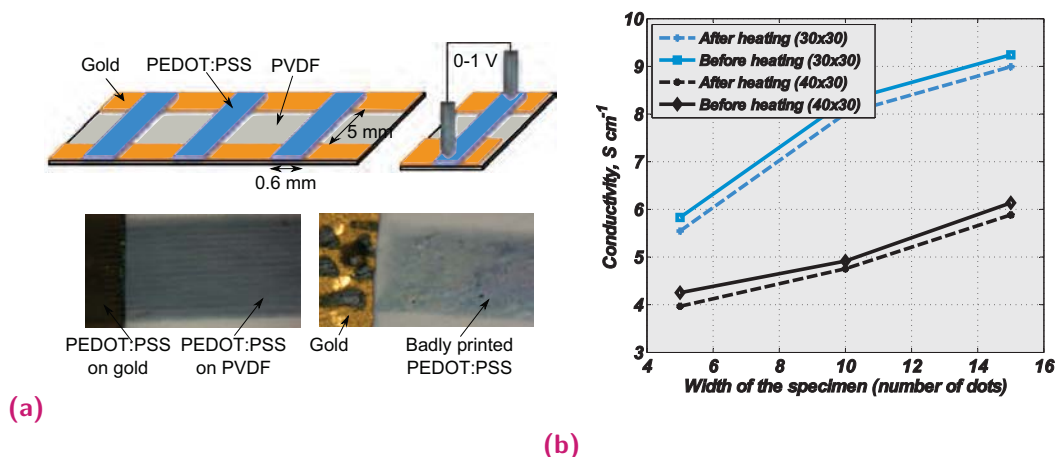


Fig. A.5. (a) Illustration of the setup used for the electrical conductivity measurements of inkjet printed lines and example of well and badly printed rectangulars. (b) Influence of the width of the line on calculated conductivity of printed *PEDOT:PSS* as well as the influence of printing resolution (indicated in legend).

they are placed on the area of the electrode (placing it on *PEDOT:PSS* or on gold does not change measured value). The conductivity was then calculated using:

$$\sigma = \frac{L}{R * W * h} \quad (\text{A.5})$$

where R is measured resistance, L , W and h are length (5 mm), width (0.6 mm) and thickness (0.5 μm) of the printed rectangular. Measured resistance for different width of the rectangular (as numbers of dots) are shown in Fig. 5.7a. As can be seen, conductivity measurement value seems to be dependent on the width of the printed line (Fig. A.5b), making this type of measurement condition dependent. Therefore for comparison of different inks, 150 dots length and 15 dots width and printing was done at lower resolution (40x40) in order to keep the symmetry. Several samples of each ink composition were printed and only well defined films were used for measurements. At least 2 good samples were used for measurements.

A.5.2 Printing and characterization of actuators

The ink-jet printing was carried out as previously described with following parameters: 10 or 20 layers of 125 x 25 drops of 30 μm diameter with 40x40 μm resolution (leading to dimensions of 5 x 0.8 mm) ejected at 24°C. The print-head was driven by a bi-polar waveform (2 μs rise time, 10 μs dwell time, 5 μs fall time, 7 μs dwell time) with a driving voltages of 20 V and -22 V and frequency of 2000 Hz. *PEDOT:PSS* doped with 5 vol% ethylene glycol was used as ink. *PEDOT:PSS* was dried per night in the oven at 80°C and printed on the other side of the membrane in the same conditions. Printed actuators was again dried at at 80°C. Printed actuators were kept in clean-room conditions for 3 months. Rectangulars of 15 x 2 mm were cut from the membrane using scalpel and keeping the actuator at one side of the rectangular as shown in Fig. 5.8a. Actuators were then immersed in ionic liquid for 3 hours. The displacement

of the actuator was measured from videos obtained during the actuation as previously explained in *Section A.4.2*.

Actuators on a dragon-fly shaped membrane were printed using *PEDOT:PSS* secondary doped with 1 *vol%* of *PEG400* and 1 *vol%* *Triton-X100*. 10 layers of 500x25 or 250x25 drops of 50 μm diameter with 40 x 40 μm resolution were printed at 25°C. The print-head was driven by a uni-polar waveform (2 μs rise time, 25 μs dwell time, 2 μs fall time, 3 μs dwell time) with a driving voltages of 30 *V* and 3000 *Hz* frequency. Printing 3 actuators on both sides of the membrane took 10 days, various parts were printed per day and the membrane was kept in the printer per night. After printing, membrane was kept in oven at 70°C for 2 hours. For electrical connections to the actuators, silver paste *EPO-TEK®H20E* (Epoxy Technology) was used and actuators were again annealed at 80°C for 3 hours for each side to cure it. Before actuation, membrane was immersed in ionic liquid until became translucent. For comparison, dragon-fly shape was cut from the trilayer fabricated as in *Section A.4.1*.

Appendix 2: additional figures

B

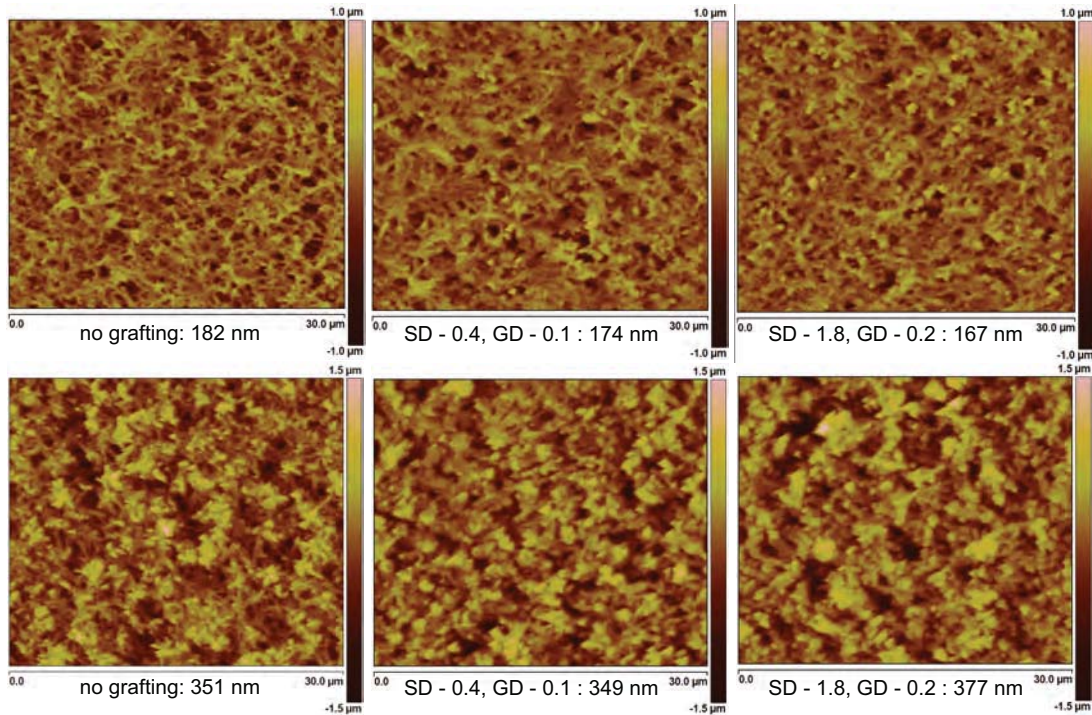


Fig. B.1. AFM surface scans of membranes functionalized with different amount of PEGMA. Measured surface roughness and the spray and graft densities are indicated below.

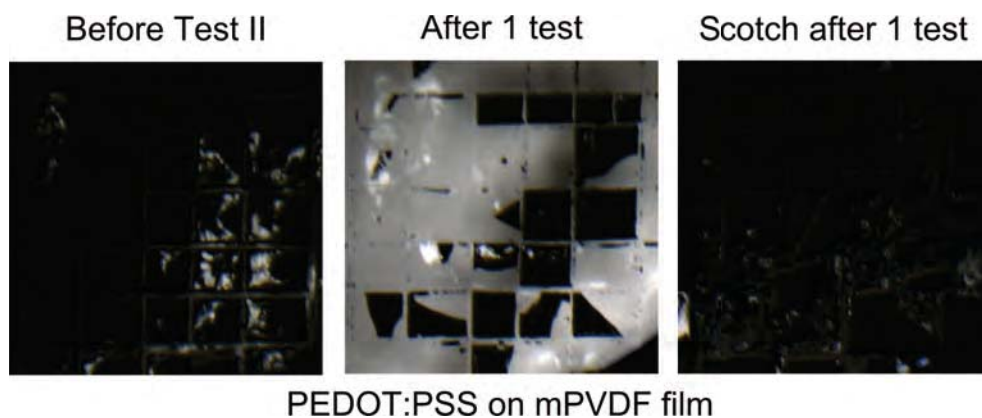


Fig. B.2. Adhesion test of *PEDOT:PSS* (with 1 vol% *PEG400*) and flat *PVDF* films after incubation in ionic liquid for 48 hours. Picture of the film before the test (*left*), after 1 Scotch™ test (*center*) and the Scotch™ after 1 test (*right*) are shown.

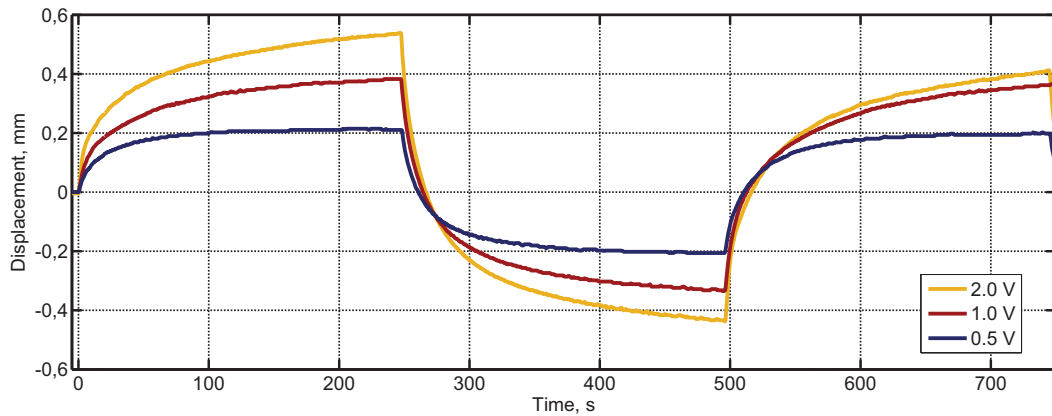


Fig. B.3. Trilayer actuator bending profiles during actuation with low frequency (2 mHz) voltage square wave. The voltage used is indicated in the legend.

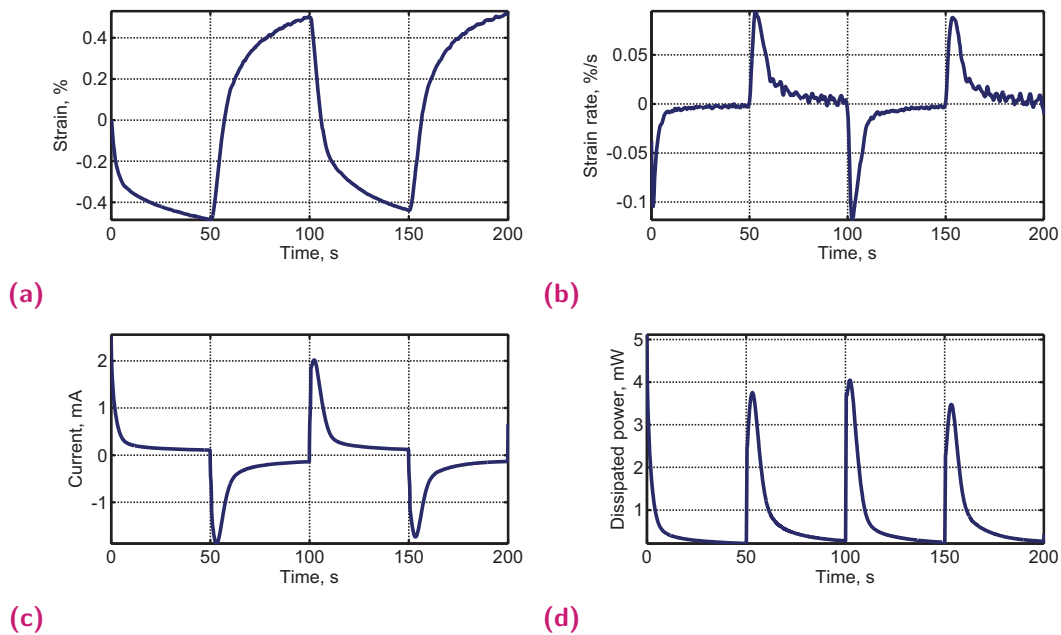


Fig. B.4. (a) Strain, (b) strain rate, (c) transferred current and (d) dissipated power profiles in time of a trilayer actuator, actuated with 2 V square voltage wave at 10 mHz .

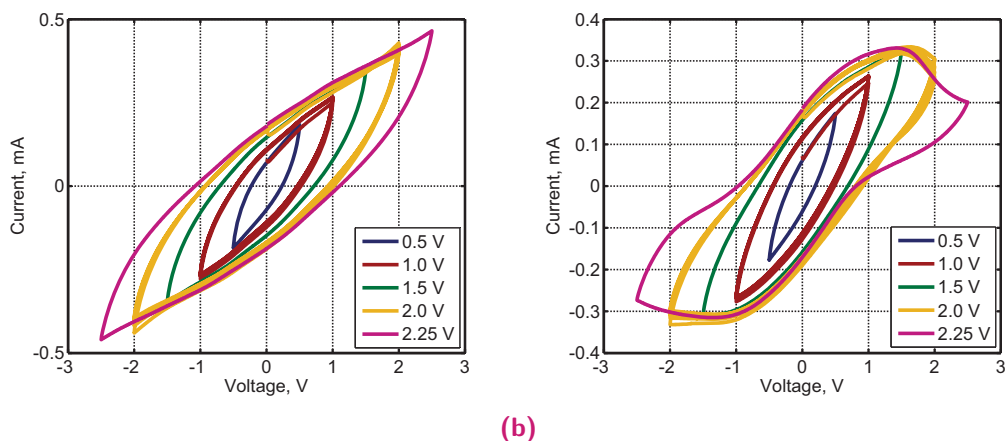


Fig. B.5. Cyclic voltammograms of the trilayer PEDOT:PSS/mPVDF/PEDOT:PSS actuators obtained with 100 mV/s scan rates and different voltages indicated in the legend. The actuators were kept in the ionic liquid for (a) 3 minutes or (b) 24 hours.

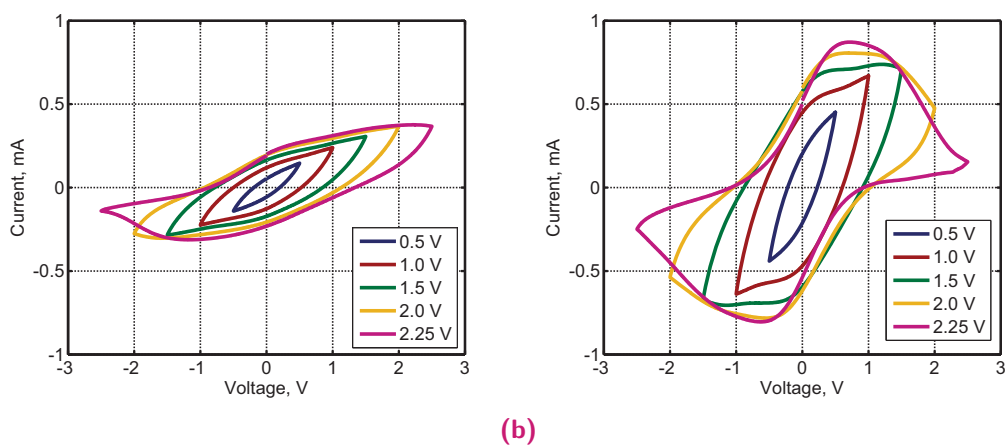


Fig. B.6. Cyclic voltammograms of the trilayer PEDOT:PSS/mPVDF/PEDOT:PSS actuators obtained with 100 mV/s scan rates and different voltages indicated in the legend. PEDOT:PSS was secondary doped with (a) 1 vol% or (b) 2 vol% of PEG400.

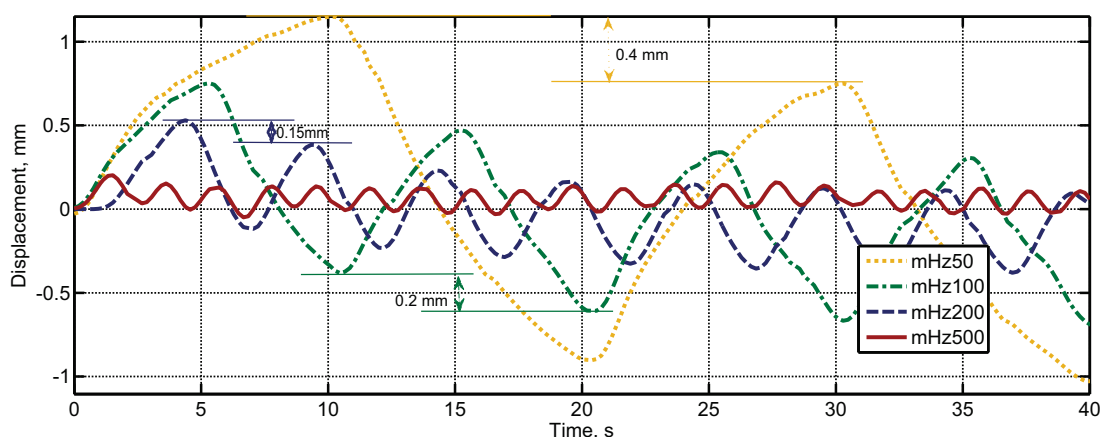


Fig. B.7. Bending profile of a trilayer actuator in time at different frequencies (indicated in the legend). Square voltage wave of 2 V was used for actuation. The level of the irreversible expansion causing creep is indicated with arrows.

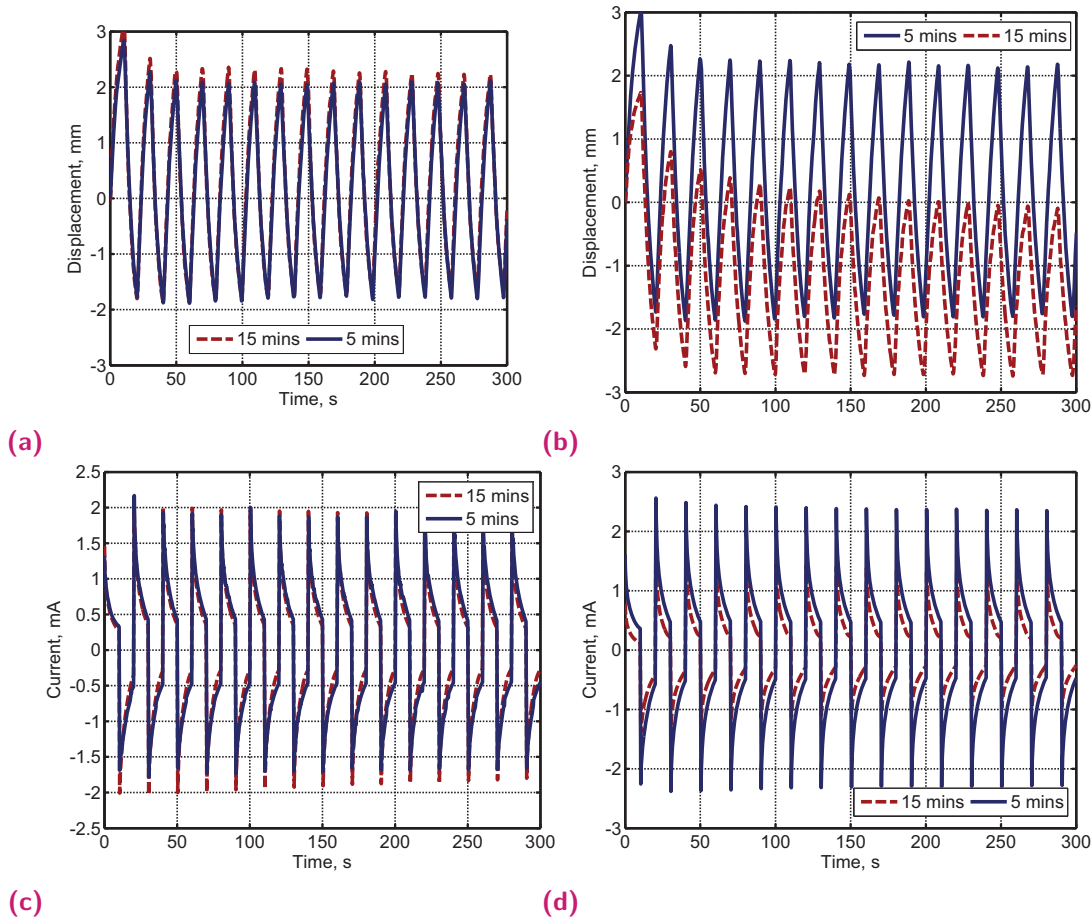


Fig. B.8. Displacement ((a)-(b)) and transferred current ((c)-(d)) profiles of the same actuator after 5 (blue) and 15 (red) minutes in the ionic liquid. (a,c) Both PEDOT:PSS layers are fine, (b,d) one of the PEDOT:PSS electrodes damaged during handling making the electrode very asymmetrical for the second measurement. 2 V square voltage wave was used for actuation at 50 mHz

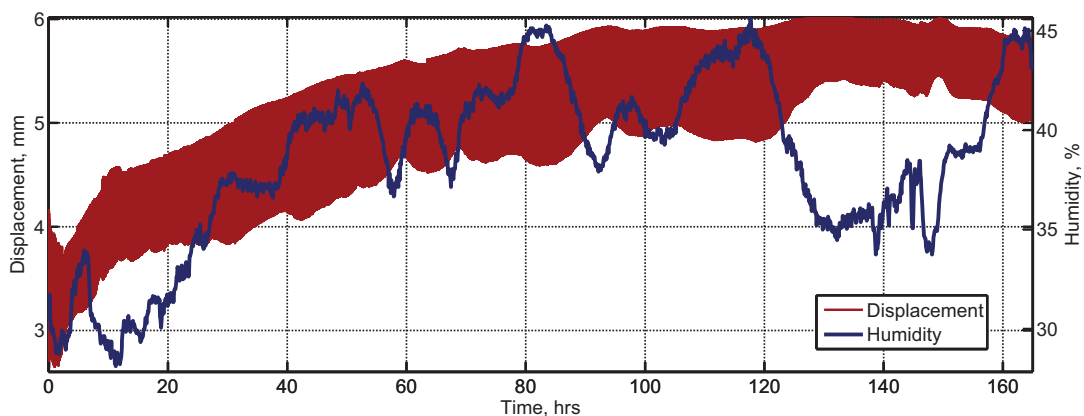


Fig. B.9. Displacement profile of the actuator during long time actuation. The ambient humidity is plotted as blue line. Square voltage wave of 1.5 V and 100 mHz frequency was used for actuation and the position was tracked with laser displacement sensor.

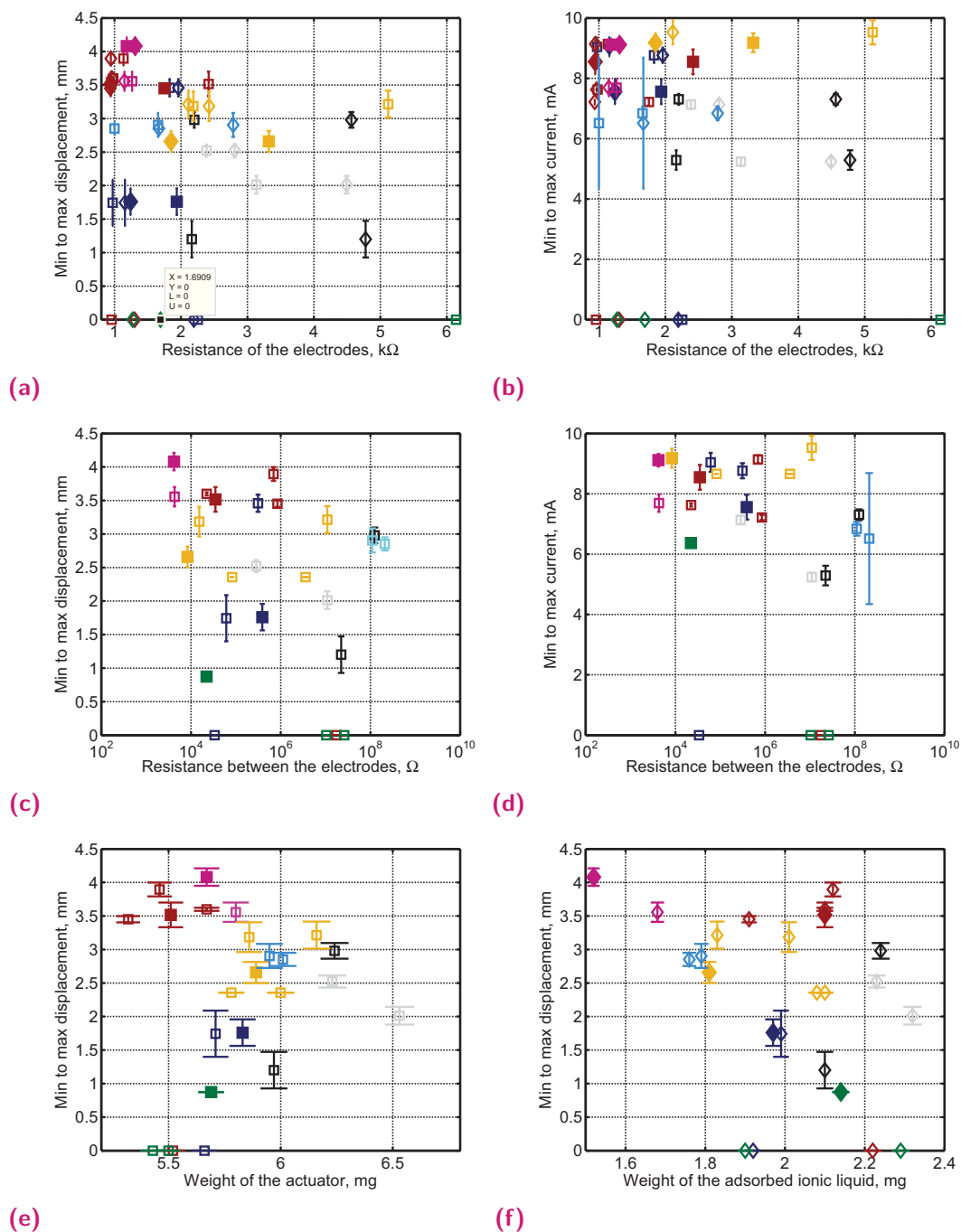
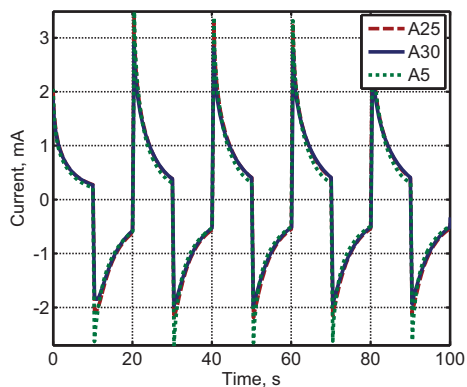
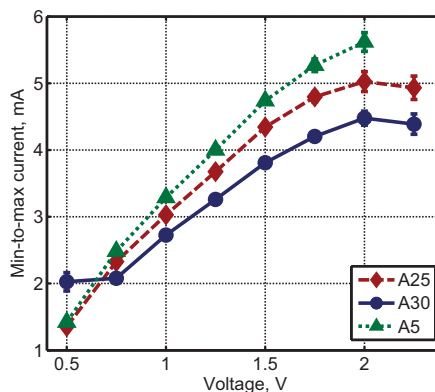


Fig. B.10. In order to identify factors affecting performance of the actuators, 4 PVDF membranes were functionalized in the equivalent way. Half of each membrane was then secondarily treated in order to create variety of resistances along the electrode and in between the electrodes as explained in *Section A.4.3* (different amount of *CNT*, *Ag* nanowires, *SDS* were deposited by spray-coating on the surface). Peak-to-peak displacement ((a), (c)-(f)) and transferred current ((b), (d)) is plotted versus measured resistance along the electrode ((a)-(b)) and between the electrodes ((c)-(d)), weight of the actuator ((e)) and the amount of the adsorbed ionic liquid ((f)). Different batches are indicated in different colours. Filled markers represent the coloured displacement profiles and images of the actuators in the Fig. 4.14.

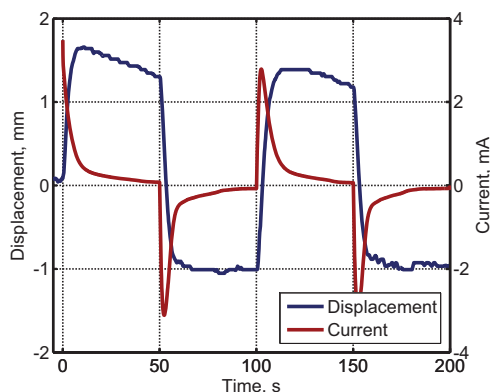


(a)

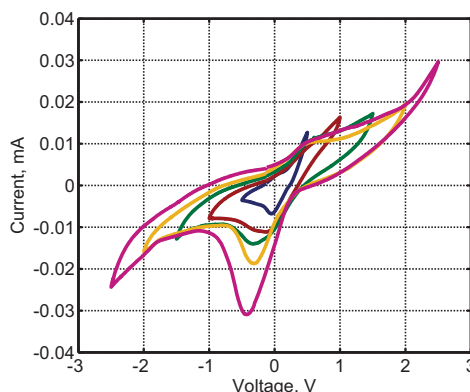


(b)

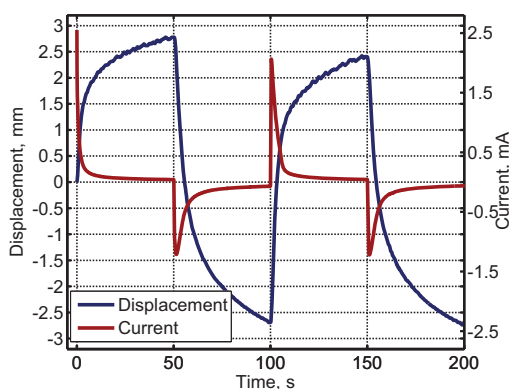
Fig. B.11. (a) Transferred current profiles of the actuators with different mixing depth during actuation with 2 V square wave at 50 mHz frequency and (b) peak-to-peak transferred current of the same actuators at different voltages.



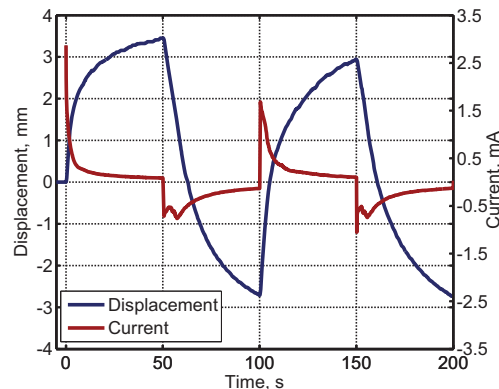
(a)



(b)



(c)



(d)

Fig. B.12. Displacement (blue) and transferred current (red) profiles of the (a) trilayer actuator made with PEDOT:PSS doped with 5 vol% PEG400 electrodes (infiltrated through and percolated), (c) A5 actuator and (d) trilayer actuator made on completely hydrophilized PVDF membrane (also infiltrated though and percolated). 2 V square wave at 10 mHz was used for actuation. (b) CV voltammograms of the actuator with the percolated electrodes (with 5 vol% PEG400) obtained during scans at 100 mV/s until different voltages.

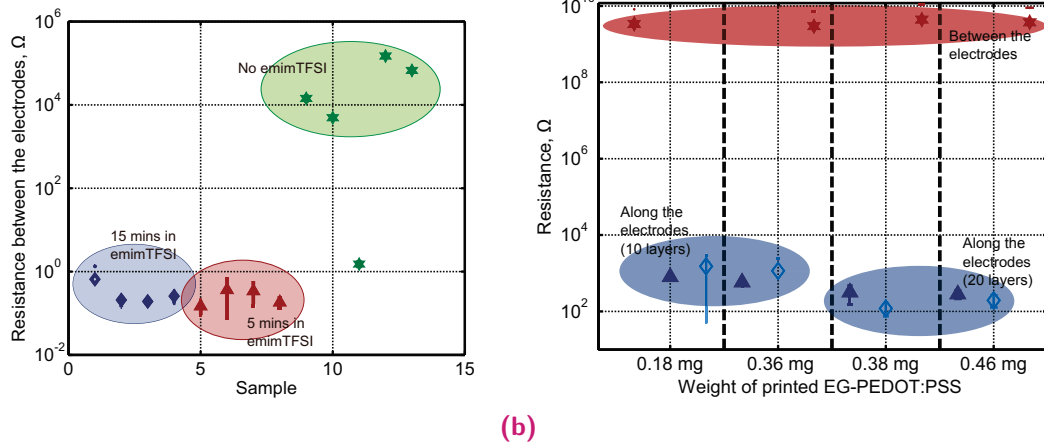


Fig. B.13. (a) Resistance between the electrodes before (green) and after incubation in ionic liquid for 5 (red) or 15 minutes of actuators fabricated by drop casting. (b) Electrical resistance measurements of printed *PEDOT:PSS* actuators. Resistance along the electrodes is shown in blue (different shades of blue indicate the conductivities measured on different sides), resistance in between the electrodes is shown in red.

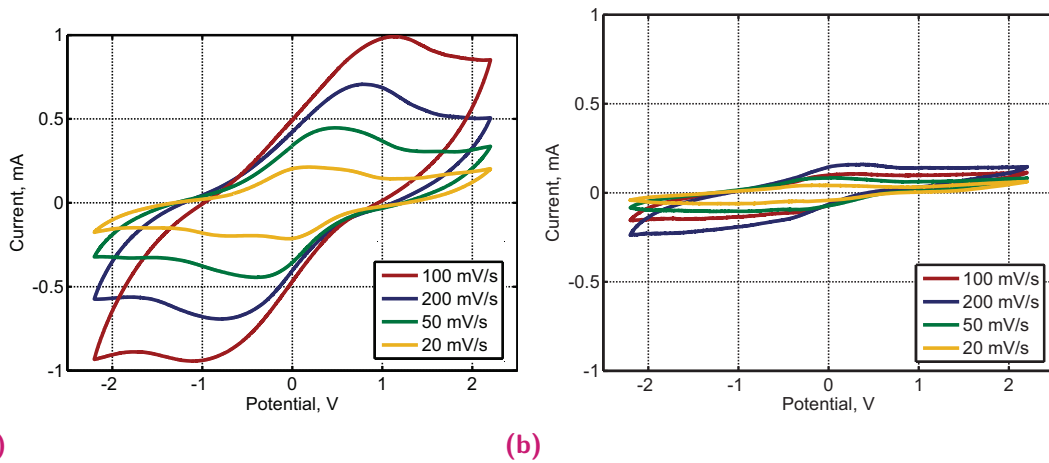


Fig. B.14. Cyclic voltammograms of actuators with (a) and (b) without post treatment with *CNT*. Scans were obtained at different scan rates indicated in the legend.

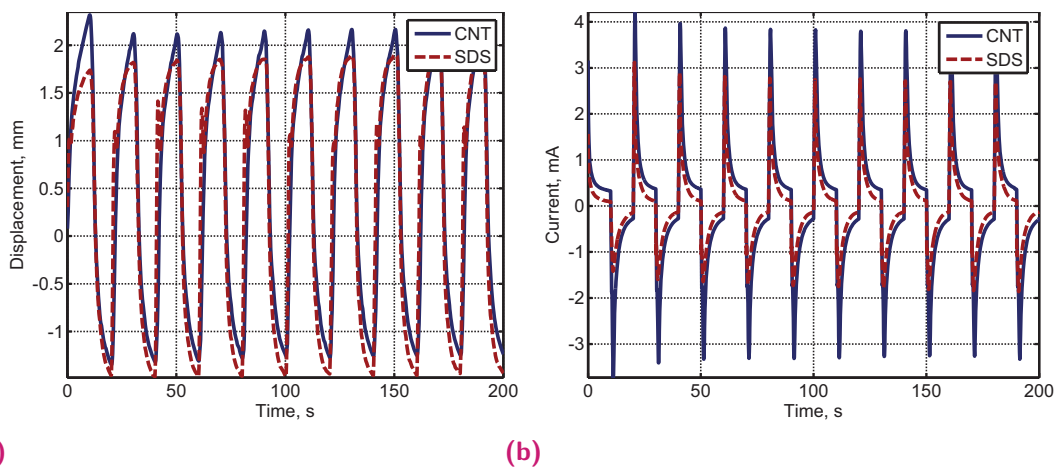
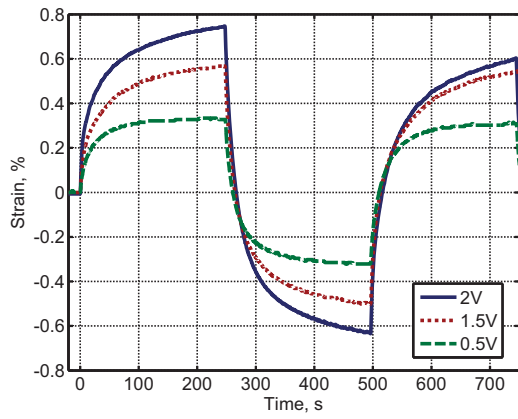
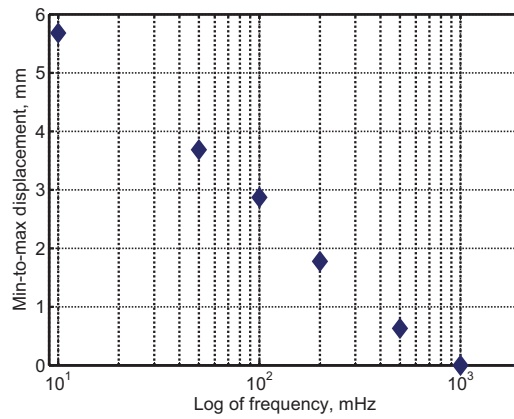


Fig. B.15. Displacement (a) and transferred current (b) profile of the actuators treated with *CNT* (blue) and with *SDS* (red). 1.5 V square voltage wave was used for actuation at 50 mHz.

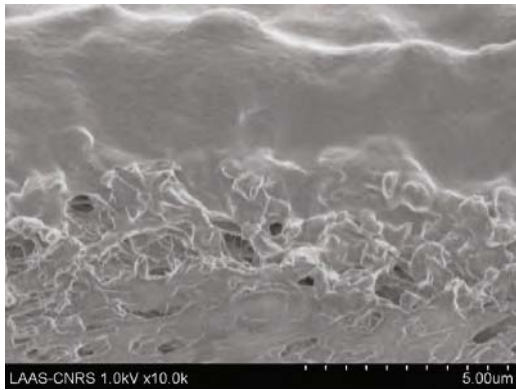


(a)

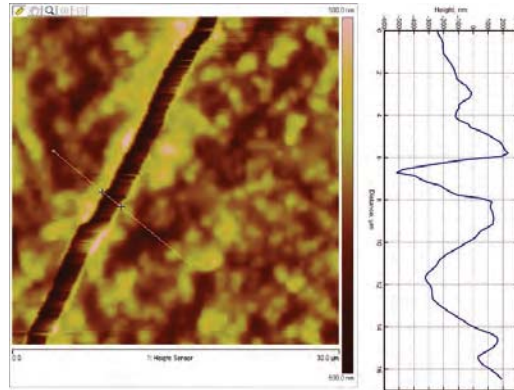


(b)

Fig. B.16. (a) Strain profile at different voltages and (b) frequency response of probably the best trilayer *PEDOT:PSS/mPVDF/PEDOT:PSS* actuator fabricated during our study.

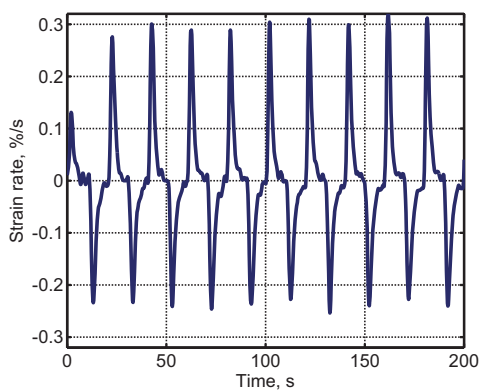


(a)

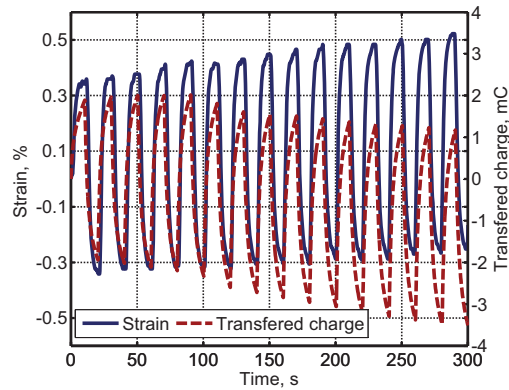


(b)

Fig. B.17. (a) SEM image of the *PEDOT:PSS* layer printed on the *PVDF* membrane (tilted) and (b) AFM image of the crack on the surface of printed *PEDOT:PSS* and the height profile.



(a)



(b)

Fig. B.18. (a) Strain rate profile of printed actuator (10 layers on each side resulting in 3.35 mg of printed *PEDOT:PSS*. Actuated with 1.5 V, 50 mHz square voltage wave.). (b) Strain and transferred charge profiles of the same actuator.

Contents

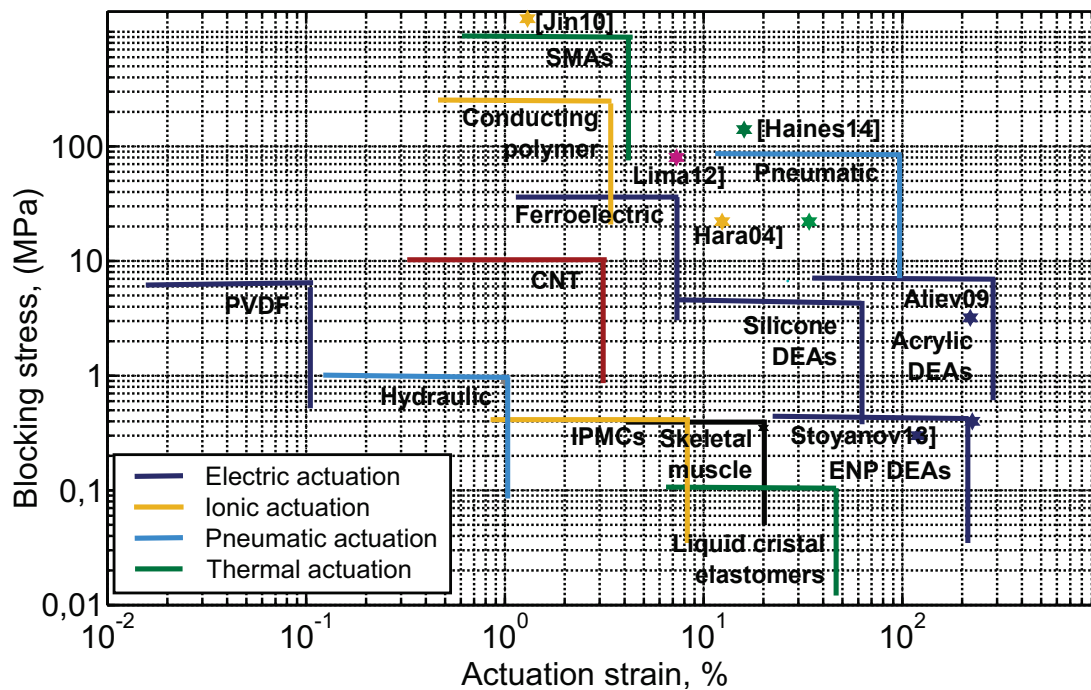
C.1	Introduction	163
C.1.1	Muscles artificiels: état de l'art	163
C.1.2	Materials	167
C.1.3	Contexte et positionnement du problème	169
C.2	Membranes hybrides PVDF/PVDF-PEGMA	171
C.2.1	Contrôle de la profondeur de pénétration	173
C.3	PEDOT :PSS et membrane en PVDF : adhésion versus infiltration . .	175
C.3.1	Conclusion	179
C.4	Actionneurs ioniques PEDOT :PSS /mPVDF	179
C.4.1	Durée de vie	182
C.4.2	Vers des muscles artificiels fabriqués par technologie jet d'encre	183

C.1 Introduction

L'étude de robots en interaction directe avec l'homme suscite un intérêt croissant depuis plusieurs années. Un des grands défis actuellement est de leur conférer une compliance proche de celle de muscles naturels. Pour la nouvelle génération de robots, des stratégies adaptées de contrôle devront être combinées avec des matériaux, des actionneurs, des capteurs et des sources d'énergies toujours plus légers. Par exemple, jusqu'à aujourd'hui, les faibles densités d'énergie générées, les rapports masse/puissance défavorables ou encore les efficacités d'actionnement médiocres ont fortement limité le développement de micro-robots dynamiques. En outre, leur coût, leur encombrement et l'absence de contrôle intégré par rétroaction sur la force ou sur la position constituent également d'autres aspects limitant leur développement pour des applications dans le domaine médical.

C.1.1 Muscles artificiels: état de l'art

L'expression «Muscle artificiel» est un terme générique utilisé pour les matériaux ou les dispositifs pouvant générer de manière réversible une contraction, une dilatation ou encore une rotation d'un corps grâce à un stimulus externe (tension, courant, température, etc.) [270]. Même si leur développement est encore limité actuellement, les polymères électroactifs (ElectroActive Polymers EAPs en anglais) pourraient à terme remplacer les actionneurs actuels dans un contexte où une réponse comparable à un muscle naturel est désirable. De plus, les EAPs offrent une flexibilité de fabrication



(a)

Fig. C.1. Contrainte en fonction de la déformation pour différents types de muscles artificiels et d'actionneurs. Types d'actionnement : bleu-électrique, orange-ionique, vert-thermique, rouge-nanotubes de carbone, gris-autres, noir-muscles naturels de mammifères. Adapté de [249, 269] et d'autres références citées dans le texte.

et peuvent potentiellement être utilisés dans des dispositifs médicaux (chirurgie peu invasive et outils de diagnostic) [131, 324, 381], prothèses (mains et bras), robotique (préhenseurs, manipulateurs) [60, 149, 377], jouets, etc.

Une classification des différents types de muscles artificiels peut être envisagée en considérant la nature du stimulus : pneumatique, thermique, électrique et ionique. La comparaison en termes de déformation (c'est-à-dire le déplacement normalisé par rapport à la longueur initiale de l'actionneur [249]) et la contrainte (c'est-à-dire la force par unité de surface, homogène à une pression [249]) des différents types de muscles artificiels est présentée sur la Fig. C.1.

En ce qui concerne les **actionneurs pneumatiques**, un mouvement de contraction est généré par gonflement et dégonflement d'un élastomère. Ces actionneurs sont légers, d'une grande compliance et sont très utilisés [74, 81, 149, 417]. Cependant, leur fonctionnement repose sur l'utilisation d'un équipement produisant une pression fluïdique qui est souvent sujette à des ruptures, des fuites avec des temps de réponse importants. De plus, la force générée est déterminée à la fois par la pression et l'état de gonflement ce qui rend ces actionneurs non linéaires et difficiles à contrôler. Cela limite leurs domaines d'applications notamment ceux pour lesquels un mouvement précis et délicat est nécessaire.

Les **muscles artificiels thermiques** à base d'alliages à mémoire de forme subissent un changement de forme avec la température. Ces matériaux bas coût sont capables de

produire d'importantes déformations jusqu'à 700% [200]. De plus, ils sont simples à produire et peuvent être élaborés de manière à répondre à des applications spécifiques [28, 360]. La dilatation thermique peut être également utilisée pour l'actionnement. Des métaux [270], des nanotubes de carbone [233], des fibres en nylon ou en polyester [134] peuvent être enroulés sous forme de tresses pour augmenter l'effet de dilatation et être ainsi utilisés comme muscles artificiels en torsion. Ces actionneurs sont capables de produire des contractions de l'ordre de 49% en produisant un travail mécanique de l'ordre de $5,3 \text{ kW/kg}$ et peuvent supporter des millions de cycles thermiques [134, 233]. Néanmoins, des études sont encore nécessaires pour améliorer leur efficacité de conversion énergétique électrothermique qui reste de l'ordre de 1 à 2%.

Les polymères peuvent voir leur forme modifiée sous l'effet d'un champ électrique comme c'est le cas pour les polymères ferroélectriques. Leurs principaux avantages ont trait à la faible dissipation de chaleur et leur temps de réponse très court [249, 269]. Cependant, leur actionnement nécessite l'application de champs électriques très importants (environ 150 MV/m). Ils sont par ailleurs sensibles aux défauts et difficiles à produire en masse. Les actionneurs électriques les plus étudiés sont les élastomères diélectriques. Ils se présentent sous la forme d'un film élastomère et de deux électrodes souples positionnées de part et d'autre du film. Quand une tension est appliquée, la pression électrostatique entre les deux électrodes due aux forces de Coulomb comprime le film élastomère dans son épaisseur et conduit à une dilatation de sa surface. Typiquement, les élastomères diélectriques produisent de grandes déformations et pressions. Ils sont aussi connus pour générer de fortes densités d'énergie ($> 0,75 \text{ J/g}$) avec une grande efficacité de conversion (90%) [37, 34]. De plus, la fabrication de ces élastomères est peu coûteuse ; ils sont légers et très souples. Les tensions nécessaires pour l'actionnement (jusqu'à 5 kV) les rendent cependant difficilement utilisables pour des applications dans le domaine biomédical ou lorsque des interactions avec le corps humain sont nécessaires [249, 269].

Dans ce cas, il est essentiel d'avoir des dispositifs fonctionnant à basse tension. Les actionnements à base d'ions reposent sur le transport de ces derniers à l'intérieur d'un polymère sous l'effet d'un champ électrique et leur distribution non uniforme conduit à un changement de volume ou de forme. De cette façon, une contrainte mécanique ou une déformation de quelques pourcents peut être obtenue en appliquant une tension de quelques volts. Plusieurs types de **polymères électroactifs ioniques** ont été étudiés pour fabriquer des muscles artificiels : gels ioniques [252], composites polymère ionique-métal [162, 374], actionneurs à base de polymères conducteurs [24] et plus récemment des composites à base de nanomatériaux carbonés [23, 204].

Les gels ioniques sont des arrangements polymériques en trois dimensions qui peuvent subir un changement de volume en réponse à un stimulus environnemental. Il s'agit d'un processus contrôlé par la diffusion ce qui limite le temps de réponse des gels ioniques à quelques secondes [22, 151]. Les composites polymère ionique-métal (Ionic Polymer Metal Composite, IPMC en anglais) sont constitués d'une membrane en polymère synthétique imprégnée d'un électrolyte et placée entre deux électrodes métalliques. Quand un champ électrique est appliqué, les cations dans le solvant se déplacent vers une des électrodes et les anions vers l'électrode opposée causant ainsi un

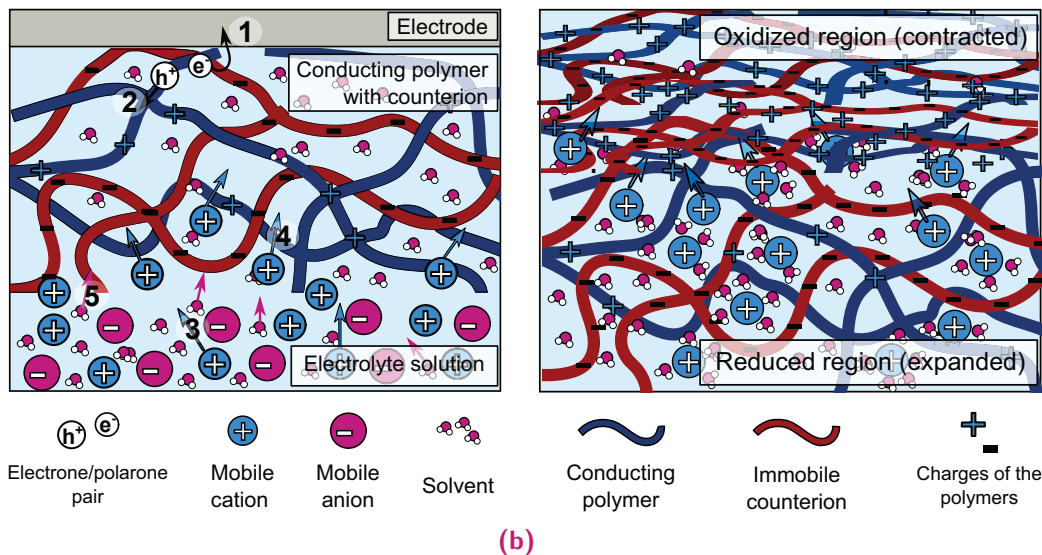


Fig. C.2. (a) Illustrations schématique du processus qui entre en jeu lors de la dilatation volumique ① les électrons sont supprimés de la chaîne polymère ② les polarons créés se propagent le long des chaînes polymères et engendrent un changement de conformation du polymère ③-④ les cations se déplacent vers l'électrolyte à travers l'interface et entre les chaînes polymères et ainsi ouvrent des canaux au sein du polymère ⑤ si elles sont présentes, les molécules du solvant peuvent pénétrer le film polymère. (b) Structure du polymère dans son état oxydé et réduit. A cause de la charge nette induite par le changement de conformation du polymère et due à la présence des ions et du solvant, l'état réduit est plus ouvert. D'un autre côté, l'état oxydé est plus compact et contient moins de molécules d'eau et réduit fortement la mobilité des ions.

gonflement et une déformation en flexion [144, 240, 286, 287]. Même si les IPMC ont un fort potentiel applicatif dans le domaine de la robotique sous-marine (préhenseurs, dispositifs « nageurs ») [109, 53, 185, 300], en médecine (micropréhenseurs, cathéters) [103, 324], leur durée de vie est limitée par l'évaporation graduelle de l'électrolyte durant l'utilisation [196, 303], la faible adhésion des électrodes métalliques sur la membrane en polymère et l'endommagement de la surface des électrodes [303, 404].

Le remplacement des électrodes métalliques par des matériaux conducteurs plus souples et moins fragiles peut apporter des solutions aux limitations des IMPC. Utiliser des polymères conducteurs comme électrodes est une des alternatives notamment grâce à la charge induite par l'oxydation et la réduction du polymère qui est compensée par le mouvement des ions. Cela cause un changement de volume du polymère qui peut être considéré comme le facteur prépondérant conduisant à l'actionnement comme illustré en Fig. C.2.

Les principaux avantages des polymères conducteurs sont les faibles tensions requises pour l'actionnement et leur biocompatibilité ce qui en fait des candidats prometteurs pour des applications médicales en particulier pour les dispositifs implantables. De plus, en comparaison de leur masse, ils peuvent générer des forces relativement importantes et de faibles courants sont nécessaires pour maintenir une déformation constante sous tension continue [154, 345]. D'un autre côté, la fatigue mécanique, la rapide détérioration de leurs propriétés sous cyclage électrique et leur temps de réponse important ($< 40 \text{ Hz}$) nécessite des améliorations notables.

Les propriétés des polymères conducteurs peuvent être exploitées sous forme d'un film monolithique (immergé dans ce cas dans un électrolyte) ou sous forme d'actionneurs bicouches ou tricouches. Ces deux derniers types d'actionneurs sont en général privilégiés pour tirer avantage de leur déformation plus importante dans le plan. Dans notre travail, seuls les actionneurs tricouches ont été considérés. Dans cette configuration, l'électrode de travail est connectée à une face du film et la contre-électrode à la face opposée. Une différence de potentiel appliquée entre les deux faces du film conduit simultanément à une oxydation et une réduction de celles-ci. Durant la dilatation volumique du polymère, un gradient de contrainte est généré à l'interface ce qui conduit à la flexion de l'actionneur tricouche.

C.1.2 Materials

Pour obtenir un mouvement en flexion, un polymère conducteur électromécaniquement actif est laminé sur un substrat passif. Les performances de l'actionneur dépendent largement des propriétés mécaniques de la couche passive entre les deux électrodes ainsi que des propriétés mécaniques et électriques du polymère conducteur et de l'électrolyte.

Polymère conducteur

Pour guider le développement de la technologie des muscles artificiels à base de polymères conducteurs vers des approches automatisées de fabrication haut débit, des techniques de fabrication simples et bas coût en utilisant des matériaux commerciaux sont nécessaires. Le poly(3,4-ethylenedioxythiophene) polystyrene sulfonate (PEDOT:PSS) (Fig. C.3a) est le seul polymère conducteur disponible commercialement qui est très largement utilisé dans le domaine de l'électronique souple imprimée [21, 174, 221]. Le poly(3,4-ethylenedioxythiophene) (PEDOT) synthétisé chimiquement et dopé avec du polystyrene sulfonate (PSS) forme des nanoparticules qui sont solubles dans l'eau. Ces particules ont une structure cœur/coquille : une couche de PSS constitue la coquille isolante et les chaînes conductrices de PEDOT le cœur de la particule [215]. Cette structuration a pour conséquence une faible conductivité électrique des solutions de PEDOT:PSS [298]. De plus, la couche isolante PSS est fortement hydratée et une barrière de molécules d'eau est créée non seulement entre les particules de PEDOT :PSS mais également entre n'importe quelle surface et le PEDOT :PSS [238]. Ceci a deux conséquences : (1) les films obtenus à partir de ces suspensions sont fragiles et cassants à faible taux d'humidité à cause du manque d'interpénétration des polymères [215] ; (2) la couche d'hydratation constituée de molécules d'eau peut gêner l'adsorption spontanée du polymère sur une surface, des recuits thermiques peuvent être nécessaires pour faire évaporer la couche d'eau.

Mais le plus problème le plus important reste la faible conductivité électrique du PEDOT :PSS. Diverses formulations de solutions ainsi que des stratégies de pré- et post-traitements ont été suggérées [100, 195, 221, 232, 400, 403]. Les additifs les plus communs sont : (1) le DMSO qui facilite le transport de charges en alignant les chaînes de PEDOT et en épaisissant les particules de PEDOT :PSS [79, 400]; (2) le glycérol qui augmente la conductivité comme le DMSO [100, 401] et (3) divers surfactants

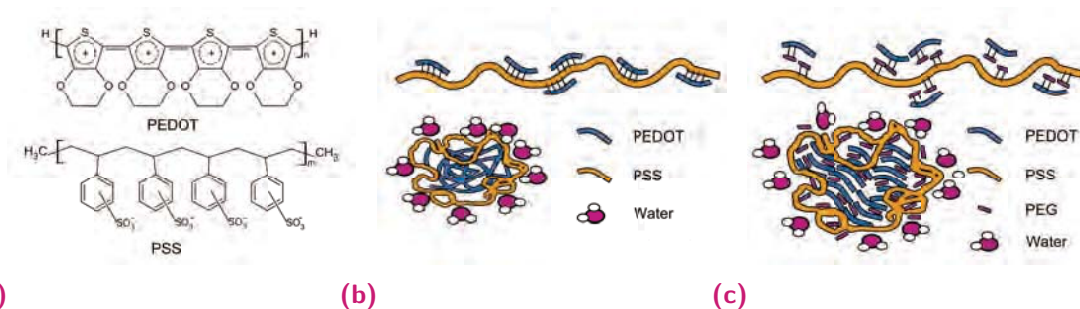


Fig. C.3. (a) Structure chimique du PEDOT :PSS et illustration schématique de la structure cœur/coquille dans une solution aqueuse (b) sans et (c) avec des additifs secondaires.

[140, 400]. Dans la plupart de nos expériences, nous avons utilisé le poly(éthylène glycol) (PEG) de masse molaire 400 comme dopant secondaire dans la solution de PEDOT :PSS. De faibles quantités de PEG400 (jusqu'à 2 % en volume) accroissent la conductivité de couches minces de PEDOT :PSS de 0,3 S/cm à 800 S/cm . Cet effet est attribué à la rupture de la structure cœur/coquille du PEDOT :PSS. Des dopants secondaires ayant un effet similaire sur la destruction de la structure cœur/coquille ont également pour effet de réduire le module élastique et d'accroître l'élongation des films de PEDOT :PSS à la rupture [47, 148, 228, 329]. Ainsi, 1% en volume de PEG400 accroît significativement non seulement la conductivité électrique mais conduit également à la formation de films continus sans détérioration même après un recuit thermique. La Fig. C.3c illustre la structure probable du PEDOT :PSS en présence du PEG comme dopant secondaire.

Membrane de stockage des ions

Une couche de bonne qualité isolante entre les deux électrodes constituées d'un polymère conducteur doit satisfaire plusieurs critères. Tout d'abord, elle doit être suffisamment flexible pour permettre d'obtenir des déformations de plusieurs pourcents. Ceci est possible en utilisant des couches ou membranes très fines. Les membranes sont plus avantageuses parce qu'elles permettent de stocker l'électrolyte et ainsi, les actionneurs peuvent être utilisés à l'air ambiant. Dans ce cas, un important volume libre est nécessaire ainsi qu'une grande stabilité chimique et une bonne conductivité ionique. Lorsque le polymère conducteur est synthétisé électrochimiquement, la membrane doit jouer également le rôle de couche conductrice initiale. Enfin, une bonne adhésion entre la couche isolante et le polymère conducteur est cruciale pour la durée de vie de l'actionneur.

L'isolant le plus utilisé pour les actionneurs à base de polymères conducteurs est probablement le polyvinylidène fluorure (PVDF). Il est utilisé comme membrane de filtration. Ces membranes sont commerciales et elles ont d'excellentes propriétés mécaniques (module d'Young de l'ordre de 260 MPa , déformation à la rupture de 28 %) et une excellente résistance chimique. Les membranes utilisées dans ce travail ont une porosité de 70% et un diamètre des pores de 100 nm ce qui permet d'obtenir une grande capacité de stockage.

Electrolyte

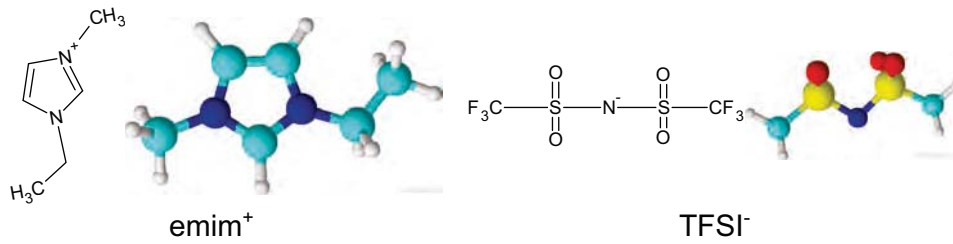


Fig. C.4. Chemical and 3D structures of the ionic liquid 1-Ethyl-3-methylimidazolium bis(trifluoromethanesulfonyl)imide (emimTFSI)

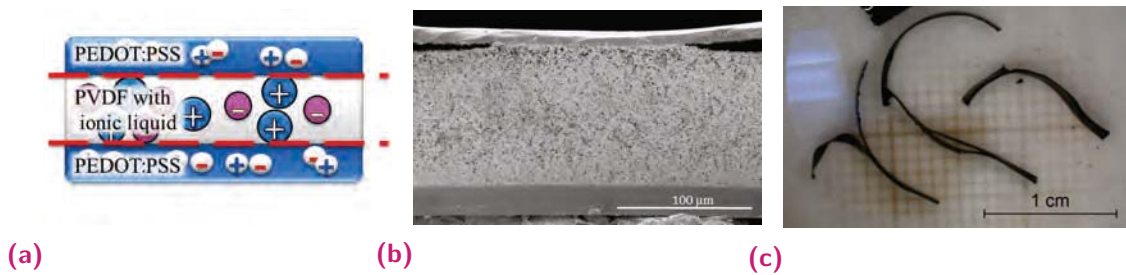


Fig. C.5. (a) Illustration schématique d'actionneurs PEDOT: PSS / PVDF / PEDOT: PSS avec un liquide ionique avec une défaillance potentielle dans la zone d'adhésion entre les couches (ligne pointillée rouge). (b) Image par microscopie à balayage (MEB) d'une coupe transversale de l'actionneur tricouche où l'on peut observer très clairement la délamination de la couche de PEDOT: PSS de la membrane PVDF (c) Actionneurs avec une mauvaise adhésion interfaciale après immersion dans un liquide ionique.

A cause de l'évaporation du solvant, les électrolytes conventionnels limitent la durée de vie des dispositifs, c'est la raison pour laquelle ils ont été remplacés progressivement par des liquides ioniques (Ionic Liquids ILs en anglais) [13, 29, 89, 243, 386]. Les liquides ioniques sont des sels constitués d'ions à faible coordination, ils sont liquides à une température inférieure à 100°C et même pour certains à température ambiante. Durant cette étude, le 1-Ethyl-3-methylimidazolium bis(trifluoromethanesulfonyl)imide (emimTFSI) a été utilisé comme liquide ionique (Fig. C.4).

C.1.3 Contexte et positionnement du problème

L'objectif de cette thèse est de développer des actionneurs électroactifs ioniques pour des applications dans le domaine de la robotique. A cette fin, une technologie de fabrication robuste, rapide et à grande échelle est nécessaire. L'impression jet d'encre est une technologie clé pour le dépôt de polymères [120] et une des plus prometteuses pour la production d'actionneurs électroactifs ioniques. De plus, elle peut être utilisée pour fabriquer et intégrer des capteurs de déformation [8, 40, 69, 330, 325]. Néanmoins, plusieurs verrous limitent le potentiel d'application de cette technique: (1) solubilité du polymère conducteur et disponibilité d'encres adéquates; (2) viscosité et tension de surface des solutions contenant les polymères conducteurs et stabilité de l'éjection; (3) adhésion entre la membrane de stockage des ions et le film de polymère conducteur; (4) diffusion de l'encre à travers les pores de la membrane. Ces verrous sont principalement liés à la nature chimique de la solution de polymère conducteur et de la membrane poreuse. La solution de polymère conducteur doit répondre à un certain nombre

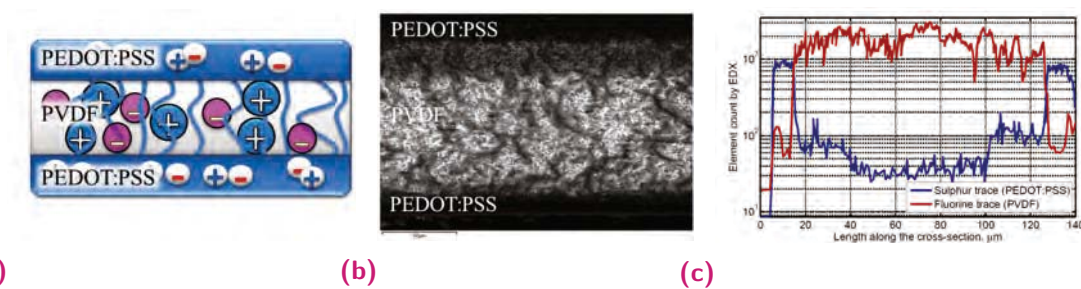


Fig. C.6. (a) Représentation schématique d'un actionneur PEDOT: PSS / PVDF / PEDOT: PSS avec des électrodes percolées (lignes bleues). (b) Image SEM d'une coupe transversale de l'actionneur tricouche avec du PEDOT: PSS dans la membrane PVDF (c) Spectres EDX le long de la coupe transversale faisant apparaître clairement des traces de soufre (PEDOT: PSS) en bleu et de fluor (PVDF) en rouge. Les traces de soufre significativement plus élevées que zéro traduisent un phénomène de percolation dans la membrane.

de prérequis pour être utilisable en technologie jet d'encre; c'est-à-dire d'un point de vue rhéologique, mais également en tant que couche active pour les actionneurs, c'est-à-dire avoir de bonnes propriétés électriques et ioniques, une bonne flexibilité mécanique et une grande résistance au vieillissement. La membrane, quant à elle, doit permettre de contenir un volume important d'électrolyte et présenter de très bonnes propriétés de conduction ionique ainsi qu'une excellente adhésion avec la couche conductrice en polymère tout en jouant le rôle d'isolant électrique entre les deux électrodes conductrices. Durant cette thèse, ces verrous sont discutés en détail et des solutions sont proposées ce qui a permis de développer les premiers actionneurs électroactifs ioniques réalisés par technologie jet d'encre.

Si une solution de PEDOT:PSS est utilisée pour la fabrication par dépôt de goutte, l'adhésion entre le PEDOT: PSS et le PVDF est mauvaise. Cela conduit à une séparation partielle des couches lors de la manipulation et une délamination complète une fois que l'actionneur est immergé dans un liquide comme représenté sur la Fig. C.5. Par conséquent, l'utilisation de membranes hydrophiles, à base de polyuréthane [295] par exemple ou de cellulose [193], remplies de liquide ionique a été récemment décrite. Le caractère hydrophile des membranes assure une bonne adhésion entre le PEDOT:PSS tandis que le liquide ionique bloque les pores empêchant les infiltrations et les connexions éventuelles entre les électrodes. Néanmoins, la fabrication de tels actionneurs se fait à l'unité et est difficilement exploitable à grande échelle. En outre, les membranes utilisées pour ce type de fabrication doivent avoir une conductivité ionique significativement plus faible ce qui influence aussi leur performance. Par exemple, la conductivité ionique de emimTFSI dans le PVDF est de $19,4 \text{ mS/cm}$ alors que dans le polyuréthane, elle est beaucoup plus faible, de l'ordre $0,9 \text{ mS/cm}$ [295, 369]. Par conséquent, il est fort probable que le rendement peut être considérablement amélioré si des membranes en PVDF sont utilisées avec les mêmes électrodes.

Une des causes possibles à l'origine de la mauvaise adhésion entre le PEDOT: PSS et le PVDF est la nature chimique des matériaux, en particulier le caractère hydrophobe du PVDF et hydrophile du PEDOT :PSS en solution aqueuse. L'angle de contact entre ces matériaux est supérieur à 130° . Néanmoins, si un PVDF hydrophile est utilisé,

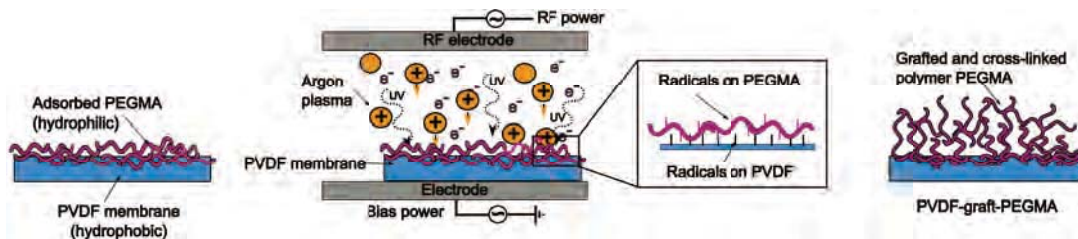


Fig. C.7. Illustration schématique d'un greffage lors de l'irradiation plasma : (1) Immobilisation du monomère ou macromonomère à la surface du substrat; (2) activation des deux: la surface du polymère et le précurseur du monomère par plasma en créant des radicaux sur chacun; (3) Réaction simultanée entre les espèces actives conduisant à la réticulation du polymère et du substrat. Si on utilise du PEGMA comme précurseur de la réaction et le PVDF en tant que substrat, cette procédure conduit à une hydrophilisation de la surface du PVDF en surface.

le PEDOT: PSS est immédiatement absorbé et dans le cas où une configuration à trois couches est nécessaire, cela provoque des connexions partielles entre les deux électrodes. Une illustration schématique de tels phénomènes ainsi que des images MEB d'actionneurs avec un phénomène de percolation des électrodes ainsi que des caractérisations par EDX le long d'une coupe transversale sont présentées sur la Fig.C.6. L'amélioration de l'adhésion est donc nécessaire mais des membranes hydrophiles ne peuvent pas être utilisées. En s'inspirant de l'approche proposée par Ikushima et al [148], nous avons développé une technique permettant la fonctionnalisation partielle des membranes. Ainsi, des membranes hybrides ayant des pores hydrophiles jusqu'à une certaine profondeur de la membrane et un centre hydrophobe ont été élaborées.

C.2 Membranes hybrides PVDF/PVDF-PEGMA

La modification de surface du PVDF et d'autres polymères fluorés a été étudiée par de nombreux chercheurs. Comme pour d'autres polymères, la défluoruration et les réactions de réduction sont plus communes et des traitements sous plasmas N_2 , O_2 , H_2 et Ar augmentent ses propriétés hydrophiles. Néanmoins, les polymères fluorés semblent être plus résistants à un plasma d'oxygène et sont fortement endommagés uniquement par l'argon [94, 304, 384]. Par conséquent, afin de réaliser un greffage pendant ou après irradiation, un plasma Ar est généralement utilisé. En outre, le contrôle de l'activation par plasma dans les pores de la membrane est souvent difficile et la fonctionnalisation de l'ensemble des pores de la membrane ne peut pas être évitée. Pour nos applications, de très minces couches de greffage ont été nécessaires, de sorte que la porosité des membranes et leur volume de stockage d'ions est resté maximal. Par conséquent, le greffage par irradiation a été considéré comme un procédé plus approprié. Une illustration schématique d'un greffage induit par plasma Ar est représentée sur la Fig. C.7.

En raison de sa disponibilité et de sa polyvalence, le polyéthylène glycol (PEG) est souvent utilisé en tant que polymère de greffage, en particulier lorsque les propriétés hydrophiles et la biocompatibilité doivent être améliorées. Le PEG fonctionnalisé avec du méthacrylate en fin de chaîne est plus réactif et peut être greffé sur une membrane en PVDF par divers moyens, par exemple, une polymérisation radicalaire par transfert

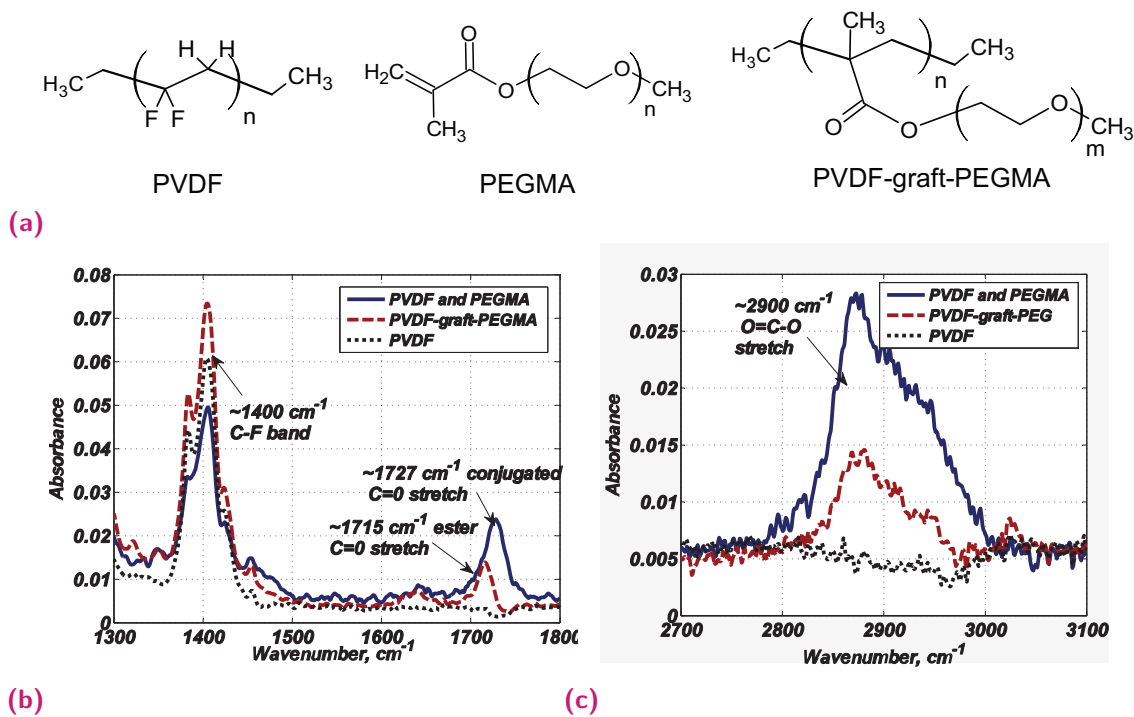


Fig. C.8. (a) Structure chimique du PVDF, du PEGMA et du PVDF-PEGMA et leur signature entre (b) $1300 - 1800\text{ cm}^{-1}$ et (c) $2700 - 3100\text{ cm}^{-1}$

d'atomes (ATRP) [45, 46], une activation par rayons ultraviolets (UV) [31, 317], un plasma [44, 46]. La structure chimique des deux, le PVDF et le poly (éthylène glycol) méthyl éther méthacrylate (PEGMA), ainsi que leur produit de réaction est représentée sur la Fig. C.8a. Les spectres obtenus par spectroscopie infrarouge par transformée de Fourier (FTIR) (Fig. C.8b-C.8c) montrent le changement dans leurs signatures IR pendant la réaction covalente.

Si le précurseur de la réaction (PEGMA) est déposé sur la surface du PVDF par une méthode de trempage, durant le traitement plasma, la surface des pores de la membrane est fonctionnalisée sur toute l'épaisseur de la membrane PVDF tel qu'illustré sur la Fig. C.9a. Cela conduit à la création de membranes PVDF hydrophiles et à la percolation du PEDOT: PSS entre les électrodes lorsque celui-ci est déposé sur la surface du PVDF.

Nous avons conclu que faire varier les paramètres du plasma n'est pas efficace pour contrôler la profondeur d'activation de la membrane. Par conséquent, deux ajustements du processus ont été considérés: (1) limiter la profondeur d'activation par plasma en bloquant les pores de la membrane (C.9b) et (2) limiter le dépôt du précurseur sur une certaine épaisseur Fig. C.9c. Les deux procédés se sont avérés adaptés pour limiter la profondeur du greffage par irradiation directe sous plasma. Néanmoins, en remplissant les pores avec les précurseurs de greffage conduit à une polymérisation très dense. Cela pourrait par conséquent bloquer les pores en surface de la membrane et avoir un impact négatif sur la conductivité ionique des électrolytes stockés dans la membrane. En outre, dans ce cas, la polymérisation est sensible à la préparation de la membrane. Un excès de liquide sur la surface (dans notre cas, il a été supprimé en plaçant les membranes

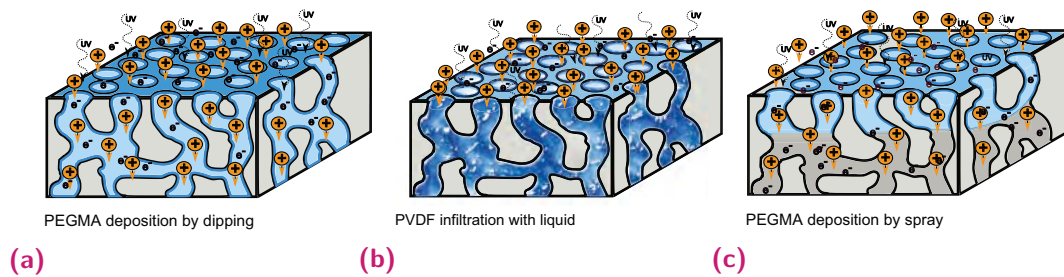


Fig. C.9. Schémas illustrant trois stratégies différentes de dépôt de précurseur et l'interaction du plasma à la surface de la membrane: (a) dle dépôt par trempage dans une solution diluée contenant le précurseur et conduisant à son adsorption sur la surface de la membrane suivi de l'activation du greffage par plasma sur toute l'épaisseur; (b) le dépôt par immersion dans un liquide visqueux qui empêche la pénétration du plasma et l'activation des pores; (c) le dépôt par pulvérisation qui limite le dépôt du précurseur à une certaine profondeur.

de filtration sur du papier absorbant) pourrait empêcher l'irradiation du PVDF, ce qui rend le processus difficile à contrôler. Par conséquent, limiter la quantité du précurseur de réaction à une certaine profondeur a été étudié durant ce travail de thèse. Pour déposer de faibles quantités et limiter l'infiltration du précurseur dans les pores de la membrane, le dépôt de PEGMA a été effectué par pulvérisation.

C.2.1 Contrôle de la profondeur de pénétration

Le PEG et le PEGMA sont de bons agents mouillants et sont immédiatement adsorbés sur la membrane PVDF. Par rapport à l'eau, leurs solutions aqueuses se propagent plus facilement (angles de contact respectifs de $53.3 \pm 2.3^\circ$ et $39.3 \pm 2.8^\circ$ pour une solution à 10 vol% en volume déposée sur la surface rugueuse et lisse du PVDF) et s'infiltrent dans ses pores. Ainsi, si au cours de la pulvérisation, le PEGMA atteint la surface avec une petite quantité de solvant résiduel, il est susceptible de diffuser à une certaine profondeur. Le processus de revêtement par pulvérisation dépend de nombreux paramètres : taille de la buse, pression, nature chimique du précurseur et du solvant, environnement de pulvérisation et substrat. L'efficacité de pulvérisation (SE) 1) et l'homogénéité du film sont donc difficilement prédictibles. Le temps de vol détermine la quantité de solvant résiduel, par conséquent, la distance entre le pistolet de pulvérisation et la membrane est l'un des paramètres essentiels déterminant l'efficacité de pulvérisation comme le montre la Fig. C.10a.

Comme illustré sur la Fig. C.10b, la densité de PEGMA greffé sur la surface du PVDF (GD : défini comme l'augmentation de la masse par rapport à la surface plane externe) dépend du dépôt par pulvérisation (SD). Le GD augmente quasi linéairement avec la densité du précurseur vaporisé pour SD inférieur à 1 ng/mm^2 mais pour SD supérieur à 2 ng/mm^2 , le taux de greffage diminue. Des effets de gravure lors du plasma pourraient être l'une des explications de ce phénomène. Néanmoins, c'est peu probable avec un traitement plasma d'une durée de l'ordre de 15s [200]. La baisse du rendement de greffage peut aussi être expliquée par une contre-polymérisation rapide du PEGMA sur la surface extérieure. Cette couverture dense de la surface peut empêcher l'activation de pores de la membrane PVDF. La rugosité de surface du substrat semble également influencer le processus de greffage du PEGMA. Lorsque le greffage s'effectue sur la face

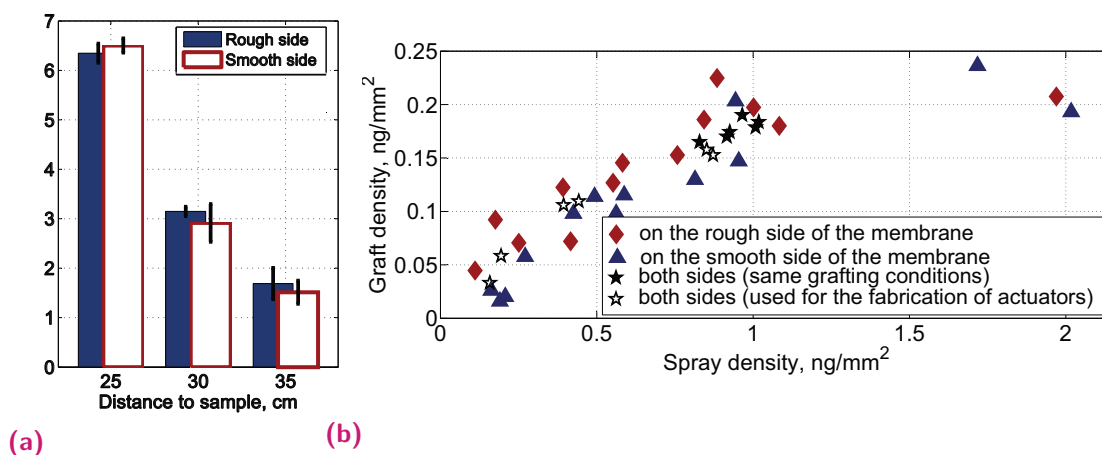


Fig. C.10. (a) Spray efficiency of poly(ethylene glycol) methyl ether methacrylate (PEGMA) in ethanol/water solution on polyvinylidene fluoride (PVDF) membranes with different spray distance, (b) Grafting density versus density of PEGMA sprayed on the rough (blue) and smooth side (red) at different conditions. Black stars - sprayed on both side and averaged.

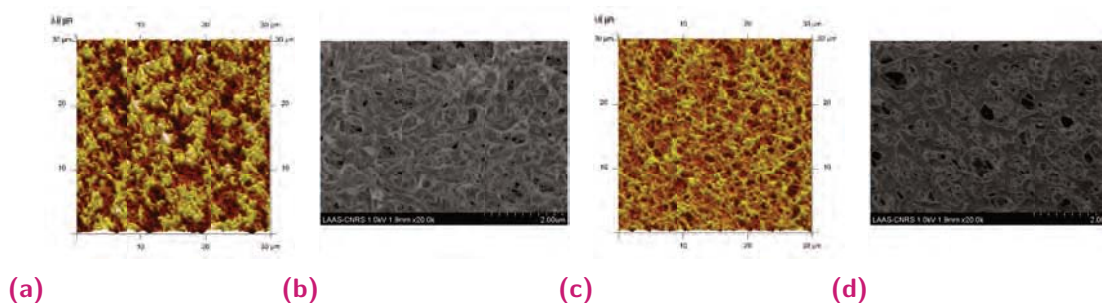


Fig. C.11. AFM and SEM images of surfaces of the pristine PVDF membrane. (a)-(b) - rough side (R_q - 351 nm) (c)-(d) - smooth side (R_q - 182 nm)

rugueuse (Fig. C.11a-C.11b), une efficacité de greffage légèrement plus importante peut être obtenue comme indiqué sur la Fig. C.10b. Nos résultats suggèrent que la réaction peut être plus rapide sur les zones topographiques les plus prononcées de la membrane ce qui augmente encore plus sa rugosité (Fig. C.12). Le dépôt sur la surface lisse semble être plus homogène (pas de changement de rugosité significative). Enfin, l'aire totale de la surface des pores de la membrane (mesurée par adsorption de krypton et estimée avec la théorie Brunauer-Emmett-Teller (BET)) ne change pas de façon significative avec la fonctionnalisation ($5.19 \pm 0.33 \text{ m}^2/\text{g}$ pour les membranes vierges et fonctionnalisées) ce qui traduit le fait que, à l'exception de la surface supérieure de la membrane, la réaction est le plus souvent limitée à une couche très mince.

Même si la densité croissante de pulvérisation (SD) et la densité de greffage (GD) ne semblent pas influencer de manière significative la morphologie de la membrane (en particulier sur la face lisse), ni la mouillabilité (même de petites densités de greffage de $< 0.05 \text{ ng}/\text{mm}^2$ diminuent l'angle de contact de l'eau à moins de $< 30^\circ$), la densité de greffage augmente toujours légèrement au-dessus de $> 0.07 \text{ ng}/\text{mm}^2$. Ceci suggère que la surface des pores de la membrane peut être fonctionnalisée et la profondeur affectée de la membrane (dans l'épaisseur) peut être influencée par les paramètres de pulvérisation.

La profondeur de fonctionnalisation, estimée par spectroscopie à rayons X à dispersion d'énergie (EDX), en fonction de la densité de greffage est représentée sur la Fig. C.12. L'épaisseur de greffage augmente avec GD jusqu'à environ 30 μm . Cependant, à plus forte densité de greffage, elle semble atteindre un niveau de saturation et au-delà de 0.18 ng/mm^2 , elle commence à diminuer. Cela corrobore notre hypothèse précédente qu'en raison d'une polymérisation rapide du PEGMA sur la surface externe de la membrane, la diffusion de plasma en profondeur dans les pores de PVDF est limitée.

En considérant ces résultats, nous suggérons que les deux mécanismes en compétition lors de la polymérisation par greffage sous plasma Ar sont : (1) la diffusion du plasma dans la membrane en PVDF ce qui se traduit par une grande profondeur de greffage et de fines couches de PEGMA greffées le long des pores et (2) la polymérisation croisée du PEGMA sur la surface supérieure, qui peut provoquer un dépôt dense et limiter la diffusion du plasma à de petites profondeurs.

C.3 PEDOT :PSS et membrane en PVDF : adhésion versus infiltration

Nous avons développé des membranes hybrides en PVDF avec un greffage PEGMA afin d'améliorer l'adhésion entre les électrodes en PEDOT: PSS et la membrane en PVDF. Néanmoins, une même nature chimique ne suffit pas toujours à faire adhérer deux polymères. Les principaux mécanismes jouant un rôle dans l'adhésion entre deux matériaux polymères sont (1) les liaisons covalentes, (2) les interactions thermodynamiques, (3) l'interdiffusion de chaînes polymères et (4) l'ancrage mécanique [161]. Dans notre cas, l'ancrage mécanique est non seulement lié à la rugosité, mais il est également important pour expliquer l'adhésion d'un polymère à des matériaux poreux.

L'étape initiale dans le processus d'interaction des matériaux est le dépôt du polymère dilué en solution sur la surface de la membrane. Beaucoup de mécanismes d'adhésion reposent sur un contact intime entre les matériaux, à savoir un bon mouillage. La tension de surface du liquide (γ_L) et son angle de contact (Θ) (avec un substrat parfaitement plan) peuvent être utilisés pour estimer le coefficient d'étalement en utilisant l'équation Young-Dupré:

$$S = \gamma_L(\cos\Theta - 1) \quad (\text{C.1})$$

Un paramètre S positif traduit un mouillage complet, tandis qu'un paramètre négatif signifie un mouillage partiel. L'angle de contact initial n'augure pas nécessairement de l'intensité de la force d'adhésion entre un substrat et un film polymère. Néanmoins, il est un bon indicateur d'un mauvais mouillage et d'une immiscibilité des polymères qui mènent ensuite à une faible épaisseur d'interdiffusion.

Le PVDF est un des polymères ayant la plus faible énergie de surface (25 mN m^{-1}). Ainsi, le WCA sur du PVDF est proche de 130° comme représenté sur la Fig. C.13. Des solutions aqueuses de PEDOT: PSS ont une tension superficielle élevée de 70.2 mN m^{-1}

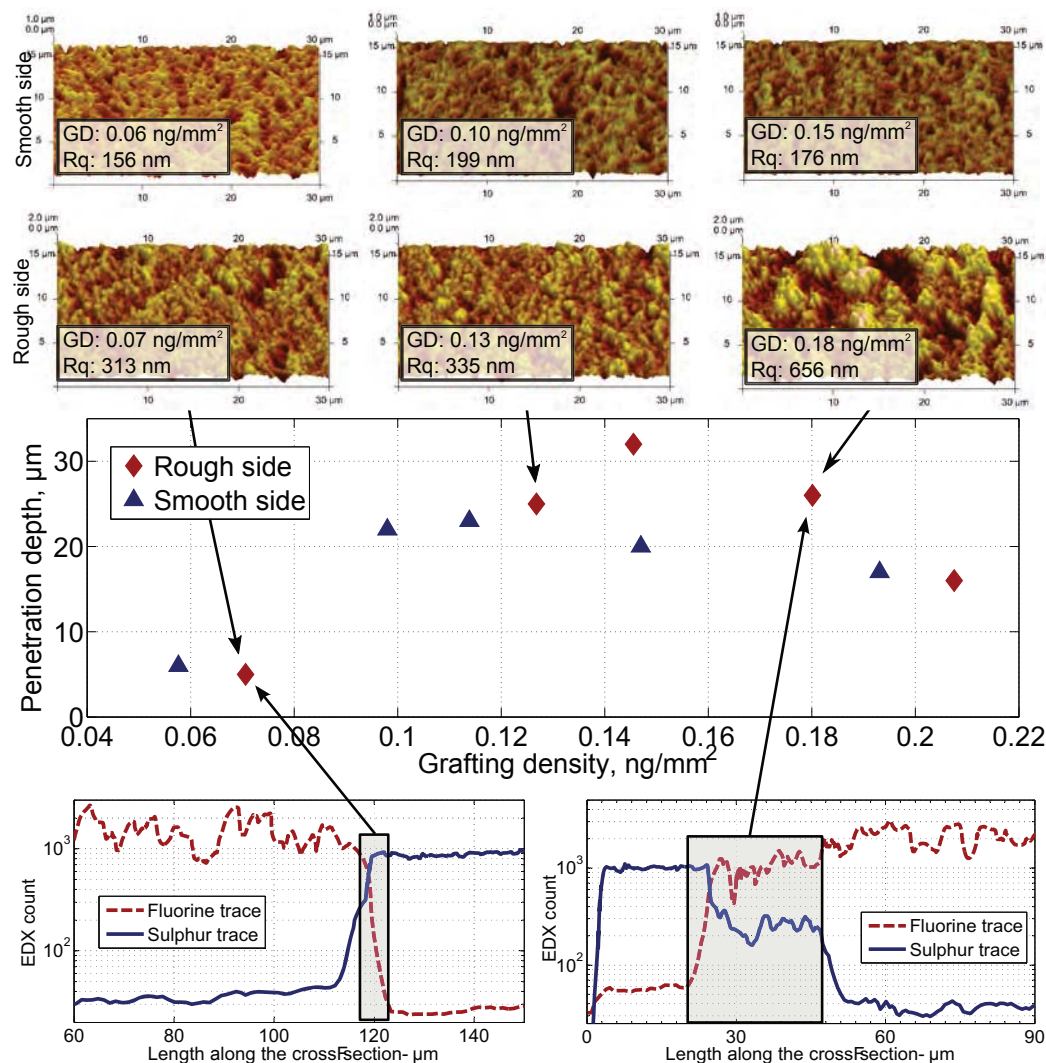


Fig. C.12. (Bas) Spectres EDX pour le soufre (bleu trait plein) et le fluor (rouge ligne pointillée) le long des sections transversales du PEDOT: PSS / PVDF avec greffage PEGMA. La densité de greffage (GD) est indiquée par les flèches. (Centre) Profondeurs de greffage par rapport à la densité de greffage (GD) tracées séparément pour du PEDOT: PSS déposé sur le côté rugueux (Δ bleu) et le côté lisse (\diamond rouge) de la membrane PVDF avec greffage PEGMA. (Haut) Images obtenues par microscopie à force atomique (AFM) des surfaces lisses et rugueuses de membranes PVDF avec greffage PEGMA pour différentes densités de greffage (GD). La densité de greffage et la rugosité sont indiquées dans les légendes.

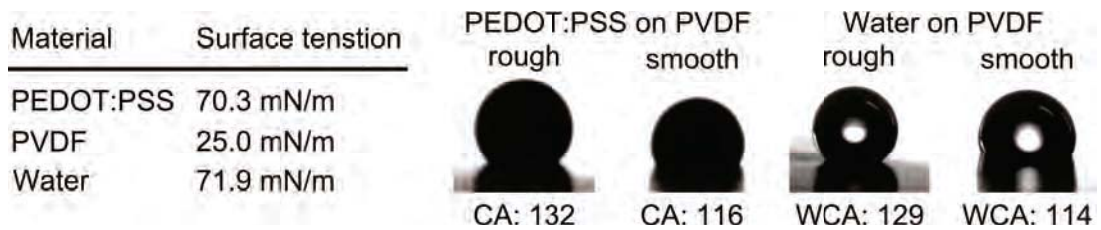


Fig. C.13. Tensions de surface mesurées (PEDOT :PSS et eau) et publiée (PVDF). Photographies de mesures d'angle de contact entre l'eau, le PEDOT :PSS et le PVDF

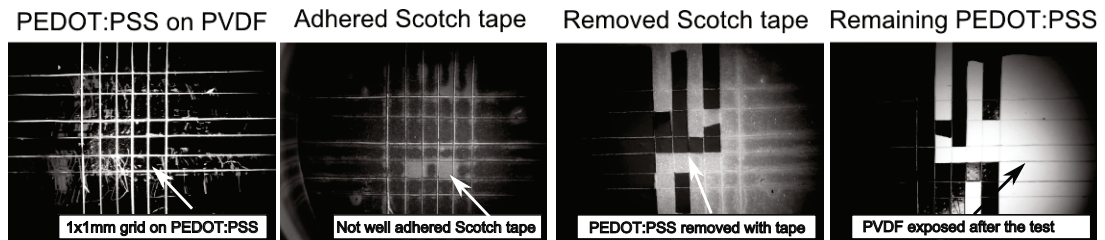


Fig. C.14. Étapes du processus d'évaluation d'adhésion (de gauche à droite): grille de 25 cases découpées sur le PEDOT: PSS jusqu'à la membrane de PVDF; Un ruban adhésif de type Scotch™ est appliqué sur la grille pour effectuer le test d'adhésion ; image du ruban adhésif après qu'il a été retiré du film; image de la membrane PVDF et du PEDOT :PSS restant sur la membrane après que le ruban adhésif a été retiré

qui est similaire à celle de l'eau pure (à 25°C). La tension de surface élevée et l'important angle de contact avec l'eau dans les deux cas conduit à un coefficient d'étalement négatif. L'état de contact intime entre les matériaux n'est donc pas satisfait et l'interdiffusion des chaînes de polymère est hautement improbable. Par conséquent, il en résulte une mauvaise adhésion.

Afin d'estimer la force d'adhésion entre des membranes sans greffage PEGMA (pPVDF) et avec greffage PEGMA (mPVDF) et les films de PEDOT :PSS déposés par goutte, le test du ruban adhésif a été utilisé (test conforme aux recommandations ISO 2409:2013 et validé par Liu et al. et Kim et al.) [241, 193]. Deux séries de découpes parallèles et orthogonales pour obtenir 25 carrés similaires ont été effectuées sur la surface du PEDOT: PSS sans découper la membrane (étapes indiquées sur la Fig. C.14). Ensuite, le ruban adhésif a été appliqué et lentement retiré. La procédure a été répétée 5 fois (essai I). En fonction de la qualité de l'adhésion, le PEDOT: PSS reste sur la membrane en PVDF ou est supprimé avec le ruban adhésif. Nous tenons à souligner que ce sont des tests qualitatifs qui ne fournissent aucune information quantitative sur la valeur de la force d'adhésion.

Les résultats des essais d'adhésion sur des membranes PVDF avec et sans greffage PEGMA sont représentés sur la Fig. C.15. Une plus grande rugosité de surface semble avoir une influence positive sur la force d'adhésion du PEDOT: PSS sur la membrane. Une surface significativement plus grande de PEDOT: PSS reste sur le côté rugueux de la membrane PVDF après le test de décollement. L'influence de la rugosité de surface sur l'adhésion est discutable, mais dans ce cas il est néanmoins plus probable en raison de l'ancrage physique du polymère sur les aspérités plus marquées et plus fréquentes sur la surface rugueuse [15]. Cependant, l'adhésion n'est pas assez importante pour

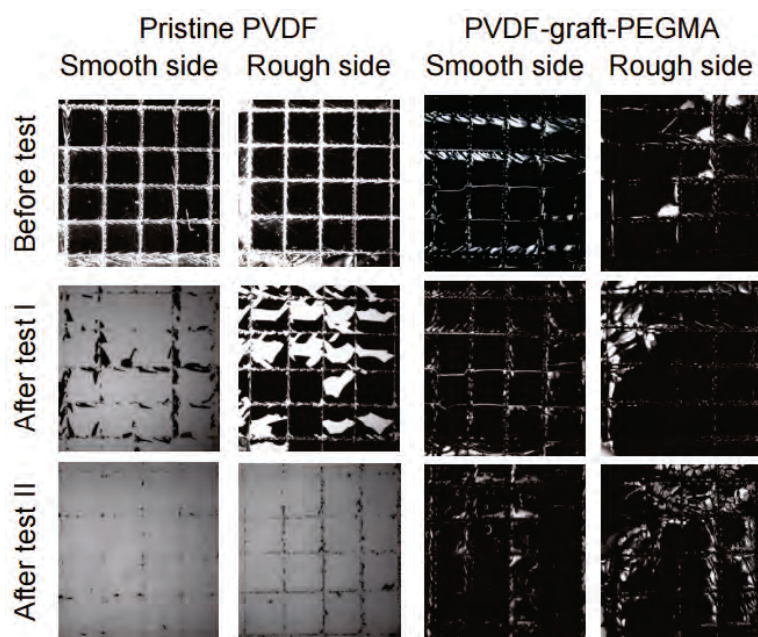


Fig. C.15. Test d'adhésion du PVDF et de membranes PVDF avec un greffage PEGMA (blanc) et PEDOT: PSS (noir). Les photos sont prises après que la grille a été découpée (avant le test), après 5 tests consécutifs de décollement (test I) et de nouveau après une incubation de la bicouche dans le liquide ionique pour 24 heures et 5 tests supplémentaires de décollement (test II).

supporter la contrainte induite à l'interface une fois que la membrane est placée dans le liquide ionique (Test II). Ainsi, le PEDOT: PSS qui est resté sur la membrane pPVDF après le test I a complètement disparu après cinq tests en présence de liquide ionique.

D'autre part, même de faibles densités de greffage PEGMA ($GD - 0.07 \text{ ng/mm}^2$) conduisent à une résistance de l'adhésion améliorée de façon significative. Le PEDOT: PSS reste sur la surface de la membrane mPVDF après des tests dans un milieu sec et après immersion dans liquide ionique (Fig. C.15). Trois mécanismes pourraient expliquer cette interaction plus forte: (1) des liaisons hydrogène entre le PEGMA et le polymère PEDOT ou le PSS; (2) l'enchevêtrement du PEDOT et du PSS avec la couche de PEGMA greffée sur le PVDF; (3) l'infiltration et l'ancrage mécanique de la couche de PEDOT: PSS dans les pores de la membrane.

Avoir une forte adhésion nécessite un contact intime entre la surface du PVDF sur laquelle sont greffés le PEGMA et le PEDOT: PSS. Plusieurs facteurs pourraient entraver cette interaction. Il a été montré que l'eau résiduelle dans le film de PEDOT: PSS est susceptible de former une couche barrière entre le PVDF et le film polymère. Par conséquent, un séchage incomplet réduit considérablement l'adhésion. Il a également été montré que l'adsorption de PEG ou d'un autre matériau hydrophile peut inhiber l'adhésion. Nous suggérons que dans le cas d'un excès de PEG dans la solution de PEDOT: PSS, il s'adsorbe sur la membrane avant évaporation du solvant, et reste à la surface après le recuit thermique. Par conséquent, au cours de l'évaporation du solvant, le PEDOT: PSS se dépose sur la surface où la couche de PEG a été adsorbée et n'atteint pas le PVDF à la surface duquel le PEGMA a été greffé.

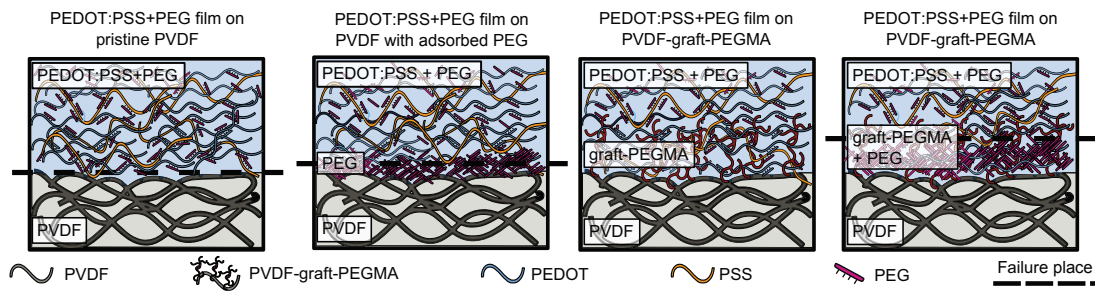


Fig. C.16. Représentation schématique de différentes méthodes de fonctionnalisation du PVDF et leur influence sur l'adhésion avec du PEDOT :PSS.

C.3.1 Conclusion

Un résumé de ces résultats est représenté sur la Fig. C.16. Nous avons montré que l'ancrage mécanique direct, qui est le résultat de l'infiltration et de la solidification du film de PEDOT: PSS dans les pores de la membrane, est l'un des moyens les plus efficaces pour assurer une bonne adhésion entre ces deux matériaux. Une autre façon d'ancrer le PEDOT: PSS et le PVDF est de rendre la surface du PVDF hydrophile grâce à un greffage de PEGMA.

L'adhésion par simple enchevêtrement ou grâce à des liaisons hydrogène avec un greffage polymère (comme cela a été testé sur un substrat lisse) est assez robuste pour passer le test de ruban adhésif dans un état sec. Dans le cas de substrats poreux, il permet l'infiltration de PEDOT: PSS dans les pores de la membrane. En outre, dans ce cas seulement, quelques micromètres de profondeur sont nécessaires pour obtenir une forte adhésion. Nous avons également montré que dans les deux cas, ancrage mécanique et fonctionnalisation par greffage, un contact intime entre les matériaux doit être assuré pour obtenir une bonne adhésion. L'eau, ou tout autre revêtement hydrophile présent entre deux matériaux, conduit irrémédiablement à une délamination.

L'adhésion et le transport de masse à travers des membranes hydrophobes sont influencés par les propriétés physico-chimiques des matériaux. Par conséquent, ces deux processus doivent être pris en considération lors de la conception de structures bi-couches ou tricouches. L'infiltration d'une solution aqueuse de polymère dans les pores de la membrane se produit sur des membranes hydrophiles, lorsque la tension superficielle de la solution est suffisamment faible ou lorsque des matériaux hydrophobes sont utilisés. Ceci limite le choix des dopants secondaires ; des tensioactifs et même des molécules légèrement hydrophobes sont susceptibles de provoquer des infiltrations de PEDOT: PSS.

C.4 Actionneurs ioniques PEDOT :PSS /mPVDF

L'utilisation de membranes PVDF hybrides est pertinente seulement si la plus grande partie de la membrane est maintenue hydrophobe. C'est le cas pour les actionneurs souples qui sont fabriqués en déposant deux électrodes constituées de polymères conducteurs sur les deux faces de la membrane. Une connexion partielle de ces électrodes à l'intérieur de la membrane aurait des effets néfastes sur leur performance

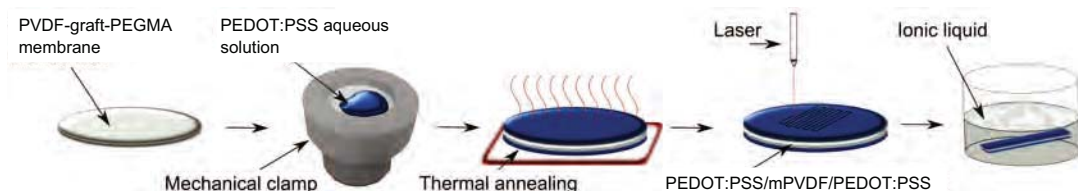


Fig. C.17. Illustration d'un procédé de fabrication d'un actionneur par dépôt en goutte de solvant. Une membrane hybride (PVDF avec greffage PEGMA) est fixée mécaniquement à un support en aluminium et une goutte de PEDOT: PSS en solution aqueuse (avec un dopage secondaire) est déposée sur la surface de la membrane. Après séchage à température ambiante, le support est inversé et le processus est répété pour l'autre côté de la membrane afin de produire un actionneur tricouches. La membrane avec du PEDOT: PSS sur les deux côtés est ensuite séchée à l'étuve à 70°C pendant deux heures. Des actionneurs rectangulaires de 1.5 mm par 2 cm sont ensuite découpés par laser, les actionneurs sont thermiquement recuits à 120°C (non représenté ici) et sont incubés dans un liquide ionique pendant 10 à 120 minutes.

[104]. Pour démontrer les bénéfices de membranes hybrides avec différentes densités de greffage, plusieurs types d'actionneurs ont été fabriqués par dépôt en goutte.

Une illustration schématique du procédé que nous avons utilisé pour la fabrication des actionneurs avec les membranes PVDF hybride / PVDF greffé PEGMA est représentée sur la Fig. C.17. Dans la plupart des cas (sauf indication contraire) des membranes en PVDF ont été fonctionnalisées avec un SD de $0.9 \pm 0.1 \text{ ng/mm}^2$ et un GD de $0.14 \pm 0.02 \text{ ng/mm}^2$. Ceci correspond à une profondeur hydrophile d'environ $20 \mu\text{m}$ à la fois pour le côté rugueux et le côté lisse comme le montre la Fig. C.18b.

Les membranes sont ensuite séchées et fixées dans un support en aluminium d'un diamètre de $\varnothing 45 \text{ mm}$ afin de compenser la contrainte mécanique causée par le séchage de PEDOT: PSS. 3 ml de solution aqueuse de 1.3 wt% en masse de PEDOT: PSS ont ensuite été déposés sur la membrane. Afin d'augmenter sa conductivité électrique et ses propriétés mécaniques avant dépôt, le PEDOT: PSS a été dopé avec 1% en volume de PEG400. Les membranes avec le dépôt de solvant PEDOT: PSS sont ensuite séchées à température ambiante (20°C) et humidité contrôlée pendant au moins 12 heures. Cette procédure a ensuite été répétée pour l'autre face, afin d'obtenir un actionneur tricouches. Enfin, afin de diminuer la quantité d'eau résiduelle, les membranes ont ensuite séchées pendant deux heures à 70°C. Les actionneurs ont été découpés en rectangles de 2 mm par 1.5 cm par laser CO₂ et recuits thermiquement à 70°C pendant deux heures. Avant chaque mesure, les actionneurs ont été maintenus dans un liquide ionique (emimTFSI) pour 3 à 120 minutes.

Les mesures de caractérisation ont été principalement effectuées avec des actionneurs tricouches (PEDOT: PSS / mPVDF / PEDOT: PSS) fixés à une extrémité. La réponse mécanique des actionneurs a été enregistrée par mesure laser du déplacement de l'extrémité lorsqu'une tension cyclique était appliquée sur les deux faces de l'actionneur. Le courant est simultanément mesuré et a permis d'estimer la charge transférée. La réponse des actionneurs pour différentes tensions électriques et fréquences d'actionnement est représentée sur la Fig. C.19a et la Fig. C.19b.

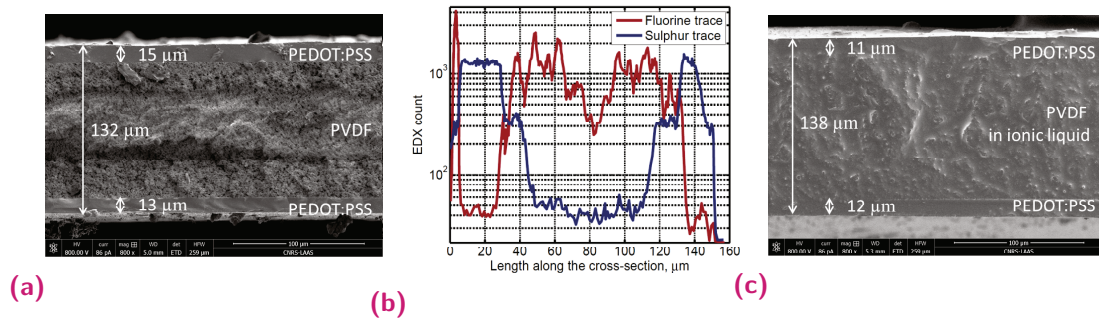


Fig. C.18. Images AFM et MEB de la surface d'une membrane PVDF sans greffage PEGMA. (a)-(b) Face rugueuse ($R_q = 351 \text{ nm}$) (c)-(d) Face lisse ($R_q = 182 \text{ nm}$)

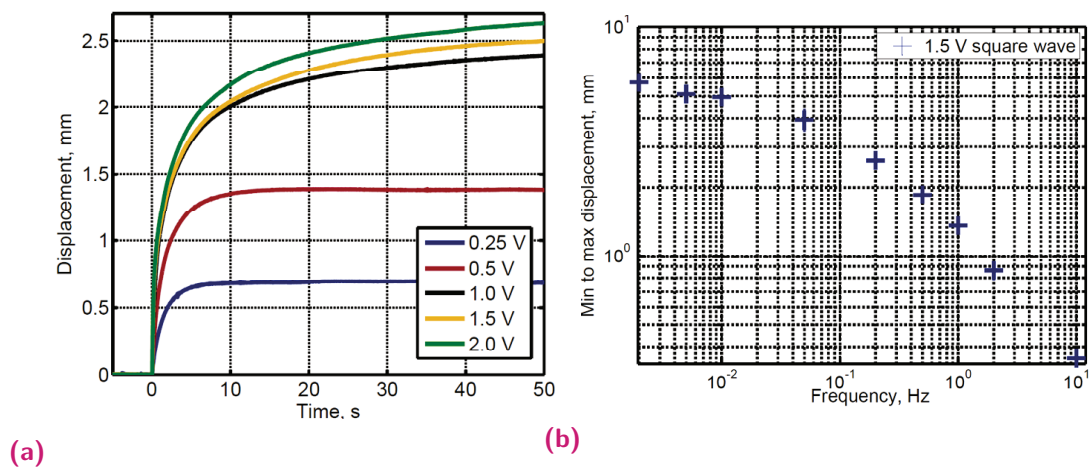


Fig. C.19. (a) Réponse d'actionneurs PEDOT: PSS / PVDF greffé PEGMA / PEDOT: PSS pour différentes tensions d'actionnement et (b) Amplitude de déplacement de ces mêmes actionneurs pour différentes fréquences.

C.4.1 Durée de vie

La durée de vie est une caractéristique importante pour de nombreux dispositifs. Dans le cas des muscles artificiels, la durée de vie dépend souvent de la fréquence d'actionnement, à savoir la différence de déformation, qui peut varier, par exemple, de 10^5 à 3 Hz , 10^3 à 1 Hz et être même inférieure à des fréquences plus faibles [247]. Les deux principaux phénomènes qui limitent la durée de vie des actionneurs polymères conducteurs sont les suivants: (1) la dégradation du polymère ou la décomposition de l'électrolyte sous cyclage électrochimique et (2) la délamination des électrodes de la membrane en raison des contraintes mécaniques à l'interface [17, 241]. La fenêtre électrochimique plus large des liquides ioniques permet de réduire l'effet de la dégradation [63, 291]. En outre, la non-volatilité des liquides ioniques rend possible un actionnement dans l'air [295, 386]. Néanmoins, la délamination des couches constituant l'actionneur reste un problème.

Sur la *Fig. C.20*, des actionneurs avec une grande densité de greffage et une importante couche interfaciale (profondeur de mélange (MD) $25\mu\text{m}$) (A25), et une densité de greffage faible et une fine couche interfaciale (MD - $5\mu\text{m}$) (A5) obtenus sur une membrane de PVDF vierge (pPVDF) (AP) sont comparées. Pour fabriquer des actionneurs fonctionnels à partir de membranes vierges en PVDF, Une solution de PEDOT: PSS avec 5% en volume de PEG400 a été utilisée ce qui provoque la pénétration du PEDOT: PSS à travers la membrane avec pour conséquence une augmentation sensible du courant mesuré entre les électrodes. La résistance entre les électrodes de membranes AP est de 6 ordres de grandeur plus faibles que pour A5 et A25 ($0.36\ \Omega$ vs $0.16\ \text{M}\Omega$) ce qui conduit à une grande dissipation d'énergie lors de l'actionnement. Une fois qu'une tension est appliquée ($1,5\text{ V}$ en signal sinusoïdal, fréquence de $0,1\text{ Hz}$) l'amplitude de déplacement de l'actionneur AP décroît continuellement et l'actionneur n'est plus fonctionnel après moins de 50 heures d'actionnement. A l'opposé, même avec une très petite profondeur de pénétration ($5\ \mu\text{m}$) et une adhésion plus forte, les actionneurs restent actifs, , pendant plus de 100 heures sans aucune diminution significative de l'amplitude de déplacement et aucun signe de délamination.

De petites variations de l'amplitude peuvent cependant être observées. Les performances des actionneurs pourraient être influencées par le milieu ambiant, en particulier parce que le PEDOT: PSS et les liquides ioniques sont des matériaux hygroscopiques qui peuvent facilement absorber l'eau. Le déplacement et la variation de l'humidité de l'environnement lors de l'actionnement du dispositif A3 sont présentés sur la *Fig. C.20b*. L'humidité peut influencer la déformation de l'actionneur de deux façons: (1) l'eau peut être absorbée et désorbée à cause de l'échauffement par effet Joule lors de l'application de la tension d'actionnement et (2) l'eau absorbée peut modifier la structuration du PEDOT: PSS et par conséquent ses propriétés mécaniques et électriques [364, 423]. D'autre part, il a été démontré que l'actionnement est dépendant de l'humidité même pour les actionneurs qui n'utilisent pas de PEDOT: PSS comme électrodes [281]. Ce phénomène est attribué à l'hygroscopicité des liquides ioniques.

Malgré la variation assez importante dans l'amplitude d'actionnement, le cyclage électrique est réversible et l'humidité ne cause pas de dommages permanents aux

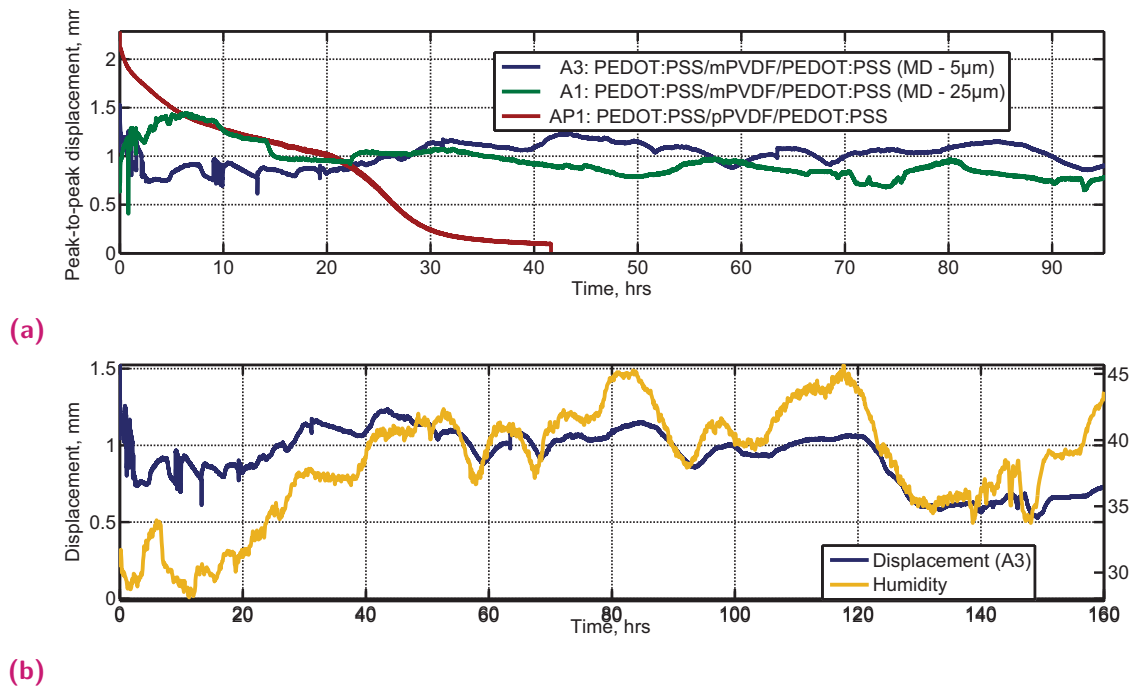


Fig. C.20. (a) Mesure de la durée de vie d'actionneurs hybrides PVDF greffé PEGMA (mPVDF) et de membranes vierges (PVDF). La profondeur d'interaction entre le PEDOT: PSS et la mPVDF est indiquée dans la légende. (b) Amplitude du déplacement d'un actionneur PEDOT: PSS / PVDF-greffage PEG / PEDOT: PSS avec un MD de 5 μm dans un liquide ionique (bleu) et changement de l'humidité de l'environnement (jaune)

actionneurs. D'autre part, si un contrôle de la position de l'actionneur est nécessaire, l'humidité doit être mesurée et les algorithmes de contrôle doivent être ajustés en conséquence.

C.4.2 Vers des muscles artificiels fabriqués par technologie jet d'encre

Afin de pousser la technologie des actionneurs souples vers une production en masse, des procédés de fabrication à grande échelle sont nécessaires. Une des solutions possibles est l'impression jet d'encre. Il s'agit d'une technique de dépôt directe sans contact qui est considérée comme l'une des technologies clés pour le dépôt de polymères en solution. En outre, elle est bas coût, rapide et précise. Elle permet également l'impression de plusieurs encres fonctionnelles de manière parallélisée. Une représentation schématique de l'impression jet d'encre de polymères conducteurs est proposée sur la Fig. C.21a. Des images SEM et AFM d'une couche de PEDOT: PSS imprimée sur une membrane de PVDF vierge sont présentées sur la Fig. C.21b. Comme l'encre utilisée pour l'impression doit satisfaire à plusieurs exigences, en particulier sa viscosité, sa densité et sa tension de surface, plusieurs dopants secondaires ont été testés pour en modifier les propriétés. En outre, les agents tensio-actifs ne peuvent pas être utilisés pour éviter des phénomènes de percolation entre les électrodes conductrices en polymères. Nous avons montré que l'éthylène glycol comme dopant secondaire améliore les propriétés mécaniques

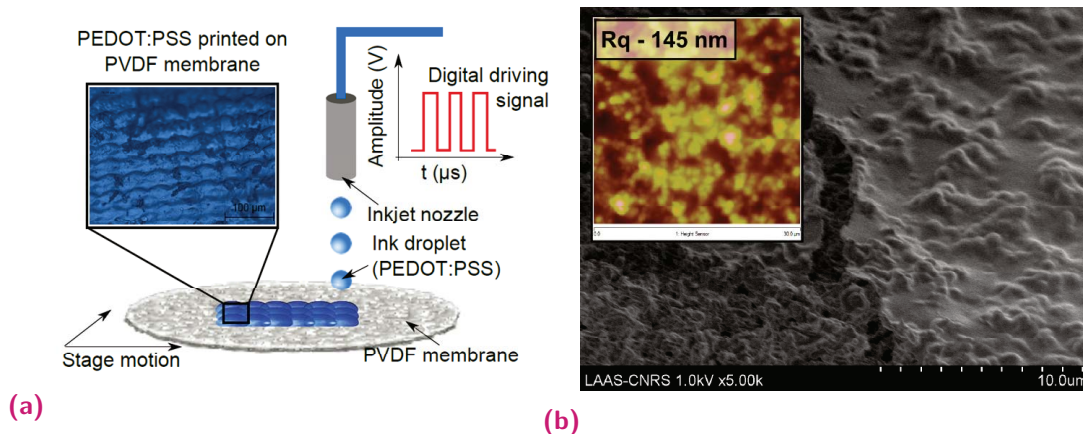


Fig. C.21. Illustration schématique d'une impression jet d'encre piézo-électrique: une tension électrique est utilisée pour déformer le matériau piézo-électrique et générer une impulsion de pression dans le fluide, qui éjecte ensuite une gouttelette d'encre (PEDOT: PSS) à partir de la buse; un motif est généré par le déplacement de la tête d'impression par rapport au substrat (membrane de PVDF) en deux dimensions. *En médaillon*: Photo prise avec un microscope optique après l'impression de 20 couches de PEDOT: PSS.

et de conductivité électrique du film sans pour autant accentuer les phénomènes d'infiltration.

Des actionneurs de forme rectangulaire ($1.5 \times 8 \text{ mm}^2$) ont été obtenus par impression jet d'encre de PEDOT: PSS sur des membranes de PVDF comme représenté sur la Fig. C.22a. Pour assurer un volume et une conductivité suffisants, 10 couches de PEDOT:PSS ont été imprimées ce qui conduit à une masse d'environ $0.27 \pm 0.13 \text{ mg}$. Le poids de la membrane de PVDF est de $3.19 \pm 0.006 \text{ mg}$. Après recuit thermique, le PVDF a été imprégnée avec $4.5 \pm 0.06 \text{ mg}$ de liquide ionique et a été immédiatement utilisé pour la caractérisation.

Le profil de la déformation de l'actionneur ainsi que le courant transféré sont tracés sur la Fig. C.22b. L'un des avantages de l'impression jet d'encre pour la fabrication d'actionneurs souples réside dans la grande flexibilité d'utilisation pour obtenir des motifs variés avec différentes solutions. Un exemple est montré sur la Fig. C.23. Des ailes mobiles d'un dispositif 2D en forme de libellule ont pu être obtenues par (1) dépôt de gouttes avec 6 ml d'une solution de PEDOT :PSS déposée sur toute la surface de la membrane (Fig. C.23c), et (2) par impression jet d'encre, où seulement une surface de $0.2 \times 1 \text{ cm}^2$ a été imprimée pour chaque aile (à l'aide de moins de 0,5 ml d'encre). Plusieurs avantages peuvent être mis en avant, notamment la possibilité de dessiner des motifs de forme très variée (spirale, forme en U, etc.) ou encore de déposer localement des électrodes sur un dispositif pour en modifier les propriétés électriques et mécaniques. Enfin, l'impression jet d'encre permet d'envisager la fabrication de dispositifs identiques à grande échelle.

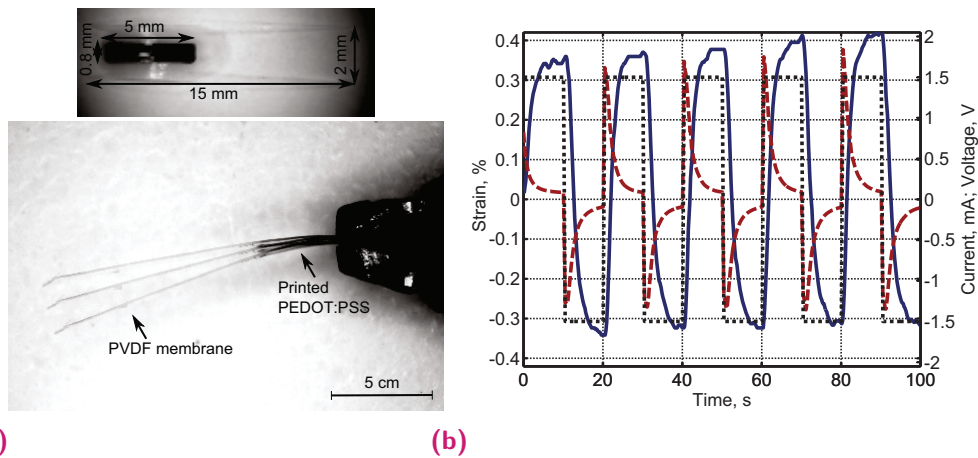


Fig. C.22. (a) Images fusionnées de l'actionneur dans sa position initiale et de ses extrémités lors de l'actionnement avec un signal carré de 1.5 V à 50 *mHz*. La position de la couche de PEDOT :PSS imprimée est indiquée par des flèches. Les dimensions de l'actionneur utilisé (2x15 *mm*) et couche de PEDOT: PSS imprimée (0.8x5 *mm*) sont indiqués ci-dessus. (b) Déplacement (ligne bleue) et courant transféré (ligne pointillée rouge) pour des actionneurs imprimés (10 couches, 0.36 *mg*) lors de l'actionnement. La forme du signal de tension utilisé est indiquée en pointillé noir.

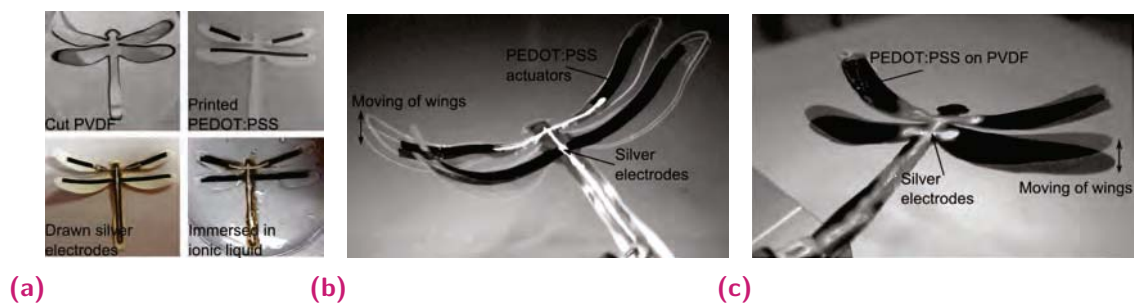


Fig. C.23. (a) Etapes de fabrication pour des actionneurs imprimés: (1) une membrane de PVDF est découpée à la forme désirée; (2) les actionneurs rectangulaires de PEDOT: PSS ont été imprimés sur chaque côté de la membrane dans la zone où l'actionnement est souhaité; (3) des zones en pâte d'argent sont déposées pour connecter les différentes électrodes; (4) la membrane PVDF est imprégnée avec le liquide ionique. Images fusionnées de deux positions d'actionnement (± 2 V à 1 *Hz*) d'une libellule avec des actionneurs (b) imprimés et (c) actionneurs obtenus dépôt de goutte et découpe.

List of Figures

1.1	(a) Stress versus strain and (b) work density versus strain rate of typical artificial muscles.	3
2.1	Scheme and example of the grafting-to reaction of acrylate to <i>PVDF</i> membrane by (a) ultraviolet (<i>UV</i>) irradiation and (b) atom transfer radical polymerisation	16
2.2	(a) Scheme of the processes during plasma induced polymerization and (b) during plasma etching.	18
2.3	(a) Scheme of simplified reaction mechanisms for post-irradiation plasma grafting and (b) functionalization during irradiation.	19
2.4	(a) Chemical structure of <i>PVDF</i> , <i>PEGMA</i> and <i>PVDF-graft-PEGMA</i> and their IR signatures between (b) $1300 - 1800\text{ cm}^{-1}$ and (c) $2700 - 3100\text{ cm}^{-1}$	21
2.5	(a) atomic force microscopy (<i>AFM</i>) surface scans of <i>PVDF</i> membranes after <i>PEGMA</i> grafting with different plasma irradiation times. (b) Fourier transform infrared spectroscopy (<i>FT-IR</i>) spectra of the same membranes and (c) ratio of integrated <i>OCO-CF FT-IR</i> peaks.	22
2.6	Schemes showing three different precursor deposition strategies and subsequent plasma membrane interactions: (a) deposition by dipping in diluted solution; (b) deposition by dipping in viscous liquid; (c) deposition by spraying	24
2.7	Comparison of membranes prepared by filling the pores (dip) and spray coating (spray): (a) grafting density; (b) water contact angle; (c) integrated <i>FT-IR OCO-CF</i> ratio; (d) roughness of the membranes.	25
2.8	<i>AFM</i> surface scans of the two sides of the pristine and functionalized membranes. <i>PEGMA</i> deposition method is indicated above.	26
2.9	<i>EDX</i> sulphur (blue) and fluorine (red) line scans across the cross-section of the <i>PEDOT:PSS/PVDF-graft-PEGMA/PEDOT:PSS</i> trilayers, where <i>PEGMA</i> was deposited on <i>PVDF</i> by (a) dipping and filling the pores, (b) spray coating.	27
2.10	Spray efficiency of <i>PEGMA</i> in ethanol/water solution on <i>PVDF</i> membranes with different spray parameters	28
2.11	Grafting density versus density of <i>PEGMA</i> sprayed on the rough and smooth side at different conditions.	29

2.12	(a) Ratio of integrated OCO and CF peaks of pristine and functionalized PVDF membranes versus sprayed amount of precursor and (b) Water contact angle of pristine PVDF and PVDF-graft-PEGMA membranes at different grafting densities. (c) TopographicAFM measurements of the cross-sectional profiles of membranes with different grafting densities for the two sides.	30
2.13	Energy-dispersive X-ray spectroscopy (EDX) line scans for sulphur and fluorine along the cross-sections of PEDOT:PSS/PVDF-graft-PEGMA, the length of the depth of mixing versus the grafting density of PVDF-graft-PEGMA. and AFM images of the rough and smooth surfaces of the PVDF-graft-PEGMA membranes with different grafting densities.	32
2.14	Scheme of functionalization of PVDF membranes.	33
3.1	Illustration of different mechanisms playing important role in the adhesion of two polymer solids.	38
3.2	Measured (for poly(3,4-ethylenedioxythiophene) polystyrene sulfonate (PEDOT:PSS) and water) or reported (for PVDF) surface tension and pictures of the contact angle measurements between water, PEDOT:PSS and PVDF.	40
3.3	Steps of adhesion evaluation process.	41
3.4	(a) Illustration of PEDOT:PSS core/shell structured nanoparticles in aqueous solution and (b) Pictures of the remaining PEDOT:PSS films on the PVDF membrane surface after adhesion tests with different annealing conditions.	42
3.5	(a) Illustration of the likely PEDOT:PSS structure in the aqueous solution with poly(ethylene glycol) of $M_r - 400$ (PEG400) as an additive and (b) pictures of the adhesion tests between PEDOT:PSS with PEG as secondary dopant (PEG-PEDOT) films and pPVDF membrane.	44
3.6	(a) Pictures of the adhesion tests between PEG-PEDOT films and pristine PVDF membrane (pPVDF) membrane in a dry state and after incubation in ionic liquid. (b) EDX scan along the cross-section of the peg-PEDOT/pPVDF/pegPEDOT trilayer.	45
3.7	(a) Pictures of PEDOT:PSS (with 1 vol% Triton X – 100) film deposited by solvent casting on pPVDF, (b) adhesion tests of such films and (c) equivalent test performed on PVDF-PEDOT:PSS (diluted with 10vol% of i-butanol) sandwich.	46
3.8	(a) Pictures of adhesion tests of PEG-PEDOT and pPVDF membrane and (a) same test with Ar plasma damaged PVDF.	48
3.9	(Table) Measured surface tension of PEG-PEDOT (1 vol%) and (pictures) contact angle measurements of PEG-PEDOT on pristine (pPVDF) and modified (PVDF-graft-PEGMA membrane (mPVDF)) membranes.	49
3.10	Qualitative adhesion test of PVDF and PVDF-graft-PEGMA membranes and PEDOT:PSS.	49
3.11	Adhesion tests of PEDOT:PSS (with 1 vol% PEG400) and flat PVDF films in a dry state.	50

3.12	Measured surface tension of <i>PEDOT:PSS</i> solutions with different <i>PEG400</i> volume concentrations and their contact angle with pristine <i>PVDF</i> membrane.	51
3.13	EDX line scans for fluorine (red) and sulphur (blue) traces along the cross-section of the trilayers <i>PEDOT:PSS/pPVDF/PEDOT:PSS</i> ((a)-(b)) and adhesion tests of the <i>PEDOT:PSS</i> film deposited on the rough side of the membrane ((c)-(d)).	52
3.14	EDX line scans for fluorine and sulphur traces along the cross-section of the trilayers <i>PEDOT:PSS/PVDF-graft-PEG/PEDOT:PSS</i> .	53
3.15	(a) Pictures of the back side of the membrane 24 hours after deposition of <i>pegPEDOT</i> (with 5 vol% <i>PEG400</i>) and (b) <i>PEDOT:PSS/pPVDF/PEDOT:PSS</i> (with 5 vol% <i>PEG400</i>) trilayer after upper <i>PEDOT:PSS</i> layer is removed.	55
3.16	Schematic drawing of different <i>PVDF</i> functionalisation methods and their influence on adhesion with <i>PEDOT:PSS</i> .	56
4.1	Chemical structure of poly(3,4-ethylenedioxythiophene) (<i>PEDOT</i>) and polystyrene sulfonate (<i>PSS</i>)	61
4.2	(a) Schematic illustration of the basic processes that are taking place during the volumetric expansion and (b) The polymer structure in the oxidized and reduced states.	62
4.3	Illustration of the interrelations between the processes during the actuation.	63
4.4	Chemical and 3D structures of the ionic liquid 1-Ethyl-3-methylimidazolium bis(trifluoromethanesulfonyl)imide (<i>emimTFSI</i>)	64
4.5	Illustration of a fabrication process flow for a solvent casted actuators.	66
4.6	Scheme of the interface and the mixing depth of <i>PEDOT:PSS</i> and <i>PVDF-graft-PEGMA</i> and the scanning electron microscopy (<i>SEM</i>) images of the cross-sections of the <i>PEDOT:PSS/mPVDF/PEDOT:PSS</i> trilayers before and after the immersion in ionic liquid.	67
4.7	(a) Difference of the thickness of the actuators and (b) increase in the actuators weight after different times of incubation in 1-ethyl-3-methylimidazolium bis(trifluoromethanesulfonyl)imide (<i>emimTFSI</i>).	67
4.8	(a) Merged images of the actuator at its extremities during actuation applying square wave with frequency of 50 <i>mHz</i> and 2.0 <i>V</i> amplitude and (b) applied voltage, current and power dissipation measured during the actuation..	69
4.9	(a) Actuator bending profile shown as calculated strain versus time, (b) the speed, (c) transferred charge and (d) strain to charge ratio of the actuator.	70
4.10	Cyclic voltammograms of the <i>PEDOT:PSS/mPVDF/ILs</i> trilayer actuators in air at different conditions.	72
4.11	(a) Actuation displacement profile of the <i>PEDOT:PSS/mPVDF/PEDOT:PSS</i> trilayer cycled in air showing creeping effect, (b) gradual decrease in the actuators displacement and (c)-(d) training effect.	74
4.12	Picture of (a) <i>PEDOT:PSS/pPVDF/PEDOT:PSS</i> actuators just after immersion in ionic liquid when adhesion is weak, (b) <i>PEDOT:PSS/mPVDF</i> bilayer when adhesion is strong and (c) merged images of the trilayer actuator with a strong adhesion between layer at initial position and at extremities during actuation.	76

4.13	(a) Lifetime measurement of actuators produced with hybrid PVDF-graft-PEGMA and pristine membranes (PVDF) and (b) amplitude of the displacement for PEDOT:PSS/PVDF-graft-PEG/PEDOT:PSS with based actuator in ionic liquid and the change in the humidity of the environment.	77
4.14	(a) Displacement and (b) current versus time of various actuators made with or without post-treatment from four different membranes. (c) Merged images of the several actuators at the initial and extremities during actuation.	79
4.15	(a) Strain and (b) transferred current and (c) bending speed profiles of the actuators having a different mixing depth.	81
4.16	(a) Peak-to-peak strain and (b) transferred charge for actuators with different mixing depth at different voltages.	83
4.17	(a) Bending and (b) transferred current profiles of the actuators with PEDOT:PSS electrodes that were secondary doped with 1 vol% of ethylene glycol, glycerol and standard PEG400.	84
4.18	textit(a) Bending and (b) transferred current profiles of the standard actuators and actuators treated with sprayed sodium dodecyl sulfate (SDS).	85
4.19	(a) SEM image of the PEDOT:PSS electrode surface with sprayed carbon nanotubes (CNTs) carpet. (b) Displacement and transferred current profiles of the actuators with and without carbon nanotube carpet.	86
4.20	(a) The change in the actuation frequency in time for the CNTs and simple actuators and (b) their bending profiles in time.	87
5.1	Schematic diagram of (a) a drop-on-demand inkjet printer and (b) the cycle of drop ejection.	92
5.2	(a) Illustration of the range of the fluid properties that allows DoD inkjet printing. (b) Equations plotted in a coordinate system defined by the Reynolds and Weber numbers. (c) Schematic illustration of the sequence of the events that occur after droplet impact an a substrate.	93
5.3	SEM of PEDOT:PSS layer printed on (a) rough and (b) smooth side of the PVDF membrane at the printing borderline.	96
5.4	(a) SEM of one pure PEDOT:PSS layer printed on PVDF membrane cracked after drying, (b) SEM of 10 PEDOT:PSS layer having 10vol% glycerol printed on PVDF membrane showing easy delamination casued by handling and (c) SEM image of the cross-section of PEDOT:PSS/PVDF/PEDOT:PSS trilayer, when surfactant (1 vol% Triton-X100) was added to PEDOT:PSS ink.	97
5.5	Schematic illustration of some substrate-ink interactions, when (a)-(b) hydrophobic or (d)-(e) hydrophilic membrane is used as a substrate. SEM pictures of PEDOT:PSS printed on the (c) hydrophobic and (f) hydrophilic PVDF membranes.	98
5.6	Pictures and SEM images of the PEDOT:PSS electrodes printed on PVDF membrane showing formation of rings due to surface lateral diffusion. . .	99
5.7	(a) Schematic illustration of the set-up for conductivity measurement and (b)-(f) conductivity of printed PEDOT:PSS lines at various printing and post-treatment conditions.	101

5.8	(a) Merged images of the inkjet printed actuator at its initial position and extremities and (b) its displacement and transferred current profiles during the actuation.	104
5.9	(a) Fabrication steps for printed actuators and merged images of two actuation positions (+/ - 2 V at 1 Hz) of dragonfly with (b) printed actuators and (c) actuators produced by drop casting and cutting.	105
A.1	Pictures of drops of ethanol-water mixtures with different ratios on pristine PVDF membrane.	148
A.2	Pictures of the main fabrication steps of PEDOT:PSS/mPVDF/PEDOT:PSS actuators. Functionalized as in Section A.2 PVDF membranes were used. Membrane was then fixed in a metal mechanical clamp and 3 ml of PEDOT:PSS solution was drop casted on one side. After drying in air for about 24 hours, PEDOT:PSS was deposited and dried on the opposite side of the membrane. Then membrane with PEDOT:PSS on both sides was dried in oven at 70°C for 2 hours, occasionally reversing the clamp. After drying rectangular shaped actuators were cut with CO ₂ laser. Actuators were immersed in ionic liquid before characterization (not shown).	149
A.3	Picture of the experimental set-up used for bending characterization (a) by recording the bending and tracking the position of the tip and (b) by tracking bending using laser displacement meter.	150
A.4	(a) Picture of PEDOT:PSS/mPVDF/PEDOT:PSS trilayer attached on the glass slides next to silver electrodes. (b) Picture of the set-up used for spraying carbon nanotubes.	151
A.5	(a) Illustration of the setup used for the electrical conductivity measurements of inkjet printed lines and example of well and badly printed rectangulars. (b) Influence of the width of the line on calculated conductivity of printed PEDOT:PSS as well as the influence of printing resolution (indicated in legend).	152
B.1	AFM surface scans of membranes functionalized with different amount of PEGMA.	155
B.2	Adhesion test of PEDOT:PSS (with 1 vol% PEG400) and flat PVDF films after incubation in ionic liquid.	155
B.3	Trilayer actuator bending profiles during actuation with low frequency (2 mHz) voltage square wave.	156
B.4	(a) Strain, (b) strain rate, (c) transferred current and (d) dissipated power profiles in time of a trilayer actuator, actuated with 2 V square voltage wave at 10 mHz.	156
B.5	Cyclic voltammograms of the trilayer PEDOT:PSS/mPVDF/PEDOT:PSS actuators obtained with 100 mV/s scan rates, at different voltages and after inkubation in ionic liquid for various times.	157
B.6	Cyclic voltammograms of the trilayer PEDOT:PSS/mPVDF/PEDOT:PSS actuators obtained with 100 mV/s scan rates, at different voltages and different secondary doping conditions.	157

B.7	Bending profile of a trilayer actuator in time at different frequencies showing frequency influence on creep.	157
B.8	Displacement ((a)-(b)) and transferred current ((c)-(d)) profiles of new and damaged actuator.	158
B.9	Displacement profile of the actuator during long time actuation and influence of humidity.	158
B.10	Influence of various parameters, such as electrode conductivity, weight, amount of ionic liquid on performance of the actuators.	159
B.11	(a) Transferred current profiles of the actuators with different mixing depth during actuation with 2 V square wave at 50 mHz frequency and (b) peak-to-peak transferred current of the same actuators at different voltages.	160
B.12	Displacement and transferred current profiles of the (a) trilayer actuator made with PEDOT:PSS doped with 5 vol% PEG400 electrodes, (c) A5 actuator and (d) trilayer actuator made on completely hydrophilized PVDF membrane. (d) CV voltammograms of the actuator with the percolated electrodes (with 5 vol% PEG400).	160
B.13	(a) Resistance between the electrodes before and after incubation in ionic liquid for 5 or 15 minutes fabricated by drop casting and (b) electrical resistance measurements of printed PEDOT:PSS actuators.	161
B.14	Cyclic voltammograms of actuators with (a) and (b) without post treatment with CNT.	161
B.15	Displacement (a) and transferred current (b) profile of the actuators treated with CNT and with SDS.	161
B.16	(a) Strain profile at different voltages and (b) frequency response of probably the best trilayer PEDOT:PSS/mPVDF/PEDOT:PSS actuator fabricated during our study.	162
B.17	(a) SEM image of the PEDOT:PSS layer printed on the PVDF membrane (tilted) and (b) AFM image of the crack on the surface of printed PEDOT:PSS and the height profile.	162
B.18	(a) Strain rate, (b) strain and transferred charge profiles of the printed actuator (10 layers on each side resulting in 3.35 mg of printed PEDOT:PSS.	162
C.1	Contrainte en fonction de la déformation pour différents types de muscles artificiels et d'actionneurs.	164
C.2	(a) Illustrations schématique du processus qui entre en jeu lors de la dilatation volumique. (b) Structure du polymère dans son état oxydé et réduit.	166
C.3	(a) Structure chimique du PEDOT :PSS et illustration schématique de la structure cœur/coquille dans une solution aqueuse (b) sans et (c) avec des additifs secondaires.	168
C.4	Chemical and 3D structures of the ionic liquid 1-Ethyl-3-methylimidazolium bis(trifluoromethanesulfonyl)imide (emimTFSI)	169

C.5	(a) Illustration schématique d'actionneurs PEDOT: PSS / PVDF / PEDOT: PSS avec un liquide ionique avec une défaillance potentielle dans la zone d'adhésion entre les couches (ligne pointillée rouge). (b) Image par microscopie à balayage (MEB) d'une coupe transversale de l'actionneur tri-couches où l'on peut observer très clairement la délamination de la couche de PEDOT: PSS de la membrane PVDF (c) Actionneurs avec une mauvaise adhésion interfaciale après immersion dans un liquide ionique.	169
C.6	(a) Représentation schématique d'un actionneur PEDOT: PSS / PVDF / PEDOT: PSS avec des électrodes percolées (lignes bleues). (b) Image SEM d'une coupe transversale de l'actionneur tricouches avec du PEDOT: PSS dans la membrane PVDF (c) Spectres EDX le long de la coupe transversale faisant apparaître clairement des traces de soufre (PEDOT: PSS) en bleu et de fluor (PVDF) en rouge. Les traces de soufre significativement plus élevées que zéro traduisent un phénomène de percolation dans la membrane.	170
C.7	Illustration schématique d'un greffage lors de l'irradiation plasma.	171
C.8	(a) Structure chimique du PVDF, du PEGMA et du PVDF-PEGMA et leur signature entre (b) $1300 - 1800 \text{ cm}^{-1}$ et (c) $2700 - 3100 \text{ cm}^{-1}$	172
C.9	Schémas illustrant trois stratégies différentes de dépôt de précurseur et l'interaction du plasma à la surface de la membrane: (a) le dépôt par trempage dans une solution diluée contenant le précurseur; (b) le dépôt par immersion dans un liquide visqueux; (c) le dépôt par pulvérisation . . .	173
C.10	(a) Spray efficiency of PEGMA in ethanol/water solution on PVDF membranes with different spray distance, (b) Grafting density versus density of PEGMA sprayed on the rough (blue) and smooth side (red) at different conditions. Black stars - sprayed on both side and averaged.	174
C.11	AFM and SEM images of surfaces of the pristine PVDF membrane. (a)-(b) - rough side ($R_q - 351 \text{ nm}$) (c)-(d) - smooth side ($R_q - 182 \text{ nm}$)	174
C.12	Spectres EDX pour le soufre et le fluor le long des sections transversales du PEDOT: PSS / PVDF avec greffage PEGMA, profondeurs de greffage par rapport à la densité de greffage et images obtenues par microscopie à force atomique (AFM) des surfaces lisses et rugueuses de membranes PVDF avec greffage PEGMA pour différentes densités de greffage (GD). . .	176
C.13	Tensions de surface mesurées (PEDOT :PSS et eau) et publiée (PVDF). Photographies de mesures d'angle de contact entre l'eau, le PEDOT :PSS et le PVDF	177
C.14	Étapes du processus d'évaluation d'adhésion.	177
C.15	Test d'adhésion du PVDF et de membranes PVDF avec un greffage PEGMA et PEDOT: PSS.	178
C.16	Représentation schématique de différentes méthodes de fonctionnalisation du PVDF et leur influence sur l'adhésion avec du PEDOT :PSS.	179

C.17	Illustration d'un procédé de fabrication d'un actionneur par dépôt en goutte de solvant. Une membrane hybride (PVDF avec greffage PEGMA) est fixée mécaniquement à un support en aluminium et une goutte de PEDOT: PSS en solution aqueuse (avec un dopage secondaire) est déposée sur la surface de la membrane. Après séchage à température ambiante, le support est inversé et le processus est répété pour l'autre côté de la membrane afin de produire un actionneur tricouches. La membrane avec du PEDOT: PSS sur les deux côtés est ensuite séchée à l'étuve à 70°C pendant deux heures. Des actionneurs rectangulaires de 1.5 mm par 2 cm sont ensuite découpés par laser, les actionneurs sont thermiquement recuits à 120°C (non représenté ici) et sont incubés dans un liquide ionique pendant 10 à 120 minutes.	180
C.18	Images AFM et MEB de la surface d'une membrane PVDF sans greffage PEGMA.	181
C.19	(a) Réponse d'actionneurs PEDOT: PSS / PVDF greffé PEGMA / PEDOT: PSS pour différentes tensions d'actionnement et (b) Amplitude de déplacement de ces mêmes actionneurs pour différentes fréquences.	181
C.20	(a) Mesure de la durée de vie d'actionneurs hybrides PVDF greffé PEGMA (mPVDF) et de membranes vierges (PVDF). La profondeur d'interaction entre le PEDOT: PSS et la mPVDF est indiquée dans la légende. (b) Amplitude du déplacement d'un actionneur PEDOT: PSS / PVDF-greffage PEG / PEDOT: PSS avec un MD de 5 μm dans un liquide ionique (bleu) et changement de l'humidité de l'environnement (jaune)	183
C.21	Illustration schématique d'une impression jet d'encre piézo-électrique	184
C.22	(a) Images fusionnées de l'actionneur dans sa position initiale et de ses extrémités et (b) déplacement (ligne bleue) et courant transféré (ligne pointillée rouge) pour des actionneurs imprimés (10 couches, 0.36 mg) lors de l'actionnement.	185
C.23	(a) Etapes de fabrication pour des actionneurs imprimés. Images fusionnées de deux positions d'actionnement ($\pm 2 V$ à 1 Hz) d'une libellule avec des actionneurs (b) imprimés et (c) actionneurs obtenus dépôt de goutte et découpe.	185

List of Tables

4.1	Geometry and electrical properties of actuators	80
5.1	Physical properties of PEDOT:PSS inks	103

Declaration

I declare that this work has been completed solely by me and only with the help of the references I mentioned.

Toulouse, November 24, 2015

Aiva Simaite

